Determination of Imperviousness and its Impact on Risk Based Urban Flood Modeling

Thesis
submitted in partial fulfillment of the requirements
of the degree of

DOCTOR OF PHILOSOPHY

by

Sanat Nalini Sahoo

Department of Civil Engineering

Indian Institute of Technology Guwahati

Guwahati-781039, India

February 2014

Dedicated to

The Almighty God who made it happen

CERTIFICATE

This is to certify that the thesis entitled "**Determination of Imperviousness and its Impact on Risk Based Urban Flood Modeling"** submitted by Mrs. Sanat Nalini Sahoo to the Indian Institute of Technology Guwahati, for the award of the degree of Doctor of Philosophy in Civil Engineering is a record of bonafide research work carried out by her under my supervision and guidance. The thesis work, in my opinion, has reached the requisite standard fulfilling the requirement for the degree of Doctor of Philosophy.

The results contained in this thesis have not been submitted in part or full to any other University or Institute for award of any degree or diploma.

IIT Guwahati
February 2014

(Dr. P. Sreeja)
Assistant Professor
Department of Civil Engineering
Indian Institute of Technology Guwahati
Guwahati-781039

STATEMENT

I do hereby declare that the matter embodied in this thesis is the result of investigations carried out by me in the Department of Civil Engineering, Indian Institute of Technology Guwahati, Assam, India.

In keeping with the general practice of reporting scientific observations, due acknowledgements have been made wherever the work described is based on the findings of other investigators.

IIT Guwahati
February 2014

(Sanat Nalini Sahoo)
Research Scholar
Department of Civil Engineering
Indian Institute of Technology Guwahati
Guwahati-781039

Acknowledgements

This dissertation would not have been possible without the help of several individuals who in one way or the other have extended their valuable assistance for completion of this research work.

I would like to express my profound feeling of gratitude to my supervisor Dr. Sreeja P., Assistant Professor, Civil Engineering Department, IIT Guwahati, for her inspiration, invaluable guidance and constant encouragement during this work. I am deeply indebted to her for her technical and moral support during the difficult times. Her amicability and positive disposition have always been inviting and encouraging for consultation at good and bad times. I consider it as a great opportunity to work under her and to learn from her research expertise.

I am sincerely grateful to the chairman of my Doctoral Committee, Prof. S. Dutta, Professor, Civil Engineering Department, IIT Guwahati, for his constructive suggestions and timely help during the entire period of this research work

I am also thankful to the members of the Doctoral Committee Dr. S. A. Kartha, Assistant Professor, Civil Engineering Department, IIT Guwahati, and Dr. P. Muthukumar, Associate Professor, Mechanical Engineering Department, IIT Guwahati, for very helpful discussions and their invaluable suggestions at different phases of the research work.

I would also like to express my deepest sense of reverence and indebtedness to Dr. S. Sreedeep, Associate Professor, Civil Engineering Department, IIT Guwahati, for his timely suggestions and encouragement at times of need during the period of study.

I am also heartily thankful to the authorities of different government offices in Guwahati like GMDA, ASTEC, GMC, RMC, COE, State Water Resources Department, East Water Resources department for their kind help and support during the data collection period of this thesis work.

I sincerely thank Department of Science and Technology (DST), India for providing the financial support for this research program vide project no. SR/FTP/ETA-0005/2008.

Thanks are also due to Ms. Swati, B, Dr. Malaya, C., Mr. Abhisek, B., Mr. Amol, S., Mr. A. Deka, Mr. Bazal, H. and many more who at the various stages of this work have generously extended their support for completion of this project work.

I would also like to offer my love, admiration and respect to my parents and in-laws for showering their blessing and helping me to reach where I am. I also would like to thank my husband, Mr. Ramesh Chandra Sahu and my daughter Ms. Sharmistha Sahu for their constant support and co-operation during this research work.

Lastly, I take this special occasion to thank "The Almighty God" for showing me light and blessing me with necessary strength to carry out and complete this research work.

Sanat Nalini Sahoo

Abstract

Floods are the most common and widespread disasters in a tropical country like India. While the reason for flooding in rural areas is mostly due to high river discharge, the same in urban areas is due to increased imperviousness and poor drainage. The tremendous growth of infrastructure without adequate provision for drainage has increased runoff, thereby aggravating the flooding in urban areas. The criticalities in the quantification of imperviousness and its impact on flood modeling and flood management are not very well understood for urban catchments. Flood modeling and identifying the vulnerable zones are the primary step for formulating any flood management strategy. It is also noted from the literature that there are not many studies that integrate risk factor with flood management. Therefore, the objective of the present study is to identify precise method of imperviousness determination for urban catchment in north-east India, study its role on urban flood modeling, utilize the results for flood hazard identification and demonstrating the effectiveness of flood management scheme.

Different methodologies have been employed to identify Total Impervious Area (TIA) using remote sensing and GIS technologies. The more hydraulically relevant Effective Impervious Area (EIA) has been estimated by two indirect methods and one semi automated direct method. The importance of appropriate quantification of imperviousness for accurate estimation of surface runoff is brought forth in this study. An empirical relationship between TIA and EIA has been derived for the study area and compared with those reported in the literature. The impact of imperviousness and different rainfall intensities on urban flooding is studied in detail. The study also describes the usefulness of these results for flood risk modeling and proposing suitable flood management scheme. The provision of detention pond as one of the measures for urban flood management has been demonstrated in this study.

Key words: Remote Sensing, GIS, imperviousness, urbanization, urban flooding, flood hazard, flood risk, detention pond, flood management.

Contents

List of Tables

List of Figures

Nomenclature

μ_i	Mean of class i
μ_j	Mean of class j
θ	Volumetric water content
Ψ	Tension head
α	Sorptivity number
ΔV	Change in storage in time Δt
a	Radius of disc of TI
A	Total cross sectional area of flow
A_c	Cross sectional area of flow in channel
A_f	Cross sectional area of flow in floodplain
C_i	Covariance of class i
C_j	Covariance of class j
d	Depth of water in the reservoir
d_p	Maximum depression storage
D	Divergence
E	Evaporation
F_A	Total flood affected area in the ward
F_D	Area with flood depth of more than 0.2 m in the ward
g	Acceleration due to gravity
i	Rainfall intensity
I	Infiltration
JM	Jeffris-Matusita distance
$K(\Psi)$	The hydraulic conductivity function at tension head Ψ
K_c	Conveyance of the channel
K_f	Conveyance of floodplain
K_s	Saturated hydraulic conductivity
L_1	Percentage of agricultural land affected by flood in the ward
L_2	Percentage of forests and grass land affected by flood in the ward

L_3	Percentage of swampy land and water bodies affected by flood in the ward
L_4	Percentage of scrub land affected by flood in the ward
n	Manning's roughness coefficient
P	Wetted perimeter
Q	Total flow
Q_{in}	Inflow
Q_{out}	Outflow
Q_s	Steady state flow
r	Radial coordinate
R	Hydraulic radius
R_1	Percentage of NH affected by flood in the ward
R_2	Percentage of major road affected by flood in the ward
R_3	Percentage of any other road affected by flood in the ward
S	Friction slope
$S(\Psi)$	Sorptivity at tension head Ψ
t	Time
tr	The trace function of matrix (sum of main diagonal elements)
T	Return period
T_A	Total area of the ward
TD	Transformed Divergence
w	Sub-catchment's characteristic width
x	The vector location of the pixel in the n-dimensional space
X_c	Distance along the channel between the cross sections
X_f	Distance along the floodplain between the cross sections
y	Flow depth in the channel
z	Vertical coordinate

Abbreviation

3-D	3-Dimensional
ASCE	American Society of Civil Engineers
ASTEC	Assam Science Technology and Environment Council
Cl 1	Classification 1
Cl 2	Classification 2
Cl 3	Classification 3
Cl 4	Classification 4
Cl 5	Classification 5
Cl 6	Classification 6
cm	Centimeter
CN	Curve Number
COE	Centre of Excellence
DEM	Digital Elevation Model
DN	Digital Number
EIA	Effective Impervious Area
ENVI	Environment for Visualizing Images
EPA	Environmental Protection Agency
Eq.	Equation
ETM+	Enhanced Thematic Mapper plus
FCC	False Colour Composite
FIM	Flood Inundation Map
GIS	Geographical Information System
GLCF	Global Land Cover Facility
GMC	Guwahati Municipal Corporation
GMDA	Guwahati Metropolitan Development Authority
HEC-RAS	Hydrologic Engineering Centre-River Analysis System
HI	Hazard Indicator
HR	Hazard Rank
IA	Impervious Area

IDF	Intensity-Duration-Frequency
IIT	Indian Institute of Technology
IRS	Indian Remote Sensing
km	Kilometer
LGB	Lokpriya Gopinath Bordoloi
LISS	Linear Imaging and Self Scanning Sensor
LU	Land Use
MFD	Maximum Flood Depth
MIA	Mapped Impervious Area
MSS	Multi Spectral Scanner
MXL	Maximum Likelihood
n-D	n-Dimensional
NEIA	Non Effective Impervious Area
NIR	Near-Infra Red
NRSC	National Remote Sensing Centre
PA	Pervious Area
PRI	Peak Rainfall Intensity
RCC	Rectangular Concrete Channel
R K	Ram Krishna
RE	Rainfall Event
RMC	Regional Meteorological Centre
RS	Remote Sensing
SCS	Soil Conservation Service
sec	Second
SWMM	Storm Water Management Model
TCC	True Colour Composite
TI	Tension Infiltrometer
TIA	Total Impervious Area
TIN	Triangulated Irregular Network
TM	Thematic Mapper
USA	United States of America

Chapter 1

Introduction

1.1 General

Floods are the most common and widespread disasters in a tropical country like India. Intense rainfall, drainage congestion, imperviousness of ground surface, bank erosion and breaching of embankments are the main causes of flooding (Dhar and Nandargi 2003; Mohapatra and Singh 2003). According to National Flood Commission report (2008) of India, around 40 Million hectares (Mh) of land out of total 329 Mh of geographical area is prone to flood. On an average, floods affect 75 lakhs hectares of land and result in a loss of more than 1600 lives annually. Average annual damage to crops, houses, and public utilities is more than Rs. 1800 crores. This monetary value of flood damage shows an increasing trend. The average annual damage during 1996 to 2005 was Rs. 4745 crores as against the last 53 years average of Rs. 1805 crores. This affects the economy very badly in a developing country like India. While the reason for flooding in rural areas is mostly due to high river discharge, the same in urban areas is due to increased imperviousness and poor drainage.

It is almost impossible to prevent urban flooding due to continuous developmental activities. Therefore, the major focus has shifted to flood management by using structural and non-structural measures for reducing the loss of life and property. Structural measures involves civil works in the flood plain and/or the catchments and includes construction of storage reservoirs (dams), detention basins, flood embankments(levees), drainage channels, anti-erosion works, channel improvement works etc. Since it is not always feasible to undertake structural measures due to economic, social and political constraints, non-structural measures have a very important role to play (Faisal et al. 1999, 2003). The non-structural measures includes flood forecasting and warning, flood plain zoning, flood proofing, flood plain management, disaster preparedness or emergency support, post disaster recovery (rehabilitation), flood insurance etc. In general, the flood management process can be divided into three stages i.e. flood planning, flood emergency management and post flood recovery (Simonovic and Akter 2006). During the planning stage, different alternative structural and non-structural measures are analyzed and compared for

possible implementation. Flood emergency management includes real time update of current flood situation and daily operation of flood control works. From the appraisal of current flood situation, information is used to manage the flood and steps are taken to evacuate the affected areas. For a proper flood management strategy to be developed, accurate estimation of flood volume or flood depth by hydraulic modeling is essential which in turn requires the determination of inflow hydrograph by hydrological modeling.

1.2 Motivation for the Study

Flooding scenarios in urban cities of developing countries like India is bleak even for a moderate rainfall. This is due to indiscriminate growth of city devoid of holistic planning and lackadaisical development of basic infrastructure such as drainage. In the present situation, flood management is the best alternative for minimizing the effects of flooding. This would necessitate precise information of flooding aspects as discussed above. This is quite challenging for ungauged urban catchments in India where paucity of data prevents the validation of flood modeling. Therefore, refining the existing methods of flood modeling or using spatial techniques like remote sensing and geographical information system (GIS) would be the possible solution for developing recommendations for flood management, which is not explored in detail for ungauged urban catchments. The criticalities in the quantification of imperviousness (directly related to urbanization) and its impact on flood modeling and flood management are not very well understood for urban catchments. It is noted from the literature that there are not many studies that integrates risk factor with flood management. Such needs have motivated this research work to analyze and develop appropriate guidelines for flood modeling and flood hazard identification (identifying flood vulnerable zone) for urban catchment. Such a study would be important for effective flood management.

1.3 Objective of the Study

The main objective of the present research is to study flooding attributed to urbanization in Guwahati, which is a fast growing metro city in north-east India. The study purports to identify precise method of imperviousness determination (related to urbanization) by geospatial techniques for urban catchment, and understand its impact on flood modeling. The usefulness of these results for flood risk modeling, flood hazard identification and proposing flood

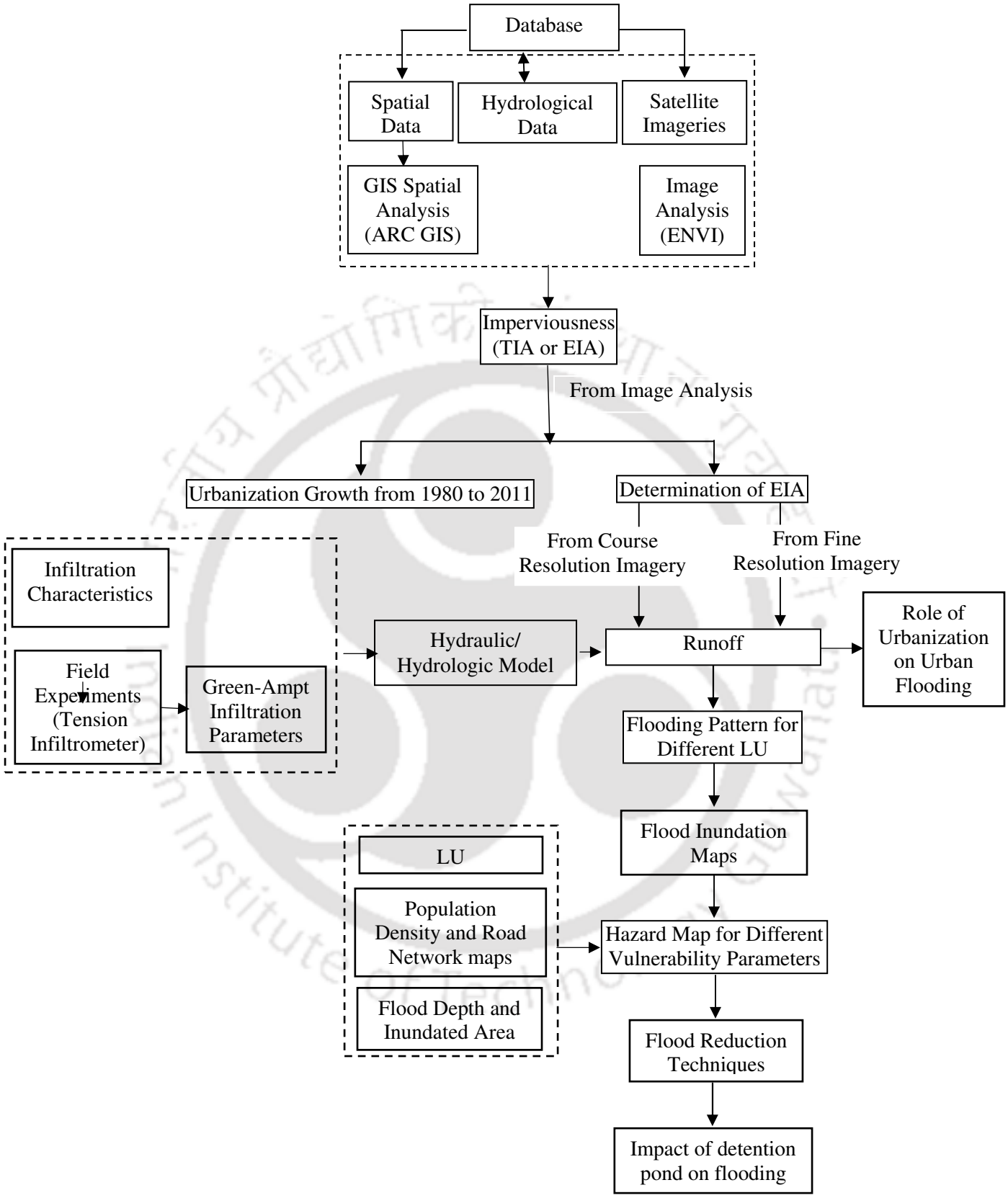

Fig. 1.1 Overview of the thesis

management scheme for the urban catchment will be demonstrated. The overview of the current research work is presented in Fig. 1.1.

1.4 Organization of Thesis

After introducing the research work, motivation and basic objective in chapter 1, chapter 2 presents comprehensive review of prominent literature on imperviousness determination methodologies, its impact on different hydrological processes, urban flood modeling and the potential application of remote sensing (RS) and Geographical Information System (GIS) in flood management. This is followed by critical appraisal of the literature discussing the need for further research. The final section of chapter 2 discusses the scope of the present research to fulfill the objective stated in chapter 1.

Chapter 3 contains the detailed description of the study area and various data collected for conducting this research work.

Chapter 4 describes the image analysis techniques for quantifying total and effective imperviousness of the study area due to urbanization. Urbanization growth from 1980 to 2011 has been determined for the study area. The procedure for improving the preciseness of imperviousness determination by integrating GIS has been discussed. Special focus has been laid to determine the more hydraulically relevant effective impervious area (EIA) by two indirect methods and a semi automated direct method. An empirical relationship between TIA and EIA has been derived for the study area with the present land use and compared with those reported in the literature.

Chapter 5 includes the experimental approach adopted to obtain the infiltration parameters in the field. Tension infiltrometer has been used to conduct experiments at 14 different locations of the study area. From the experimental result, Green Ampt infiltration parameters have been derived which is used as input for hydrologic model.

Chapter 6 presents the theory about the hydrologic model used and runoff simulated in all watersheds of the study area for different rainfall intensities and for different types of imperviousness. This section critically evaluates and quantifies the impact of imperviousness on urban flooding. The importance of appropriate quantification of imperviousness for accurate estimation of surface runoff is also brought forth in this study. A comparison is also presented

between the simulated runoff by event wise rainfall input and a continuous series of rainfall input.

Chapter 7 discusses the usefulness of urban flood modeling results for flood risk modeling and flood hazard identification. Flood inundation maps and flood risk maps have been prepared for the study area by incorporating the factors such as inundated area, flood depth, land use, population and affected road network. The influence of geographical features like hills on flooding has been explained. The provision of detention pond as one of the measures for urban flood management has been demonstrated in this chapter.

Chapter 8 presents the summary and conclusion of this research work followed by limitations and future scope of research.

Chapter 2

Literature Review

2.1 General

Several studies have been carried out in the recent past, which addresses the flood mitigation and management in natural areas where very large water bodies are present. Intense research activities have already been pursued and still ongoing in the developed countries to contribute to the systematic preparedness of urban flood management. This chapter presents a brief description about the works reported by different researchers in the field of urban flooding. The studies, which deals with modeling urban flow, the role of imperviousness in flooding and the use of remote sensing and GIS for flood related studies are discussed below in detail. Further, various studies dealing with urban flood management and risk based flood modeling are also presented. The last part presents the summary and critical appraisal of the reviewed literature.

2.2 Urban Flooding

Most part of our country is worst hit by repeated occurrence of flooding every year. It is definite that it is nearly impossible to prevent a flooding situation. The tremendous growth of infrastructure has reduced the precipitation accommodating capacity, thereby aggravating the flooding conditions. Several studies have been carried out in the recent past, which address the urban flood mitigation and management. Studies related to urban flood modeling are discussed in the following section:

2.2.1 Urban flow modeling

O'Brien et al. (1993) have performed an interactive flood or mudflow routing between channel, street, and floodplain flow using a uniform grid system to describe complex floodplain topography by making use of the two-dimensional model FLO-2D, which is a flexible tool to augment the capability of the floodplain manager and engineer to predict flood hydraulics. Simulation of the 1983 Rudd Creek mudflows with FLO-2D correlated well with the observed area of inundation, maximum flow depth at the fan apex, frontal wave flow depths, and velocities and final deposits based on mudflow cessation.

Navarro and Zorraquino (1993) have developed an explicit numerical flow-routing model based on the second order McCormack scheme. The study described the use of the finite difference scheme for the solution of the Saint-Venant's equations of the one dimensional unsteady open channel flow, and the treatment of the boundary problem by the method of characteristics. The registered inflow and outflow hydrographs were used for the simulation of the propagation of the waves along the watercourses. Results of flow computations indicated that this model can be considered as a suitable technique for hydraulic studies involving rapidly varying flows.

Molls and Molls (1998) have described a new numerical technique used to solve the one-dimensional (1D) and two-dimensional (2D) Saint-Venant's equations. This new technique differs from traditional numerical methods (i.e., finite-difference, finite element, finite-volume, spectral methods, etc.) it is quite simple, easy to implement, and can be extended to higher dimensions.

Delis et al. (2000) have presented three implicit high-resolution total variation diminishing (TVD) schemes for solving the Saint-Venant's equations used in open channel flow. The applicability, performance and validity of these methods were investigated and were reproduced for a wide range of cases, which include friction, non-uniform bed slopes and transitions between subcritical and supercritical flow, non-prismatic cross sections and hydraulic jumps. It was noticed that the tests produced satisfactory results without resorting to excessively fine grids.

Guo (2001 a) has expanded the rational method into the rational hydrograph method, in which the time of concentration has been considered as the system memory and the contributing rainfall depth to the present runoff rate has been defined as the accumulated precipitation over the past up to the time of concentration. This resulted in a complete runoff hydrograph under a continuous non-uniform hyetograph. A new formula for estimating the time of concentration was derived from 25 rainfall/runoff events observed in four urban watersheds. This approach was tested by laboratory observations, and rainfall/runoff events recorded from small watersheds in states of Maryland and Colorado.

Guo (2001 b) has compared three different approaches, which are used for the hydrologic design of flood control detention ponds in urban catchments, namely, design storm approach, continuous simulation approach and analytical probabilistic approach. It was noted that all the three approaches generated similar results. The less variable results from the analytical probabilistic approach can greatly simplify the administration of local flood control regulations.

Noto and Tucciarelli (2001) have made the computation of the unsteady-state flow in an urban drainage network by using a new methodology for the solution of shallow water equations. The algorithm employed for this purpose is based on the decomposition of the equation state variables in two components, namely kinematic and parabolic. The algorithm was tested on field example, and its performance compared with the performance of the other popular commercial codes. It was noted that the difference between the results of the different types of models was found to be negligible in most of the cases of practical interest.

Singh et al. (2001) have made design flow estimates using a regional flow-duration curve for ungauged catchments, where there are insignificant data for analysis for Himalayan watersheds. Formulation of models was based on data transfer between gauged watersheds of the same region, statistical normalization, and empirical regional relation. It was noted that the statistical approach of estimation (non-dimensional) performs satisfactorily in calibration as well as in validation. The simple power relation for mean flow-estimation, as well as the complete model, performed well in calibration and less satisfactorily in validation because of the short length of data.

Dutta et al. (2003) introduced an integral model, which is a combination of a physically based distributed hydrologic model and a distributed flood loss estimation model for flood estimation. The hydrologic model considered the major processes of water cycle through physically based equations. The loss estimation model is formulated based on stage damage relationships between different flood inundation parameters and land use features. Due to the dynamic linking of the flood inundation model with loss estimation model, it could yield a spatial distribution of flood losses at any given time as well as total losses for any given flood event.

Bruen and Yang (2006) have developed a model combination technique to improve the performance of hydraulic models for urban drainage systems using simple black-box models. This technique was applied to a storm water drainage system in a small urbanizing catchment using the HYDROWORKS modeling software package. Four black-box models were tested as an updating procedure to improve on the output of the hydraulic model for real-time forecasting. The study emphasized that the model was useful for small urban catchments and/or for catchments with steep slopes and with short catchment response times.

Guo (2006) has presented a theoretical derivation of a dimensionless unit hydrograph using the kinematic wave approach. The dimensionless kinematic wave unit hydrograph (KWUH) was normalized by the parameters associated with the equilibrium condition and generated according to the selected rainfall duration. For comparison, a KWUH whose

rainfall duration is equal to the time of equilibrium produced good agreement with the Soil Conservation Service dimensionless unit hydrograph (SCSUH). The predicted 100-year peak flow rates from five hypothetical rectangular watersheds were compared with the SCSUH method and the Colorado Unit Hydrograph Procedures (CUHP). In general, the KWUH produced good agreement with the CUHP when the catchment has an area between 60 and 120 acres. Based on the study of hypothetical rectangular watersheds, it was recommended that the KWUH be applicable to urban catchments with a drainage area of up to 120 acres.

Quader and Guo (2006) have used the recently developed analytical probabilistic approach for estimation of peak discharge rates in a practical design case. The results were compared with those from the commonly used design storm approach. Differences in meteorological data analysis and representation of rainfall input, sub-catchment aggregation, and the treatment of the catchment time of concentration between the two approaches were identified as the three main causes contributing to the discrepancy in peak discharge estimates.

Sreeja and Gupta (2006) have developed a dynamic numerical model for modeling the transient flows in the urban drainage based on transfer function approach. It was opined that such a model can be used to determine the suitable flood control strategy without conducting an in-depth survey of the urban drainage systems. The efficiency of the model has been demonstrated by applying it to a representative catchment in Mumbai, India. The study indicated that for conventional finite difference approach, the simulation time is more. However, the use of transfer function approach reduced the simulation time drastically, which is desirable for real time control of urban drainage systems. However, a need for further extensive experimentation and in-situ studies is felt to ascertain its effectiveness in real time applications.

2.2.2 Role of imperviousness on urban flooding

Imperviousness is the indicator of land development on the landscape. It consists of two components: the rooftops under which we live, work and shop and the transport facilities (roads, driveways and parking lots) that we use to move from one location to other. Determination of imperviousness is important for urban water quantity assessment. Following few studies are presented to focus on various methodologies adopted for determination of imperviousness.

Alley and Veenhuis (1983) used aerial photographs along with field survey to find out a relationship between total impervious area (TIA) and effective impervious area (EIA) in

Denver metropolitan, United States. They suggested that since TIA is considerably higher than EIA, overestimation in simulated runoff may occur if TIA is used in runoff models in place of EIA which may be misleading in ungauged watersheds.

Boyd et al. (1993) evaluated rainfall and runoff depths for 26 urban watersheds from 12 countries. Out of 26 watersheds, 17 watersheds found to show impervious surfaces as the prime source of runoff. Further rainfall depths and corresponding runoff depths for all the watersheds were plotted and effective impervious fraction was derived from the same. The impervious fraction thus derived matched well with the TIA and EIA estimated from the basin map.

Boyd et al. (1994) analyzed rainfall and runoff depths obtained for 47 storms in three urban basins in Canberra, Australia to detect the relative contribution of pervious and impervious surfaces to total runoff. The total rainfall depths are plotted against the runoff depths and the data points were fitted by least square regression to obtain a straight line. The slope of the line is determined as the effective impervious area and the intercept on the rainfall axis is the initial loss before the runoff occurs. The effective impervious area thus found was close to the mapped impervious area of the basin.

Sutherland (1995) suggested a set of empirical equations under different basin connectivity conditions for determining the effective impervious area (EIA). EIA has been related with a physical parameter of the basin named as mapped impervious area (MIA), that is easy to estimate. The equations were developed for different basin conditions like average connected basins, highly connected basins, totally connected basins, less disconnected basins and extremely disconnected basins.

Chabaeva et al. (2009) assessed the potential of six techniques for determination of impervious surface and compared the result with the impervious surface obtained from high resolution digital planimetric data. National Land Cover Data (NLCD) of the year 2001 and Connecticut's Changing Landscape (CCL) of the year 2002 have been used to estimate percentage imperviousness. It has been found that the imperviousness derived from population density and land cover based regression model gives highest accuracy.

Theobald et al. (2009) estimated impervious surface from the housing density data in United States. Regression tree method has been used to relate the estimated impervious surface with the imperviousness derived from National Land Cover Database (NLCD) of United States. Further the authors have identified the watersheds in US that will be under risk due to urbanization by the year 2030. It was observed that 3.6% watersheds of United States

was having impervious surface less than 5% in 2000 and it was predicted that the percentage of watersheds that will be having imperviousness less than 5% will be 8.5% by 2030.

Han and Burian (2009) suggested a fully automated two step method that employs GIS and remote sensing technologies to designate the impervious areas in the urban watershed as effective impervious area (EIA) or non-effective impervious area (NEIA). In first step, the multispectral imageries are classified into urban land covers to classify total impervious area (TIA). The second step applies a GIS code written in Visual Basic application (VBA) to the TIA data layer, DEM of the watershed and drainage network of the area to identify the EIA.

Ravagnani et al. (2009) in their study assessed the effect of error introduced in determination of imperviousness from satellite images on the determination of peak discharge. The drainage system connectivity has been ensured by conducting field survey. They have also investigated the effect of connectivity between the drainage network and the pervious and impervious surfaces on the peak discharges. The results obtained show that the satellite based image classification provides reliable estimation of impervious surface and the variation is about 8% from the impervious surface obtained by conducting field study. Also TIA if used in the hydrologic model found to have overestimated runoff by 30%.

2.2.3 Impact of imperviousness on urban flooding

The increase in impervious surfaces is a major controlling factor in watershed's hydrologic cycle. Hence to assess the impact of increased imperviousness on the watershed hydrology, a few studies are presented that exhibit the same on different hydrological processes.

Brun and Band (2000) assessed the effect of urbanization on watershed behavior. Hydrologic model HSPF along with ArcView GIS has been used for this purpose. It has been observed that increase in imperviousness decreases the base flow up to 20%. A threshold of percentage imperviousness of 20% has also been detected beyond which the runoff ratio has been found to change drastically.

Lee and Heaney (2003) performed hydrological and spatial analysis in a residential area in Miami to evaluate the long term impact of imperviousness on storm water systems. A linear rainfall-runoff model was applied to the hourly rainfall data for 52 years to predict the flow. It was observed that the EIA contributes 72% of total runoff volume during these 52 years. Further imperviousness was derived by applying five different methods. First two types are of imperviousness collected from literature and the TIA derived from GIS data. Third type of imperviousness is obtained from the isolated impervious areas referred as

indirectly connected impervious area, which was deducted from the TIA. The indirectly connected impervious area found from field visits were deducted from the third type of imperviousness to get the fourth type of imperviousness. From the fourth type of imperviousness, the roof tops that were found to be directly connected to the collection network were evaluated through field visits. It has been observed that the peak discharge produced due to these five types of imperviousness differs maximum by 265%.

Burns et al. (2005) evaluated the impact of impervious area on runoff processes. Precipitation, stream discharge and ground water levels in the wells have been measured to demonstrate the impact of urbanization. It has been observed that peak runoff increases and recession time decreases with increase in imperviousness. It was also found that the relationship between peak rainfall and peak runoff (as given by rational method to estimate peak discharge in urbanized watersheds) further strengthens with increase in percentage impervious area.

Pappas et al. (2008) simulated rainfall artificially in the laboratory and observed the impact of spatial distribution of impervious surfaces on runoff and sediment discharge. A series of sloped soil boxes were arranged in the laboratory representing either pervious land use (boxes containing soil) or impervious land use (boxes fitted with impervious cover to resemble asphalt or concrete surfaces). Rainfall is simulated artificially by using a nozzle rainfall simulator and runoff volume was determined by gravimetric method. It was observed that impervious surfaces at upslope are subjected to high erosion risk than their counterparts located at down slope.

Shuster et al. (2008) opined that different spatial distribution of impervious and pervious surfaces in the catchment affects the shape of the runoff hydrograph. Impervious and pervious surfaces are arranged in different manner in the laboratory to demonstrate its effect on runoff production mechanism. They have observed that increase in percentage imperviousness leads to reduction in the infiltration loss allowing the runoff to start quickly that further increases due to its connectivity.

Beighley et al. (2009) analyzed different methods that estimate the effect of imperviousness on simulated peak discharges. Imperviousness has been determined by two methods: by manually digitizing the aerial photograph and from interpretation of medium resolution satellite data. HEC-HMS has been used to assess the sensitivity of imperviousness in runoff modeling. The imperviousness determined by digitization was found to be more than that obtained from image classification. At the watershed scale, the effect of imperviousness determination on simulated peak discharge ranges from 16% for 2 year event

to 9% for 100 year event. Overall the two impervious surface estimation methods result in different peak discharges but neither method consistently results in discharges less than flood frequency based discharges.

Kauffman et al. (2009) evaluated the relationship between imperviousness and base flow in the stream for 19 watersheds near University of Delaware campus, United States. Impervious cover has been estimated by using GIS. Velocity in the stream and the cross sectional area of the stream has been measured and base flow in the stream was estimated by continuity equation. It was observed that increase in imperviousness decreases the base flow.

Shuster and Pappas (2011) used artificial rainfall in the laboratory to generate runoff for pervious and impervious surfaces of different connectivity conditions. Curve Number was estimated from measured rainfall and runoff data and used to predict the runoff by Storm Water Management Model (SWMM). The runoff response with these experimental curve numbers showed the result in good agreement with the observed one.

Giacomoni et al. (2012) opined that urbanization alters the natural hydrologic flow regime of receiving water bodies in a catchment. Hence peak flow increases significantly in an urban area and this increases the potential for urban flooding. In the study, it has been suggested that these hydrologic impacts of urbanization can be mitigated through best management practices (BMP) and low impact development (LID).

Barron et al. (2013) investigated the impact of increased urbanization on catchment water balance. A coupled surface water and ground water model MODHMS has been used for this purpose. It has been observed that a significant increase in total annual discharge occurred due to urbanization. Infiltration has been found to be reduced from 70% to 20% due to urbanization. Reduction in evaporation loss and infiltration has been found as the main cause for increase in runoff in urban areas.

2.3 Flood Management

Several studies were reported in this area during past years. The following section presents the details of studies related to flood management.

Bradley et al. (1996) have proposed a new approach for flood plain mapping using continuous simulation modeling. Generally, use of rainfall-runoff models in flood plain mapping has the assumptions that the flow is steady and secondly the design storm and the simulated peak stages have the same return period. In this proposed approach these assumptions are not necessary as frequency analysis has been done on water levels rather than the peak flow values. Hydraulic model has been coupled with a continuous simulation

hydrologic model and hence the river peak stages were estimated. A new statistical approach was then applied to these peak stages to estimate peak stage exceedance probabilities. Forty years of runoff data have been simulated using LANDS module of Hydrocomp Simulation Programme (HSP) and routed with a fully dynamic flood wave routing model to simulate the flow and stages. Then these simulated peak stages were compared with the reported high water marks. In this study flood frequency estimates were made by three approaches i.e. the design storm approach, conventional frequency analysis approach and peak-to-volume approach. The results were then used to estimate 100-yr flood. It was found that the estimated water levels for the present approach (peak-to-volume approach) gives the intermediate values between the other two approaches and it was opined that this method can be applied to the problems where flood plain storage and back water effects are important.

Guo (1999) suggested a volume based approach to fix the size of the storm water detention basins for small watersheds. He suggested that for preliminary design stage, sizing a small detention basin is a hydrologic problem rather than a hydraulic problem. Hence without knowing the detailed outlet hydraulics, estimation of storage volume can be addressed by volume based approach.

Olsen et al. (2000) have presented a dynamic model for floodplain management to better deal with the changing hydrologic, hydraulic and economic conditions like land use change, channel modifications, economic development, climate variability etc. The model has been formulated as a Markov decision process and linear programming technique has been used to solve the multi objective flood management problem. Developed dynamic model has been applied to the Chester Creek flood damage reduction plan, Pennsylvania. Discharge-frequency function has been developed from 65 years of annual maximum discharge data, stage-discharge function was generated using HEC-2 computer program and stage-damage relationship was developed by categorizing all the structures in flood plain and assessing average inundation - damage relationship for each category. The frequency - damage function was obtained from the above three relationships. If hydrological changes were considered, this case study no more gives the levee construction as the optimal policy rather it chooses the non-structural measures as the optimal policy.

Lund (2002) has proposed a two phase linear programming approach for developing floodplain management plans to minimize the sum of expected annual damages and costs for flood management. The constraints considered were flood damage calculation, conditional implementation of some options and interaction of implemented options. The two phase linear programming problem has been solved by using spreadsheet linear program solver.

This optimization approach was opined to be very useful for risk based flood and floodplain management problems. However some limitations were also reported which includes the assumption of implementation of ideally perfect emergency plans and additive nature of reductions in damage due to implementation of permanent and emergency options.

Dhar and Nandagri (2003) have analyzed the hydro meteorological aspects of floods in India. The study shows the major flooding phenomenon in India occurs in the states that are located in the Indo-Gangetic plains, north east India and in some of the rivers in central India. It has been opined that the unequal distribution of monsoon rainfall along with the antecedent moisture condition during the monsoon period has been the major cause of flood in Indian rivers. From the study, it has been put forward that the flood water in river Brahmaputra can be used effectively for power generation by storing it at the "Great Bend" of the Dihing River thereby reducing the impact of flood hazards in north east states of India.

Dutta et al. (2003) have introduced a mathematical model for flood loss estimation, which can be very useful in allocating resources for recovery after the disaster. This model has two components i.e. a distributed hydrologic model and a loss estimation model. In the hydrological model, the hydrologic processes like interception, evapotranspiration, river flow, overland flow, unsaturated zone flow, and saturated zone flow have been considered and their governing equations were solved using finite difference method to obtain flood inundation parameters like flood depth, duration, and velocity for each grid. The loss estimation model has been formulated as a grid based model with a similar grid network to that used in the first model. The probable flood damage has been estimated for each grid cell by using the inundation parameters obtained from the first model, with the help of stage-damage functions derived from the historical flood damage information.

Faisal et al. (2003) have developed a set of long term strategies for flood mitigation in Dhaka city which can be used as guidelines for flood management in other cities. As a part of the study the authors reviewed the documents of past flood events in the study area, evaluated the flood management practices followed, conducted field visits, talked with professionals and local people. From these observations, it has been concluded that the major causes of flooding in Dhaka city are mainly due to the failure of some of the structural measures taken earlier and the lack of coordination between the authorities responsible for flood protection and drainage. Hence a combination of structural and non-structural measures has been suggested for preventing flooding as a long term measure.

Koussis et al. (2003) have proposed a system for flood forecasting in an urban basin by making use of an integrated hydro-meteorological model. The rainfall has been predicted by a

chain of nested numerical weather prediction (NWP) models. Bologna Limited Area Model (BOLAM) has been used for local scale precipitation forecast which was initialized with the forecast of global scale numerical weather model aviation (AVN). The rainfall predicted by this model has been fed as input to the flow model. HYBNAT rainfall-runoff model has been implemented which employs curve number approach to predict the runoff. WASPLA hydraulic model has been implemented to calculate flood profiles by standard step method. The flood risk of Kifissos basin, Athens, was assessed for two flood events and it was observed that flow peaks have been underestimated and hydrographs were broader than the actual.

Mohapatra and Singh (2003) have presented various causes for flooding in India in different zones. It has been found that the flooding in India occurs mainly due to drainage congestion and bank erosion, as well as heavy rainfall. Flood problem has been described in Brahmaputra river basin, Ganga river basin, Central India river basin and North West river basin. Structural and Non-structural measures undertaken through some years has been discussed. It was also felt necessary that proper flood plain zoning, flood insurance scheme, flood accommodation in reservoirs, provision of data centers etc. should be made for better management of flood in future.

Abebe and Price (2005) developed a DSS for urban flood management. The purpose of this DSS was to manage the information obtained by telemetry, to feed the obtained data along with other collected data to a series of modeling tools, to forecast flooding conditions and to assist authorities in decision making process to manage the flood. Flood inundation depth and time of inundation has been used to identify the worst flood affected scenario and accordingly emergency management options have been proposed.

Li et al. (2006) have presented a web-based flood forecasting system (WFFS) which takes less time to forecast the flood than by the manual calculation by the hydrologists. The proposed WFFS has got five modules namely, real time rainfall data conversion, hydrologic forecasting by models, model calibration, precipitation forecasting, and flood analysis. It has been developed by using Java programming language. The web- based distributed system has got a multilayered architecture. In this architecture, different nodes like WFFS, FOS (flood operating system), and ISS (information services system) are there. Each node is composed of three tiers; web server (presentation tier), application server (application tier) and data base (data tier). Web server contains the components dealing with user interface; application server contains the components dealing with hydrologic forecasting and data tier deals with the data base. The developed WFFS has been applied to Shuangpai reservoir, China.

Xinanjiang model and Dahuofang model have been used for runoff prediction. The flood event occurred on August 30 of 1999 was selected to illustrate the application of WFFS. It was observed that, Xinanjiang model simulate the peak timing and peak flow well whereas Dahuofang model differed significantly in peak flow from the observed one.

Simonovic and Akter (2006) have proposed the methodology to be followed for participation of stake holders in floodplain management using fuzzy set theory and fuzzy logic. The floodplain management problems which are multi objective functions have been solved in two phases: firstly, the aggregation of the judgments per decision alternative and secondly, the ranking of the decision alternatives. Inputs from all stakeholders were collected and aggregated to find a representative value. The input may be in any form i.e. numerical, linguistic, or conditional input. The proposed methodology has been applied to floodplain management in Red River Basin. The inputs were processed through Fuzzy Expected Value (FEV). From the results, it has been found that there exists a good correlation between the numeric scale type and linguistic type of inputs. The conditional type results show consistently a slightly lower value.

Boni et al. (2007) have proposed a methodology for the estimation of flood discharge for un-gauged watersheds. Generally for un-gauged sites, as no discharge-time series data is available, the magnitude of flood discharges are estimated by either regional frequency analysis method or modeling rainfall-runoff processes. In this study, a regional scale analysis has been performed by index flood method. In this method, the regression parameters were estimated by using the growth curve, obtained by drawing the best fit curve to the plotted observed data for annual discharge maxima. These parameters which are obtained were applied to the ungauged sites having similar hydrologic condition. In this study, a semi-distributed hydrologic model called DRiFt (Discharge River Forecast) developed by F. Giannoni (2005) has been used for the estimation of effective runoff rate.

Friedel et al. (2008) have presented a new regionalization procedure to predict the flooding in ungauged coastal river basins of EI Salvador, Latin America. The flood prediction problem has been solved in two regions i.e. upstream mountains and downstream alluvial plains. From recurrent peak flow discharge data of gauged basins, model parameters (curve numbers) were determined. Those parameters were used in the models to estimate the peak flow limits in ungauged basins. Then this model is validated with the known events. The tributary basin parameters and recurrent hydrographs for upstream mountains were estimated. The governing equations (continuity and momentum equation) for unsteady, unconfined flow were solved to get the flood flow depths taking the minimum and maximum estimated peak

flow discharge hydrographs as boundary conditions. This method has been applied to four of the ungauged basins in EI Salvador and found that the observed and simulated peak flow tributary hydrographs matches well.

Price and Vojinovic (2008) introduced the digital city concept in urban flood disaster management planning. Disaster management activities have been grouped into three stages such as pre-disaster or preparation stage, during disaster or supportive phase and post disaster or restoration phase. It was suggested that urban hydro informatics is a valuable tool to effectively manage different activities in the context of urban flood. Also it was opined that GIS based maps showing the areas under flood risk are important information that has to be widely circulated to minimize the flood hazard.

Sahapure et al. (2011) in their study analyzed flooding condition in an urban catchment in Navi Mumbai, India. Their model simulates flood in the urban catchment by finite element method and uses GIS and Remote Sensing for data base management. Overland flow is modeled by kinematic wave method and channel flow has been modeled by diffusion wave method. Also they have employed the detention ponds at different locations of the city that are based on mass balance approach to reduce flooding.

2.4 Remote Sensing and GIS for Flood Management

Accurate delineation of flood extent and depths within the flood plain areas is essential for proper flood management. **S**patial analysis tools like GIS and RS can be effectively used for this purpose and hence to generate and evaluate hydraulic models for floodplain inundation (Wright et al. 2008). Since floodplain mapping is a multidimensional problem, a hydraulic simulation model can be integrated with some GIS technique to accurately delineate the floodplain. In recent years satellite data have been used to get vital information in terms of precipitation forecast, flood warning, inundation mapping, damage assessment and flood plain management towards flood management. Few studies that deal with the use of RS and GIS technique in flood management are given below:

Tao and Kouwen (1989) have examined the advantage of introducing land cover information derived from landsat data into a flood forecasting model. In this study the runoff for the same catchment has been calculated in two ways, i.e. with and without landsat data. Without landsat data the model was considered as a lumped model and with landsat data, the model was treated as a distributed model. The hourly flood forecasting model (SIMPLE) developed by Kouwen (1973) has been used for this purpose, which models the processes like interception, depression storage, infiltration, overland flow and channel flow. In the

model, the runoff has been calculated for each land cover class for each of the element in the catchment. The modeling parameters were identical throughout the watershed for a particular land cover class. The topographic and physiographic information required by the model were obtained from land cover and topographic maps, landsat imagery and other sources. The land cover of each area had been classified into six categories. SIMPLE was applied to a grid of 10 km x 10 km size, with and without landsat input. Four storm events were chosen for optimization of the model parameters like soil permeability, interflow coefficient, overland roughness and channel roughness and another set of events were used for validation of the model. The results were then compared in terms of volume of runoff, peak flow rate and time to peak. It was seen that the distributed model showed better agreement with the measured values.

Jayaraman et al. (1997) have evaluated the role of satellite remote sensing in natural disaster management like flood, drought etc. It has been suggested that disaster warning system (DWS), data collection platform (DCP), and emergency terminals etc. can be widely used to provide information and services towards flood forecast. It was also pointed out that satellite remote sensing and GIS technique can be integrated in Brahmaputra river basin to provide information on flooded area and damage to crop lands, roads and rail tracks etc. Also, it was mentioned that satellites provide precipitation forecast and warning, inundation mapping, damage assessment and flood plain management.

Crooks and Davies (2001) have investigated the effect of land use change on flood frequency through rainfall-runoff modeling. Land use changes over a period of 30 years have been incorporated into a semi-distributed continuous simulation rainfall-runoff model known as CLASSIC. The model incorporates soil water balance module, drainage module and channel routing module on a grid basis using rainfall and evapotranspiration as inputs. Land use classes were incorporated in soil water balance module allowing for different evapotranspiration rates and soil rooting depths for each one. The model was run for 30 years period from 1961 to 1990 using both land use scenarios and flood frequency analysis performed on the resulting daily flow series. A good agreement has been found between flood frequency curves from the observed and modeled continuous flow data using the two land use scenarios.

Jain et al. (2004) developed a GIS based distributed rainfall-runoff model to deal with the variable nature of the model parameters like slope, land use, soil and rainfall. In this model the catchment has been divided into a number of cells or grid areas. Topography, soil, land use etc. for each of the cell has been provided to the model through GIS analysis. Flow

direction from one cell to the neighboring cell was obtained by choosing the steepest route among the eight available routes by eight direction pour point algorithm suggested by Maidment (1983). Thus the drainage path from individual cell to the catchment outlet is obtained. The infiltration has been calculated by Phillip two term infiltration model by using physical properties of the cell. Overflow mechanism was taken care of by diffusion wave approximation of St. Venant's equation which was solved by finite volume method to obtain the depth of flow and runoff. The performance of the developed model has been tested by applying it on 11 sub catchments. Input data file for all the catchments were prepared by using GIS and RS analysis. A sensitivity analysis was also conducted to evaluate the effect of any change in the model parameters over the peak discharge, and total discharge. From the results it was observed that, peak runoff, time to peak and volume of runoff computed from the model for all the catchments were in well agreement with the corresponding observed values.

Han and Burian (2005) determined TIA from high resolution multi spectral data using maximum likelihood supervised classification and compared the result with the TIA value obtained by unsupervised classification. The study found that use of high resolution data produces accurate TIA value in the study area with small tree canopy coverage and less accurate TIA value in the study area having high tree canopy coverage.

Jain et al. (2005) mapped flood inundation area in Koa catchment in Bihar, India. IRS LISS III and Landsat TM satellite data just before and after the flood event along with the DEM of the study area have been used for this purpose. Originally supervised and unsupervised classification methods were followed to identify inundated area. But it did not yield good result hence density slicing approach, Tasseled Cap Transformation approach and water index (NDWI-Normalized Difference Water Index) approach have been applied. NDWI has been found to produce good result.

Jain et al. (2006) used NOAA-AVHRR (National Oceanographic Atmospheric Administrative – Advanced Very High Resolution Radiometer) data for flood inundation mapping in Assam in 2003. Three methods of water identification have been employed on the basis of spectral characteristics of land and water. After identification of water pixels the inundated area is estimated. It has been found that 25-30% of the area was flood affected during flood period.

Gall et al. (2007) have presented methods for delineating flood zones when detailed digital flood plain maps are not available. Two approaches for this purpose were assessed. One is by using USGS's stream flow model (SFM-3.3) and other is by using FEMA's natural

hazard loss estimation software (HAZUS-MH) which operates on ArcGIS 8.0. Both the models require a DEM as data input, with a resolution of 30 m. The lowest threshold for stream initiation in SFM 3.3 is a stream length of 15 km and in HAZUS-MH it is the drainage area of 1 sq. mile. In other words, a collection of cells that drain an area of 1 sq. mile or more is considered as a stream in HAZUS-MH and in SFM 3.3, a stream is only generated with at least 500 (15 km/ 30 m) raster cells. Thus, both the models have got the demerit of not identifying the small tributaries. However this drawback could be overcome by using higher resolution DEMs. These models have been applied to three counties of South Carolina and the model outputs have been compared with the corresponding flood data. The accuracy of output has been assessed by the use of error matrices, Kappa analysis and percentage overlap with the corresponding flood data. It was found that both the models did well in these case studies; more specifically HAZUS-MH performed best in coastal areas and no model was found to do well in steep topography.

Sanders (2007) has evaluated the online DEMs for using in flood inundation modeling if recent and accurate topographic data cannot be used due to lack of time or budget. DEMs based on LiDAR (Light Detection and Ranging), IfSAR (Interferometric Synthetic Aperature Radar), SRTM (shuttle radar topography mission) and NED (National elevation data) were evaluated on two test sites, Santa Clara River (SCR) in South California and Houstan, Texas. IfSAR- based DEMs have good horizontal resolution (1/9 s). So bridges and buildings were well resolved. However these are DSMs (digital surface model) and hence needs further processing to get bare earth elevation. DEMs based on 1/3 s and 1 s NED are truly DTMs (digital terrain model) and can map terrain with smoothness but, vertical accuracy was poor. In this case flood zones were predicted to be 25% smaller than predicted by other DEMs. DEMs based on 1 and 3 s SRTM may have data gaps caused due to radar shadow and predicted flood zone may contain non-physical pools. Among all these LiDAR-based DEMs found to be the best source for this purpose, due to its horizontal resolution and vertical accuracy.

Ramlal and Baban (2008) have used GIS to identify the areas which are prone to erosion and predict the sediment loading in a river, which was the major cause of flooding. In this study, more emphasis has been given for the processes such as, soil erosion, sediment transport and river morphological processes for the identification of the sub-basins and waterways that are mostly affected by erosion and siltation respectively for proposing suitable mitigation measures. The flood management plan for the case study of Caparo River Basin, West Indies included the soil conservation measures like reforestation in steep slopes,

construction of retention ponds, bypass channels, upgrading of channels to increase its capacity and overall the allowance of flood plain area.

Salimi et al. (2008) have integrated the hydraulic simulation model HEC-RAS and GIS to get the areal extent and depth of the spreading flood. It was assumed that the flow is steady over the considered river reach and the flow profile is GVF between the cross sections. Since steady flow was assumed, time dependent variables were not included in the energy equation and this equation was solved by standard step method. Annual peak flow data for 24 years have been taken and frequency analysis was conducted to get the peak flows at different return periods. These data have been used as the steady flow data for simulation. Normal depth for upstream and critical depth for downstream has been considered as boundary conditions. By simulating through HEC-RAS, water surface profiles for different return periods were obtained and this has been exported to GIS to get flood plain zonation map.

Wardah (2008) has developed an algorithm for rainfall estimation using Geostationary Meteorological Sattelite-5 (GMS-5) infrared images as input to flood forecasting and warning system. The images from GNS-5 used in this study are hourly images with a spatial resolution of 7 km x 5 km. The accurate geographic location of the image pixels closest to a particular rainfall station have been calculated from these images, by knowing its latitude and longitude point on earth. Using the pixel brightness value the temperature has also been estimated. Hourly temperature data (pixel cloud top brightness temp) has been then produced for each image frame. This temperature for a particular location is then compared with the radar rain rate at the same grid location. Now these combinations of temperature and rain rate were fed into ANN to get the estimated rainfall at any location and time.

Wright et al. (2008) have used the remotely sensed data for flood inundation modeling. In this study, four things, such as, topography, stage data for inflow and outflow boundary conditions, friction parameters for each model cell and a source of validation data have been used to construct a flood inundation model. The validation data set has been generated for river Severn, U. K. with the help of remote sensing. In this study, 1D model MIKE-11 and one 2D model LISFLOOD-FP have been applied to this data. From the study, it has been observed that the set up time for both the models were roughly same but the run time was 12 min for MIKE-11 and 36 hours for LISFLOOD-FP. It was also observed that the MIKE-11 under predicts the inundation extent whereas LISFLOOD-FP over predicts the inundation extent.

2.5 Flood Risk Analysis

Risk is generally defined as the probability of loss of life or property or belongings and risk management refers to actions taken to reduce the consequences. Advanced tools are now available to calculate the actual flood risk. A few studies dealing with risk management are presented as follows:

Arnell (1986) has proposed a less time-consuming approach to estimate average annual damage using a set of typical values for buildings in specific locations. The method requires the definition of a range of flood hazard factors (difference between the 10 year and 100 year flood levels) and associated depth-frequency relationships, and the computation for each flood hazard factor of the average annual damage for properties located with their lowest floors at specified frequency levels. A graph can then be prepared showing variations in damages with the flood hazard factor for structures located at different flood return period levels. Although damage estimates based on zonal annual damage may not be particularly accurate for individual properties, the method can be used to make initial estimates of flood damage in a floodplain, and can also be used as the basis for flood insurance premiums.

Karlsson and Haimes (1988) have performed a study on risk based analysis of extreme events. Mathematical expectation has traditionally been used in solving risk-based decision making problems. In this study, it is reported that, this concept is not appropriate for decision making that affects public policy because it conceals extremes by commensurating events of different magnitudes and probabilities of occurrence. If a decision maker instead uses an expected value function in addition to a conditional expectation that captures extreme and catastrophic events, he will gain a more meaningful and more encompassing representation of the trade-offs at hand. A theory relating conditional expectation to the statistics of extreme has been developed in this study. The theory highlights the importance of using both the conditional and the unconditional expected risk in decision making. This fact has previously been recognized in the partitioned multi-objective risk method (PMRM), a risk analysis methodology based on the concept of conditional expectation. The theory proposed in this study provides a formulation for analyzing the sensitivity of subjectively chosen parameters in the PMRM. The study emphasizes the importance of considering extreme events in parallel with the notion of expected risk.

Anselmo et al. (1996) have presented a technique for flood risk assessment of an area by using both hydrologic and hydraulic model. The hydrologic and cartographic data were collected for estimation of Probable Maximum Precipitation (PMP). This precipitation was converted to run-off by the application of rainfall-runoff model. This rainfall-runoff model

has been previously calibrated based on the data observed during the recent flood events. The runoff thus obtained acts as the input to the hydraulic model to simulate the flood plain inundation. The technique developed has been applied to a thermoelectric power plant in Italy to assess the flood risk. The ARNO rainfall-runoff model developed by Todini (1996) has been used for runoff simulation and a two dimensional hydraulic model has been used for simulation of flood inundation area. Flood inundation area simulated by this approach was found to match well with that of the measured experimentally.

Islam and Sado (2002) developed a methodology to prepare flood hazard map for Bangladesh. An interactive effect of flood frequency and flood depth were taken into account. Flood hazard ranks were estimated based on a weighted score for land cover, physiographical and geological data for each pixel of the land area of Bangladesh. It was opined that this type of maps will help the responsible authorities to better understand the flooding pattern in the floodplain.

Plate (2002) has reported that flood risk management takes place in three different levels such as, operational level, project planning level and project design level. The operational level includes the actions for risk management operation of the existing flood management system. It includes the process of risk analysis through preparing hazard maps, maintenance and improvement of the system by taking technical and non technical measures, preparedness by issuing early warning systems and disaster response by planning disaster relief, reconstruction and emergency help. When the existing system needs any modification or replacement by a new system, the project needs to be planned and designed properly which come in subsequent levels. In these levels, one has to choose the best among the possible alternatives which meet the objective of the project. It was concluded that, since natural environment is constantly undergoing change due to natural processes or human interference, this change should be taken into consideration while planning any flood management strategy.

vanManen and Brinkhuis (2005) have described how to calculate the flood risk in an area surrounded by protecting dykes (polders). An area at the centre of the Netherlands enclosed with two branches of river Rhine has been considered as the case study. The parts of the dyke were identified that will give rise to similar flooding condition if failure occurs anywhere within these parts. The probability of failure of each of the above parts was calculated. Out of these several options, one point of actual dyke failure has been selected and the amount of breach growth and incoming water through that breach were calculated. Flow and distribution of incoming water in the area was also calculated. The damage which was assumed as a

deterministic quantity has been estimated for each case. Then the product of probability and estimated damage over all dike ring parts were summed up to give the flood risk.

Buchele et al. (2006) have conducted a study on flood risk mapping to enhance the existing methods for hazard and risk assessment for extreme events. The study has been divided into three parts. In the first part, a regionalization approach for flood peak discharges was done, especially for large recurrence intervals for small ungauged catchments. Model comparisons show that more confidence in such flood estimates for ungauged areas. The hydraulic simulation in the second part is oriented towards hazard mapping and risk analyses covering the whole spectrum of relevant flood events. As the hydrodynamic simulation is directly coupled with a GIS, the results can be easily processed as local inundation depths for spatial risk analyses. For this, a new GIS-based software tool was developed, being presented in the third part, which enables estimations of the direct flood damage to single buildings or areas based on different established stage-damage functions. The methods and results from this study form the base for comprehensive risk analyses and flood management strategies.

Blade et al. (2009) developed a web based DSS for the flood risk assessment and management of emergency scenarios. The risk analysis provides data for the DSS in order to define risk zones and emergency scenarios. Risk criteria considered was associated either to human risk in terms of critical water levels, velocities or a combination of both the parameters and to water permanence. According to these criteria, a risk database is developed. The developed DSS was able to produce flood risk maps, maximum depth and velocity maps and time of flooding maps for the area of interest.

Dietrich et al. (2009) have conducted a study to assess the uncertainties in flood forecasts for decision making. According to their study, a probabilistic evaluation can be used to communicate forecast uncertainty to decision makers. An operational system for ensemble based flood forecasting has been presented, which combines forecasts from the European COSMO-LEPS, SRNWP-PEPS and COSMO-DE prediction systems. However these techniques, in particular the probabilistic assessment and the derivation of decision rules are still in their infancy. These aspects need further research.

Luino et al. (2009) have developed a model for flood damage estimation using GIS. The model simulates flood scenarios and evaluates expected economic losses from the impact of floodwaters on exposed elements, through the application of a computational model developed using GIS. The main objective of this study was to devise a method that could enable real time assessment of potential economic direct loss due to a natural process. The method requires a thorough knowledge of the local area coupled with descriptions of some

physical aspects of natural events. When a catastrophic natural event of a given intensity affects a particular area, the value of economic losses connected to direct damages to goods depends on the number and economic value of the units of each element in the area and on the degree of damage to the exposed units, commonly defined as vulnerability, varying from 0 for undamaged to 1 for completely destroyed. The economic worth of loss has been defined as the sum of the product of unit value, number of units of exposed element and damage degree.

Pingel and Watkins (2010) have carried out a study on multiple flood sources expected annual damage computations. From this study, it has been observed that for flood damage reduction analysis, the standard for measuring risk is expected annual damage (EAD). This index represents a long-term average annual flood damage for a given structure or area. This index has been computed by integrating a probability-damage function. In practice, the required function has been developed by generating a water level (stage) - probability function and an elevation-damage relationship. The analysis becomes complex when the stage-probability function is dependent upon multiple flooding sources.

Gain and Haque (2011) assessed the flood risk of eastern part of Dhaka city. In their study, the flood inundation map has been produced using geo-informatics tools. The depth-duration-damage function has been used to produce vulnerability map. The expected damage map is generated and is classified into several classes where each class represents risk of study area.

Nieto et al. (2012) constructed a simple water balance model which is based on GIS technology for urban surfaces. Locations at risk of surface water flooding are identified and the flood management opportunities were explored. The pieces of land available for redevelopment within the city area are given emphasis and it has been suggested that redevelopment should take place in a way, which maximizes the opportunities for flood risk reduction.

Sikorska et al. (2012) have performed a Bayesian uncertainty assessment of flood predictions in ungauged urban basins for conceptual rainfall-runoff models. Urbanization and the resulting land-use change strongly affect the water cycle and runoff-processes in watersheds. Unfortunately, small urban watersheds, which are most affected by urban sprawl, are mostly ungauged. This makes it intrinsically difficult to assess the consequences of urbanization. In this study, the uncertainty of flood predictions in ungauged urban basins from structurally uncertain rainfall-runoff models has been investigated. In addition, they proposed a concise procedure to derive prior parameter distributions from base data and

successfully apply the methodology to an urban catchment in Warsaw, Poland. Based on the results, it was demonstrated that the autoregressive error model greatly helps to meet the statistical assumptions and to compute reliable prediction intervals. In addition, the analysis suggests that imprecise rainfall information and model structure deficits contribute mostly to the total prediction uncertainty. In the future, flood predictions in ungauged basins will become more important due to ongoing urbanization as well as anthropogenic and climatic changes. Thus, providing reliable measures of uncertainty is crucial to support decision making.

2.6 Critical Appraisal of Reviewed Literature

The reviewed literature highlights procedures for determination of imperviousness, which is an important input for urban flood modeling. The importance of estimating representative imperviousness for an urban catchment precisely is asserted by researchers. However, there are only a few studies that investigate the sensitivity of imperviousness on urban runoff results. Even though it is known that a high value of imperviousness would result in high runoff, its quantification is not dealt in detail for urban catchments.

Space technology outputs in terms of RS and GIS are potential tools for estimating the imperviousness. Runoff co-efficient (Jackson et al., 1977), Curve Number (Ragan and Jackson 1980; Alexander and Rao 1985), rainfall excess estimation (Tao and Kouwen 1989), and imperviousness estimation (Alley and Veenhuis 1983; Sutherland 1995; Han and Burian 2009) can be obtained from the change in land use data. A number of studies have reported the determination of TIA, but a few of them distinguished between TIA and EIA by ensuring its hydraulic connectivity (Lee and Heaney 2003; Ravagnani et al. 2009). Since TIA is likely to overestimate runoff (Alley and Veenhuis 1983), it is desirable that EIA should be estimated for flood management studies, which require accurate prediction of runoff. Distinction between TIA and EIA cannot be ascertained from remote sensing data alone, field visits need to be conducted to ensure the connectivity between impervious surfaces and sewer network, which is not always feasible (Lee and Heaney 2003; Ravagnani et al. 2009). Hence an integrated approach between the remote sensing data and digital format of the drainage network is essential to ensure the connectivity of the impervious surface with the collection network.

The imperviousness, which is a critical parameter for urban flood modeling is highly site specific and difficult to measure directly. Hence it is not transferable to other cities having heterogeneous urban sprawl characteristics. From the reviewed literature it has been found

that not many studies have been conducted pertaining to the development of a relationship between TIA and EIA. This necessitates the development of a unique relationship between the critical parameter for urban flooding (EIA) and other land use types (TIA), which is easily obtained. It was noted that most of the reviewed literature deals with TIA, even though EIA is the vital parameter for runoff prediction in the catchment. However direct determination of EIA is difficult since it requires the knowledge about the connectivity of the drainage network with the impervious surface. In a large area where assessment of the drainage network connectivity is tedious and time consuming, an indirect determination of EIA can be done to estimate the runoff. Sutherland (1995) and Alley and Veenhuis (1983) equations can be used to estimate the EIA for different type of basin conditions. It may be noted that for Indian catchments, there are no such equations reported in the literature correlating TIA to EIA and the applicability of existing equations are not evaluated. Such studies are important for estimating the increase in EIA with urbanization, which becomes a mandatory input for surface water management planning process.

The reviewed literatures discuss about various measures to manage the flooding problem, the potential application of GIS and RS techniques for risk based flood modeling and development of flood management schemes. The flood damages are increasing over time and there are a lot of uncertainties involved in flood damage calculations. Owing to these uncertainties and lack of data in ungauged urban catchments (issue of most of the developing countries like India), flood risk studies are considered to be appropriate for appraising flood damages. A risk based approach will fine tune the decisions for managing the flood situation. Therefore, a lot of intense research is required for flood risk management in urban areas.

Following this, a comprehensive review of studies conducted by various researchers (Olsen et al. 2000; Salimi et al. 2008; Wright et al. 2008) for modeling different flood inundation conditions was done. Studies have highlighted the potential of integrating hydraulic simulation model with some GIS technique to accurately delineate the floodplain for flood inundation mapping (FIM). In recent years satellite data have been used to get vital information in terms of flood forecasting (Tao and Kouwen 1989; Jayaraman et al. 1997), inundation mapping (Jain et al. 2005; Jain et al. 2006), damage assessment (Luino et al. 2009) and flood plain management (Price and Vojinovic 2008). The flood risk zones are identified by estimating the flood depth and duration (Abebe and Price 2005; Gain and Haque 2011, 2012), which will help to prepare flood hazard map.

The flood inundation and flood hazard maps can be used by the municipal authorities for proposing suitable flood management schemes. Best Management Practice (BMP) has been

found to help urban cities to mitigate hydrologic impact of urbanization (Giacomoni et al. 2012). BMPs can be of structural type such as civil works in the flood plains, which includes construction of detention basins, drainage channels, channel improvement works etc., or non-structural type like flood forecasting and warning, flood plain zoning, flood proofing, and flood plain management. Detention ponds have been found to be effective in reducing the effect of urban flood (Guo 1999; Sahapure et al. 2011) and hence can be proposed as a suitable measure for flood management.

There are not many studies conducted for flood risk modeling in ungauged urban catchments. The existing studies are based on the in-depth surveys and real life data available for flow data and flood damages. However, in the case of developing countries like India, there is always a dearth of data and survey records especially for urban watersheds. This necessitates precise modeling of urban catchments with the available data. Also, the reviewed literature indicates that there is a lack of an integrated approach for modeling urban catchments that can be employed to generate output for the flood mitigation by using flood risk modeling.

2.7 Scope of the Work

The quantification of imperviousness and its impact on flood modeling and flood management are not very well understood for ungauged urban catchments in developing countries like India. Therefore, the objective of the present study is to identify precise method of imperviousness determination for urban catchment and study its role in risk based flood modeling. To address this objective, the present research has the following scope:

i. To utilize geo spatial techniques for determining the imperviousness due to urbanization.
ii. To demonstrate the criticalities involved in the imperviousness quantification and to identify a precise procedure for its determination for urban catchment.
iii. To evaluate indirect estimation of imperviousness for Indian catchments and, if required, propose a new estimation procedure.
iv. To determine the infiltration characteristics of the study area.
v. To carry out the hydrological and hydraulic flood modeling for the study area.
vi. To quantify the effect of imperviousness on urban runoff.
vii. To develop the flood inundation map of the study area for different rainfall intensities.
viii. To perform flood risk analysis to identify the potential flood risk zones of the study area.

ix. To demonstrate the use of existing detention pond as an alternative measure for flood management.

Chapter 3

Description of the Study Area

3.1 General

The important features of urban growth is development in infrastructure and population. Since the spatial concentration of people and property is high in urban areas, the damage potential of flood in cities is high and increasing with time. Hence there is the need to critically analyze the phenomenon of urban flooding and propose suitable measures for flood management in cities. Guwahati city is considered as one of the fast growing cities in India. It experiences unacceptable magnitude of flooding both with respect to space and time. Increased urbanization, prolonged and high intensity rainfall and encroachment in natural channels have resulted in severe urban flood in Guwahati. Water logging, ill functioning of drain and its inadequate capacity together with excessive rain water inundates vast areas of the city. During peak flood period, the high flood level of river Brahmaputra obstructs the normal discharge of flood water from Guwahati city. This along with the lack of a comprehensive storm water drainage system leads to artificial flooding and water logging in the Guwahati city mostly in monsoon season. Since this study deals with flood management in urban condition, Guwahati city is considered as the study area. This chapter gives details about the study area and various data collected for the study.

3.2 Study Area

Guwahati metro city is a gateway to northeast India and business hub promoting rapid urbanization since last decade. Guwahati city is a part of Kamrup District in Assam (India), and is situated between 26° 4' 45" and 26° 13' 25" North Latitude and between 91° 34' 25" and 91° 52' 00" East Longitude. Located on the bank of river Brahmaputra, it is the largest commercial, industrial and educational centre of the North East India.

As depicted in Fig. 3.1, Guwahati is located towards the South-Eastern side of Kamrup District. It is surrounded by Nalbari District in the North, Darrang and Marrigaon Districts in the East, Meghalaya State in the South and Goalpara and Barpeta Districts in the West. The city is situated on an undulating plane of varying altitude of 49.5 m to 55.5 m above mean sea level

(MSL). The southern and eastern parts of the city are surrounded by hillocks. Apart from the hilly tracts, swampy/marshy lands and water bodies cover a considerable portion of the city. The average annual rainfall for the study area is 1600 mm. Monsoon rainfall season starts from June and continues up to September. Most of the rainfall (about 900 mm) in this region occurs in the month of July and August. Only the urban Guwahati city (South Guwahati) with an area of 227.81 km^2 is considered to assess the impact of urbanization on flooding phenomenon. In this study, the impact of urbanization is quantified by observing the changes in built-up area.

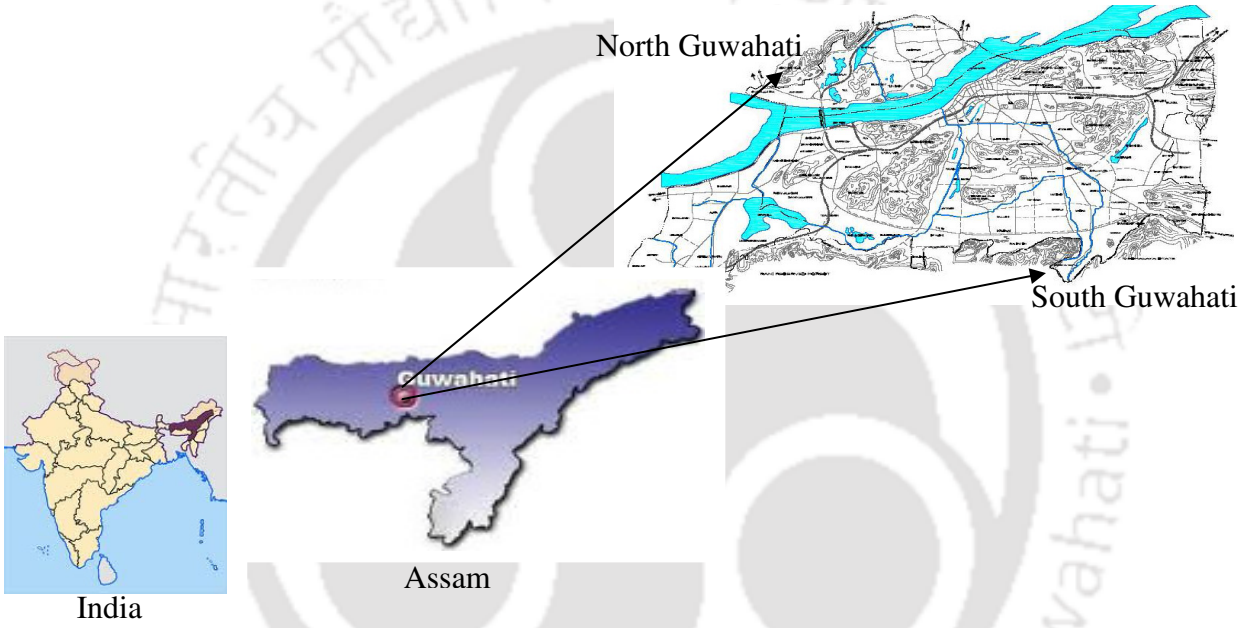

Fig. 3.1 Location of Guwahati city

3.3 Developing Database

All the available land use and hydrologic data have been collected from the respective government authorities. Besides the hydro-meteorological data, physical data related to the characteristics of watershed are also obtained. The list of the collected data is given as follows:

i. The base map of the Guwahati city has been collected from Guwahati Metropolitan Development Authority (GMDA). The existing building footprints, road network and the contours of 5 m interval were digitized from this collected base map.

ii. The map showing detailed drainage network for natural drainage system has been collected from Guwahati East Water Resources Division. The manmade drainage network and its cross sectional details have been collected from GMDA, Guwahati.

iii. A paper map showing the land use of Guwahati for the year 2002 has been collected from ASTEC. The land use in the catchment has been developed using the information available from Map of 2002. Different land use classes of Guwahati city are built up area, forest land, water body, agricultural land and waste land which has been again divided into subclasses of swampy/marshy land, scrub land and grass land.

iv. For preparing the flood inundation map of Guwahati city, a map has been collected from Guwahati Municipal Corporation (GMC) showing different wards of the study area.

v. The latest census data for the study area is for the year 2001. The ward wise population of the city corresponding to 2001 census has been collected from GMC for preparing the flood hazard ranking maps.

vi. Rainfall data

Daily rainfall data have been collected for the rain gauge station at Guwahati Airport from the period 1980 to 2012 from Regional Meteorological Centre, Guwahati. The mean, standard deviation and coefficient of variation are calculated for the monthly, seasonal and annual rainfall data series. From this, it has been found that mean rainfall in July is 328.3 mm which is the highest and contributes 18.9% of annual rainfall having mean 1735.8 mm. June and August rainfall are almost similar contributing about 16.5% and 15.64% of the annual rainfall respectively. September rainfall is lower than the previous month and contributes 11.2% of the annual rainfall. May rainfall contributes about 13.93% of annual rainfall. The variation of rainfall over Guwahati in different seasons is depicted in Fig. 3.2. Monsoon season rainfall from the month of June to September contributes 62% of the annual rainfall which has the highest contribution among the four seasons. Contribution of pre-monsoon (1^{st} Mar – 31^{st} May), post-monsoon (1^{st} Oct – 31^{st} Nov) and winter (1^{st} Dec – 28^{th} Feb) are 28.3%, 7.4% and 2.3% of the annual rainfall, respectively.

The mean total rainfall, mean number of rainy days, standard deviation, and coefficient of variation for each month from the period of 1980-2012 are shown in Table 3.1. The maximum mean number of rainy days and mean total rainfall is in the month of

July whereas December month has the minimum mean number of rainy days and minimum mean total rainfall. From the daily rainfall data, the day that shows the maximum depth of rainfall in a year is chosen and the corresponding rainfall event was collected. Accordingly three rainfall events of 13th October 1991, 2nd October 2006 and 26th July 2011 are collected for event wise rainfall-runoff analysis. Henceforth the rainfall event on 13th October 1991 will be referred as RE-1; the rainfall event on 2nd October 2006 will be referred as RE-2 and the rainfall event on 26th July 2011 will be referred as RE-3. The rainfall hyetographs for these events are given in Fig. 3.3.

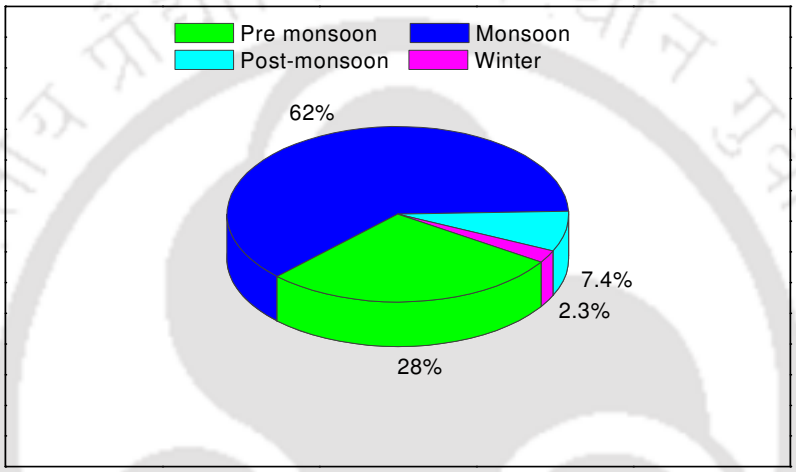

Fig. 3.2 Rainfall variation over Guwahati city in different seasons (i) pre monsoon (ii) monsoon (iii) post monsoon and (iv) winter

Table 3.1 Details of the statistical parameters of monthly rainfall in Guwahati city

Month	Mean total rainfall (mm)	Mean number of rainy days	Standard deviation	Coefficient of variation
January	12.0	1.13	15.45	129.15
February	24.2	2.33	21.66	89.40
March	58.3	4.67	42.99	73.71
April	178.4	10.17	106.31	59.60
May	241.9	13.37	130.1	53.76
June	286.7	14.33	120.13	41.90
July	328.3	15.83	113.40	34.55
August	271.5	13.07	139.42	51.34
September	193.7	9.8	86.89	44.86
October	112.5	4.67	91.34	81.23
November	16.3	0.97	22.13	136.08
December	6.1	0.6	8.71	143.23

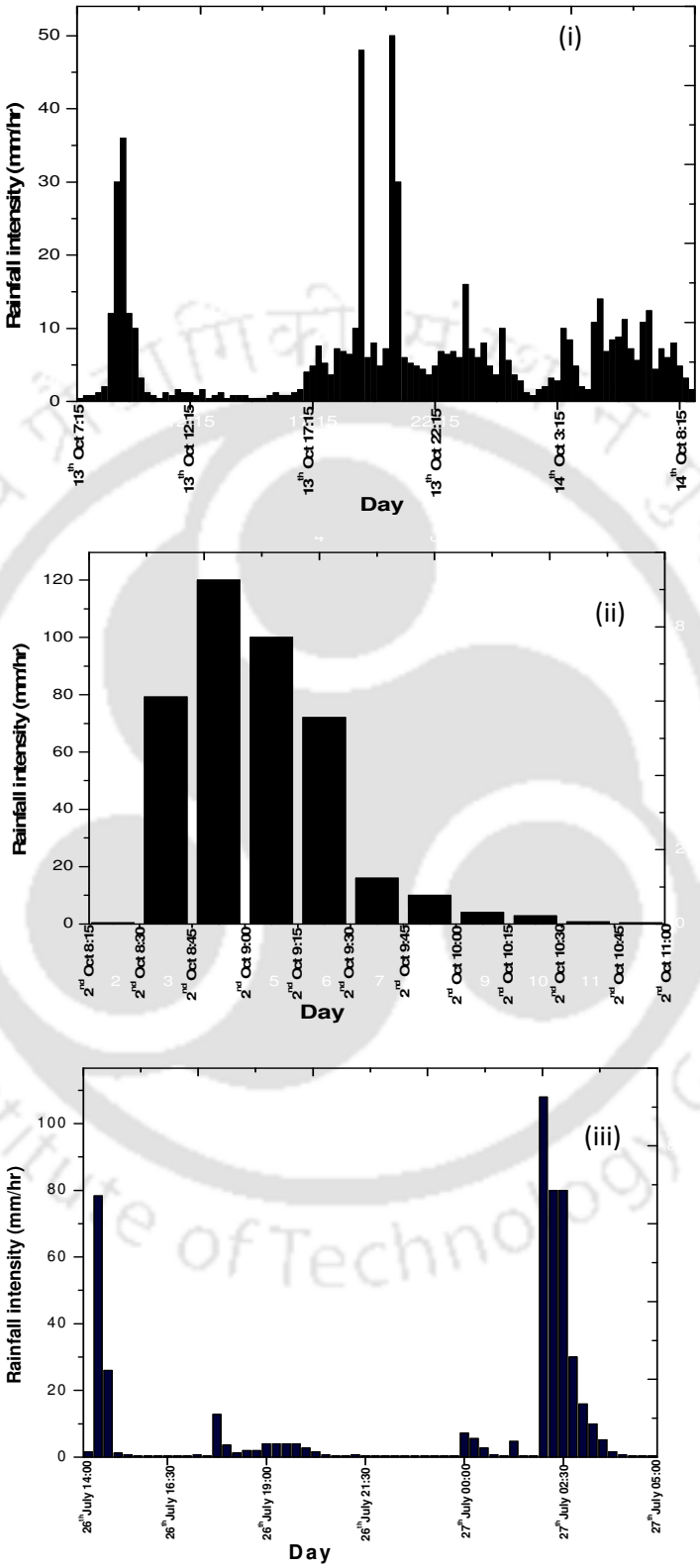

Fig. 3.3 Rainfall hyetographs for (i) RE-1 (ii) RE-2 and (iii) RE- 3

vii. Toposheet of Guwahati city has been collected from the Centre of Excellence (COE) project, Water Resources Engineering and Management, IIT Guwahati.

viii. Soil map of Guwahati city has been collected from Assam Science Technology and Environment Council (ASTEC).

ix. Satellite imageries listed in Table 3.2 have been collected for studying the land use changes of urban Guwahati city through different years. All the available bands of the images mentioned were either downloaded (Landsat ETM+, TM, MSS images) from GLCF (Global Land Cover Facility, USA) or procured from National Remote Sensing Centre (NRSC), India. Three LISS-3 images of 24 m spatial resolution corresponding to the years 1997, 2000 and 2004 and two LISS-4 images of spatial resolution of 5 m have been procured for the year 2006 and 2011 from NRSC.

Table 3.2 Satellite images for different years

Sl. No.	Date of Imagery	Spatial Resolution	Source of Collection
1	8th Feb 1980	60 m	Landsat MSS, GLCF
2	26th Nov 1991	30 m	Landsat TM, GLCF
3	5th March 1997	24 m	LISS-3, IRS1C
4	7th Jan 2000	24 m	LISS-3, IRS1D
5	17th Feb 2002	30 m	Landsat ETM+, GLCF
6	29th Dec 2004	24 m	LISS-3, IRSP6
7	April-2006	5 m	LISS-4, IRSP6
8	26th Oct 2006	30 m	Landsat ETM+, GLCF
9	Nov- 2011	5 m	LISS-4, Resourcesat-2

3.4 Delineation of Watersheds

For hydrologic study, the geographical area of urban Guwahati city is delineated into seven watersheds. The methodology adopted for watershed delineation in ArcGIS platform (Lyon 2010) is represented by flowchart depicted in Fig. 3.4. All the seven watersheds along with the stream network are shown in Fig. 3.5. The details of the watersheds are described as follows:

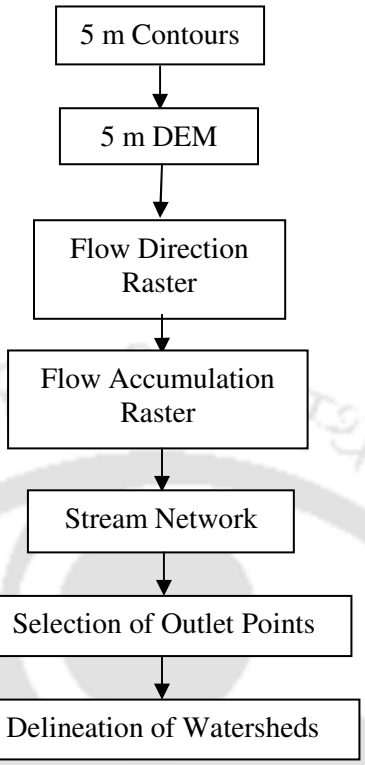

Fig. 3.4 Methodology adopted for watershed delineation

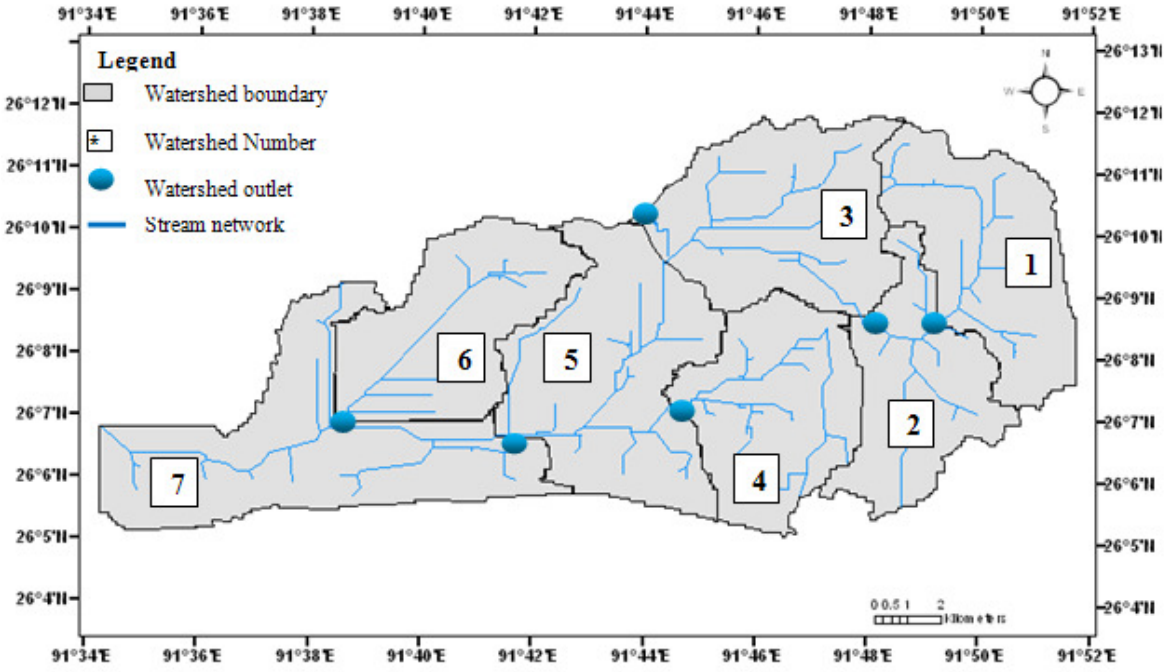

Fig. 3.5 Seven watersheds of Guwahati city with the stream network and the outlets

Watershed 1

Watershed 1 covers an area of 27.85 km^2 in the east of Guwahati as shown in Fig 3.6. The basin includes military area, refinery, townships of various industrial establishments and major portion of Narkalbari hill and Sunsili hill in the east. All the areas are sloping towards a wetland named Silsako Bil (lake) and at present this Bil receives all the runoff from watershed 1.

Watershed 2

Watershed 2 is the extended portion of the city having a catchment area of 24.47 km^2 as depicted in Fig 3.7. Major portion of the storm water in this basin is carried by river Bahini. Bahini starts from the hills in Meghalaya to the south of Guwahati and flows northwards. This river is a tributary of river Bharalu.

Fig. 3.6 Satellite imagery (5 m spatial resolution) for watershed 1

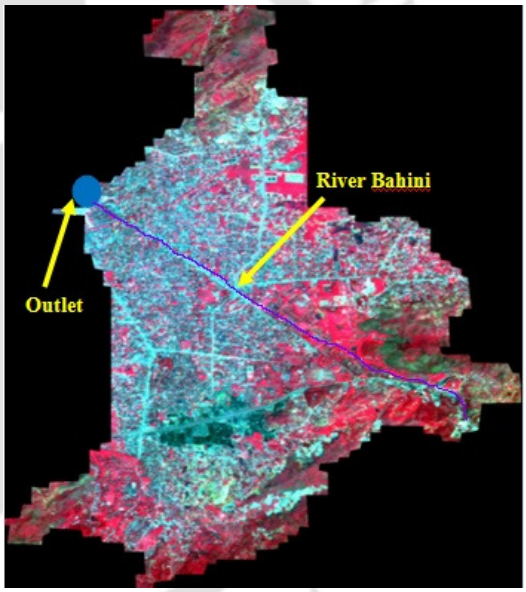

Fig. 3.7 Satellite imagery (5 m spatial resolution) for watershed 2

Watershed 3

This watershed is an important urban area of the entire Guwahati city with a catchment area of 28.3 km^2, as shown in Fig. 3.8. It includes main residential, commercial, institutional and business areas in Guwahati. The entire storm water for this basin is carried by river Bharalu which finally discharges to river Brahmaputra near Baralumukh, the outlet of watershed 3 as shown in Fig. 3.8. This is the most flood prone region of the study area and hence gets the top

priority in the drainage scheme. The proximate catchment of River Bharalu includes some discontinuous hills and is almost flat with several pockets of low-lying areas. From the figure it can be noticed that a number of water bodies are present in this watershed. Some of the major wetlands or ponds are Dighalipukhuri, Borosola Bil and Ram Krishna (R K) Mission pond. Out of these three ponds, Borosola Bil and R K Mission pond are situated near the outlet of the watershed where as Dighali pukhuri is situated at a higher elevation.

Watershed 4

This basin constitutes the southern portion of the study area and has a catchment area of 28.03 km^2, as shown in Fig 3.9. The major portion of the storm water produced by this area is carried by river Basistha. Basistha river enters Guwahati from the southern side from Meghalaya. It flows northwards until it reaches near the Assam State Secretariat and then continues westwards and flows gradually downwards till it discharges to watershed 5 and finally into Dipor Bil, which is the largest lake in the study area through Pamohi nallah (stream) as shown in Fig. 3.10.

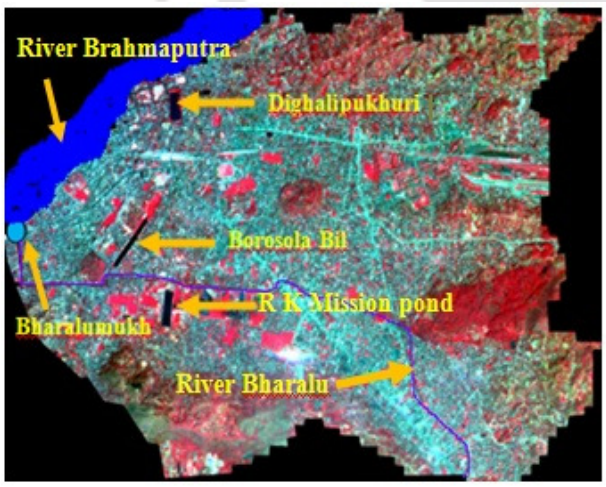

Fig. 3.8 Satellite imagery (5 m spatial resolution) for watershed 3

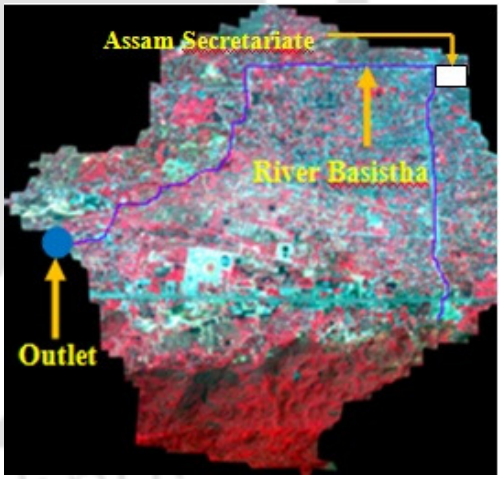

Fig. 3.9 Satellite imagery (5 m spatial resolution) for watershed 4

Watershed 5

Watershed 5 is having a catchment area of 37.4 km^2 which is mostly spread around the river Morabharalu, as shown in Fig 3.10. Morabharalu starts from the river Bharalu and moves southwards into Guwahati. Morabharalu flows southwards till it discharges to Dipor Bil.

Watershed 6 and 7

As shown in Figs. 3.11 and 3.12, watershed 6 and 7 are located at the southern most part of the Guwahati Metropolitan Area with an area of 27.7 and 35.35 km^2, respectively. Dipor Bil, which is the largest lake of the city, connects these two basins. Major portion of these watersheds are swampy/marshy lands or agricultural lands. Some hilly portions are also found to be present in watershed 6. The airport of Guwahati (LGB international airport) is located in watershed 7.

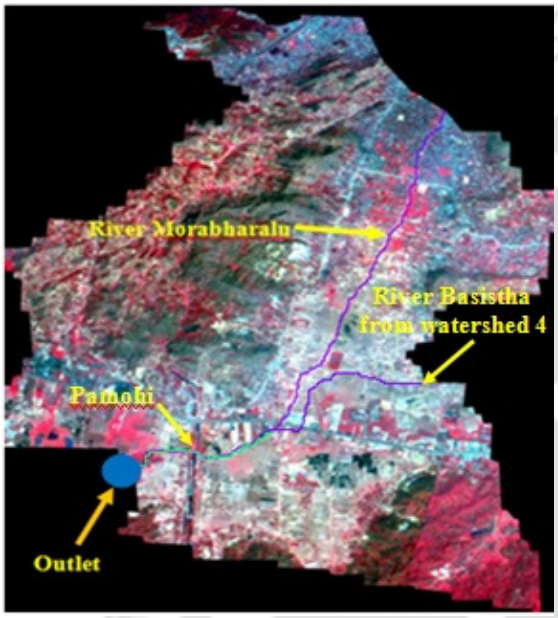

Fig. 3.10 Satellite imagery (5 m spatial resolution) for watershed 5

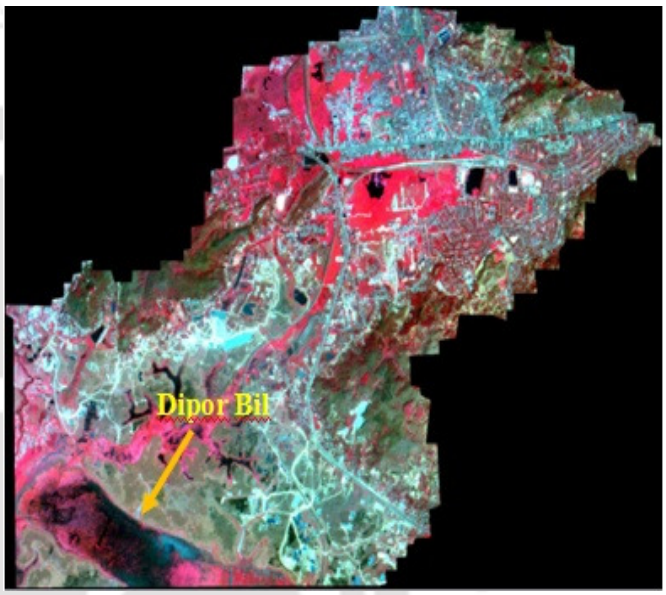

Fig. 3.11 Satellite imagery (5 m spatial resolution) for watershed 6

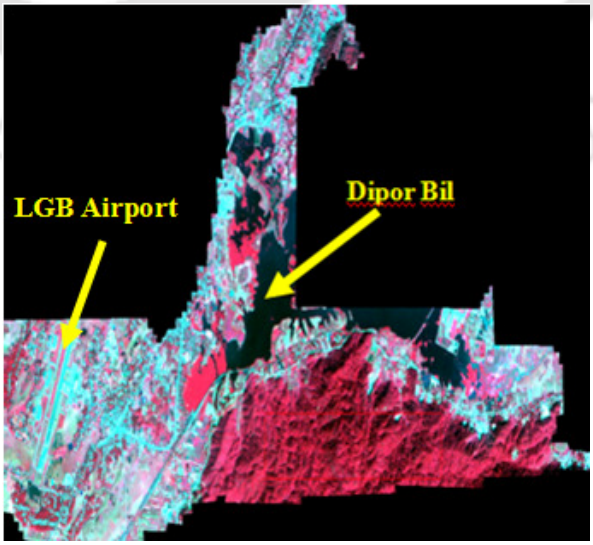

Fig. 3.12 Satellite imagery (5 m spatial resolution) for watershed 7

3.5 Delineation of Watersheds into Sub watersheds

For predicting runoff, it is generally necessary to divide the watersheds into sub watersheds with uniform characteristics. Runoff parameters vary among sub watersheds but assumed to be homogeneous within them. Thus the delineated watersheds in section 3.4 were again sub divided into 87 different sub watersheds as given in Table 3.3 and shown in Fig 3.13. The physical characteristics of the sub watersheds are reported in Table 3.4.

Table 3.3 Watershed division into sub watersheds

Watershed Number	Number of sub watersheds
1	22
2	14
3	14
4	14
5	10
6	5
7	8
Total	**87**

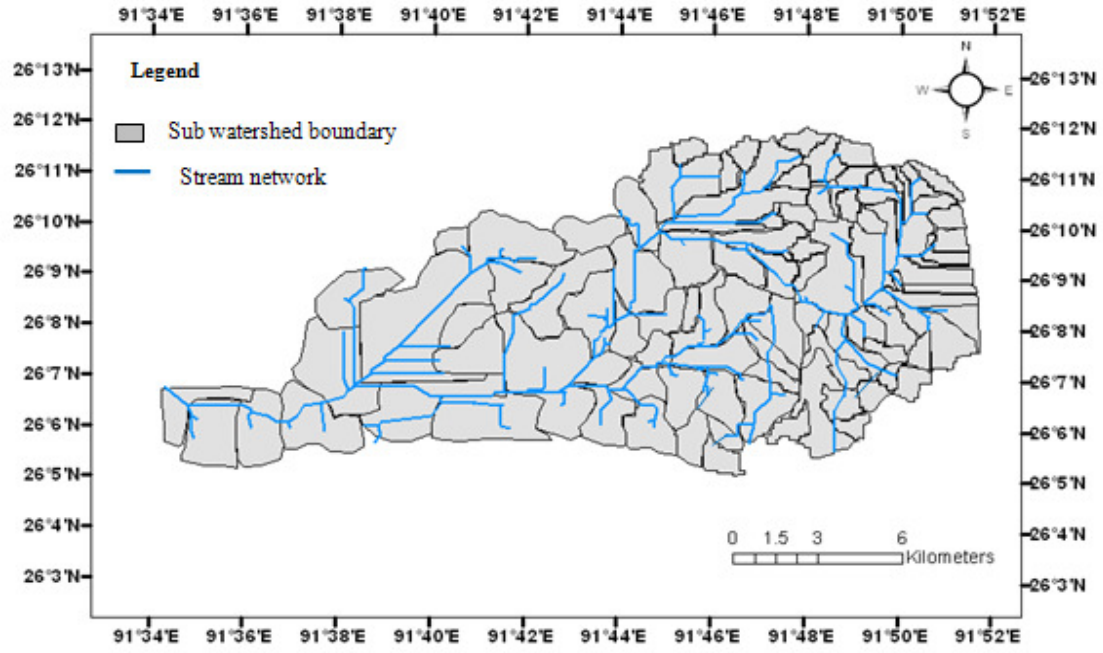

Fig. 3.13 Seven watersheds subdivided into 87 sub watersheds

Table 3.4 Physical characteristics of the sub watersheds

Watershed No.	Sub watershed No.	Sub watershed property		
		Area (km^2)	Width (m)	Slope (%)
1	1	1.01	733	5.0
	2	1.6	910	5.1
	3	0.95	698	5.5
	4	0.68	278	4.1
	5	0.74	580	7.4
	6	0.7	592	4.2
	7	0.33	274	9.5
	8	0.68	498	6.7
	9	1.14	498	4.9
	10	0.92	530	0.18
	11	0.89	603	10.3
	12	0.78	402	2.4
	13	0.97	727	0.7
	14	0.72	415	0.3
	15	2.99	448	2.0
	16	0.93	277	0.24
	17	0.74	506	4.09
	18	1.38	582	1.49
	19	2.95	933	3.9
	20	1.5	422	0.2
	21	2.73	960	0.28
	22	2.52	500	1.9
2	1	1.19	947	7.9
	2	0.6	652	6.5
	3	0.95	826	5.2
	4	0.78	684	3.5
	5	1.2	589	4.8
	6	1.4	917	3.9
	7	0.86	503	4.8
	8	1.42	761	2.5
	9	1.58	953	0.48
	10	2.12	791	1.75
	11	2.05	829	1.9
	12	4.12	1044	1.6
	13	1.2	650	0.16
	14	5.0	1455	2.8

Table 3.4 Physical characteristics of the sub watersheds (Contd..)

Watershed No.	Sub watershed No.	Sub watershed property		
		Area (km^2)	Width (m)	Slope (%)
3	1	4.9	1736	2.8
	2	0.83	762	4.0
	3	0.78	780	10.8
	4	0.88	663	11.0
	5	1.04	813	4.7
	6	0.85	508	1.79
	7	0.88	604	4.4
	8	0.6	359	1.49
	9	7.27	1261	1.2
	10	3.29	1328	4.0
	11	0.71	467	5.3
	12	0.79	502	5.8
	13	1.7	684	2.2
	14	3.78	1093	3.3
4	1	1.4	954	4.1
	2	2.81	755	2.8
	3	0.84	779	4.4
	4	1.78	739	0.2
	5	1.58	621	0.2
	6	2.56	943	3.6
	7	2.98	992	0.1
	8	1.28	590	0.3
	9	3.54	1419	1.9
	10	1.23	674	4.3
	11	1.01	553	5.7
	12	1.37	703	2.2
	13	2.86	1070	1.8
	14	2.79	1247	0.4
5	1	2.43	932	4.2
	2	4.1	1352	4.2
	3	2.25	913	2.8
	4	4.53	1167	5.1
	5	3.68	1119	7.0
	6	2.07	777	1.6
	7	1.56	848	0.3
	8	2.82	1190	2.5
	9	2.54	1131	6.7
	10	11.42	2654	3.5
	5	18.73	1972	1.6

Table 3.4 Physical characteristics of the sub watersheds (Contd..)

Watershed No.	Sub watershed No.	Sub watershed property		
		Area (km^2)	Width (m)	Slope (%)
6	1	1.0	751	0
	2	2.97	1311	4
	3	2.86	1265	5
	4	2.14	866	7
	5	18.73	1972	1.6
7	1	5.6	1315	0.09
	2	5.12	1547	0.12
	3	3.02	1252	0
	4	3.82	1470	0.03
	5	3.39	1690	0.05
	6	5.05	2241	6.7
	7	5.32	2128	0
	8	4.03	1642	3.7

Chapter 4

Determination of Imperviousness of the Study Area

4.1 General

Monitoring of urbanization and its impact on hydrological processes in a watershed is an important process in urban planning. One of the impacts of urbanization is the increase in built-up area due to which impervious surface increases. Increased imperviousness leads to high runoff in a short interval of time during precipitation as compared to rural areas. This indicates that quantification of land use in terms of imperviousness becomes mandatory for studying hydrological process in urban area. Satellite remote sensing has long been an important tool for urban land use analysis. Recently due to availability of cost effective high resolution satellite images, the focus on urban remote sensing has shifted more towards the use of digital images than the aerial photographs. The advantage of having digital images is that it can be processed by computer. A variety of commercial packages are available in the market for digital image processing. Out of these, ENVI (Environment for Visualizing Images) has the capability to perform numerous image analysis techniques, including multispectral classification, various types of spatial filtering, image registration and image statistics. Hence in the present study ENVI – 4.6 software has been used for the visualization, analysis and processing of all types of digital imageries. The data obtained from image processing are mapped to a geographic or spatial grid and analyzed to extract further information required for hydrologic modeling. Since surface water runoff is a function of many interrelated factors including climate, soil, land use and physiography of the basin, spatial database is critical component of hydrologic models. In the present study, ArcGIS 9.3.1 has been used to store, manipulate and manage different types of spatial data required for the study.

4.2 Overview of Image Analysis

The images collected for the study, listed in Table 3.2 (chapter 3), are in multi-spectral bands. A photographic product or a computer display generated from each spectral band gives different shades of black (grey) and white pictures. However any three bands can be combined to

give colour imagery. Human eyes can differentiate only about 16-20 grey levels in the black and white photograph while more than hundred colours can be distinguished in a colour photograph (Joseph 2003). Therefore coloured images are preferred over black and white for visual image interpretation. If the images are taken in blue (band 1), green (band 2) and red (band 3) bands, they can be combined to give natural colour called True Colour Composite (TCC) in which vegetation appears to be green. In the case of vegetation, maximum reflectance takes place in the near-Infra Red (NIR) region, i.e. in band 4 or between wavelength of (0.76 to 0.9) µm. To take advantage of this, remote sensing data usually combines green, red and near-IR bands representing blue, green and red bands respectively for image formation. Thus the representative colour is not the actual colour rather is a false colour and hence known as False Colour Composite (FCC) in remote sensing. Hence in FCC, the vegetation appears red. As an initial step in image analysis, False Colour Composites (FCC) of all the images was developed by using image processing software ENVI. The FCC images were then classified into seven different classes by supervised classification to obtain the classified images, which is explained in the following section.

4.3 Classification Process

Objects of similar nature have similar spectral properties. Hence the electromagnetic radiation reflected by objects of the same nature is similar and will have similar spectral signatures. Since the spectral signatures of the objects observed by satellites are converted into different colours in digital images, objects of the same kind will appear in closely related colours. Since the colours in a digital image are merely a conventional transposition of numerical values, it is possible to exploit the computer's computational power to classify the pixels by their numerical values. This is the basic principle of image classification. Thus the process of classification involves the conversion of satellite derived spectral data i.e. digital number (DN) values from the imagery into different land covers (Gupta 2003) of interest.

Classification may be supervised or unsupervised. In unsupervised classification, the classes are grouped by the computer on the basis of DN values and are separated based on certain algorithms. In supervised classification, the analyst supervises the process of classification by locating representative samples known as training areas prior to the classification process (Han and Burian 2009). Some classification algorithm is then applied to classify the image resulting in

the classified images. In the present study Supervised Maximum Likelihood classifier algorithm has been applied as it gives the highest overall accuracy as compared to other classification schemes (Sharif et al. 2010).

4.3.1 Supervised classification

Supervised classification procedures are the analytical tools most often used for quantitative information extraction in remote sensing data. Many procedures or algorithms are available (parallelepiped classifier, minimum distance classifier, maximum likelihood classifier etc.) for this purpose to classify the pixels in an image. Irrespective of the algorithm chosen, the steps generally followed (Richards 1999) for supervised classification is as follows:

i. To decide different classes into which the image has to be classified.
ii. To choose the sample pixels (training data) in the image to represent each of the above desired class well.
iii. To estimate the parameters of the particular classifier algorithm from the training data. The set of parameters for a given class is called signature of that class and it should be unique.
iv. To apply the classifier algorithm using the training data.
v. To obtain the quantitative class summary.

Hence for application of supervised classification, a training data needs to be selected and from that signatures can be developed for each class. Signatures generated from the training data will be of a different form depending on the classifier to be used. For example, for parallelepiped classification the class signatures will be the upper and lower bounds of brightness in each spectral band, for minimum distance classification the signature will be the mean vector of the training data while for maximum likelihood classification both class mean vectors and covariance matrices constitute the signature. The number of pixels in each training class should be large enough to reliably estimate the statistical properties of the class. If there are ‘n’ number of bands used in the analysis there should be at least (n+1) pixels per each training class (Joseph 2003) and preferably it should be more than 10n (Swain and Davis 1978). Some studies (Richards 1999) suggest that the training area should be approximately 1% to 5% of the total area to be classified. Since the cost of classification in terms of computational time can be considerably reduced by using optimum number of bands, after training is complete, bands

(feature) selection can be carried out using the separability measures. In other words the separability of different training classes can also be checked for the bands used in the image analysis. It may be done by utilizing various separability indices such as divergence, transformed divergence, J-M distance etc.

Divergence is computed using Eq.4.1.

$$D_{ij} = \frac{1}{2}\,\mathrm{tr}\left((C_i - C_j)(C_i^{-1} - C_j^{-1})\right) + \frac{1}{2}\,\mathrm{tr}\left((C_i^{-1} - C_j^{-1})(\mu_i - \mu_j)(\mu_i - \mu_j)^T\right) \quad (4.1)$$

Transformed Divergence is determined based on Eq. 4.2 as,

$$TD_{ij} = 2000\left(1 - \exp\left(\frac{-D_{ij}}{8}\right)\right) \quad (4.2)$$

Jeffries-Matusita (J-M distance) is given as follows:

$$JM_{ij} = \sqrt{2(1 - e^{-\propto})} \quad (4.3)$$

$$\propto = \frac{1}{8}(\mu_i - \mu_j)^T\left(\frac{C_i + C_j}{2}\right)^{-1}(\mu_i - \mu_j) + \frac{1}{2}\ln\left(\frac{|(C_i + C_j)/2|}{\sqrt{|C_i| \times |C_j|}}\right) \quad (4.4)$$

where i and j are the two signatures (classes) compared; C_i and C_j are the covariance of classes i and j respectively; μ_i and μ_j are the mean of classes i and j respectively; T is the transposition function; and tr is the trace function of matrix (sum of main diagonal elements).

Training set separability is a statistical measure of distance between two signatures and can be calculated for any combination of bands, which are used in the classification. For distance evaluation, the spectral distance between the mean vectors of each pair of signatures is computed. If the spectral distance between two samples is not significant for any pair of bands, then they may not be distinct enough to produce a successful classification. The formulae used to

calculate divergence are related to the maximum likelihood decision rule. Therefore evaluating signature divergence helps predict the results of maximum likelihood classification. The separability is calculated by Eqs. 4.2 and 4.4 which take into account the mean and covariance of the signatures.

4.3.1.1 Maximum likelihood (MXL) classification

An important assumption in supervised classification is that each spectral class can be described by a probability distribution in multispectral space. This distribution describes the chance (probability) of finding a pixel at any location belonging to that class. Maximum likelihood classifier is based on the principle that a given pixel will be assigned to the class to which it has the maximum probability of belonging (Gupta 2003). Also it assumes that the statistics for each class in each band are normally distributed (Donnay et al. 2001) and calculates the probability that a given pixel belongs to a specific class using Eq. 4.5,

$$p(x) = \frac{1}{(2\pi)^{N/2}|C|^{1/2}} \exp\left\{-\frac{1}{2}(x-\mu)^{t}C^{-1}(x-\mu)\right\} \qquad (4.5)$$

where x is the vector location of the pixel in the N dimensional space; μ is the mean of the distribution; and C is the covariance. Thus the normal distribution is specified completely by its mean (μ) and the covariance (C). Hence the probabilities of the pixel under consideration for each class can be calculated. Then the pixel is assigned to that class which has got the highest probability (i. e., the maximum likelihood). A pixel close to the mean of a class will have highest probability for that class and as it moves away from the mean, the probability will decrease. Unless a probability threshold is selected, all pixels will be classified. If the highest probability is smaller than a threshold, the pixel remains unclassified.

4.4 Methodology Adopted for Image Analysis

The summary of methodology adopted in this study for analysis of IRS (NRSC) imageries can be explained with help of a flowchart depicted in Fig. 4.1. Similarly the methodology adopted for analysis of Landsat (GLCF) imageries is represented by Fig. 4.2. Since the image resolution here is low (24 m), the study area fits well in one scene unlike the LISS-4 imagery case where three scenes were required to be mosaicked to get the study area.

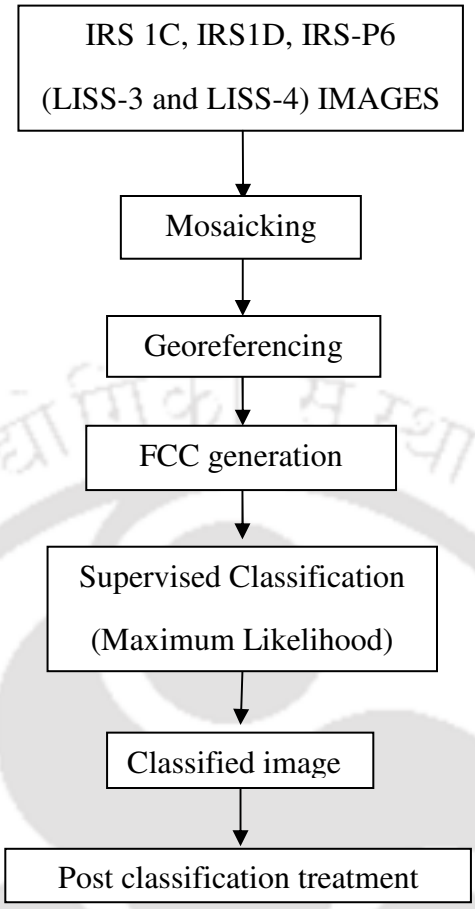

Fig. 4.1 Methodology adopted for analysis of IRS (NRSC) imageries

To access the impact of land use change on urbanization, supervised classification has been applied by following the step by step procedure mentioned in Fig. 4.1 and 4.2 for all the images. All the imageries in Table 3.2 have been classified into seven basic classes namely built-up area, water body, forest, scrub land, agricultural land, swampy/marshy land and grass land. For classification process, training areas having good separability values were selected from various locations of the image. In the present study, the image for the year 2002 was taken as the standard for analysis of the rest of the images. The classification result of 2002 image was validated from a classified paper map of the corresponding year. Training areas are then selected from this validated classified image and are referred for other images' classification process. The evaluation of the training areas suggest that the areas selected would be adequate for the classification process in this study. The selected training areas were then used to classify the imageries by MXL method. Suitable post classification treatment was then applied to get a

smooth classified image. Land use changes are then detected by comparing the classified images of different years through "change detection statistics".

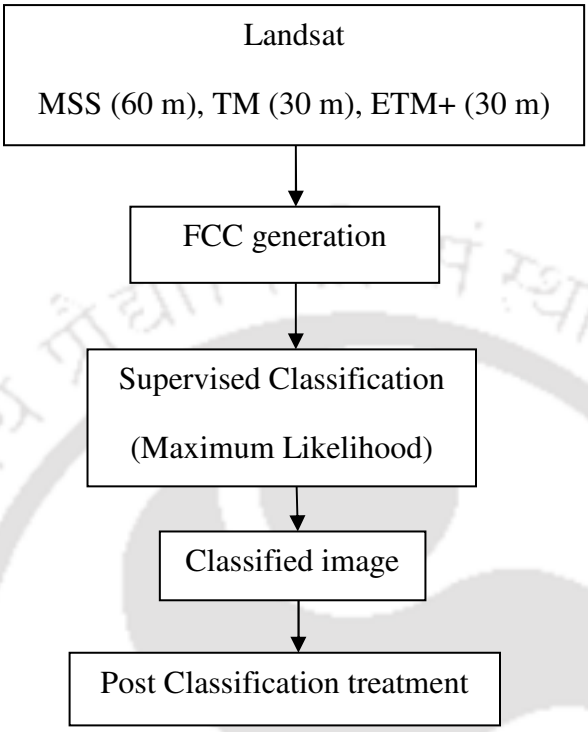

Fig. 4.2 Methodology adopted for analysis of Landsat (GLCF) imageries

4.5 Determination of Imperviousness

Information regarding imperviousness is essential for urban hydrology and watershed management. Imperviousness broadly refers to the built up area that obstructs the infiltration of water into the soil, which mainly includes the building rooftops and the transportation networks. Collectively they are called Total Impervious Area (TIA), and include both Effective Impervious Area (EIA) and Non Effective Impervious Area (NEIA) (Han and Burian 2009). The commonly used measure of imperviousness is TIA which is a measure of the area that prevents water infiltrating into the soil. EIA is that fraction of TIA that has a direct hydraulic connection to the downstream drainage. TIA tends to overestimate the runoff (Ravagnani et al. 2009) whereas EIA is found to give more accurate result (Lee and Heaney 2003). Hence, from hydrology prospective, EIA is considered as a better predictor of runoff. In the present study, efforts have been made to determine EIA from satellite imageries. For the determination of EIA, it is ideal to use fine resolution satellite imageries. However, for the study area this was not available for all

the years. For those years, coarse resolution imageries were used. The methodology adopted for the determination of TIA and EIA based on coarse and fine resolution imageries are discussed as follows.

.

4.5.1 Determination of TIA and EIA from coarse resolution imageries

Direct determination of EIA is difficult and needs high resolution satellite imageries. Therefore, indirect method of EIA determination is used when only coarse resolution imageries are available. Alley and Veenhuis (1983) suggested an empirical equation for the determination of EIA from TIA as represented by Eq. 4.6. This empirical equation has been developed for 19 basins in Denver city of Colorado, United States, out of which 16 basins are of single family residential type of size 4047 m^2 and less. From the collected building foot prints of the present study area, it is observed that maximum number of building size comes within this range. Keeping in view the socio-economic status of the study site it is assumed that it falls under the single residential type of land use. However, there are no studies in the literature that evaluate the efficiency of such empirical equation in Indian catchment. TIA (builtup area) has been determined by following the procedure shown in Fig. 4.1 and 4.2 and applying supervised maximum likelihood classification algorithm to the coarse resolution imageries. Further, Eq. 4.6 has been used for indirect estimation of EIA from the TIA of study area. Application of this empirical equation is an intermediate option when data for direct estimation of EIA is not available and hence runoff modeling becomes difficult.

$$EIA = 0.15\ TIA^{1.41} \tag{4.6}$$

Also Sutherland (1995) suggested a set of empirical equations under different basin connectivity conditions for determining EIA. Here TIA has been presented as Mapped Impervious Area (MIA). The general form of the equation is given by

$$EIA = A\ (TIA)^{B} \tag{4.7}$$

where A and B are unique combination of numbers such that, (i) if TIA = 1 then EIA = 0% and (ii) if TIA = 100 then EIA = 100%

The equations were developed for different basin conditions like average connected basins, highly connected basins, totally connected basins, less disconnected basins and extremely disconnected basins. From the collected drainage network of the study area it is ensured that the study area is poorly connected with the drainage network and can be assumed as extremely

disconnected basin. Based on this, following equation of Sutherland (1995) is used in the present study.

$$EIA = 0.01\ TIA^{2.0} \quad (4.8)$$

The suitability of Eqs. 4.6 and 4.8 for the study area has been evaluated by comparing indirectly estimated EIA with those determined directly from fine resolution imageries for the years 2006 and 2011.

4.5.2 Determination of TIA from fine resolution imagery

In this study a combination of remote sensing and GIS techniques has been used to estimate TIA from the high resolution imageries (Ravagnani et al. 2009). The study area was classified using remote sensing software ENVI into different urban land covers like builtup area, swampy/ marshy land, scrub land, grass land, agricultural land, forest and water body. These classes were again grouped into two: (a) impervious area consisting of building roof tops, asphalt/concrete pavements and (b) pervious area consisting of swampy/marshy land, scrub land, agricultural land, grass land, forest and water body. A suitable set of training areas for each class was then selected to carry out the MXL supervised classification. Training areas were selected at different locations of the image depending on the knowledge about the land use in image and the corresponding area in the field. A total of 102 regions were selected for training (impervious-74, pervious-28), which is about 2.3% of the study area. MXL algorithm allows a threshold value to be set for each of the classes. If the probability for any pixel falls below this threshold value, that pixel remains unclassified. Thus it puts a limit on the classification of pixels for each of the classes. Hence setting threshold value enables to obtain more reliable classifications. Therefore, it was decided to create three different classification methodologies (while maintaining the same number of classes and training regions) such as:

Cl 1: no threshold value;

Cl 2: threshold value of 0.5 for all classes;

Cl 3: different threshold values for each class (0.1 for pervious type and 0.5 for impervious type of land cover).

Cl 2 and Cl 3 (where threshold values were imposed) had some unclassified pixels (pixels whose probability was found to be less than the imposed threshold value). These unclassified pixels were proportionately distributed among all the classes.

Some cases of misclassifications, such as roof top and brick kilns were found in the study area due to classification of satellite imageries using RS only. Hence to obtain a more reliable classification process a set of GIS data set in terms of building footprints and road network (collected from Guwahati Metropolitan Development Authority) was deployed in the classification process. An effort has been made to obtain a modified classification over Cl 1, Cl 2 and Cl 3. The polygons of buildings and roads were rasterised (Endreny and Thomas 2009) using the same georeferencing and the same pixel size of 5 m as in the satellite classifications and were overlaid on Cl 1, Cl 2 and Cl 3 to get the classifications Cl 4, Cl 5 and Cl 6.

Thus

Cl 4: modified Cl 1 incorporating buildings and road pixels derived from GIS data.

Cl 5: modified Cl 2 incorporating buildings and road pixels derived from GIS data.

Cl 6: modified Cl 3 incorporating buildings and road pixels derived from GIS data.

In Cl 5 and Cl 6, since the GIS data have been used for rooftop and asphalt/concrete (impervious) classes, the unclassified pixels were proportionately distributed among the pervious group classes according to their respective percentage in Cl 2 and Cl 3 respectively. Thus six different values of TIA have been obtained corresponding to six classifications. The TIA has been used to determine EIA by two methods: (i) a semi-automated direct method (described in section 4.5.3.1) and (ii) using Eqs. 4.6 and 4.8. These EIAs were employed for flood modeling using Storm Water Management Model (SWMM) to simulate the runoff for study area.

4.5.3 Determination of EIA from fine resolution imagery

Many earlier reported studies deal with various direct and indirect methods (Canters et al. 2006) of determination of EIA. Direct method of EIA determination includes visual interpretation of aerial photos (Goetz et al. 2003), automated or semi-automated interpretation of satellite imagery (Han and Burian 2009) and conducting ground surveys (Ravagnani et al. 2009). The method of conducting ground survey is a very time consuming process and hence practically adopted in small areas. In the indirect method, EIA has been estimated based on the land use (Kauffman et al. 2009), TIA (Alley and Veenhuis 1983), population density (Heaney et al. 1977) or any other watershed characteristics such as curb length (Novotny and Olem 1994) SCS CN (Debo and Reese 1995) etc. Irrespective of the methods used, imperviousness estimation techniques can be grouped into three groups (Chabaeva et al. 2009) namely, (i) interpretive

detection (ii) spectral pattern recognition and (iii) statistical and mathematical modeling. Interpretive approach deals with the quantification of imperviousness by visual interpretation of the image by a human analyst whereas if interpretation is done by computer through classification algorithms then the approach is called spectral pattern recognition approach. These two approaches fall under direct method. The modeling methods utilize numerical or statistical techniques to derive coefficients that have to be applied to any spatial data like land cover and population to generate impervious surfaces. This can be regarded as an indirect method. In this study, a combination of interpretive detection and spectral pattern recognition has been used to quantify EIA directly from fine resolution satellite imageries. This method can be considered as a semi-automated method to determine EIA as discussed in the following sub section.

4.5.3.1 Determination of EIA by semi-automated direct method

In this method, GIS data of building footprints and road networks have been used to estimate TIA as described in section 4.5.2. The EIA is estimated from TIA by following the methodology described below.

The entire study area is classified into either impervious or pervious class. The land cover data which is termed as TIA data layer is exported from ENVI platform to ArcGIS platform and combined in a project with a 5 m resolution DEM and a vector layer of drainage network layer. The drainage network layer is rasterized and all the three layers were converted to a consistent co-ordinate system. Each TIA data layer grid cell that is connected to drainage network layer has been evaluated. If the connected cell is found to be of impervious class then it is selected and its adjacent pixels were checked. If the adjacent pixels are of impervious class those are selected and others are neglected. With respect to the selected adjacent pixels, the corresponding flow direction raster was established. If the flow direction is from the adjacent pixels to the pixel under consideration then they are designated as EIA, else neglected. Thus water moves over totally impervious path before getting discharged to the drainage network and this impervious area over which water travels is the effective impervious area or EIA (Han and Burian 2009). Since the exact location of the gutters and manholes in the drainage network was not mentioned, it was assumed that the drainage system is open throughout its length and allows entry of storm water anywhere along its length. To eliminate flat areas (when all the adjacent cells will have the same elevations), the sinks have been filled in the DEM. Each TIA data layer grid cell that is

connected to drainage network layer was checked and EIA designation was done. The summary of step by step procedure for EIA designation is shown in Fig. 4.3.

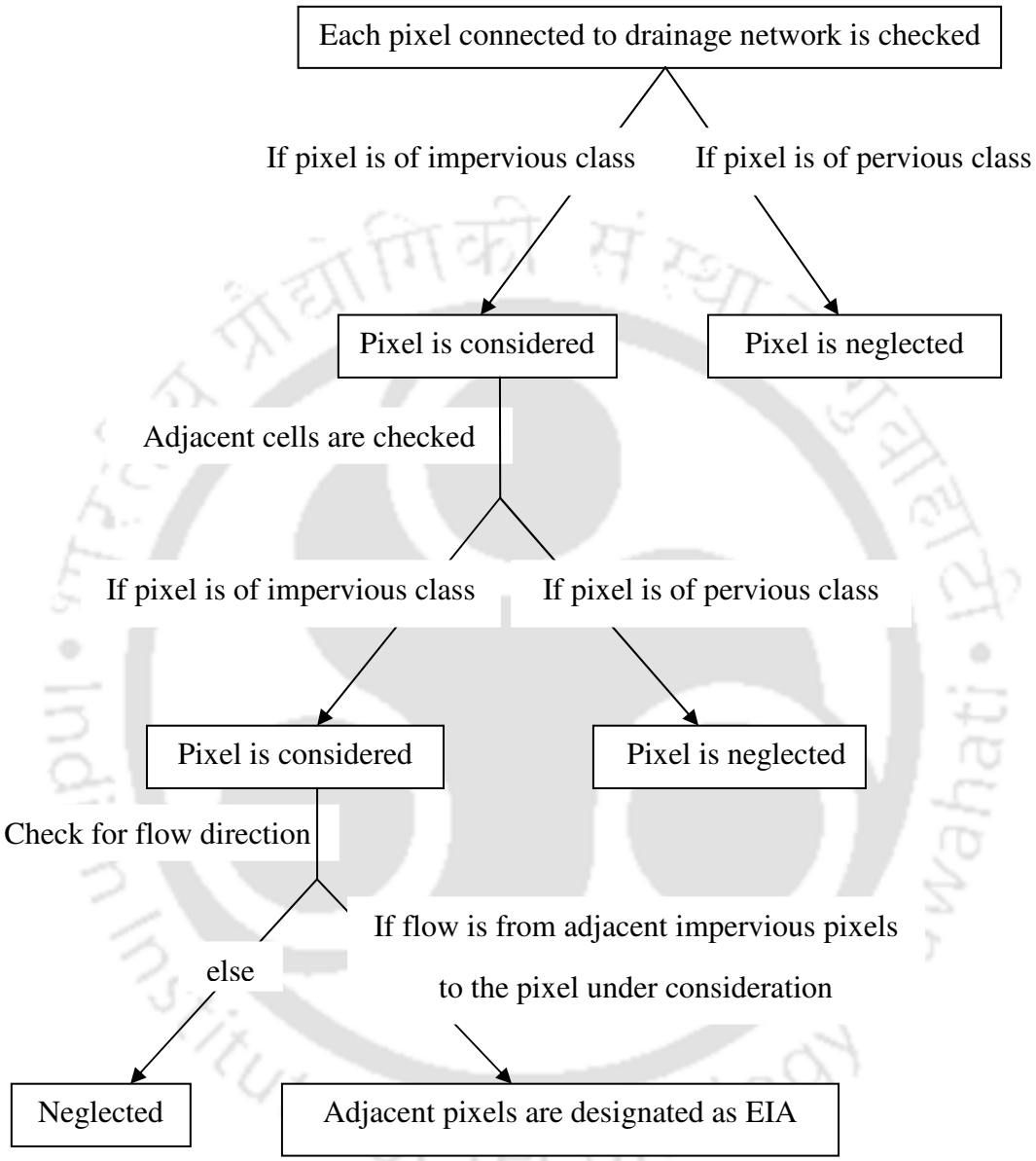

Fig. 4.3 Methodology followed for EIA designation in the direct method

4.6 Results of Image Classification

The basic objective of image analysis is to find out the urbanization growth pattern in the study area. For this purpose satellite image of the study area for a time span of around 30 years (from 1980 to 2011) were considered to quantify imperviousness (TIA and EIA). For analysis of

all images, the image of 2002 was taken as the standard. In analysis of 2002 imagery, different training areas were chosen for classification which had a good separability values. Here both the J-M distance and Transformed Divergence separability measures are adopted. The spectral separability between selected training area pairs for classification of 2002 imagery is listed in Table 4.1.

Table 4.1 Spectral variability for different training areas used for classification of 2002-image

grass land [Sea Green]: agricultural land [Purple]: (2.0; 2.0) scrub land [Magenta]: (1.99; 2.0) forest [Green]: (2.0; 2.0) waterbody [Cyan]: (2.0; 2.0) swampy/marshy land [Maroon]: (1.99; 2.0) builtup area [Yellow]: (2.0; 2.0)	agricultural land [Purple]: grass land [Sea Green]: (2.0; 2.0) scrub land [Magenta]: (2.0; 2.0) forest [Green]: (2.0; 2.0) waterbody [Cyan]: (2.0; 2.0) swampy/marshy land [Maroon]: (1.99; 2.0) builtup area [Yellow]: (2.0; 2.0)
scrub land [Magenta]: grass land [Sea Green]: (1.99; 2.0) agricultural land [Purple]: (2.0; 2.0) forest [Green]: (1.99; 2.0) waterbody [Cyan]: (2.0; 2.0) swampy/marshy land [Maroon]: (1.98; 1.99) builtup area [Yellow]: (2.0; 2.0)	forest [Green]: grass land [Sea Green]: (2.0; 2.0) agricultural land [Purple]: (2.0; 2.0) scrub land [Magenta]: (1.99; 2.0) waterbody [Cyan]: (1.99; 2.0) swampy/marshy land [Maroon]: (1.76; 1.98) builtup area [Yellow]: (1.99; 2.0)
Waterbody [Cyan]: grass land [Sea Green]: (2.0; 2.0) agricultural land [Purple]: (2.0; 2.0) scrub land [Magenta]: (2.0; 2.0) forest [Green]: (1.99; 2.0) swampy/marshy land [Maroon]: (2.0; 2.0) builtup area [Yellow]: (1.99; 2.0)	swampy/marshy land [Maroon]: grass land [Sea Green]: (1.99; 2.0) agricultural land [Purple]: (1.99; 2.0) scrub land [Magenta]: (1.98; 1.99) forest [Green]: (1.76; 1.98) waterbody [Cyan]: (2.0; 2.0) builtup area [Yellow]: (2.0; 2.0)
Builtup area [Yellow]: grass land [Sea Green]: (2.0; 2.0) agricultural land [Purple]: (2.0; 2.0) scrub land [Magenta]: (2.0; 2.0) forest [Green]: (1.99; 2.0) waterbody [Cyan]: (1.99; 2.0) swampy/marshy land [Maroon]: (2.0; 2.0)	

Values greater than 1.9 indicate that the pairs have good separability. For pairs with lower (less than 1.8) separability values, attempts have been made to improve the separability by editing the training areas or by selecting new training areas. These values range from 0 to 2.0

(Richards 1999) and indicate that the selected training pairs are statistically separated. From Table 4.1, it can be observed that the J-M distance for forest class and swampy/marshy land is found to be 1.76 after several trials, which is less than 1.8. This can also be observed in Fig 4.4 that the two classes (forest in green colour and swampy/ marshy land in maroon colour) are close to each other. This similarity in reflectance values between both the classes is due to the vegetation cover of the swampy/ marshy land and the leafy forest cover. But the transform divergence for the particular combination of classes was found to be 1.98, which is more than 1.9. Hence this can be accepted in the current study.

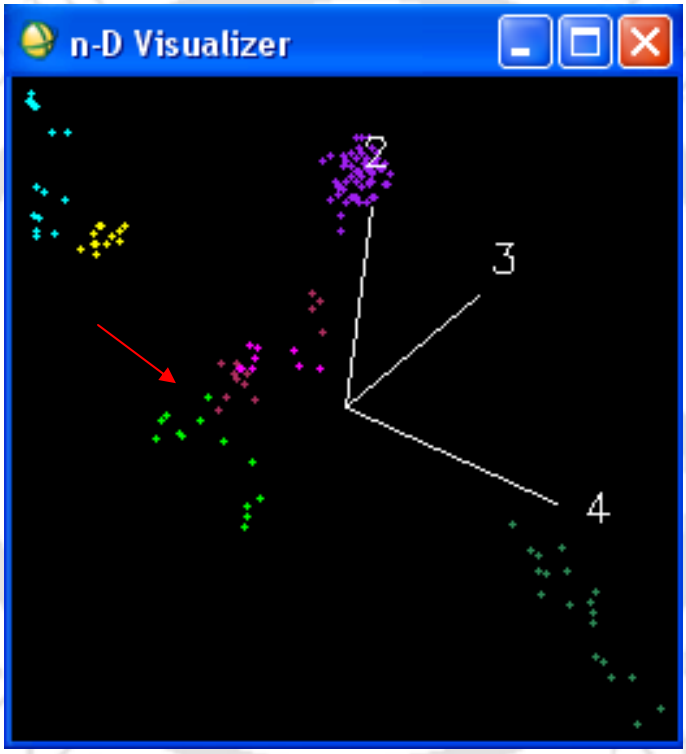

Fig. 4.4 Scatter plot for different classes in 3-D spectral space demonstrating separability of different training regions in 2002 imagery

In ENVI, n-D visualizer has been programmed to visualize the shape of training data clouds that results from plotting image data in spectral space (with image bands as plot axes). Since 3 bands (band 4 as **R**ed band, band 3 as **G**reen band and band 2 as **B**lue band) have been used, Fig.4.4 shows the reflectance values for different training classes taking the bands 2, 3, 4 as plot axes. The co-ordinates of the points in the 3-D space consist of 3 spectral reflectance values in

each band for a given pixel. From Fig. 4.4, it can be noticed that the classes (in different colours) are clustered in different groups to give a distinct separability. Since MXL classification has been applied, training data need to have normal distribution. The details of the basic statistics representing the mean and standard deviation of the training areas for the classification of 2002 imagery are listed in Table 4.2.

Table 4.2 Basic statistics for the training classes for MXL classification of 2002 imagery

Description	Band	Mean	Standard Deviation
Grass land [Sea Green]	1	79.36	1.64
	2	103.23	1.86
	3	123.31	1.90
Agricultural land [Purple]	1	86.37	1.95
	2	75.25	1.48
	3	90.43	1.43
Scrub land [Magenta]	1	64.55	1.87
	2	64.44	1.51
	3	85.44	1.33
Forest [Green]	1	47.92	1.75
	2	53.53	1.39
	3	83.84	1.95
Water body [Cyan]	1	51.73	1.43
	2	41.00	1.36
	3	37.40	1.60
Swampy/marshy land [Maroon]	1	61.06	3.28
	2	83.73	3.61
	3	73.00	3.92
Built-up area [Yellow]	1	56.76	1.36
	2	59.15	0.89
	3	81.07	0.95

It can be observed from Table 4.2 that the mean vectors of different classes agree with the known spectral characteristics of the cover types. Essentially, each class of training data should have a distinct range (Han and Burian 2005) of mean values. In Table 4.2, a perfectly distinct range of mean values is not observed for all classes, which is mainly due to the coarse resolution of the imagery. Since the accuracy of classification is not very much sensitive to violation of the assumption that the classes are normal, minimal degree of overlapping is always permissible (Richards 1999). The standard deviation in all the bands was found to be small for water body

due to its homogeneous nature. The standard deviation in all the bands for built-up area is high due to its heterogeneous nature. The evaluation of the training areas suggest that the areas selected would be adequate for the classification process in this study. Thus supervised MXL classification was applied to the image with the above mentioned training areas to obtain the corresponding classified images. The FCC images for all the years are shown in Fig. 4.5 (a) to (c).

From Fig. 4.5 (c) (i) (the FCC of the study area for the year 2006), it can be noticed that a cloud cover of approximately 11 km^2 covers the eastern portion of the study area. However this area has been masked before applying MXL classification algorithm and deducted from the overall area while analyzing the change detection statistics of the study area. From all FCCs, it can be observed that the urbanization (built-up area in bluish green colour) is growing gradually from 1980 to 2011. The results have been used to quantify the urbanization as discussed in the following section:

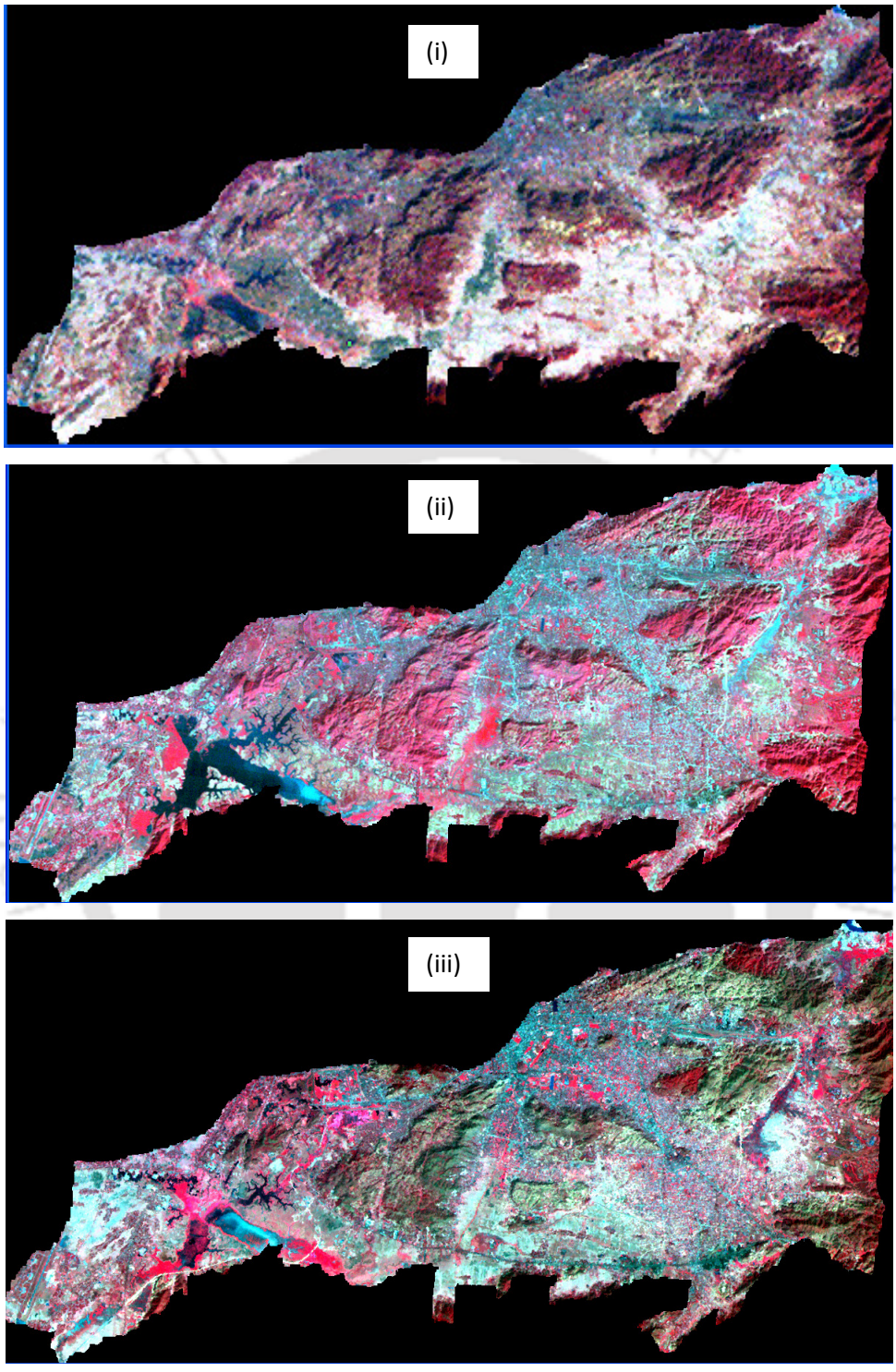

Fig. 4.5 (a) False Colour Composite of the study area for the years (i) 1980, (ii) 1991 and (iii) 1997

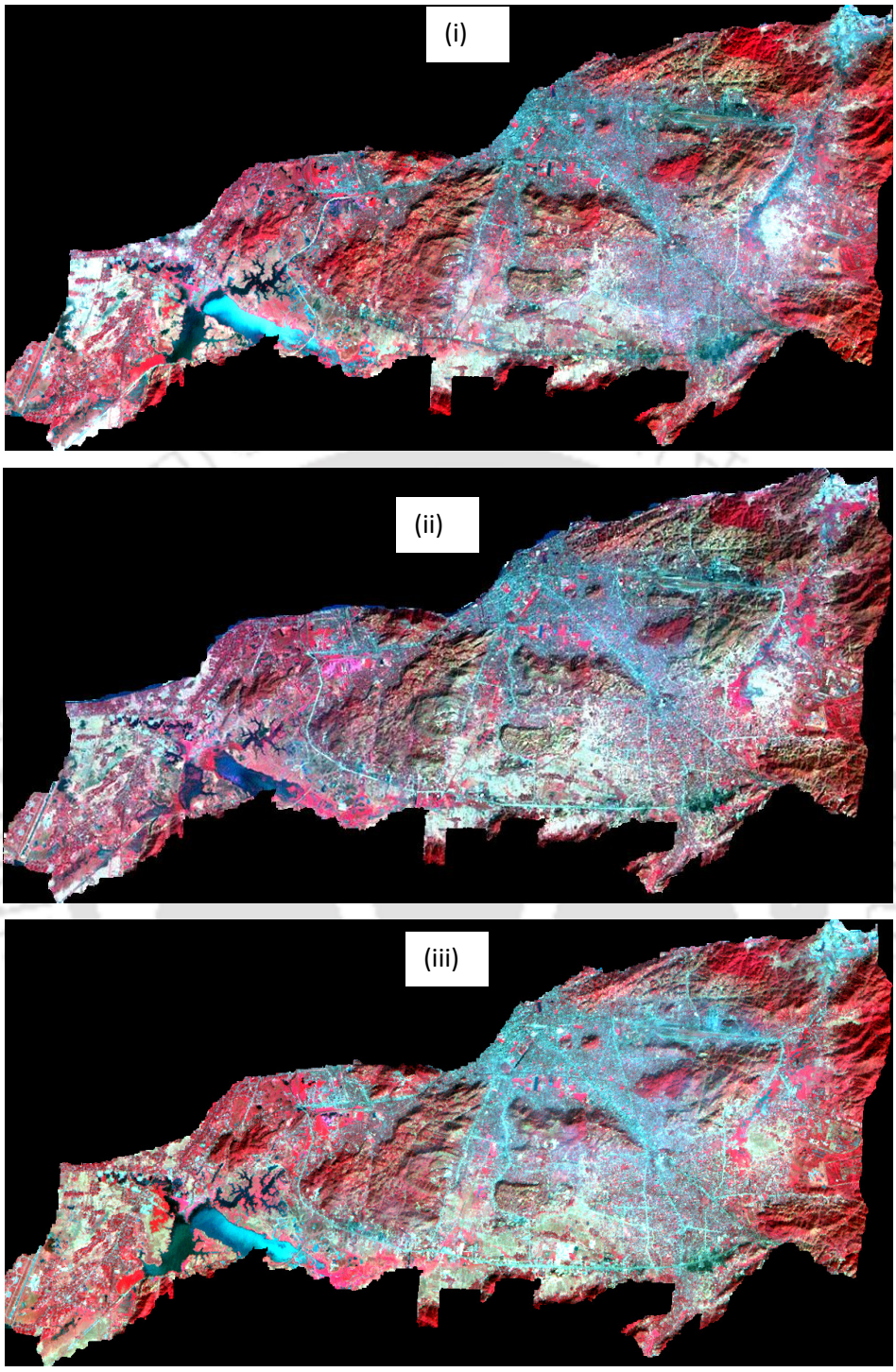

Fig. 4.5 (b) False Colour Composite of the study area for the years (i) 2000, (ii) 2002, and (iii) 2004

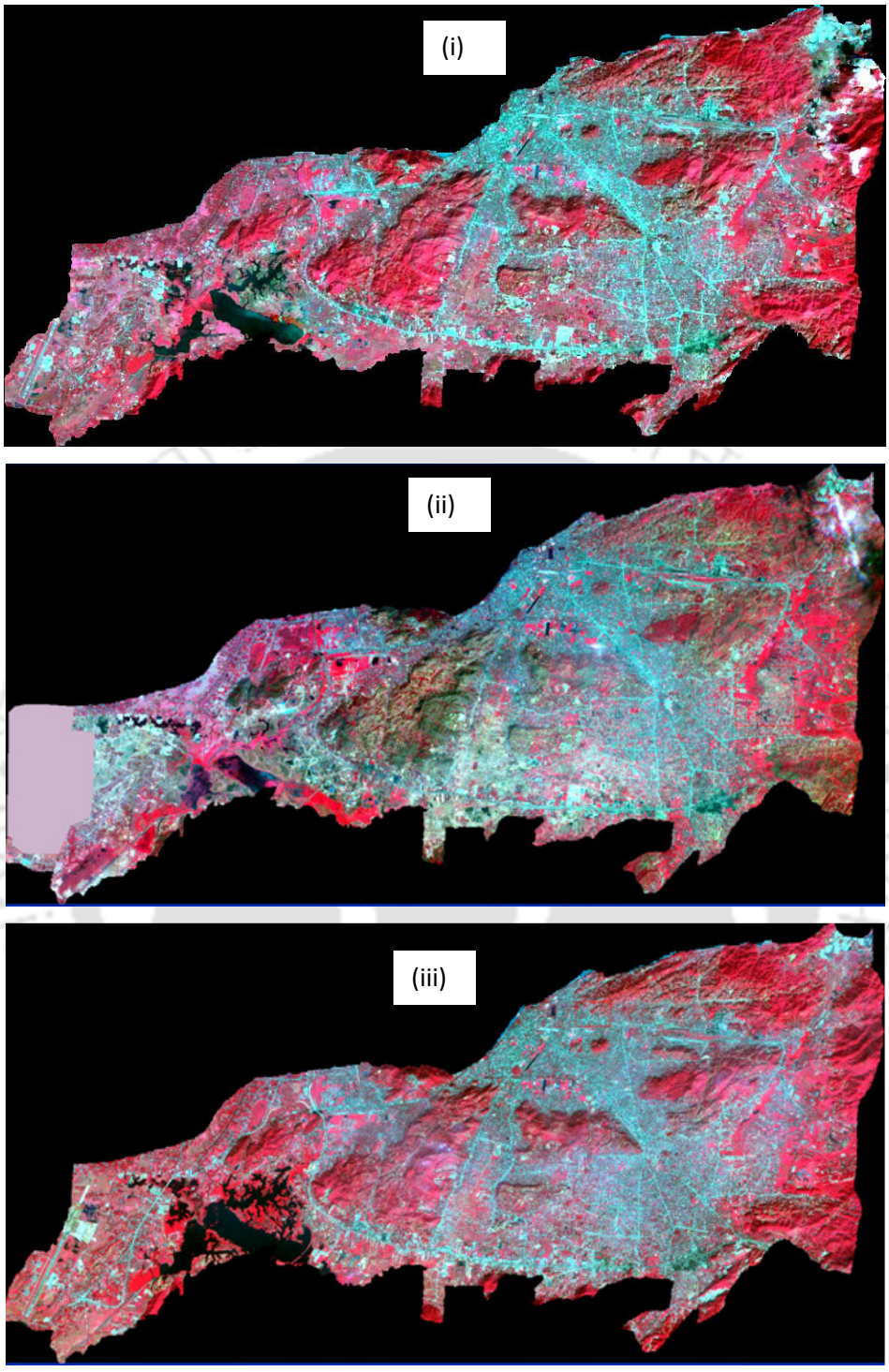

Fig. 4.5 (c) False Colour Composite of the study area for the years (i) 2006 - ETM+ of Landsat (ii) 2006 -LISS 4, and (iii) 2011-Resourcesat-2

4.6.1 Assessment of classification result

A classified paper map (scale = 1:25000) of total Guwahati city was collected for the year 2002 from ASTEC (Assam Science Technology and Environment Council, India) for assessing the accuracy of the classification process. It is prepared based on the classification result of LISS-III (IRS 1D) imagery of spatial resolution 24 m for the study area corresponding to the year 2002. Different classified areas were measured from the map using a planimeter. A Comparison between the land uses obtained from classification of 2002 image (landsat imagery of spatial resolution 30 m) and collected paper map is listed in Table 4.3. A little discrepancy is observed between different classes obtained from both the paper map and the landsat imagery. This discrepancy may be attributed to the spatial resolution of the imageries.

Table 4.3 Comparison between the land uses obtained from classification of 2002 image and collected paper map

Sl No.	Land use class	Areas in km^2	
		Landsat image in 2002	Paper map collected
1	Builtup area	34.62	37.58
2	Forest	37.55	39.23
3	Agricultural land	32.07	28.86
4	Scrub land	43.08	45.31
5	Grass land	6.24	4.67
6	Swamp/ marshy land	67.31	66.25
7	Waterbody	6.94	5.91

From Table 4.3, it can be observed that the land use distribution in the paper map is in good agreement with that of the result obtained using image analysis. The training areas from the validated image of 2002 were then imported to other images of different years and taken as the reference for choosing training sites for their respective classification. Hence a series of classified images, which are depicted in Fig. 4.6 (a) to 4.6 (c), were obtained for a period of 30 years from 1980 to 2011 for the study area.

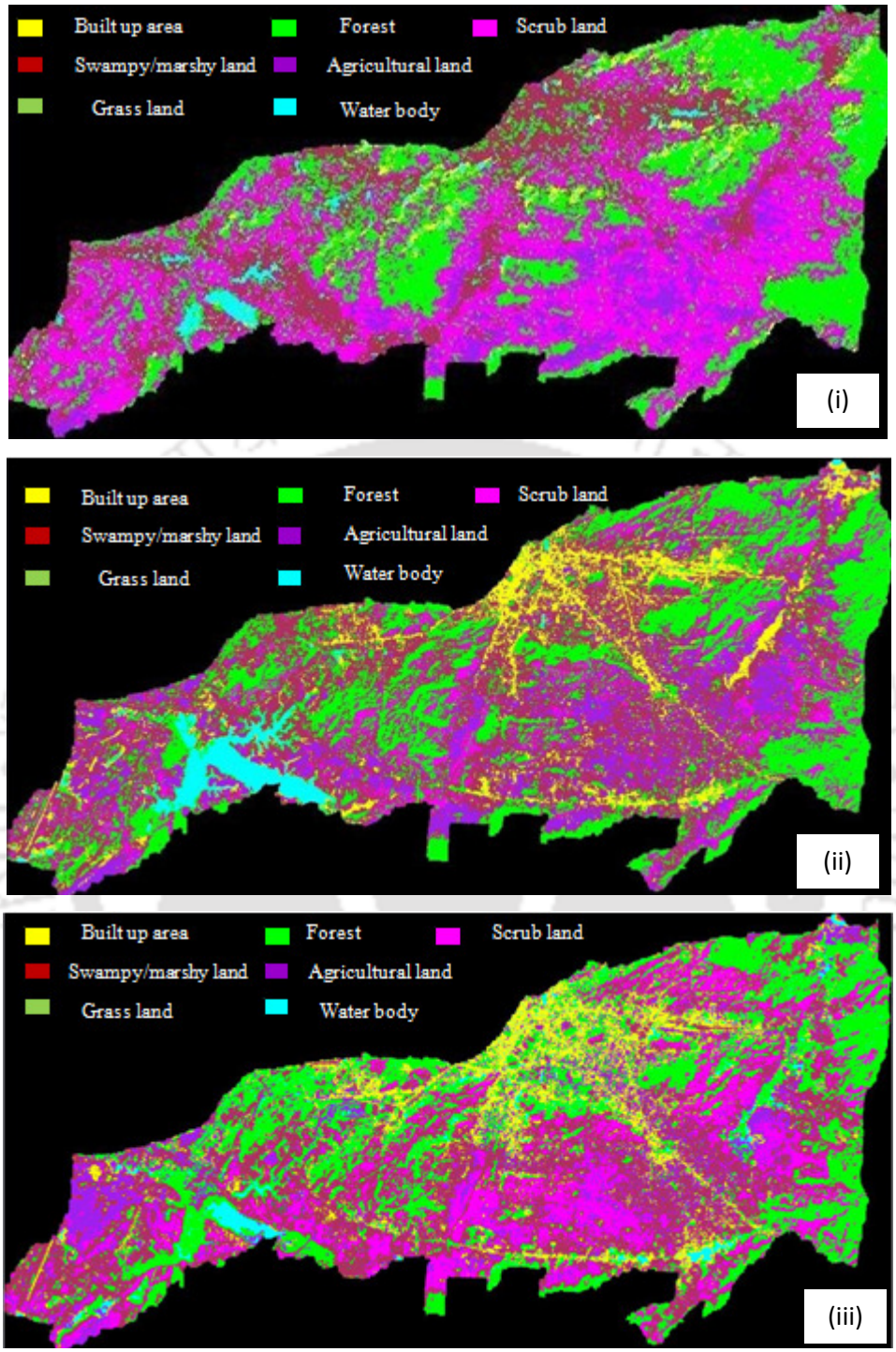

Fig. 4.6 (a) Classified image of the study area for the year (i) 1980, (ii)1991, and (iii)1997

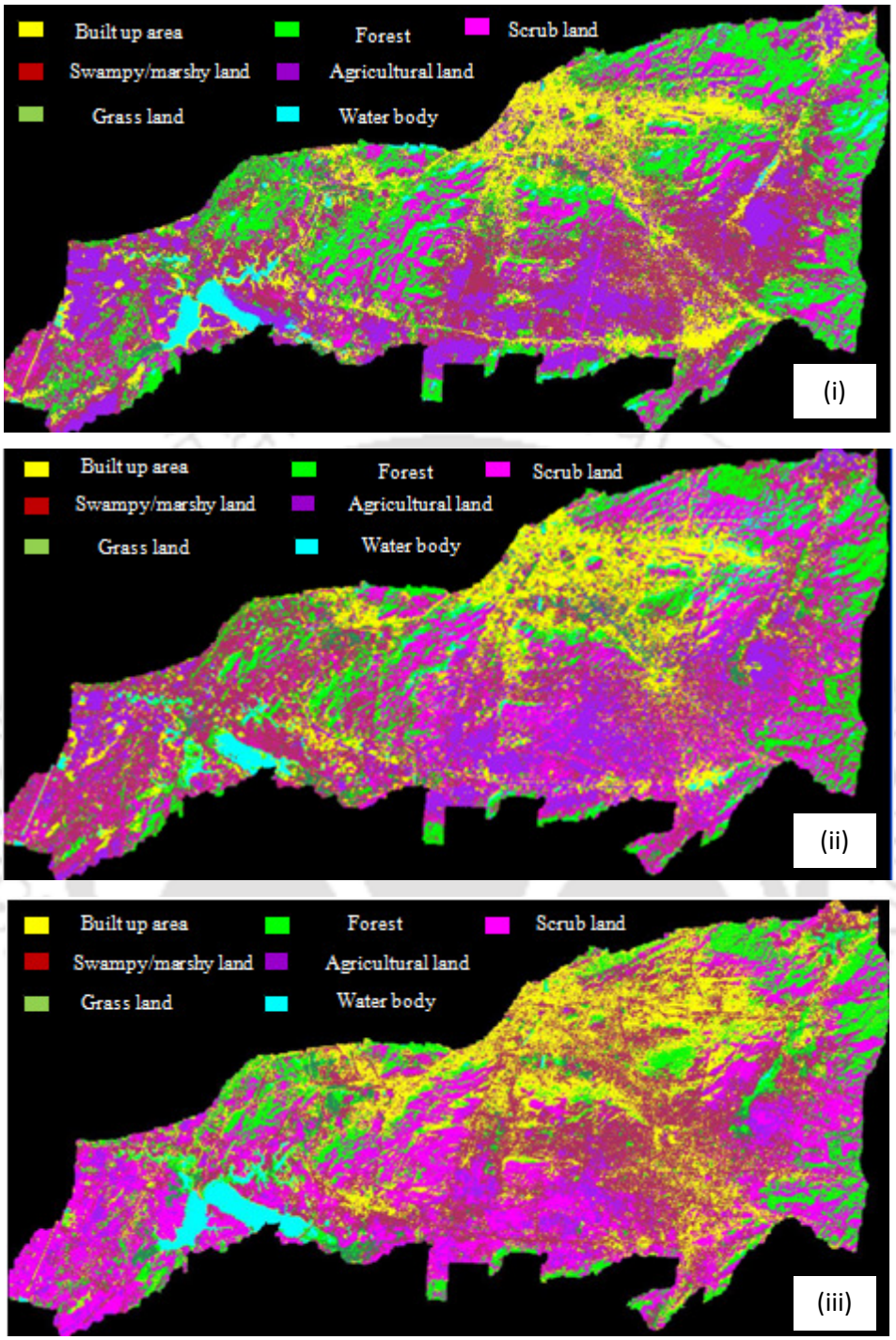

Fig. 4.6 (b) Classified image of the study area for the year (i) 2000, (ii) 2002, and (iii) 2004

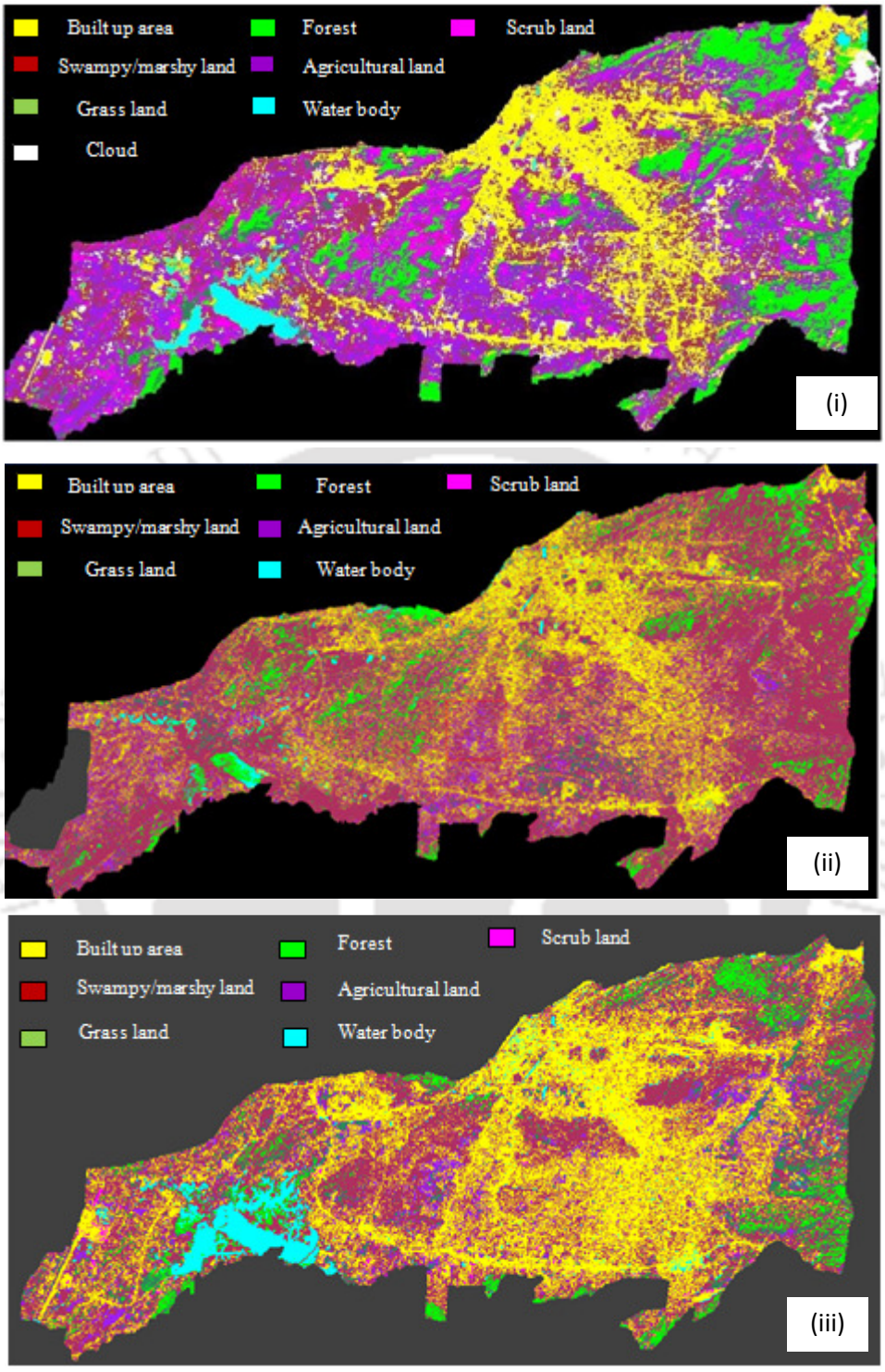

Fig. 4.6 (c) Classified image of the study area (i) 2006- ETM+ of Landsat, (ii) 2006-LISS4, and (iii) 2011-Resourcesat-2

4.6.2 Determination of land use changes

From the classified images, the land cover changes for urban Guwahati are determined for 30 years from 1980 to 2011, and the same is listed in Tables 4.4 and 4.5. In table 4.4, the source of the imagery and its spatial resolution is indicated.

Table 4.4 Land cover distribution over Guwahati from 1980 through 2011

Class type	Representative colour in the classified image	Area (km^2)							
		1980	**1991**	**1997**	**2000**	**2002**	**2004**	**2006**	**2011**
		Landsat MSS (60 m)	Landsat TM (30 m)	LISS 3 (24 m)	LISS 3 (24 m)	Landsat ETM+ (30 m)	LISS 3 (24 m)	Landsat ETM+ (30 m)	LISS 4 (5 m)
Builtup area	Yellow	6.5	20.42	23.67	34.36	34.62	45.58	46.68	82.94
Forest	Green	71.3	65.88	62.03	54.97	37.55	36.2	26.9	22.07
Agricultural land	Purple	13.83	29.78	26.33	39.79	32.07	22.49	38.12	32.15
Scrub land	Magneta	85.69	22.45	38.13	29.23	43.08	50.02	41.93	25.89
Grass land	Sea green	0.08	1.91	0.44	6.94	6.24	4.47	12.96	13.81
Swampy/ marshy land	Maroon	44.27	80.18	69.92	57.27	67.31	63.51	45.5	44.98
Water body	Cyan	6.14	7.19	7.29	5.41	6.94	5.54	4.72	5.97
Cloud	White	0	0	0	0	0	0	11.00	0
Total area		227.81							

In this study, the urbanization growth is defined in terms of TIA as shown in Figs. 4.7 and 4.8. From the Fig. 4.7 it is clear that there is a steady rise in urbanization from 1980 to 2006 and a steep rise from 2006 to 2011. This sudden growth in built-up area can also be noticed from Fig 4.6 c (ii) and Fig 4.6 c (iii), where the built-up area is represented in yellow colour. From Fig. 4.7 a major change of built-up area equal to 6.12% was noticed to occur from 1980 to 1991. The built-up area of 1980 is less accurate due to coarse resolution of the imagery (60 m). However, this would not influence the quantification of imperviousness because the major urbanization of the study area took place post 2000. Another major increase of 4.8% in urbanization occurred during 2002 to 2004. This increase can be attributed to a large scale migration of people to towns and cities in search of a better livelihood and safe socio-economic condition that prevailed in the city after 2002. Also a remarkable increase in imperviousness of 15.91% is noticed from 2006 to

2011. Total area remaining constant, the increase in built-up area occurred at the expense of reduction in waste lands (swampy/marshy land or scrub land or grass land) or forest, as it is a common practice to adopt land alteration for better habitat. Also it can be observed from Fig. 4.5 c (i) that in 2006 imagery, a considerable portion (approximately 11 km^2) of the city is covered by cloud. However, by comparing Fig. 4.6 b (iii) and 4.5 c (i), it can be seen that the areas covered by cloud in 2006 imagery might be either forest or scrub lands.

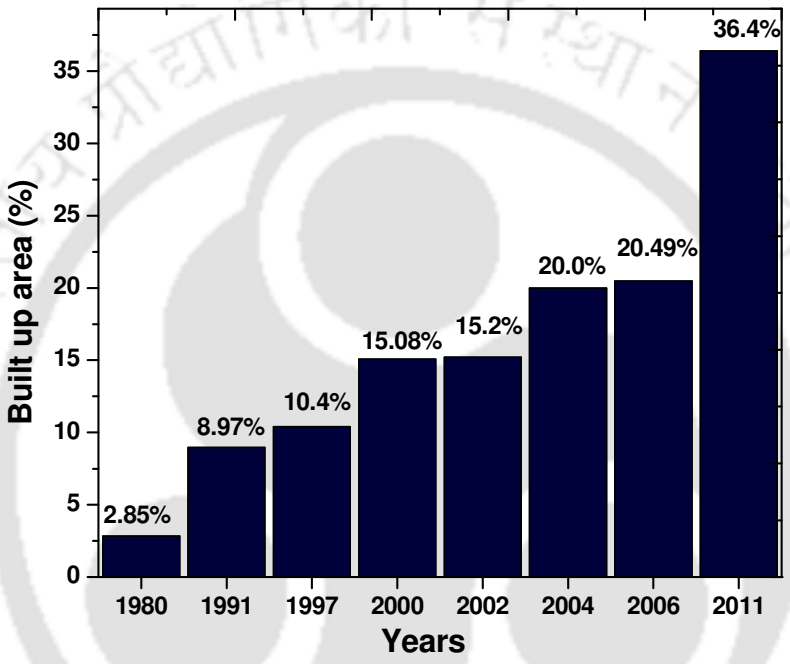

Fig. 4.7 Urbanization growth from 1980 to 2011

TIA obtained for the study area for different years have been plotted as shown in Fig. 4.8 to assess the trend of the urbanization growth of the study area. From Fig. 4.8 it can be noticed that urbanization in the study area follows an exponential growth trend from 1980 to 2011.

It can be observed from Tables 4.4, 4.5 and Fig. 4.9, that the various land classes listed show a remarkable change in the land use pattern from 1980 to 2011. From table 4.5 it can be noticed that the urbanization gradually increased from 6.5 km^2 in 1980 to 46.68 km^2 in 2006 and 82.94 km^2 in 2011 (from 2.85% in 1980 to 36.4% in 2011 of total area) in terms of builtup area. This resulted in an increase of 33.55% in the built-up area and decrease of 21.61% in the forest cover from 1980 to 2011.

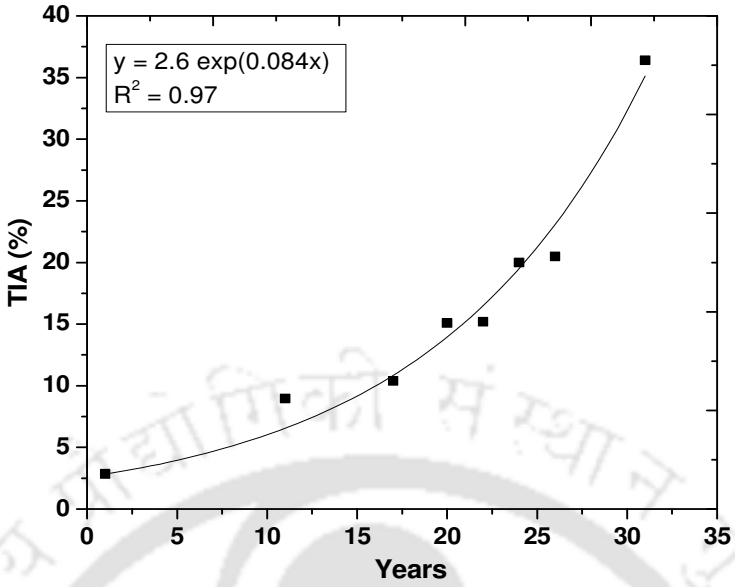

Fig. 4.8 Trend of urbanization growth of the study area

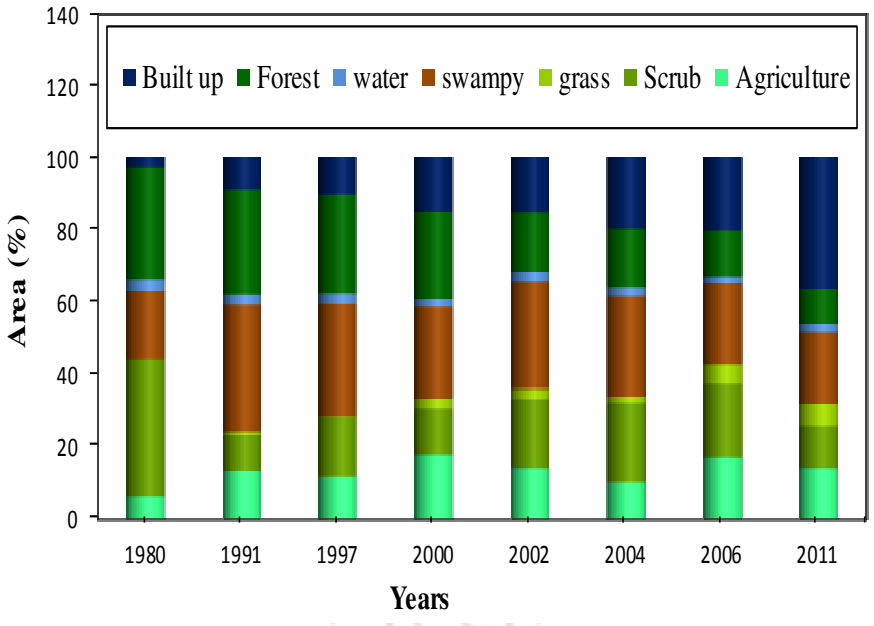

Fig. 4.9 Temporal change of different land classes

Table 4.5 Change detection of various land covers from 1980 to 2011

Land cover type		Area determined from image analysis								Change in area from 1980 to 2006		Change in area from 2006 to 2011	
		1980			2006			2011					
		km^2		% of total area	km^2		% of total area	km^2		% of total area	km^2	% of total area	km^2	% of total area
Built up area		6.5		2.85	46.68		20.49	82.94		36.4	+40.18*	+17.6	+36.26	15.91
Forest		71.3		31.3	26.9		11.8	22.07		9.69	-44.4**	-19.5	-4.83	-2.11
Agricultural land	Waste land	13.83	143.87	63.1	38.12	138.51	60.8	32.15	116.83	51.29	-5.36	-2.3	-21.68	-9.51
Scrub land		85.69			41.93			25.89						
Grass land		0.08			12.96			13.81						
Swampy/ marshy land		44.27			45.5			44.98						
Water body		6.14		2.7	4.72		2.1	5.97	2.62		-1.42	-0.6	-1.25	-0.52

* +ve value shows an increase in area

** -ve value shows a decrease in area

4.6.3 Determination of EIA from coarse resolution imageries

EIA for the study area estimated from TIA (discussed in section 4.5.1) by using Eqs. 4.6 and 4.8 are given in Table 4.6 and plotted in Fig. 4.10. EIAs determined using both the equations are found to follow similar trends. However it is noticed that Sutherland equation (Eq. 4.8) predicts EIA values that are less than those predicted by Alley and Veenhuis equation (Eq. 4.6). The suitability of these equations for the study area can be evaluated only by comparing the values with EIA determined by the direct method presented in section 4.6.5.

Table 4.6 TIA and EIA of the study area for different years

Sl. No.	Year	TIA (km^2)	TIA (%)	EIA by Alley and Veenhuis equation (Eq. 4.6)		EIA by Sutherland equation (Eq. 4.8)	
				EIA (km^2)	EIA (%)	EIA (km^2)	EIA (%)
1	1980	6.5	2.85	1.5	0.65	0.2	0.08
2	1991	20.42	8.97	7.6	3.3	1.83	0.8
3	1997	23.67	10.4	9.3	4.08	2.46	1.08
4	2000	34.36	15.08	15.6	6.88	5.2	2.28
5	2002	34.62	15.2	15.9	6.96	5.3	2.31
6	2004	45.58	20.0	23.4	10.25	9.1	4.0
7	2006	46.68	20.49	24.2	10.6	9.6	4.2

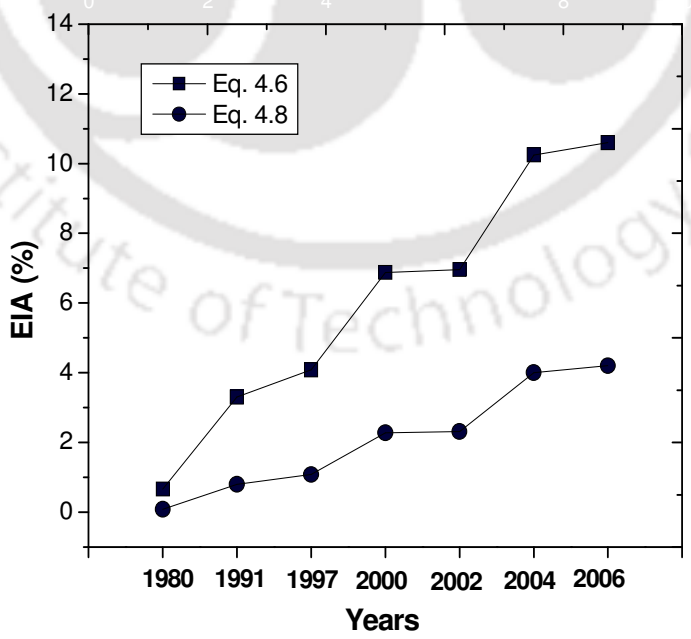

Fig. 4.10 Comparison of EIA estimated from TIA using two different equations

4.6.4 Determination of total imperviousness from fine resolution imageries

The TIA of all the watersheds were determined by the classification methodologies described in sub section 4.5.2 for the year 2006 and 2011 (fine resolution imageries of the study area available only for these two years). The fine resolution (5 m) image of the study area for the year 2006 has a mask applied over the airport region (9.817 km^2) for security reason which falls in watershed 7. Since airport area in terms of its runway can contribute towards the imperviousness of the city, it cannot be neglected. Hence it was decided to analyze the said area from the low resolution (30 m) Landsat ETM+ imagery of the same year. The accuracy of estimation of imperviousness using low resolution image will be less than the fine resolution imagery. The details of the classification of airport area from Landsat ETM+ image for the year 2006 is listed in Table 4.7.

Table 4.7 Classification of airport area from Landsat ETM+ image of the year 2006

Class name	Area (km^2)
Rooftop	0.454
Asphalt/Concrete	2.63
Swampy/ Marshy land	3.6
Agricultural land	2.4
Grass land	0.38
Forest	0.074
Scrub land	0.019
Water body	0.26
Total Area	9.817

The classification result of the study area by adopting all the techniques (Cl 1 to Cl 6) discussed in sub section 4.5.2 for the year 2006 and 2011 is given in Table 4.8. From Table 4.8 it can be observed that watershed 3 has the highest percentage of imperviousness in all the classifications. Being the active part of the city it is quite evident that watershed 3 will have high urbanization and hence more imperviousness.

The results of Table 4.8 have been used to plot Fig. 4.11 for better analysis of TIA determination when GIS data is not used. It can be observed that the results of the three classifications (Cl 1 to Cl 3) for a particular year show similar trend for both the years (2006 and 2011). A distinct difference can be noticed between imperviousness obtained using Cl 1, Cl 2 and Cl 3 in watersheds-2, 3 and 4. This difference in imperviousness is minimal in watersheds 1,

6, 5 and 7. However in all the watersheds it can be observed that imperviousness obtained from Cl 2 is maximum followed by Cl 3 and lowest for Cl 1. This difference can be sequentially represented as imperv (Cl 2 > Cl 3 > Cl 1) and can be explained as follows.

Table 4.8 TIA of all watersheds of Guwahati city from fine resolution imageries

Watershed No.	Year	Impervious Area (%)					
		Image Analysis without GIS data			Image Analysis with GIS data		
		Cl 1	Cl 2	Cl 3	Cl 4	Cl 5	Cl 6
1	2006	11.94	17.8	15.2	23.85	25.04	24.23
	2011	20.0	25.8	23.2	25.6	28.1	26.0
2	2006	27.46	36.83	32.17	32.92	36.62	34.12
	2011	37.7	47.1	42.5	43.25	46.9	44.4
3	2006	47.0	54.2	51.82	53.17	55.86	54.14
	2011	58.22	65.4	63.0	64.3	67.0	65.3
4	2006	27.28	35.29	32.56	31.38	36.13	32.75
	2011	50.68	57.5	54.7	53.4	58.0	54.6
5	2006	28.64	32.05	30.6	36.17	36.37	36.25
	2011	41.03	44.3	43.0	48.5	48.9	48.7
6	2006	20.3	26.34	24.4	23.53	27.1	25.03
	2011	27.62	33.6	31.7	30.83	34.4	32.3
7	2006	17.63	22.0	20.59	19.74	22.07	20.44
	2011	29.42	33.7	32.3	31.4	33.7	32.0

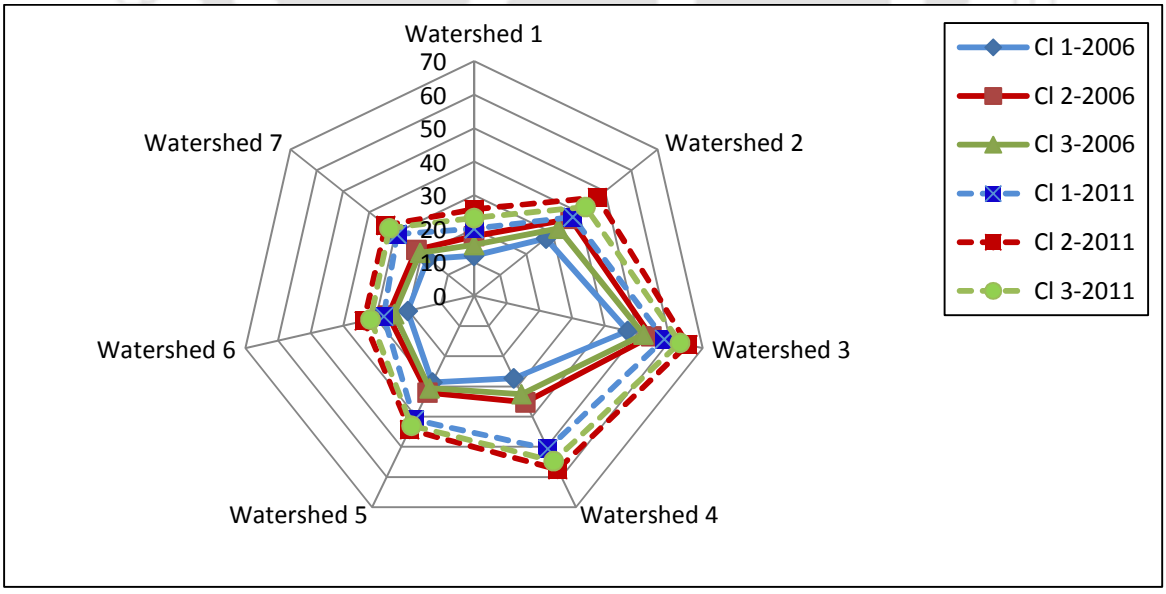

Fig. 4.11 Growth of TIA (%) estimated by satellite image classification without using GIS data

Since threshold imposed for both pervious and impervious areas in Cl 1 is less than that of Cl 2, logically imperviousness of Cl 1 should be more than imperviousness of Cl 2. But use of higher threshold in Cl 2 leaves maximum pixels as unclassified which are later proportionately distributed among the classes according to their respective percentage. In Cl 3 the threshold value for pervious area is less than that of Cl 2. Hence, this classification produces same number of impervious pixels, more number of pervious pixels and less no. of unclassified pixels than that of Cl 2. Thus less number of unclassified pixels (as land use percentage) is contributed towards imperviousness in Cl 3 as compared to Cl 2. Hence imperviousness determined using Cl 2 is more than that of Cl 3. Similar trends are observed for Cl 4, Cl 5 and Cl 6 as depicted in Fig. 4.12. However, the difference among the classification is minimal for a particular year as compared to Fig. 4.11. This is mainly due to the fact that since GIS data has been used in the classification process, the unclassified pixel produced due to the application of the threshold values in Cl 5 and Cl 6 are proportionately distributed among the pervious classes only. Hence, TIA determined by different classification becomes comparable when GIS is incorporated.

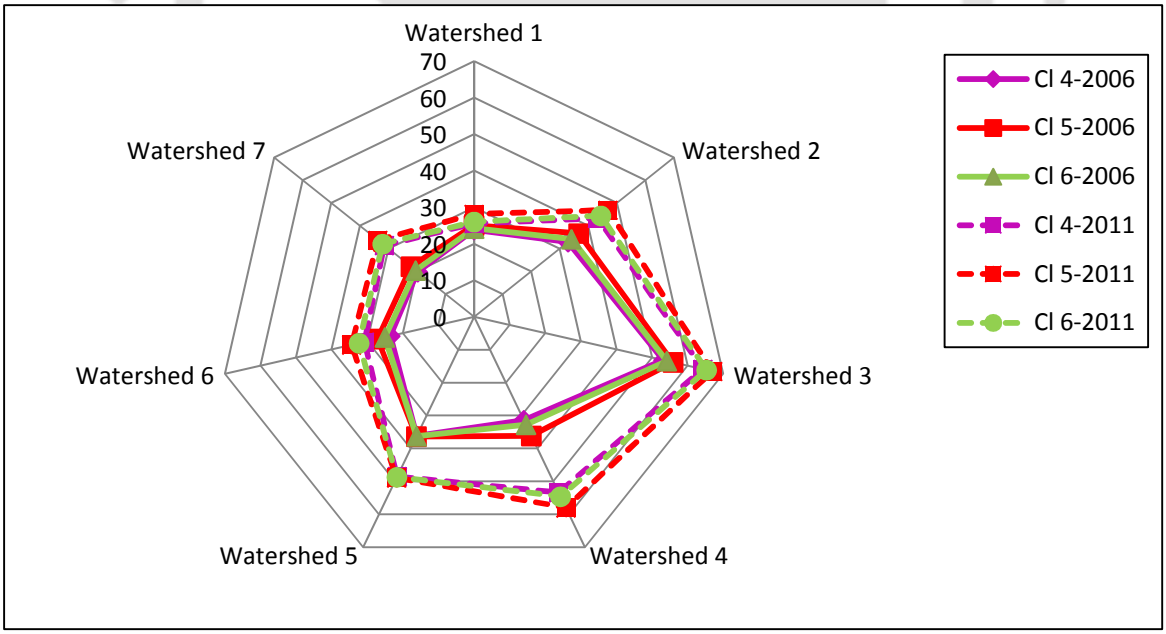

Fig. 4.12 Growth of TIA (%) estimated by satellite image classification by using GIS data

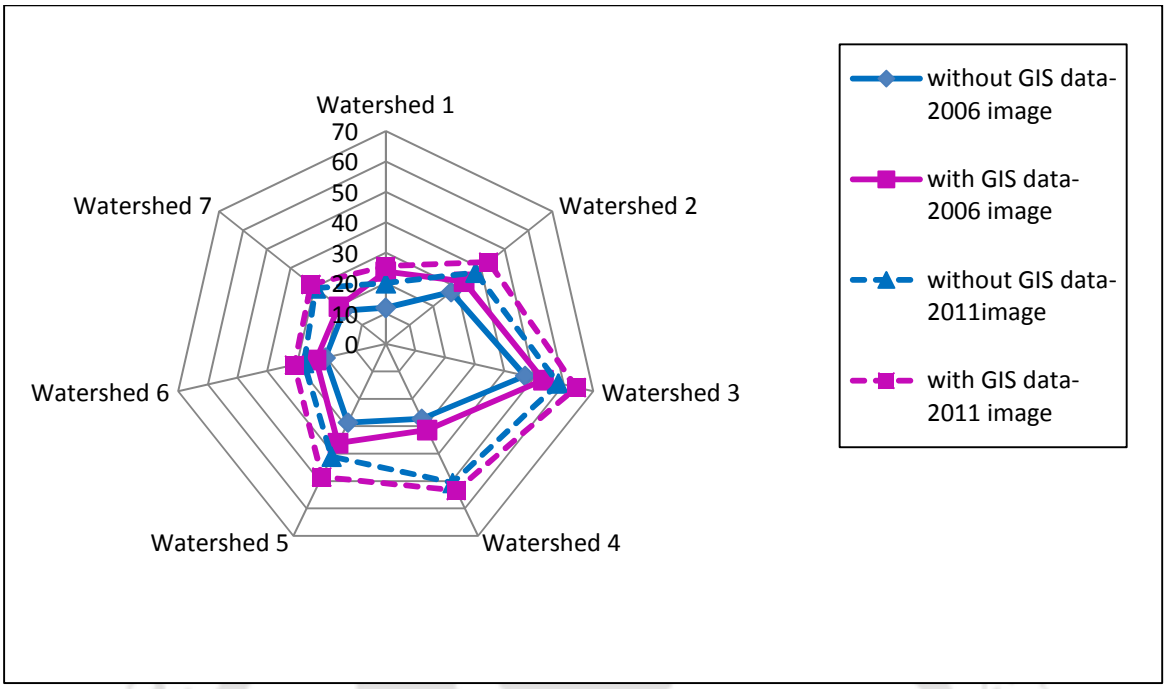

Fig. 4.13 Comparison of TIA (%) obtained from image classification with and without using GIS data (for Cl 1 and Cl 4)

The TIA obtained with and without GIS data is compared as shown in Fig. 4.13. Watershed 4 shows maximum increase (85%) in TIA from 2006 to 2011 if image classification is not supported by GIS data. However the increase in TIA in these years is maximum 70% in watershed 4 if GIS data is used for classification process. It can be noted that the TIA estimated by incorporating GIS data is found to be more than classification by satellite imagery alone. Use of GIS data increases TIA by maximum 28% in 2011 in watershed 1. This indicates that GIS data is effective in improving the classification accuracy. In the absence of GIS data, the rooftops were misclassified due to their colour and material. This could be correctly traced with the help of GIS data. Based on this observation, this study recommends using GIS data along with remote sensing data (fine resolution satellite imagery) for improving the accuracy of imperviousness determination. Eqs. 4.6 and 4.8 have been used to estimate EIA from the TIA listed in Table 4.8 and the same is listed in Table 4.9 and Table 4.10.

Table 4.9 EIA estimated by Alley and Veenhuis equation (Eq. 4.6) for the study area

Watershed No.	Year	Impervious Area (%)					
		Image analysis without GIS data			Image analysis with GIS data		
		Cl 1	Cl 2	Cl 3	Cl 4	Cl 5	Cl 6
1	2006	3.36	5.90	4.72	7.73	9.53	9.13
	2011	6.95	9.94	8.57	8.78	11.22	10.06
2	2006	8.93	13.51	11.16	11.53	13.40	12.13
	2011	13.96	19.11	16.54	16.96	18.99	17.58
3	2006	21.42	26.18	24.57	25.48	27.31	26.13
	2011	28.99	34.09	32.38	33.31	35.29	34.07
4	2006	9.06	13.02	11.61	11.03	13.45	11.71
	2011	21.70	25.92	24.16	23.36	26.22	24.11
5	2006	11.10	13.01	12.18	15.42	15.54	15.47
	2011	18.42	20.52	19.69	23.32	23.59	23.46
6	2006	6.39	9.22	8.28	7.87	9.60	8.58
	2011	9.87	13.00	11.97	11.51	13.44	12.29
7	2006	5.90	8.07	7.34	6.92	8.09	7.27
	2011	12.14	14.68	13.84	13.32	14.70	13.66

For better comparison, EIA quantification has been represented in Figs. 4.14 to 4.16. Fig. 4.14 shows EIA estimated for the study area in the year 2006 and 2011 using Eq. 4.6. It is observed that watershed 3 has the maximum imperviousness of 34.09% in 2011 due to Cl 2. However imperviousness in watershed 3 in 2011 varies from 28.99% to 34.09% irrespective of the classification process adopted. Watershed 1 shows the least fraction of imperviousness of 3.36% due to Cl 1.

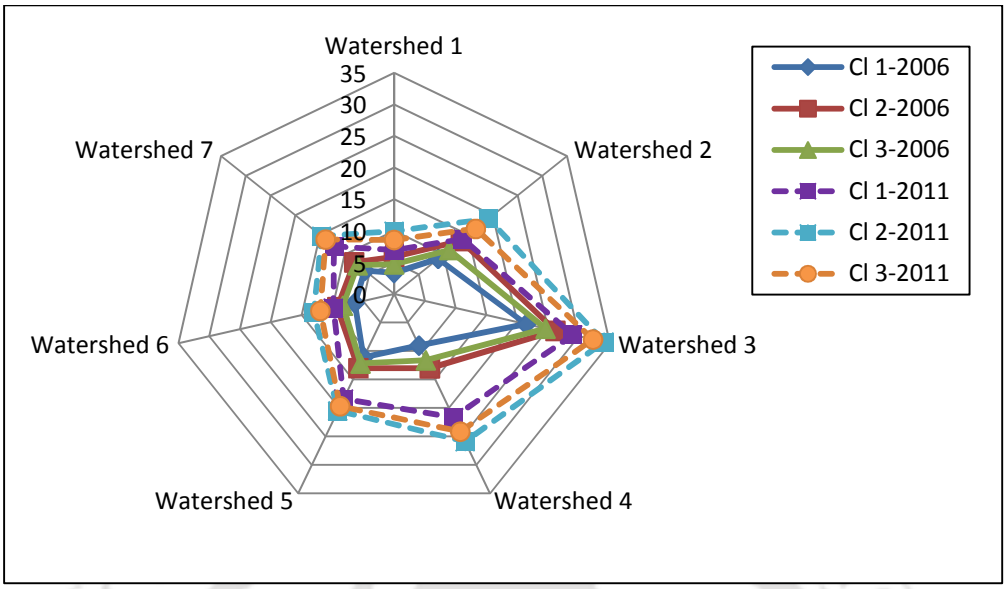

Fig. 4.14 EIA (%) estimated by satellite image classification and Eq. 4.6

Fig. 4.15 shows EIA estimated for the study area in the year 2006 and 2011 using the TIA derived by using GIS data and Eq. 4.6. Fig. 4.15 is observed to show similar trend like that of Fig. 4.14. It is observed that watershed 3 has the maximum imperviousness of 35.29% in 2011 due to Cl 5. However its imperviousness in 2011 varies from 33.31% to 35.29% irrespective of the classification process adopted. Watershed 7 in 2006 shows the least fraction of imperviousness of 6.92% due to Cl 4. Further EIA has been found to increase maximum by 111% from 2006 to 2011 in watershed 4.

Fig. 4.16 depicts a comparison between estimated EIA values for the study area with and without use of GIS data. For different watersheds of the study area it was found that the EIA value varies between 3.36% to 21.42% in 2006 and 6.95% to 28.99% in 2011 if classification result is not supported by GIS data. However if GIS data is used in classification process, the result is found to have improved by maximum 26.6% in 2011 in watershed 5.

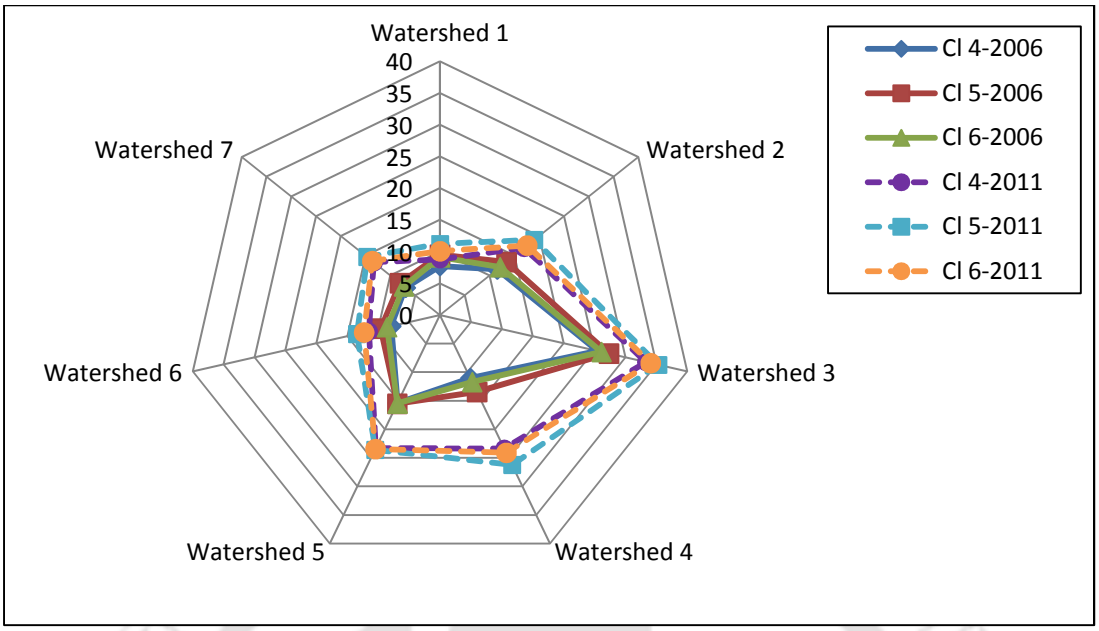

Fig. 4.15 EIA (%) estimated by satellite image classification incorporated with GIS data and Eq. 4.6

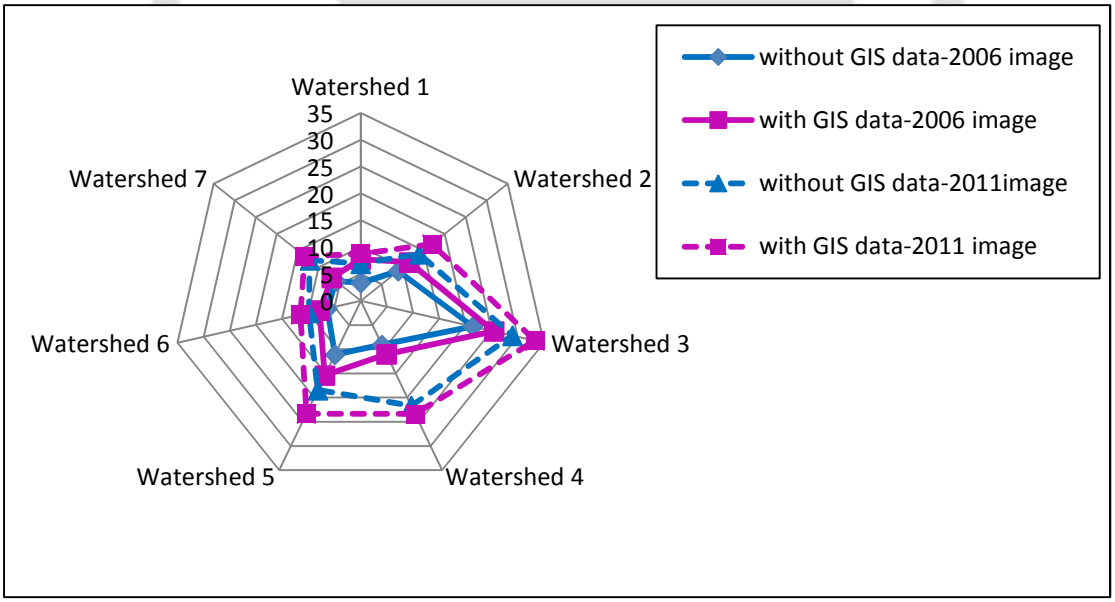

Fig. 4.16 Comparison of EIA (%) estimated by Eq. 4.6 and image classification with and without using GIS data (for Cl 1 and Cl 4)

Table 4.10 EIA estimated by Sutherland equation (Eq. 4.8) for the study area

Watershed No.	Year	Impervious Area (%)					
		Image analysis without GIS data			Image analysis with GIS data		
		Cl 1	Cl 2	Cl 3	Cl 4	Cl 5	Cl 6
1	2006	0.55	1.23	0.90	2.20	2.42	2.27
	2011	1.55	2.58	2.09	2.54	3.06	2.62
2	2006	1.81	3.26	2.49	2.60	3.22	2.80
	2011	3.42	5.33	4.35	4.50	5.29	4.74
3	2006	7.06	9.39	8.59	9.04	9.97	9.37
	2011	10.85	13.66	12.70	13.22	14.35	13.65
4	2006	1.89	3.17	2.69	2.50	3.32	2.73
	2011	6.54	8.41	7.62	7.26	8.55	7.59
5	2006	2.90	3.63	3.31	4.62	4.67	4.64
	2011	5.95	6.93	6.54	8.31	8.45	8.38
6	2006	1.24	2.08	1.79	1.66	2.20	1.88
	2011	2.29	3.39	3.01	2.85	3.55	3.13
7	2006	1.25	1.94	1.70	1.56	1.95	1.68
	2011	3.47	4.54	4.18	3.96	4.55	4.10

Fig. 4.17 shows EIA estimated for the study area in the year 2006 and 2011 using Eq. 4.8. It is observed that watershed 3 has the maximum imperviousness of 13.66% in 2011 due to Cl 2. However imperviousness of watershed 3 varies from 7.06% to 9.39% in 2006 and 10.85% to 13.66% in 2011 irrespective of the classification process adopted. Watershed 1 shows the least fraction of imperviousness of 0.55% due to Cl 1. Also comparing Fig. 4.14 and Fig. 4.17 it is observed that for the same watershed, Eq. 4.6 predicts EIA value more than Eq. 4.8 by any of the classification methodologies.

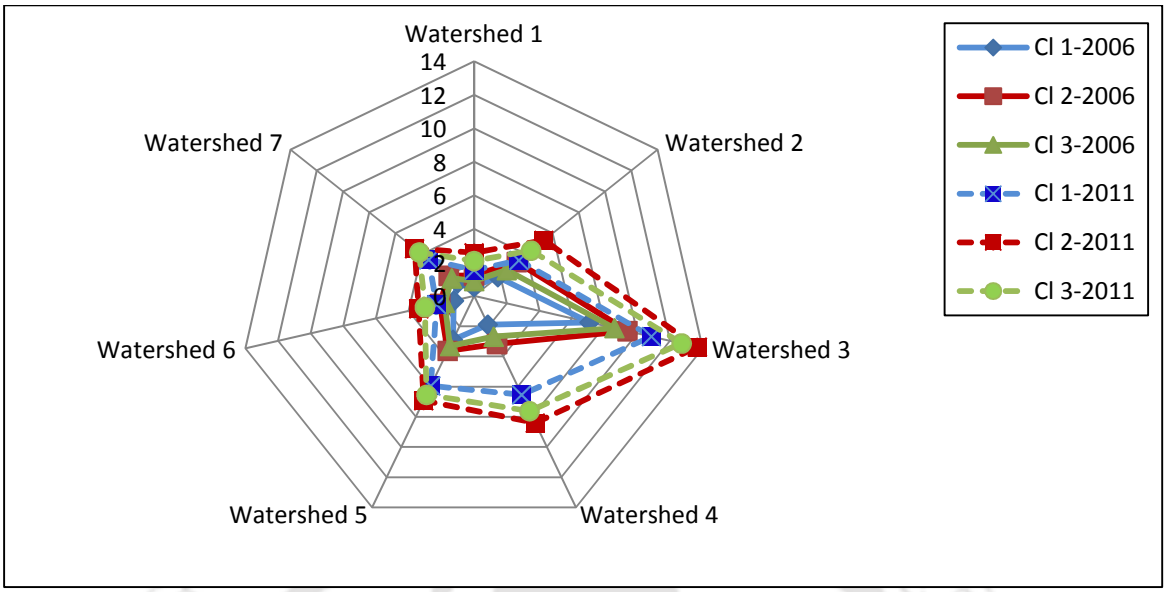

Fig. 4.17 EIA (%) estimated by satellite image classification and Eq. 4.8

Fig. 4.18 shows EIA estimated for the study area in the year 2006 and 2011 using the TIA derived by using GIS data and Eq. 4.8. Fig. 4.18 is observed to show similar trend like that of Fig. 4.15. It is observed that watershed 3 has the maximum imperviousness of 14.35% in 2011 due to Cl5. However its imperviousness varies from 9.04% to 9.37% in 2006 and 13.22% to 14.35% in 2011 irrespective of the classification process adopted. Watershed 7 shows the least fraction of imperviousness of 1.56% in 2006 due to Cl 4. EIA has been found to increase maximum by 190% from 2006 to 2011 in watershed 4.

Fig. 4.19 presents a comparison between estimated EIA values for the study area with and without use of GIS data. For different watersheds of the study area it was found that the EIA value varies between 0.55% to 7.06% in 2006 and 1.55% to 10.85% in 2011 if classification result is not supported by GIS data. However if GIS data is used the result is found to have improved by maximum 64% in 2011 in watershed 1.

It needs to be mentioned here that the accuracy of the classification processes for TIA determination cannot be ascertained due to the non-availability of ground truth data. However, of all these classification schemes (Cl 1 to Cl 6), Cl 6 is expected to give reliable TIA values as GIS data has been incorporated and different threshold values have been used for identification of pervious and impervious land covers. However from the comparison between directly estimated EIA and the indirectly estimated EIA values it can be compared.

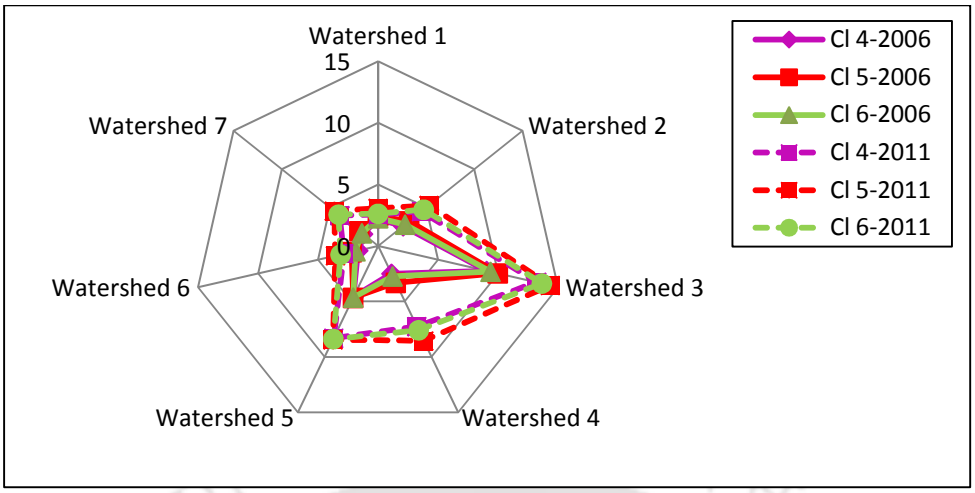

Fig. 4.18 EIA (%) estimated by satellite image classification incorporated with GIS data and Eq. 4.8

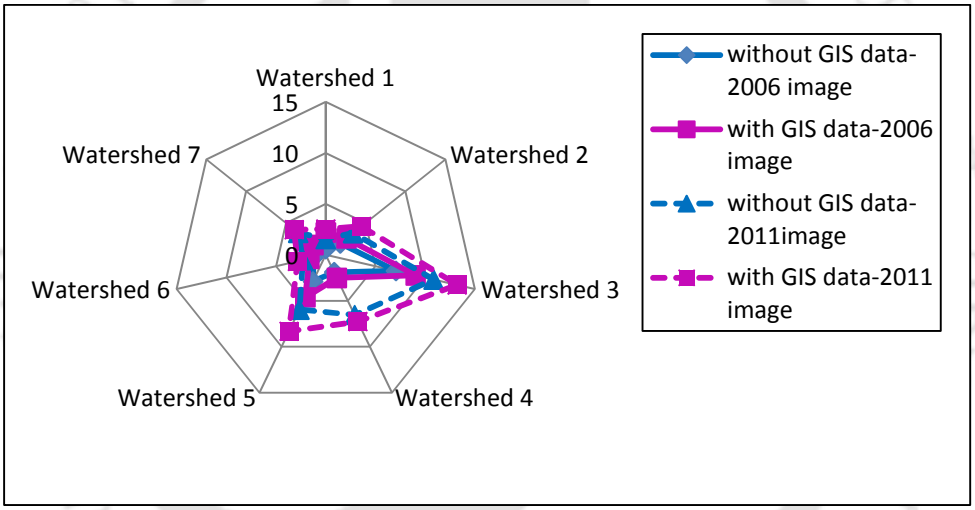

Fig. 4.19 Comparison of EIA (%) estimated by Eq. 4.8 and image classification with and without using GIS data

4.6.5 Determination of EIA from fine resolution imageries

Table 4.11 presents the EIA estimated for different watersheds of the study area by using the semi-automated direct method explained in section 4.5.3.1. It can be observed from Table 4.11 that EIA in watershed 1 increased maximum by 96.09% from 2006 to 2011. Watershed 2 was observed to have least (32.73%) rate of EIA growth in these years. All other watersheds show moderate increase in EIA values from 2006 to 2011. Watershed 3 shows 54.68%, watershed 4 shows 55.45%, watershed 5 shows 62.6%, watershed 6 shows 42.1% and watershed 7 shows 35.41% increase in EIA from 2006 to 2011. These results signifies the density of developmental

activities leading to imperviousness in the study area. It may be noted that the rate of developmental activities is not the same in all the watersheds of the study area.

Table 4.11 EIA estimated for the study area by direct method

Watershed No.	EIA (%) estimated by semi-automated direct method		% Increase from 2006 to 2011
	In the year 2006	In the year 2011	
1	1.28	2.51	96.09
2	4.98	6.61	32.73
3	7.9	12.22	54.68
4	1.1	1.71	55.45
5	1.07	1.74	62.6
6	0.38	0.54	42.1
7	4.8	6.5	35.41

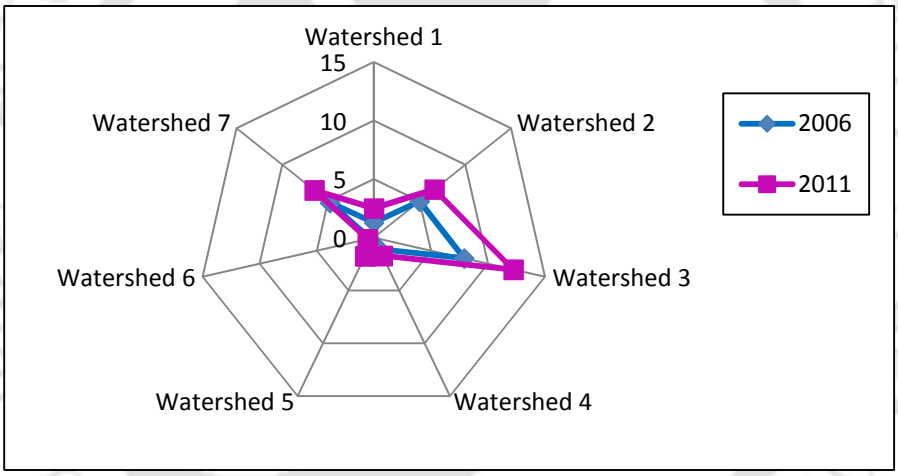

Fig. 4.20 EIA (%) estimated for the study area by semi- automated direct method

The EIA (obtained by direct and indirect methods) are compared in Table 4.12. Also comparisons are presented in Figs. 4.21 and 4.22, for the year 2006 and 2011, respectively. It can be observed that the EIA estimated by Eq. 4.8 are close to the EIA values determined by semi-automated direct method. Hence the assumption that the drainage network is poorly connected is appropriate for the study area. EIA estimated by Eq. 4.6 is an overestimation for the given study area.

Table 4.12 Comparison of EIA of the study area in 2011

Watershed No.	EIA (%) by indirect method												EIA (%) by direct method
	By Eq. 4.6						By Eq. 4.8						
	Cl 1	Cl 2	Cl 3	Cl 4	Cl 5	Cl 6	Cl 1	Cl 2	Cl 3	Cl 4	Cl 5	Cl 6	
1	6.95	9.94	8.57	8.78	11.22	10.06	1.55	2.58	2.09	2.54	3.06	2.62	2.51
2	13.96	19.11	16.54	16.96	18.99	17.58	3.42	5.33	4.35	4.50	5.29	4.74	6.61
3	28.99	34.09	32.38	33.31	35.29	34.07	10.85	13.66	12.70	13.22	14.35	10.85	12.22
4	21.70	25.92	24.16	23.36	26.22	24.11	6.54	8.41	7.62	7.26	8.55	7.59	1.71
5	18.42	20.52	19.69	23.32	23.59	23.46	5.95	6.93	6.54	8.31	8.45	8.38	1.74
6	9.87	13.00	11.97	11.51	13.44	12.29	2.29	3.39	3.01	2.85	3.55	3.13	0.54
7	12.14	14.68	13.84	13.32	14.70	13.66	3.47	4.54	4.18	3.96	4.55	4.10	6.5

Table 4.12 indicates that there is a distinct difference between the EIA values obtained for the study area by direct and indirect methods. Among indirect methods, Eq. 4.8 is observed to predict closer EIA values with the directly determined EIA than that of Eq. 4.6. It is also observed that there is no single classification methodology that is consistently showing accurate EIA value that of the directly derived EIA values in all watersheds. Cl4 was found to show EIA values with good agreement to that of the directly estimated EIAs in watershed 1. Cl 2 was found to perform well in watershed 2 whereas Cl 3 performed well in watershed 3. Also Cl 1 observed to produce good result in watersheds 4, 5, 6 and 7. However it can be said that Cl4 was found to give close EIA value with that of the directly estimated EIA value in the most urbanized watershed (watershed 3) with an error of 8.1%. The difference in EIA value obtained by direct and indirect methods varies from 1.2% in watershed 1 to 427% in watershed 6 due to Cl 4.

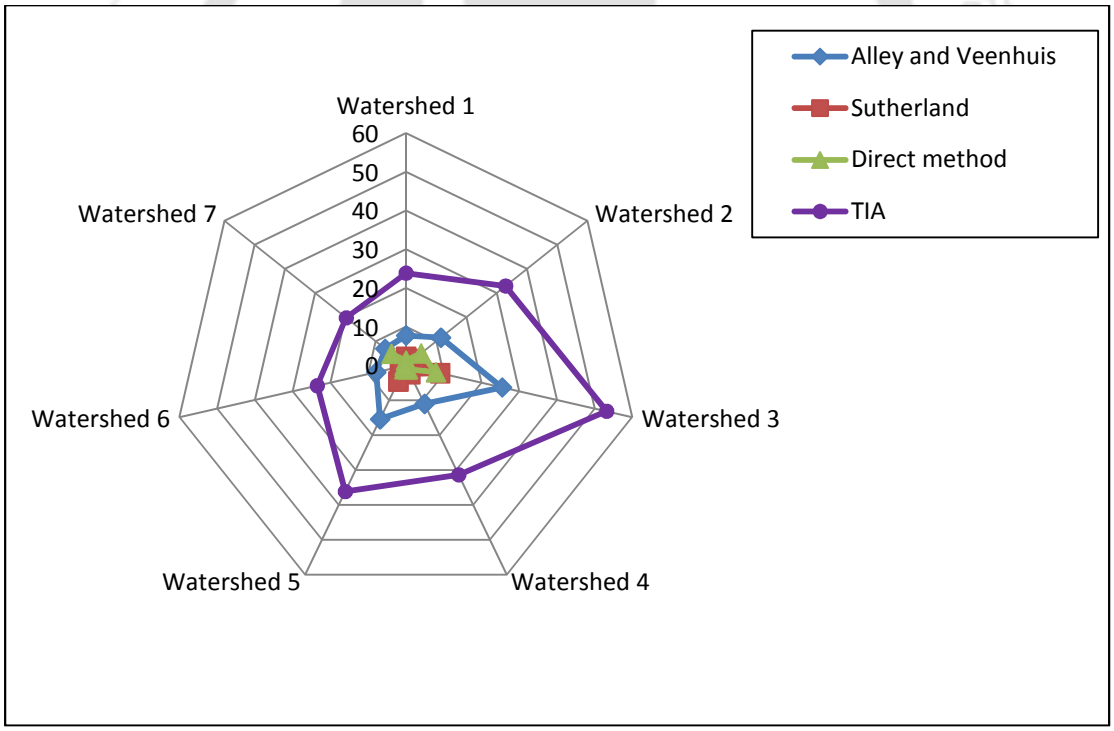

Fig. 4.21 EIA estimated for the study area for the year 2006

From Figs. 4.21 and 4.22 it is observed that Sutherland equation (Eq. 4.8) overestimates EIA value maximum by three times in 2006 and by four times in 2011 in watershed 6. Alley and Veenhuis equation (Eq. 4.6) overestimates EIA value maximum by 19 times in 2006 and by 20

times in watershed 6. TIA in watershed 6 has been observed to be 52 times more than the directly estimated EIA in 2006 and 56 times more than the directly estimated EIA in 2011.

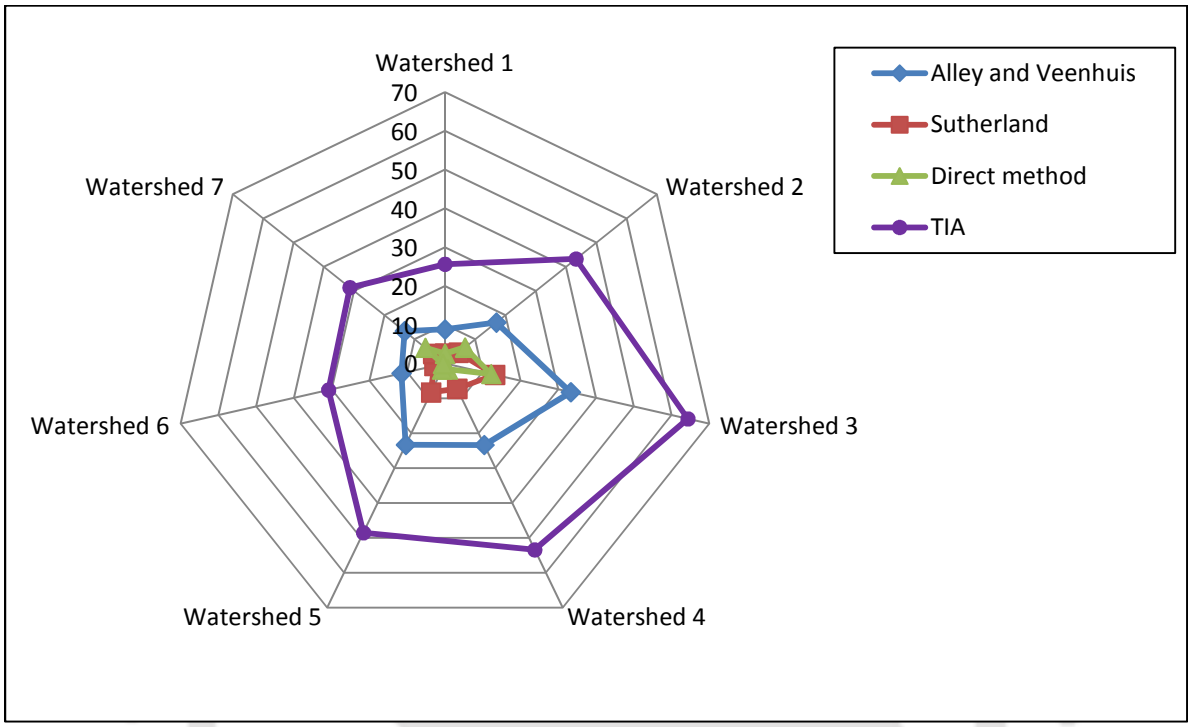

Fig. 4.22 EIA estimated for the study area for the year 2011

In addition, an effort has been made to obtain relationship between TIA and EIA for the study area based on the results of semi-automated direct method. For this purpose EIA and TIA results obtained for 87 sub watersheds (7 watersheds divided into sub watersheds as mentioned in section 3.5 of Chapter 3) have been plotted for the years 2006 and 2011, as depicted in Fig. 4.23. A power curve (represented by Eq. 4.9) fitted to the data points yields a good coefficient of regression close to 0.9 for both the years. A comparison of the fitting constants (A and B) of Eq. 4.9 is listed in Table 4.13.

$$\mathrm{EIA} = \mathrm{A} \times (\mathrm{TIA})^{\mathrm{B}} \qquad (4.9)$$

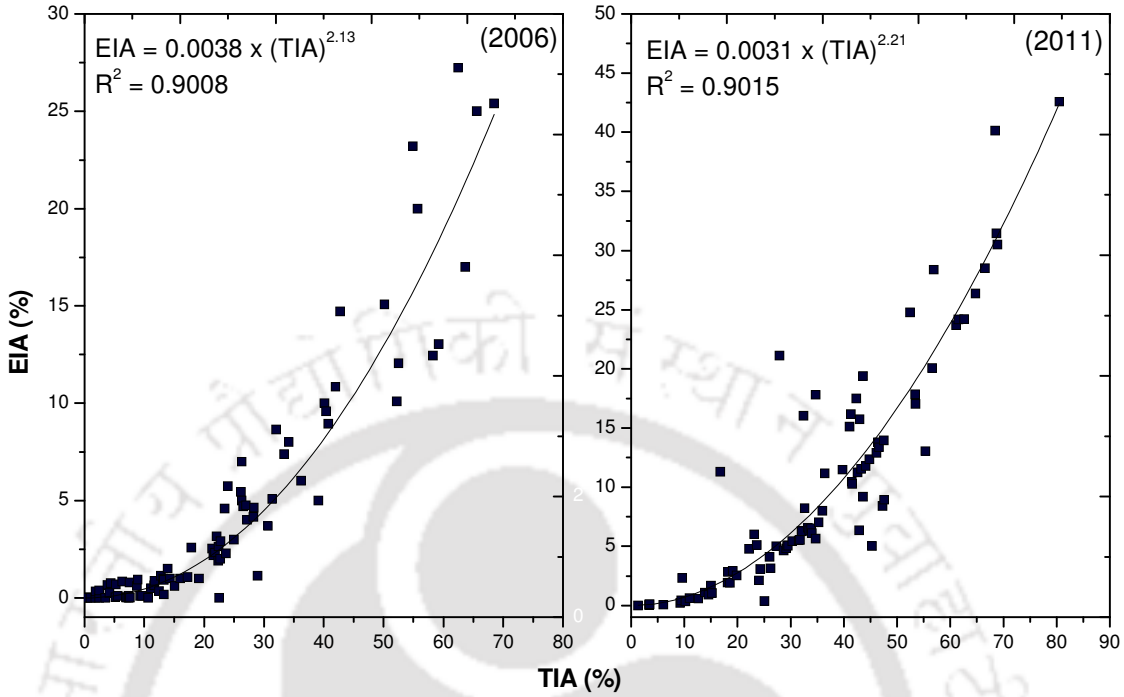

Fig. 4.23 Relation between EIA and TIA of the study area for the years 2006 and 2011

Table 4.13 Comparison of fitting constants of Eq. 4.9

Equation Number	Value of 'A'	Value of 'B'
Eq. 4.6	0.15	1.41
Eq. 4.8	0.01	2.0
Eq. 4.9 for the year 2006	0.0038	2.13
Eq. 4.9 for the year 2011	0.0031	2.21

It can be noted from Table 4.13 that the fitting constants of regression power equation obtained for the years 2006 and 2011 are comparable. These constants are in good agreement with Eq. 4.8. Thus a relationship between TIA and EIA is developed for the study area based on 2011 LU and is given by Eq. 4.10.

$$\text{EIA} = 0.0031 \times (\text{TIA})^{2.21} \qquad (4.10)$$

4.7 Imperviousness of Total Study Area

The various land covers of the entire study area was determined by taking the summation of built up area of all the watersheds and the details are listed in Table 4.14. The details obtained from classification of airport area from 2006 image (listed in Table 4.7) are added to the areas listed in Table 4.14 to obtain the total area reported in Table 4.15.

Table 4.14 Land cover of study area (excluding airport area) in 2006

Class name		Area (km^2)					
		Classification without GIS data			Classification with GIS data		
		Cl 1	Cl 2	Cl 3	Cl 4	Cl 5	Cl 6
Rooftop	IA	17.54	18.39	18.15	28.02	29.421	29.777
Asphalt/ Concrete	IA	35.856	48.651	43.635	35.566	40.175	36.349
Swampy/Marshy land	PA	55.58	47.33	48.578	50.68	45.33	46.09
Scrub land	PA	50.82	47.44	48.39	49.714	42.451	44.642
Agricultural land	PA	23.5	23.451	22.09	22.8	24.26	23.8
Grass land	PA	5.07	4.52	4.47	5.27	4.75	5.12
Forest	PA	26.77	25.56	27.75	25.77	25.77	28.17
Waterbody	PA	2.851	2.645	2.931	3.167	3.32	3.04

IA: Impervious area PA: Pervious area

Table 4.15 Land cover of the study area

Class name		Year	Area (km^2)					
			Classification without GIS data			Classification with GIS data		
			Cl 1	Cl 2	Cl 3	Cl 4	Cl 5	Cl 6
Rooftop	IA	2006	18.0	18.85	18.60	28.48	29.88	30.23
		2011	40.36	45.76	46.3	41.2	43.54	42.56
Asphalt/Concrete		2006	38.48	51.28	46.27	38.2	42.80	38.33
		2011	42.58	50.32	44.65	51.5	55.14	51.93
TIA		**2006**	**56.48**	**70.13**	**64.87**	**66.68**	**72.68**	**68.56**
		2011	**82.94**	**96.08**	**90.95**	**92.7**	**98.68**	**94.49**
Swampy/ Marshy land	PA	2006	59.18	50.93	52.18	51.28	50.93	51.34
		2011	44.98	37.56	40.66	39.87	35.27	40.23
Scrub land		2006	50.84	47.46	48.41	49.74	42.98	44.66
		2011	25.89	22.67	23.7	24.1	23.0	23.4
Agricultural land		2006	25.9	25.85	26.49	25.2	26.66	26.2
		2011	32.15	29.3	30.5	29.3	29.14	29.01
Grass land		2006	5.45	4.9	4.85	5.65	5.13	5.5
		2011	13.81	14.12	14.0	13.52	13.21	13.4
Forest		2006	26.85	25.64	27.83	25.85	25.85	28.25
		2011	22.07	21.97	21.77	22.31	22.41	21.2
Water body		2006	3.11	2.91	3.19	3.43	3.58	3.3
		2011	5.97	6.11	6.23	6.01	6.1	6.08
Total pervious area		**2006**	**171.33**	**157.69**	**162.95**	**161.13**	**155.13**	**159.25**
		2011	**144.87**	**131.73**	**136.86**	**135.11**	**129.13**	**133.32**
Total Area of Study Area			**227.81**					

IA: Impervious area PA: Pervious area

Till now the imperviousness of the total study area has been reported for all seven watersheds of the study area for hydrologic analysis. However sometimes for urban planning purpose, it may be necessary to know the impervious fraction and pervious fraction of the total study area. Hence the imperviousness (TIA) percentage of study area is listed in Table 4.16.

Table 4.16 Imperviousness (TIA) of study area

Classifications	2006		2011	
	Impervious area (%)	Pervious area (%)	Impervious area (%)	Pervious area (%)
Cl 1	24.8	75.2	36.4	63.6
Cl 2	30.8	69.2	42.18	57.82
Cl 3	28.5	71.5	40.0	60.0
Cl 4	29.26	70.74	40.7	59.3
Cl 5	31.9	68.1	43.32	56.68
Cl 6	30.01	69.99	41.48	58.52

From Table 4.16 it can be observed that, TIA of the study area in 2011 varies from 36.4% to 43.32% and pervious area varies from 56.68% to 63.6% irrespective of the classification methodology employed. For better comparison the growth of imperviousness of study area from 2006 to 2011 is also plotted in Fig. 4.24. From the figure, the TIA growth trend of the study area was found to be similar for all classification methodologies. Also TIA of total study area found to vary from 24.8% to 31.9% in 2006 and from 36.4% to 43.32% in 2011 irrespective of the classification methodology employed. Maximum TIA growth by 46% was observed from 2006 to 2011 due to Cl 1.

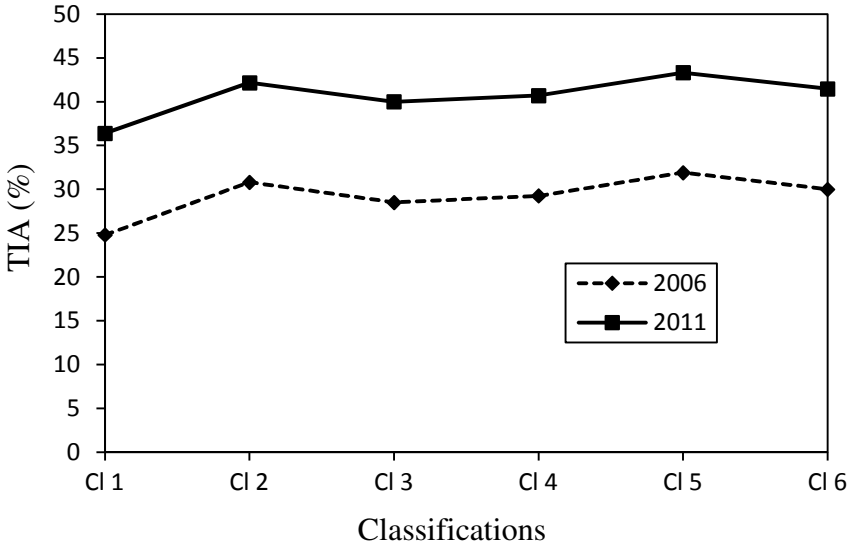

Fig. 4.24 TIA growth of the study area from 2006 to 2011

Table 4.17 shows the summary of TIA and EIA (obtained by direct and indirect methods) of study area for the years 2006 and 2011. From Table 4.17 it can be observed that, TIA of the study area in 2011 varies from 36.4% to 43.32% irrespective of the classification methodology and EIA varies from 4.9% to 20.5% irrespective of the empirical equation used. For better comparison, TIA and EIA of the study area in 2011 for different type of classifications are plotted in Fig. 4.25. It is observed from Fig. 4.25 that Eq. 4.8 estimates EIA value that is close to the directly determined EIA value and hence fits with the study area better than Eq. 4.6.

Table 4.17 Summary of TIA and EIA of study area for the years 2006 and 2011

Classification	In 2006				In 2011			
	TIA (%)	EIA (%)			TIA (%)	EIA (%)		
		by direct method	using Eq. 4.6	using Eq. 4.8		by direct method	using Eq. 4.6.	using Eq. 4.8
Cl 1	24.8	3.02	9.43	2.39	36.4	4.46	16.05	4.9
Cl 2	30.8		12.57	3.5	42.18		19.53	6.4
Cl 3	28.5		11.34	3.05	40.0		18.15	5.8
Cl 4	29.26		12.28	3.47	40.7		18.74	6.1
Cl 5	31.9		13.76	3.95	43.32		20.5	6.9
Cl 6	30.01		12.88	3.63	41.48		19.38	6.4

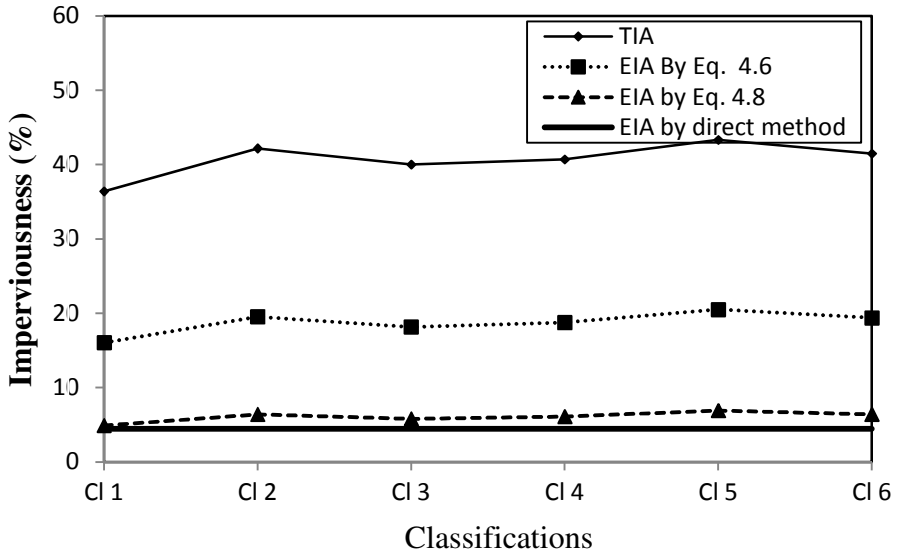

Fig. 4.25 TIA and EIA of the study area in 2011 for different type of classifications

4.8 Comparison of Coarse and Fine Resolution Imageries for the Determination of Imperviousness

Since the images of the study area of different spatial resolution (30 m and 5 m) are available for the same year (2006), the capability of poor resolution (30 m) imageries for urban classification can also be analyzed. For this purpose the imperviousness determined from coarse resolution image and fine resolution image of the year 2006 has been used and the results are presented in Table 4.18 (all land use classes) and Table 4.19 (for TIA and EIA). Since analysis of Landsat imagery has been done by applying zero threshold for all the classes, Cl 1 (zero thresholds, without GIS data) and Cl 4 (zero thresholds, with GIS data) have been used for comparison purpose in the case of fine resolution imagery.

Table 4.18 Comparison of land use of study area for the year 2006 from Landsat ETM+ image (30 m resolution) and IRS LISS-4 image (5 m resolution)

Land cover type		Landsat-2006		LISS-4-2006			
				Cl 1		Cl 4	
		Area (km^2)	Area (%)	Area (km^2)	Area (%)	Area (km^2)	Area (%)
Builtup area	Impervious area	46.68	20.49	56.48	24.8	66.67	29.26
Swampy/marshy land	Pervious area	45.5	19.97	59.18	25.97	51.28	22.5
Scrub land		41.93	18.4	50.839	22.31	49.733	21.83
Agricultural land		38.12	16.73	25.9	11.37	25.2	11.07
Grass land		12.96	5.7	5.45	2.4	5.65	2.5
Forest		26.9	11.8	26.85	11.78	25.85	11.34
Water body		4.72	2.07	3.111	1.37	3.427	1.5

From Table 4.18 it can be observed that the impervious class (built up area) is under estimated and the pervious classes are over estimated in Landsat image. Underestimation of builtup area is due to the sparsely located small settlements which are misclassified as vegetation in coarse resolution imagery. Also since the collection periods of both the images are different, a large change in vegetation was found. While analyzing the classification result of Landsat-2006 image it should be kept in mind that, an area of approximately 11 km^2 is covered by cloud in the said image. Comparing the classified image of 2006 (Fig.4.6 c (i)) and it's immediate past counterpart of 2004 (Fig. 4.6 b (iii)), it can be predicted that the cloud cover area is mostly scrub

land. Hence a remarkable difference in scrub land is found. Various land covers of the study area obtained from different resolution imageries for the year 2006 are also plotted in Fig. 4.26. It is noticed from Fig. 4.26 that built-up area shows maximum distinction and forest land cover shows least distinction with respect to the spatial resolution of the satellite image. As the GIS data used buildings and road network, it will have least impact on land covers like forest and water body as is evident from Fig. 4.26.

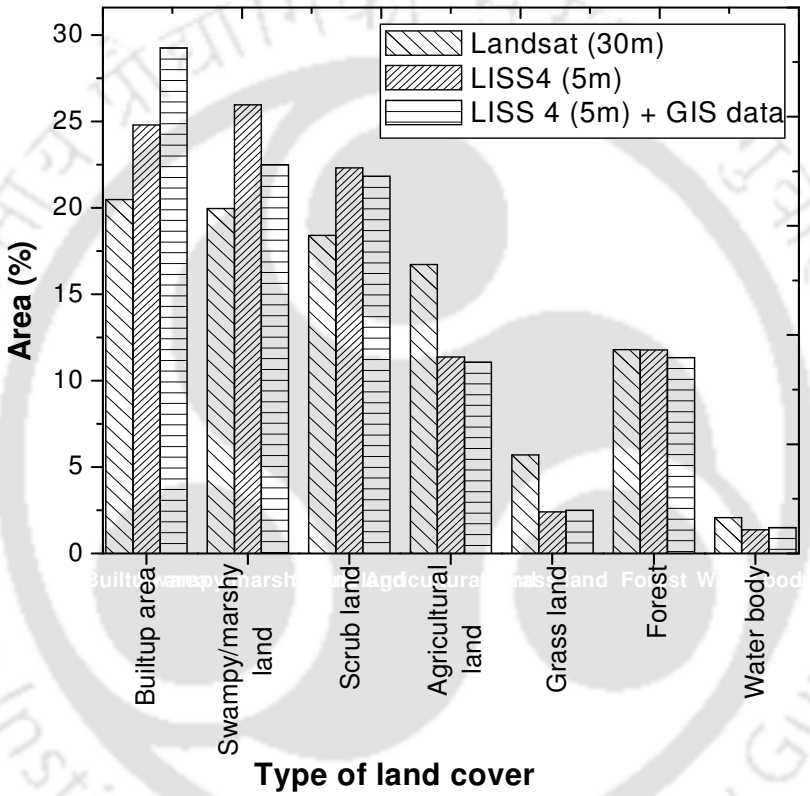

Fig. 4.26 Comparison of land use of study area for the year 2006 obtained from coarse and fine resolution imagery

A comparison is presented in Table 4.19 between the TIA and EIA values of the study area obtained from different spatial resolution imageries. It can be observed from Table 4.19 that TIA estimated by coarse resolution imagery are 17.4% less than the corresponding estimation by fine resolution imageries without using GIS data and with zero thresholds applied. However if GIS data are used, fine resolution imagery estimates TIA 30% more than that of the coarse resolution imagery. EIA value estimated by using Eq. 4.6 was found to be 12.38% more in coarse

resolution imagery than that of the fine resolution imagery if image classification is not supported by GIS data. EIA value estimated by using Eq. 4.6 was found to be 13.69% less in coarse resolution imagery than that of the fine resolution imagery if image classification is supported by GIS data. Also it is observed that EIA estimated by Eq. 4.6 from coarse resolution imagery is 251% more than the directly estimated EIA and EIA estimated by Eq. 4.8 from coarse resolution imagery is 39% more than the directly estimated EIA of the study area.

Table 4.19 Comparison of EIA of Guwahati city for the year 2006 from Landsat ETM+ image (30 m resolution) and IRS LISS-4 image (5 m resolution)

Image type		TIA (%)	EIA (%)		
			By direct method	using Eq. 4.6	using Eq. 4.8
Landsat ETM+ of 2006		20.49	3.02	10.6	4.2
IRS LISS-4 of 2006	Cl 1	24.8		9.43	2.39
	Cl 4	29.26		12.28	3.47

Chapter 5

Infiltration Characteristics of the Study Area

5.1 General

Infiltration is the process whereby water enters the soil from surfacial sources, such as flooding, snowmelt, irrigation, liquid waste spills, etc. (Stephens 1995). Thus infiltration rate is the volume rate of water flowing into a unit area of soil surface. The infiltration in any geometry is controlled by many factors, such as the rate of water application, antecedent moisture in the soil, soil hydraulic properties, topography etc. Infiltration is considered as a major hydrologic process controlling the amount of runoff and is difficult to estimate due to its spatial and temporal variability. Many empirical (Horton 1933) and physically based models (Green and Ampt 1911; Richards 1931; Philip 1957) have been developed to understand infiltration of water into soil (Habili and Heidarpour 2011). The infiltration parameters are normally determined through model calibration (Jain and Kumar, 2006) or field measurements (Bouwer et al., 1999). Traditionally infiltration rates have been determined with cylinder infiltrometers (Bouwer 1986). To eliminate the effects of divergence on the measured infiltration, the double ring infiltrometer was introduced (Bouwer 1986, 1994). In ring infiltrometers, water at atmospheric pressure is allowed to infiltrate into the underlying soil. Once the rate of infiltration has stabilized, this steady infiltration rate is then measured and used to compute the saturated hydraulic conductivity. However, because water is ponded on the soil surface with ring infiltrometers, a large portion of the water might infiltrate through cracks or wormholes (macropores), and thus result in over prediction of saturated hydraulic conductivity values (Cameira et al., 2000), which are not representative of the soil matrix. Hence by maintaining a small negative pressure (or tension) on the soil as water is infiltrating, water will not enter the large cracks or wormholes, but will infiltrate through the soil matrix. This is achieved by use of a tension infiltrometer (TI). Thus tension infiltrometer excludes the macropore effect in the flow process and the measurements obtained with this are more representative of the soil as a whole. Conventional methods of infiltration measurement are applicable for full saturation conditions only. However, TI is capable for measuring infiltration corresponding to near saturation conditions as well.

Accurate determination of infiltration characteristics of soil being indispensable for flood management, an effort has been made in the current study to determine infiltration characteristics by using a tension infiltrometer. Many earlier reported studies deal with the determination of soil hydraulic properties from TI tests conducted in the field (Bodhinayake et al., 2004; Yoon et al., 2007) and laboratory (Schwartz and Evett, 2002). Since field methods are considered more realistic (Ramos et al., 2006) than laboratory methods, it is preferred in the present study. The details of the measuring methodology and the test set up adopted are presented in the following sections. The details obtained from this study would be quite helpful for flood modeling as realistic infiltration characteristics of the catchment are being incorporated.

5.2 Tension Infiltrometer (TI)

The Tension Infiltrometer (TI) attachments (2825K1 Tension Infiltrometer, Soilmoisture Equipment Corporation, USA) shown in Fig. 5.1. It consists of three major components namely, Guelph permeameter reservoir assembly, infiltrometer foot assembly and Marriot bubbler assembly.

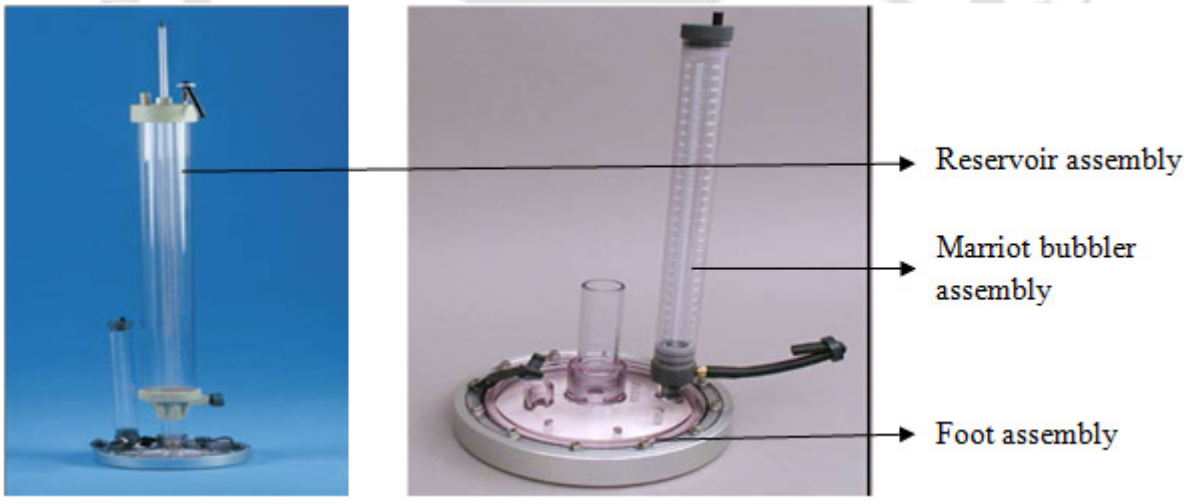

Fig. 5.1 Parts of Tension Infiltrometer

5.3 Working Principle of Tension Infiltrometer

The saturated hydraulic conductivity of soils is often determined with single or double ring infiltrometers (Scotter et al. 1982; Bouwer et al. 1999) in contrast with the tension

infiltrometers, which are designed to measure the unsaturated hydraulic properties of soils as well. In tension infiltrometer water is allowed to infiltrate the under lying soil at a slower rate than the infiltration rate that would have been established when water is ponded on the soil surface. This is accomplished by maintaining a small negative pressure (tension) on the water as it moves out of the infiltrometer disc into the soil. Water can only flow out of the infiltrometer disc at the base and infiltrate into the soil, if air can enter the sealed reservoir through a narrow tube in which the tension is Ψ. This capillary attraction of water into the air entry tube means that the soil has to suck with a pressure head 'Ψ' to get the water out of the basal disc. The tension infiltrometer works on this principle (shown in Fig. 5.2) and the Marriot bubbler (Bubble Tower in the figure) establishes the required tension head. Perroux and White (1988) incorporated these principles and developed tension disk permeameter.

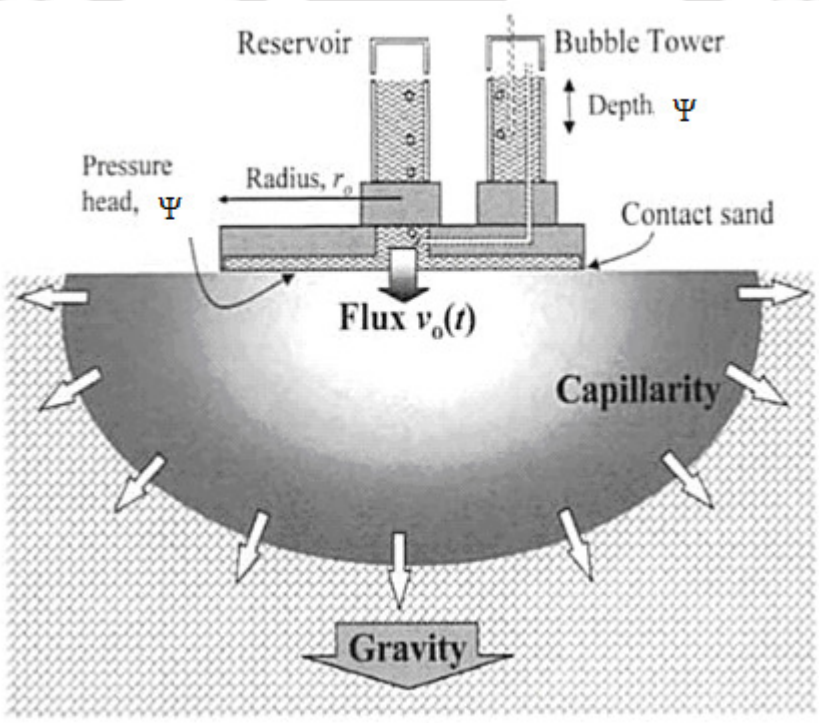

Fig. 5.2 Transverse section through a disk permeameter of radius r_0 (Smith and Mullins 2001)

In situ test with TI ensures a minimum degree of disturbance to the soil structure. The flow of water beneath the tension infiltrometer disk is three dimensional. The three dimensional wetting under the tension infiltrometer disk (Clothier and Scotter 2002) is schematically shown in Fig. 5.3. This flow into unsaturated soil reflects the dual influences of soil's capillarity and of

gravity and can be described by Richard's equation (Eq. 5.1) (Warrick 1992; Angullo-Jaramillo et al. 2000).

$$C(\Psi)\frac{\partial \Psi}{\partial t} = \frac{\partial}{\partial z}\left[K(\Psi)\left(\frac{\partial \Psi}{\partial z} - 1\right)\right] + \frac{\partial}{\partial r}\left[K(\Psi)\frac{\partial \Psi}{\partial r}\right] + \frac{K(\Psi)}{r}\frac{\partial \Psi}{\partial r} \qquad (5.1)$$

where $C(\Psi) = d\theta/d\Psi$ is the soil water capillary capacity function; θ is the volumetric water content; Ψ is the water pressure head; $K(\Psi)$ is the hydraulic conductivity function; r and z are radial and vertical coordinates respectively.

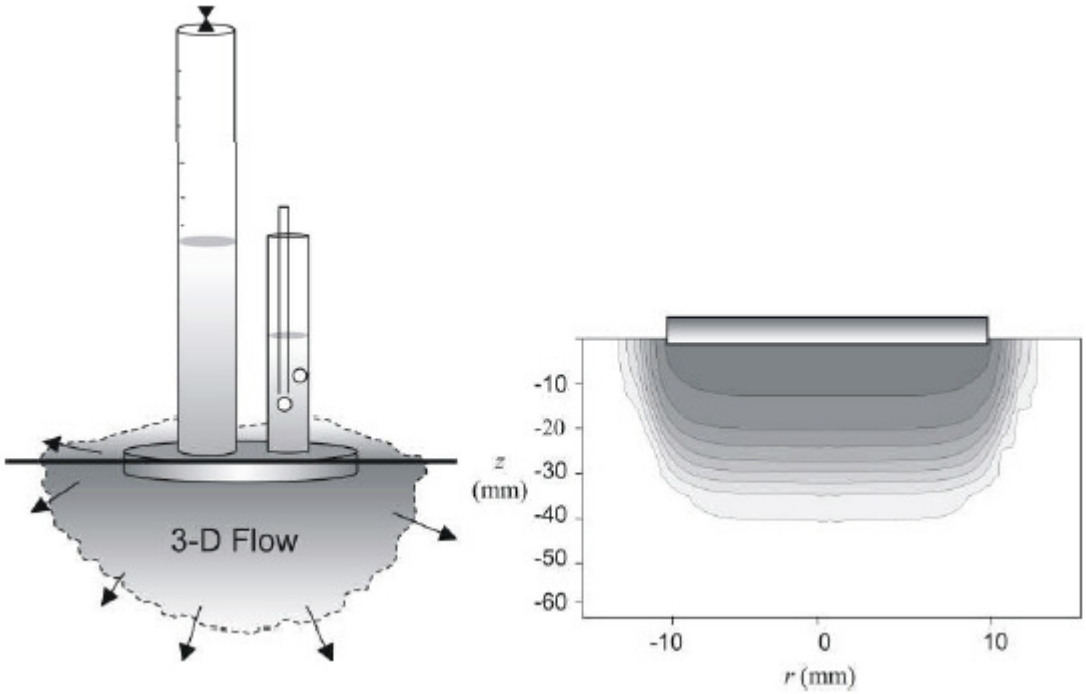

Fig. 5.3 Three dimensional wetting under tension disk infiltrometer (Clothier and Scotter 2002)

Eq. 5.1 can be solved to obtain soil hydraulic properties by taking measurements of either steady flow rate or transient flow rates from TI experimental observations. In the current study, steady state flow rates have been measured for two tension heads and the soil hydraulic properties have been calculated (Ankeny et al. 1991) as described in the next section.

5.4 Field Experiments Carried out with Tension Infiltrometer

To deal with the spatial variability of infiltration characteristics, the experiments have been carried out at 14 different locations of the study area as shown in Figs. 5.4 and 5.5. Care has

been taken to carry out experiments at locations that are subjected to least possible intervention due to human activities.

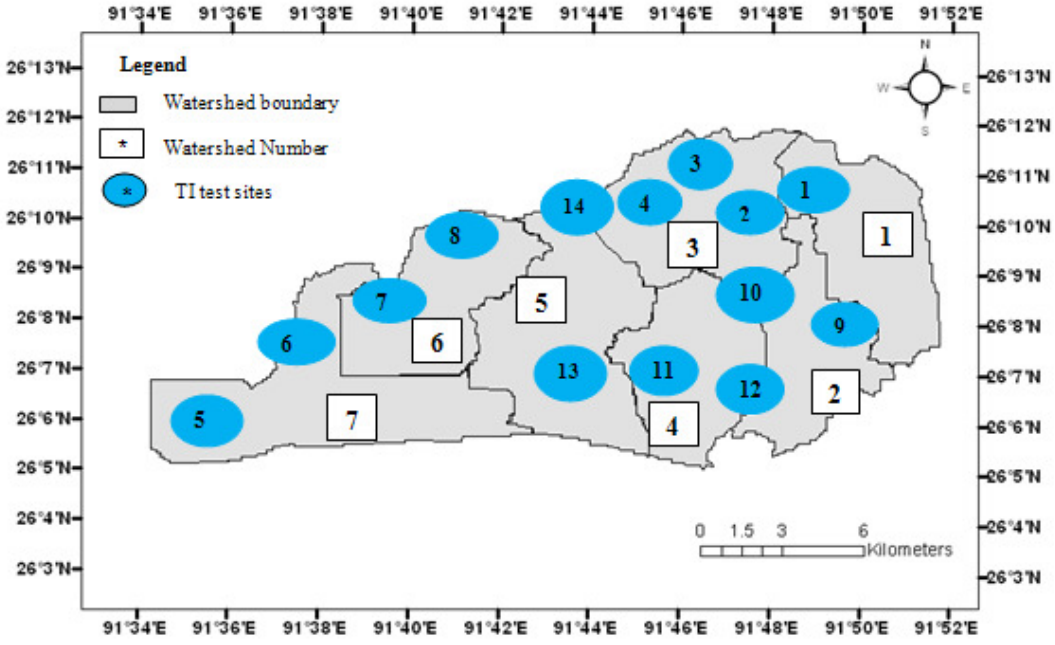

Fig. 5.4 Location of 14 TI test sites in 7 watersheds of the study area

Fig.5.5 TI tests carried out in the field

In the field, three components of the equipment were assembled and the reservoir assembly was filled with water with the help of supplied vacuum hand pump. The Marriot

bubbler is then filled with water and the head is adjusted to the desired level of tension head. Before operating the TI, all entrapped air bubbles were removed from the foot assembly and the Marriot bubbler. A sequence of TI measurements was taken for tension equal to 20 cm, 10 cm, 2 cm and 0 cm at all the measuring location. Prior to the experiments, the selected site was scraped and made level. 2 mm thick layer of fine sand (of diameter = 0.1–0.4 mm) was then laid over the scrapped surface to ensure proper contact between the base membrane of the TI and the soil surface (Bagarello et al. 2000; Wahl et al., 2004; Ramos et al., 2006). The infiltrometer base was placed onto the sand surface. Care was taken that the base plate of TI was level.

The rate of water level drop against time is then recorded till it attains a constant rate, which is called steady state infiltration. A sequence of measurements of steady state flows Q_{s1} and Q_{s2} were taken at successive potentials Ψ_1 and Ψ_2 respectively using tension infiltrometer at a single location. The use of single infiltration radius at different tensions in a single location minimizes the disturbance that might be there due to repeated equipment setup (Joel and Messing 2000). From the steady state flow values obtained from the TI readings, the saturated hydraulic conductivity (K_s) and unsaturated hydraulic conductivity (K) were calculated (Ankeny et al. 1991) for different tension heads making use of the following equations.

$$K(\Psi_1) = \frac{Q_{s1}}{\pi a^2 + 2\Delta\Psi\, a\left(\frac{Q_{s1}+Q_{s2}}{Q_{s1}-Q_{s2}}\right)} \tag{5.2}$$

$$K(\Psi_2) = K(\Psi_1)\frac{Q_{s2}}{Q_{s1}} \tag{5.3}$$

Corresponding values of sorptivity number ($\propto$) and saturated hydraulic conductivities were then calculated from Eqs. 5.4 and 5.5 respectively.

$$\frac{1}{\propto} = \Delta\Psi \frac{K(\Psi_1) + K(\Psi_2)}{2\lceil K(\Psi_1) - K(\Psi_2)\rceil} \tag{5.4}$$

$$K = K_s \exp(\propto \Psi) \tag{5.5}$$

where K_s is saturated hydraulic conductivity; Ψ_1 and Ψ_2 are tension heads; $K(\Psi_1)$ and $K(\Psi_2)$ are unsaturated hydraulic conductivities at tension heads of Ψ_1 and Ψ_2 respectively; Q_{s1} and Q_{s2} are

steady state flow rate at tension heads of Ψ_1 and Ψ_2 respectively; a is radius of disc of tension infiltrometer = 10 cm; $\propto$ is sorptivity number.

There are various means by which tension infiltrometer observations can be used to infer the soil's hydraulic character. Here steady state readings have been taken. However first few minutes readings can be taken as early time readings or short time observations and can be used to calculate sorptivity (S) (Perroux and White, 1988) at a particular tension value. Hence sorptivity at different tension heads can be calculated by Eq. 5.6.

$$S(\Psi) = \frac{I}{\sqrt{t}} \qquad (5.6)$$

where I is cumulative infiltration in cm; t is cumulative time. So a plot is made between I and $\sqrt{t}$ and the slope of the curve for initial time was found out to be the sorptivity (Zhang 1997) at that tension head.

5.5 Infiltration Result

The infiltration characteristics obtained by conducting field tests with the help of TI are presented in Table 5.1.

Table 5.1 Spatial variation of infiltration characteristics of study area

Sl. No.	Experimental site	Hydraulic Conductivity K(mm/hr) at different suction heads (Ψ)				Sorptivity at zero suction (cm/$\sqrt{s}$)
		Ψ = 0 mm	Ψ = 20 mm	Ψ = 10 cm	Ψ = 20 cm	
1	Noonmati	64.8	57.7	19.32	4.5	0.002
2	Geetanagar	19.44	17.05	5.68	2.3	0.009
3	Silpukhri	72	68.8	12.78	4.3	0.006
4	Ulubari	75.6	65.26	15.34	6.45	0.008
5	Airport	60.12	51.17	11.17	2.79	0.009
6	Azara	25.2	18.61	6.15	3.1	0.005
7	AEC	61.2	58.39	25.3	8.7	0.009
8	Maligaon	6.48	4.48	1.9	0.78	0.006
9	Kalakshetra	46.9	42.3	10.9	4.3	0.098
10	Secretariate	30.24	28.07	4.81	1.39	0.037
11	I G Stadium	50.4	44.3	7.1	2.8	0.012
12	Brahmaputra Board	46.8	39.7	9.2	4.6	0.008
13	Balaji Temple	46.8	38.3	12.55	3.9	0.009
14	Bharalumukh	6.48	3.31	2.1	0.64	0.026

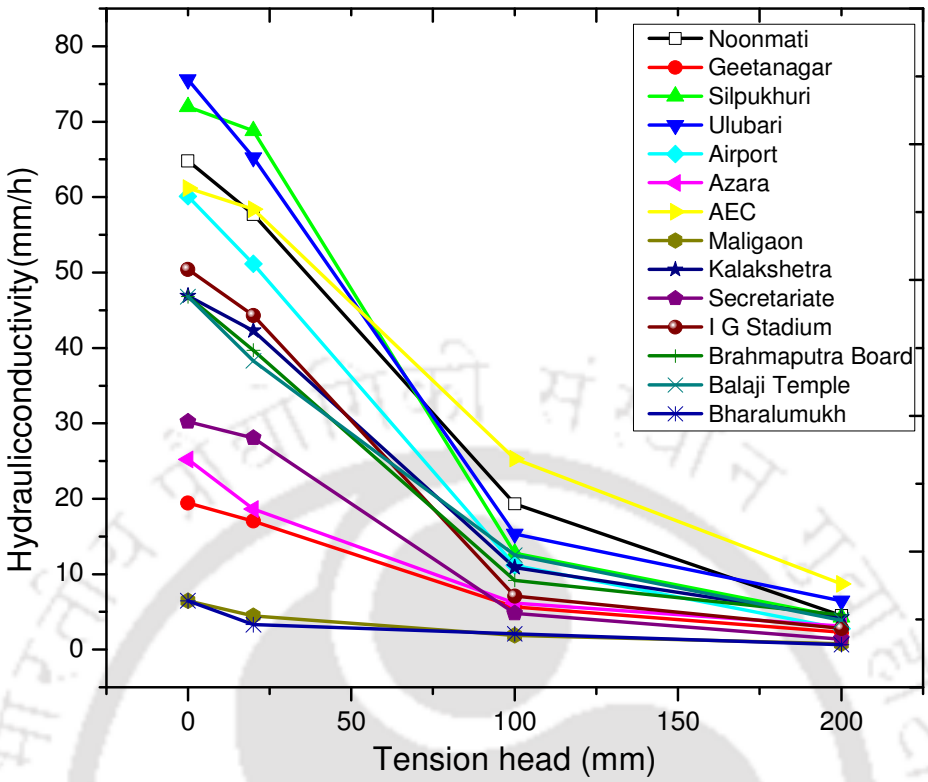

Fig. 5.6 Variation of saturated hydraulic conductivity in the study area

From Fig. 5.6 it is observed that the saturated hydraulic conductivity (hydraulic conductivity at zero tension head) varies from 6.48 mm/hr to 75.6 mm/hr for the study area. The hydraulic conductivity has been found to decrease with increase in tension heads. Also it is noticed that the variation in hydraulic conductivity is much at low tension heads and is less at high tension heads.

5.6 Green Ampt Infiltration Parameters for the Study Area

For runoff simulation in SWMM (Storm Water Management Model, Rossman 2005), the infiltration can be modeled by Horton Method, Green Ampt method or by Curve Number Method. Green Ampt model being a physically based method allows more flexibility (Jumadar et al., 2008) in application. Moreover Green Ampt parameters can be easily determined from the TI test readings conducted at various places in the study area. Hence it is adopted in the present study for infiltration modeling. The Green Ampt parameters required in SWMM for infiltration modeling are suction or tension head (Ψ), saturated hydraulic conductivity (K_s), and initial

moisture deficit. 'K_s' has been calculated above from the TI readings for a particular Ψ value. Soil samples were collected before and after conducting the test at each site for determining moisture content. The type of soil has been assessed from the soil map collected for the study area. The porosity value for that type of soil has been approximately obtained from the literature (Rawls et al. 1983). The difference between the porosity value and the initial moisture content obtained before the test, gives the fraction of soil moisture deficit. Thus the following Green Ampt parameters (Table 5.2) were calculated for the study area.

Table 5.2 Green Ampt model parameters for the study area

Watershed No.	Location	Soil type from soil map	Tension head (Ψ) in mm	K_s in mm/hr	Moisture deficit
1	Noonmati	Clay loam	0	64.8	0.350
2	Kalakshetra	Clay Loam	0	46.9	0.305
	Secretariat	Silty Clay	0	30.24	0.314
3	Geetanagar	Clay Loam	0	19.44	0.253
	Silpukhuri	Clay Loam	0	72	0.344
	Ulubari	Silty Clay	0	75.6	0.385
4	I G Stadium	Sandy Loam	0	50.4	0.232
	Brahmaputra Board	Clay Loam	0	46.8	0.305
5	Balaji Temple	Sandy Loam	0	46.8	0.273
	Bharalumukh	Sandy Clay	0	6.48	0.272
6	A E C	Sandy Loam	0	61.2	0.343
	Maligaon	Clay Loam	0	6.48	0.354
7	Airport	Sandy Loam	0	60.12	0.361
	Azara	Sandy Clay Loam	0	25.2	0.282

Green Ampt parameters obtained above are employed in the runoff simulation model (described in chapter 6) for obtaining a realistic flooding scenario.

Chapter 6

Impact of Imperviousness Determination on Urban Flood Modeling

6.1 General

Flood is the result of a complex interaction among components like rainfall, land use, soil type, topography and drainage capacity in a watershed. These components are connected by hydrological processes like infiltration, depression storage, evapotranspiration, surface runoff and ground water flow, which are depicted in Fig. 6.1. The issue of flooding in urban watershed is more severe due to increased imperviousness. The growth of infrastructure such as drainage facilities in urban cities of developing countries like India does not keep adequate pace with the rapid urbanization resulting in artificial floods. For proper flood management strategies to be undertaken in urban watershed, precise estimation of flood depth and its dependence on rainfall intensity and rapidly changing imperviousness is essential. The estimation of flood depth using hydraulic models depends on the inflow hydrographs determined by the hydrological models. This chapter investigates the role of imperviousness determination and rainfall events on flood modeling of the urban study area. The main objective is to quantify the increase in run off (flooding) due to a certain increase in imperviousness and corresponding to a particular rainfall event. These results will be used to identify flood risk zones and for suggesting suitable flood management strategies in the next chapter.

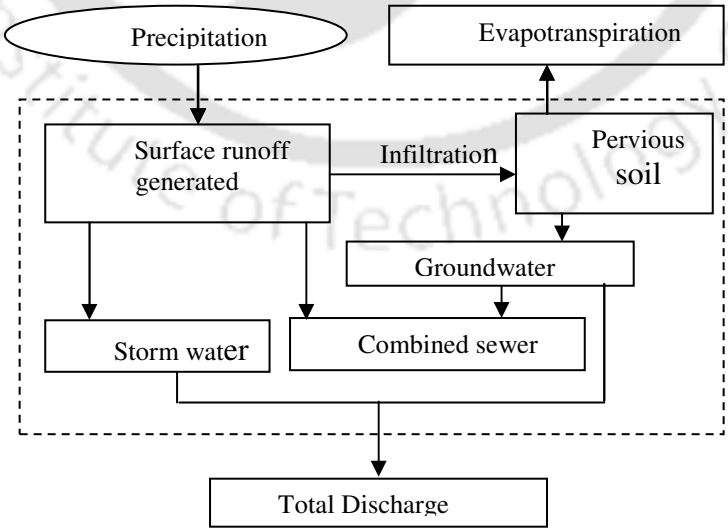

Fig. 6.1 Visualization of hydrologic processes in a watershed

6.2 Description of the Hydrologic Model

There are different types of hydrologic models available for runoff simulation that differs in terms of required inputs, representation of hydrologic process and algorithms for calculating outputs. The model's utility may vary depending on the characteristics of the watershed, availability of data and the objectives of the user. In the present study, Storm Water Management Model (SWMM) has been chosen because of its success in hydrologic modeling of urban watersheds (Delleur 2003; Spry and Zhang 2006). SWMM developed by EPA (Environmental Protection Agency, USA) is a dynamic rainfall-runoff simulation model that computes runoff originating primarily from urban areas due to single or continuous rainfall events (Rossman 2005).

Wang and Altunkaynak (2012) have used SWMM to predict total runoff in an urban watershed in Italy. The study demonstrated that the predicted runoff is in good agreement with the observed runoff as well as the runoff estimated by fuzzy logic approach. Barco et al. (2008) employed SWMM for runoff simulation in a large urban watershed in California and observed that the model predicts the observed runoff with reasonable accuracy. Also in their study SWMM model has been found to be more sensitive to imperviousness and least sensitive to Manning's roughness coefficient for generation of surface flow. Such a finding justifies the use of SWMM for present study where the role of imperviousness on runoff is of prime importance. Warwick and Tadepalli (1991) investigated the efficacy of SWMM for runoff simulation in an urban watershed Dallas, Texas and the performance was found to be well with good forecasting efficiency for both runoff volume and peak runoff prediction. These studies show that SWMM is a widely accepted hydrologic model for runoff simulation in urban areas. Moreover surface runoff in SWMM is simulated by considering the watershed as a non linear reservoir. Since non linear reservoir method does not take into account the time of concentration of the watershed, it simulates the runoff in urban watersheds with higher accuracy where time of concentration is relatively small (Xiong and Melching 2005). Hence in the current study SWMM has been chosen as the hydrologic model.

SWMM can also be used to simulate other aspects of hydrological and quality cycle like snow melt calculations, transport through drainage network, storage and receiving water effects etc. (Huber and Dickinson 1988). SWMM consists of several blocks, which need to be simulated separately. Blocks used in the current study are the runoff block for runoff estimation and

transport block for routing the estimated runoff to the common outlet point of the total watershed.

6.2.1 Runoff block

The runoff block generates hydrographs by inputting weather data like rainfall, evaporation etc. and a set of runoff parameters. These runoff parameters describe the physical characteristics such as area, width and slope of basin and hydrologic characteristics such as percentage of imperviousness, depression storage, Manning's roughness coefficient and infiltration parameters of the basin. These parameters vary in space and their heterogeneity can be captured by a process called model subdivision (Ghosh and Hellweger 2012). Hence, seven watersheds of the study area are divided into smaller sub watersheds by delineation process as described in section 3.5 to capture the effect of topography variation, land use variation, soil type variation on runoff. Each sub watershed is then modeled as a nonlinear reservoir with rainfall as input. Both the pervious and impervious areas of the watershed are characterized by a value of maximum depression storage, which represents the capacity of the nonlinear reservoirs (ASCE Manual 1992). Surface runoff occurs only when the depth of water in the reservoir is higher than the maximum depression storage. In pervious area, infiltration can be modeled by Horton's equation or by Green-Ampt's equation. The schematic representation of estimation of runoff using SWMM by following different physical processes is depicted in Fig. 6.2.

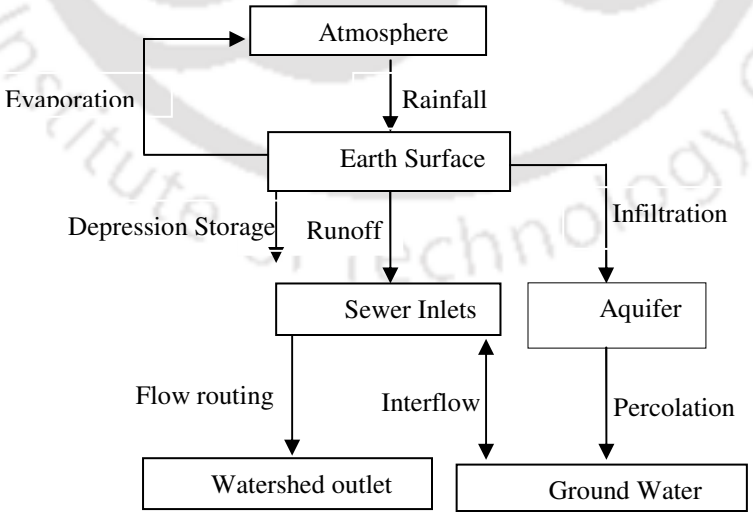

Fig. 6.2 Modeling processes in SWMM for the determination of runoff

The inflow to the SWMM comes from rainfall or snow melt or any upstream sub-catchment. The sub-catchment is treated as a non-linear reservoir whose capacity is taken as the maximum depression storage. Surface runoff, Q occurs only when the depth of water, d in the reservoir exceeds the maximum depression storage, d_p. The outflow is given by Manning's equation (Eq. 6.1).

$$Q = w \frac{1.49}{n} (d - d_p)^{5/3} S^{1/2} \quad (6.1)$$

where w is the sub-catchment's characteristic width, S is its slope, and n is the Manning's roughness coefficient. Depth of water over the sub-catchment is continuously updated with time by solving numerically the water balance equation (Eq. 6.2) over the sub-catchment.

$$P = Q + I + E \quad (6.2)$$

where P is the precipitation; Q is the surface runoff; I is the infiltration and E is the evaporation.

SWMM models the surface runoff as overland flow over the sub-catchment surface. In urban catchments, true overland flow can be very short before it is collected into open channels or pipes. Gironas et al. (2009) opined that a maximum overland flow length of 152.4 m or less is appropriate for urban catchments while the typical overland flow length is the length from the farthest point of a sub watershed to its outlet. Hence if the overland flow length varies greatly within the sub-watershed, then an area-weighted average should be used.

The physical characteristics such as area, width and slope of the sub-watersheds are determined using ArcGIS 9.3.1. The contour map was collected from the relevant municipal authorities and the DEM has been generated in the ArcGIS platform. Since SWMM uses the Manning's equation to compute the overland flow rate, the roughness coefficient of the sub-watersheds are taken same as Manning's roughness coefficient n. Manning's 'n' for impervious and pervious surfaces are taken as 0.01 and 0.1 corresponding to its value for asphalt/concrete and vegetation, respectively (McCuen et al. 1996). The values of depression storage for impervious and pervious areas are taken as 1.27 mm and 2.54 mm, respectively (ASCE Manual 1992). The impervious areas such as roofs and roadways, through which rainfall cannot infiltrate

are considered as TIA, which has been estimated as described in section 4.5. The percentage imperviousness is input to SWMM for estimating the runoff. Other hydrologic characteristics of the sub-catchments are defined by the following set of input parameters in SWMM.

Percentage of impervious area without depression storage

This parameter accounts for immediate runoff that occurs at the beginning of rainfall before depression storage is satisfied. It represents pavement close to the gutters that has no surface storage, pitched rooftops that drain directly to street gutters, new pavement that may not have surface ponding etc. Since no relevant data was obtained for this the default value of 25% is taken for each sub watershed (Rossman 2005).

Infiltration model

Three different methods for computing infiltration loss for pervious areas of sub-catchment are available in SWMM such as Horton, Green-Ampt and Curve Number. In this study, Green Ampt model has been adopted whose parameters have been determined by conducting field experiment as described in Chapter 5. The Green Ampt parameters listed in Table 5.2 are used in SWMM.

Precipitation input

Precipitation is the principal driving variable in rainfall-runoff simulation. The volume and rate of storm water runoff depends directly on the precipitation magnitude and its spatial and temporal distribution over the catchment. Each sub-catchment in SWMM is linked to a single rain gauge station located in that area. A continuous simulation has been done by considering the daily rainfall data from 1980 to 2012 as input file. Also rainfall events corresponding to high intensity (mentioned in section 3.3) have been inputted to study the flooding response of the catchment.

6.2.2 Transport block

The runoff simulated at the outlet of the sub watershed is used as the input for the subsequent transport block, which models the sewer system as a series of geometrical hydraulic "elements", that are nodes or conduits. Nodes provide the linkage among conduits and they consist of manholes, pump stations, storage units and flow dividers. The surface runoff is considered entering the sewer system at nodes. The existing drainage network details collected from Guwahati metropolitan development authority (GMDA) were used for hydraulic modeling

of the study area. All the conduit properties and the node properties were derived from the available drainage network details. The open channel properties considered in the current study are the length of the channel, roughness of the material of the channel, shape of the channel such as the width, side slope and depth. Most of the channels are found to be open rectangular channels, which are RCC (rectangular concrete channels) in some places and unlined channels in other places. The roughness values for the channel material were taken from ASCE Manual, (1982). The junction property includes only the elevation of the junction measured from sea level. This property has been derived from the available contour map of the study area.

The modeling of the transport of runoff is based on the Saint-Venant's continuity and momentum equations. SWMM can perform hydraulic routing by three different methods, namely, steady flow routing, kinematic wave routing and dynamic wave routing. Each of these routing methods employs Manning equation to relate flow rate to flow depth and bed (or friction) slope. Dynamic wave routing is the most powerful method of the flow routing because it solves the complete one-dimensional Saint Venant equations represented by Eqs. 6.3 and 6.4 for the entire conveyance network. This method can simulate all gradually-varied flow conditions observed in urban drainage systems such as backwater, surcharged flow and flooding. Hence this method of flow routing is employed in the current study to estimate the runoff at the watershed outlet.

$$\frac{\partial Q}{\partial x} + \frac{\partial A}{\partial t} = 0 \tag{6.3}$$

$$\frac{1}{A}\frac{\partial Q}{\partial t} + \frac{1}{A}\frac{\partial}{\partial x}\left(\frac{Q^2}{A}\right) + g\frac{\partial y}{\partial x} - g(S_0 - S_f) = 0 \tag{6.4}$$

where Q is the flow rate in the channel; A is the channel cross sectional area; y is the flow depth; S_0 is the channel bottom slope; S_f is the friction slope; g is the acceleration due to gravity; x is the distance along flow direction and t is the time.

6.3 Application of SWMM to the Study Area

The model is applied to the study area and runoff is simulated for two types of rainfall data as input, such as the continuous daily rainfall data from 1980 to 2012 and then for event wise rainfall data mentioned in section 3.3. A continuous hydrologic modeling synthesizes hydrologic processes and phenomena (response of the basin to a number of rain events and their cumulative effects) over a longer time period that includes both wet and dry conditions (Chu and Steinman 2009). To assess the change in runoff due to difference in land use caused due to rapid urbanization, continuous simulation has been performed in the study area. Event based hydrologic modeling reveals how a basin responds to an individual rainfall event (e.g., quantity of surface runoff, peak, time to peak, and detention, etc.). It is particularly useful for understanding detailed hydrologic processes like infiltration and surface runoff in a particular watershed (Daniel et al. 2010). In progressively urbanizing catchments, short duration high intensity rainfall are important for studying urban flooding attributed to increased imperviousness. However, this needs the input rainfall data in small time steps. The various simulated runoffs for different watersheds are presented in the following sections for continuous and event wise rainfall. Such a study would help to understand the extent of underestimation caused by considering continuous rainfall event for urban flood modeling.

6.3.1 Runoff simulation using continuous rainfall data

To assess the change in runoff produced due to land use change from 1980 to 2011, the runoff is estimated in the study area by using imperviousness determined as described in section 4.5 (chapter 4). Runoff has been simulated for total impervious area (TIA) and effective impervious area (EIA) to understand the amount of over prediction when the former is used instead of later. The daily rainfall data collected for the study area from 1980 to 2012 has been used in the model to simulate the runoff in different watersheds. Monsoon rainfall season starts in the study area from June and continues up to September. Most of the rainfall (about 900 mm) in this region occurs in the month of July and August. The runoff determined for continuous rainfall for different watersheds in the study area are presented as follows.

Fig.6.3 shows the variation of runoff in the monsoon season (1st June to 30th September) for the years 1980, 2006 and 2011 by considering TIA and EIA. EIA has been determined from Eq. 4.10 developed for the study area. In the absence of fine resolution imagery for the year 1980, it

is presumed that the same equation for EIA determination is valid. Comparatively high flood events occurred in the study area more frequently in 2006. By considering TIA, peak runoff of 16.26 m^3/s was observed on 29th July 1980, 36.3 m^3/s on 11th June 2006 and 48.58 m^3/s on 6th August 2011. The peak runoff was reduced to 7.59 m^3/s on 29th July 1980, 13.08 m^3/s on 11th June 2006, and 21.12 m^3/s on 6th August 2011 by considering EIA. These results indicate that the peak runoff estimated using TIA is 2.14 times than those estimated by EIA for the year of 1980, 2.78 times in 2006 and 2.3 times in 2011.

Figs. 6.4 to 6.9 shows the variation of estimated runoff in the monsoon season for the years 1980, 2006 and 2011 for watersheds 2 to 7, respectively by considering both TIA and EIA. The summary of peak runoff determined for different watersheds are listed in Table 6.1. It can be noted from Figures and table that runoff increases with time for all watersheds. With all other physical characteristics of the watershed remaining constant, the increase in runoff is a combined effect of the change in rainfall intensity and increase in imperviousness (attributed to urbanization). As expected, TIA overestimates peak runoff as compared to EIA predicted runoff for all watersheds and for years 1980, 2006 and 2011. Even though this is expected, the amount of such possible over prediction is not reported in the literature for urban catchments. It must be noted here that EIA is more hydrologically relevant than easily determined TIA. Such over prediction can have important consequence on flood management schemes to be proposed. It can be noted from Table 6.1 that the ratio of TIA runoff to EIA runoff gives an average value of 2.46. Irrespective of the year considered, land use and the rainfall, the runoff modeling result indicate that there is an overprediction in runoff by an average of 2.46 times if TIA is used instead of EIA. Such an overprediction will have high economical impact on the flood management schemes that need to be implemented for a particular urban area. The study clearly highlights the need to estimate EIA more precisely for an urban catchment for a realistic flood modeling.

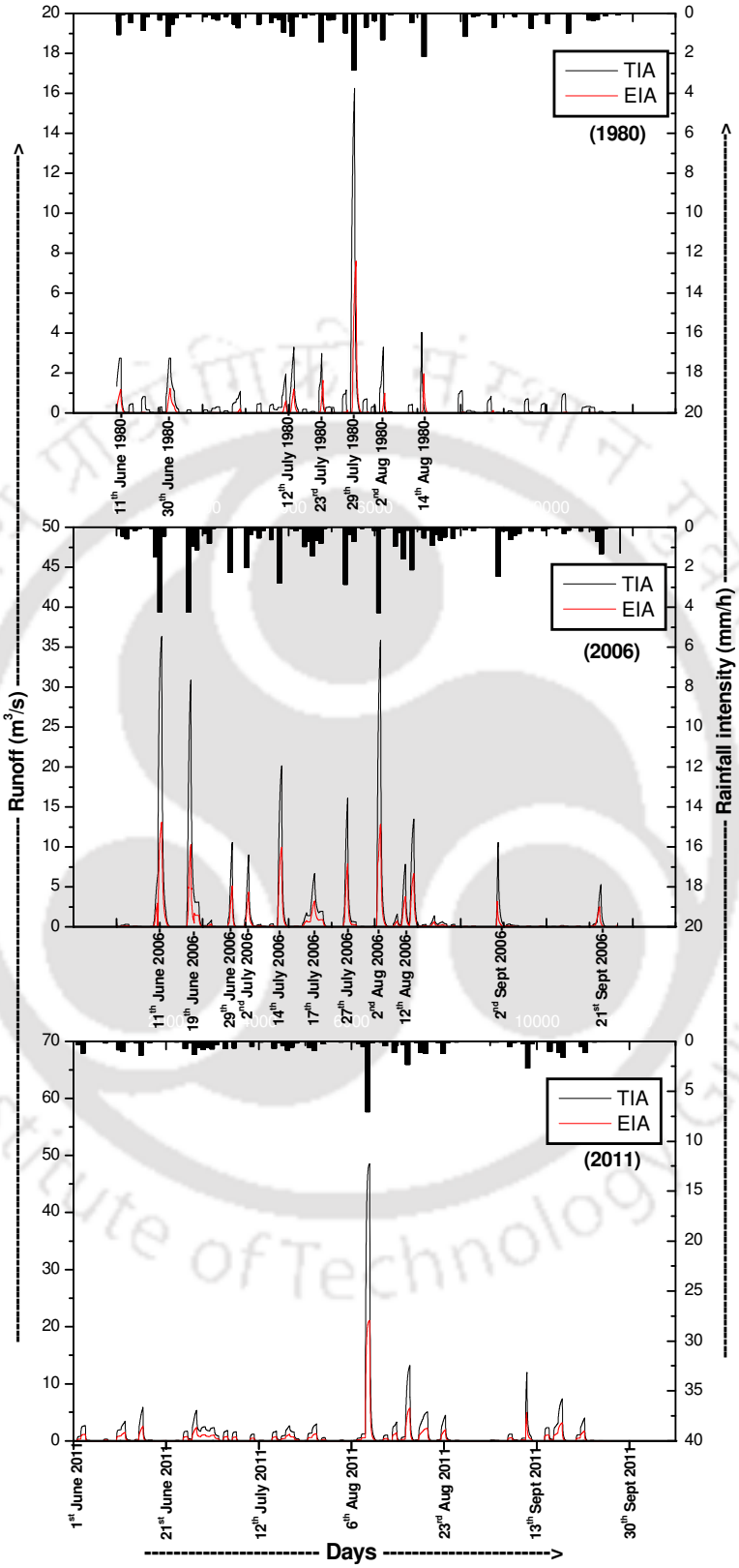

Fig. 6.3 Simulated runoff of watershed 1 using continuous rainfall data for TIA and EIA

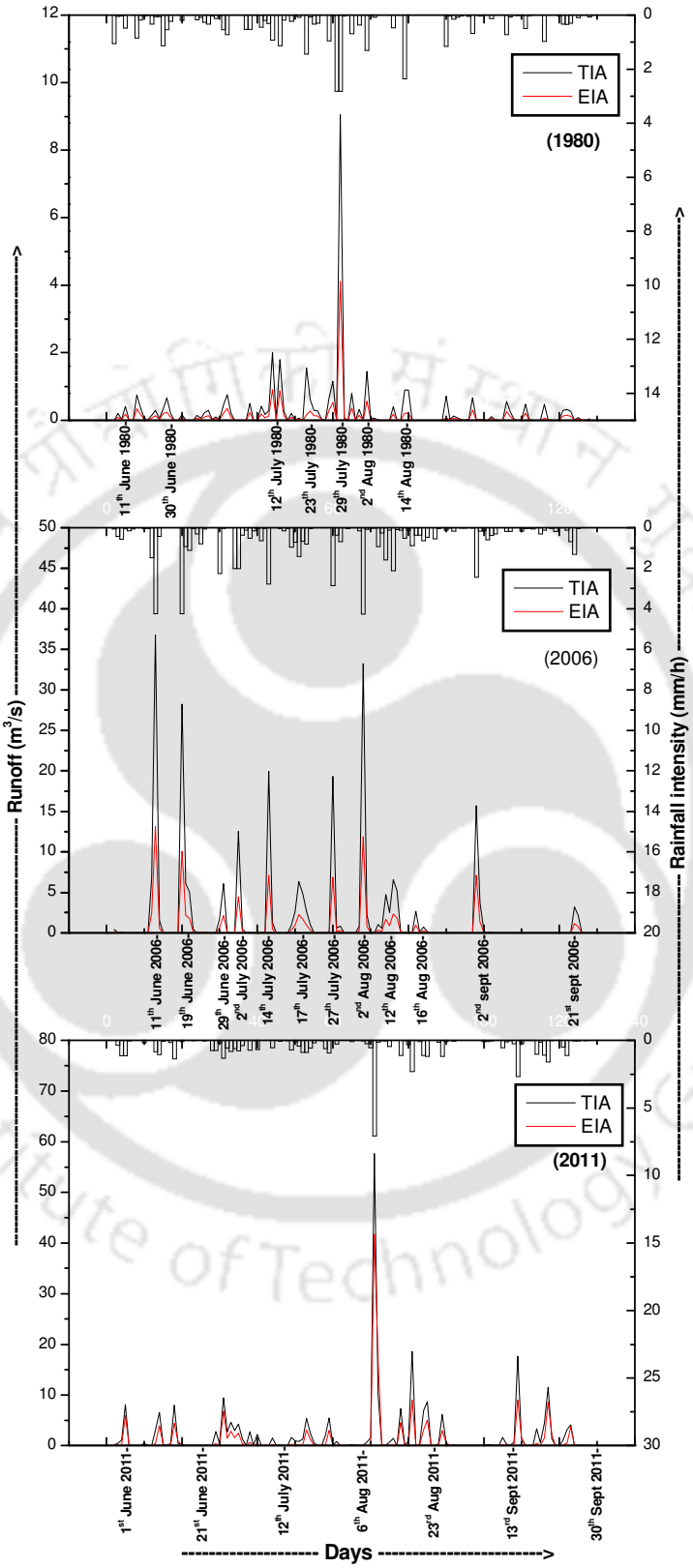

Fig. 6.4 Simulated runoff of watershed 2 using continuous rainfall data for TIA and EIA

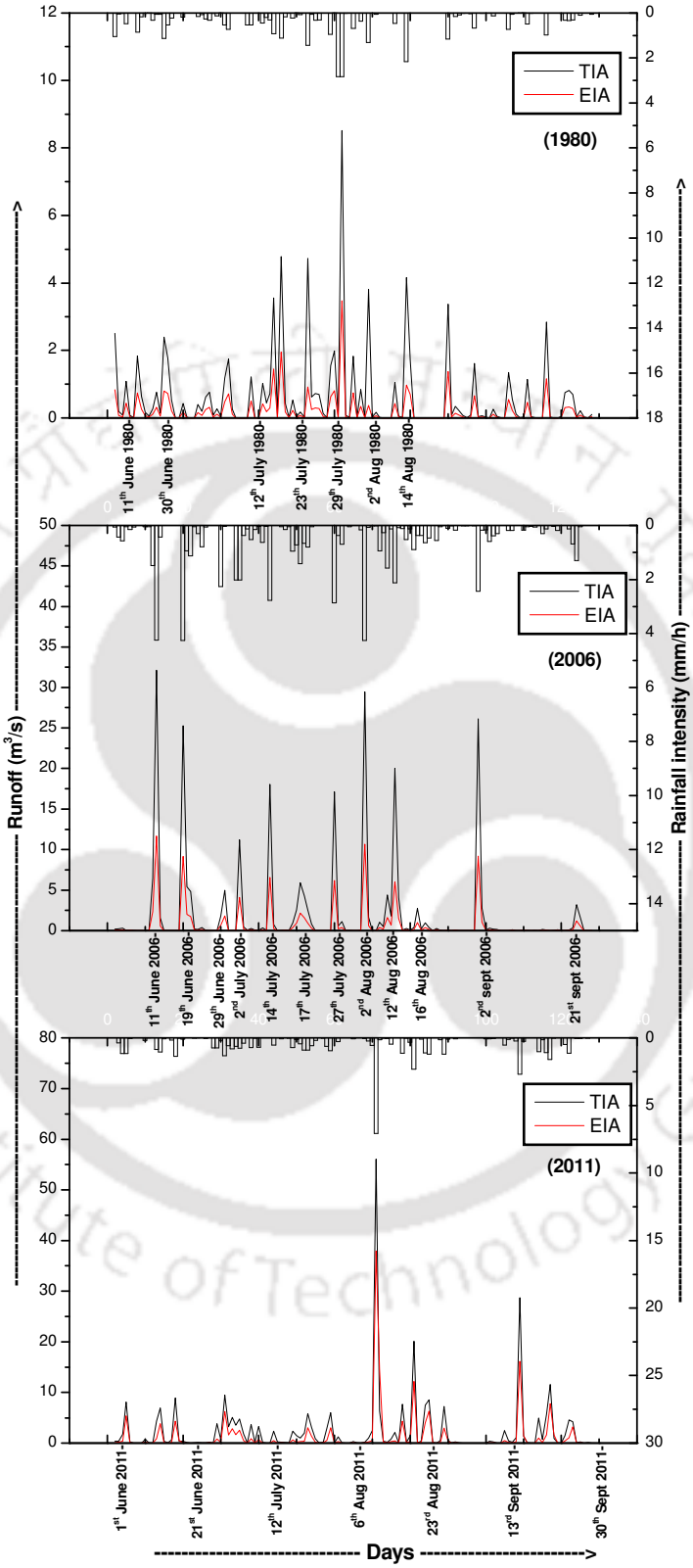

Fig. 6.5 Simulated runoff of watershed 3 using continuous rainfall data for TIA and EIA

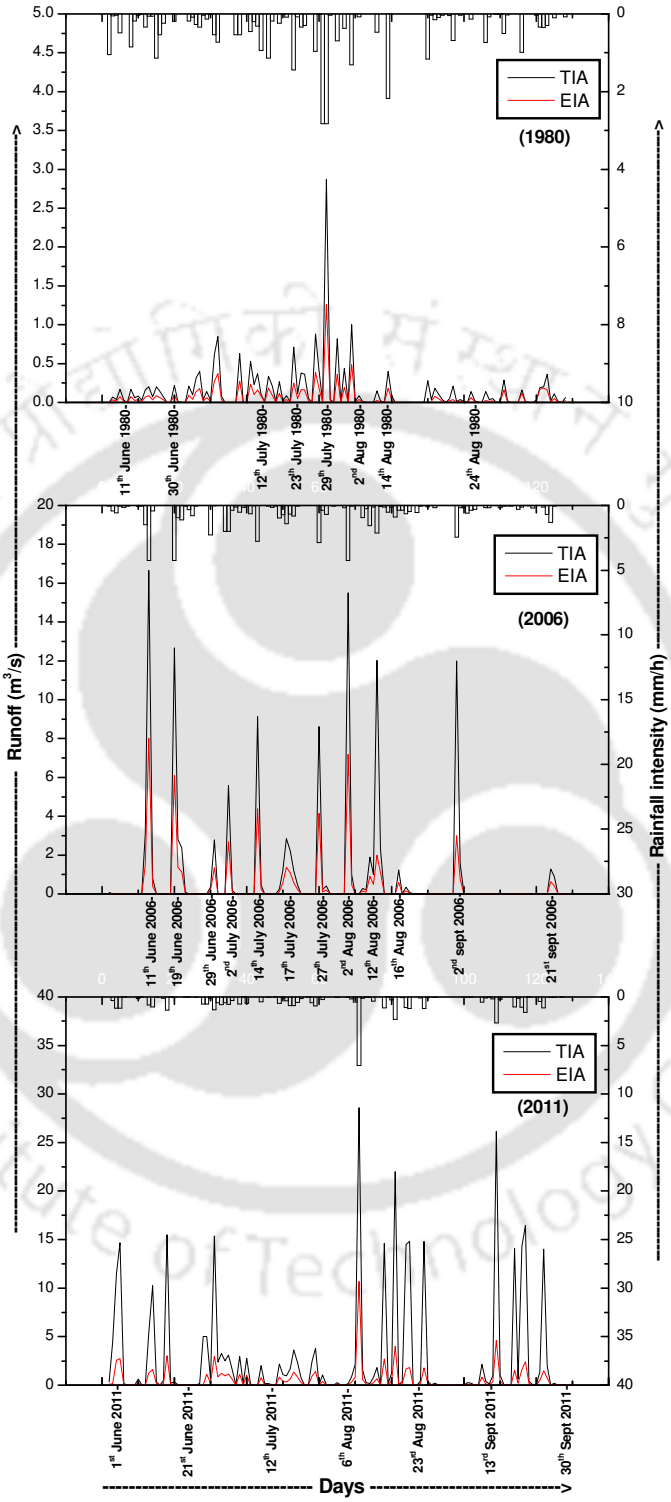

Fig.6.6 Simulated runoff of watershed 4 using continuous rainfall data for TIA and EIA

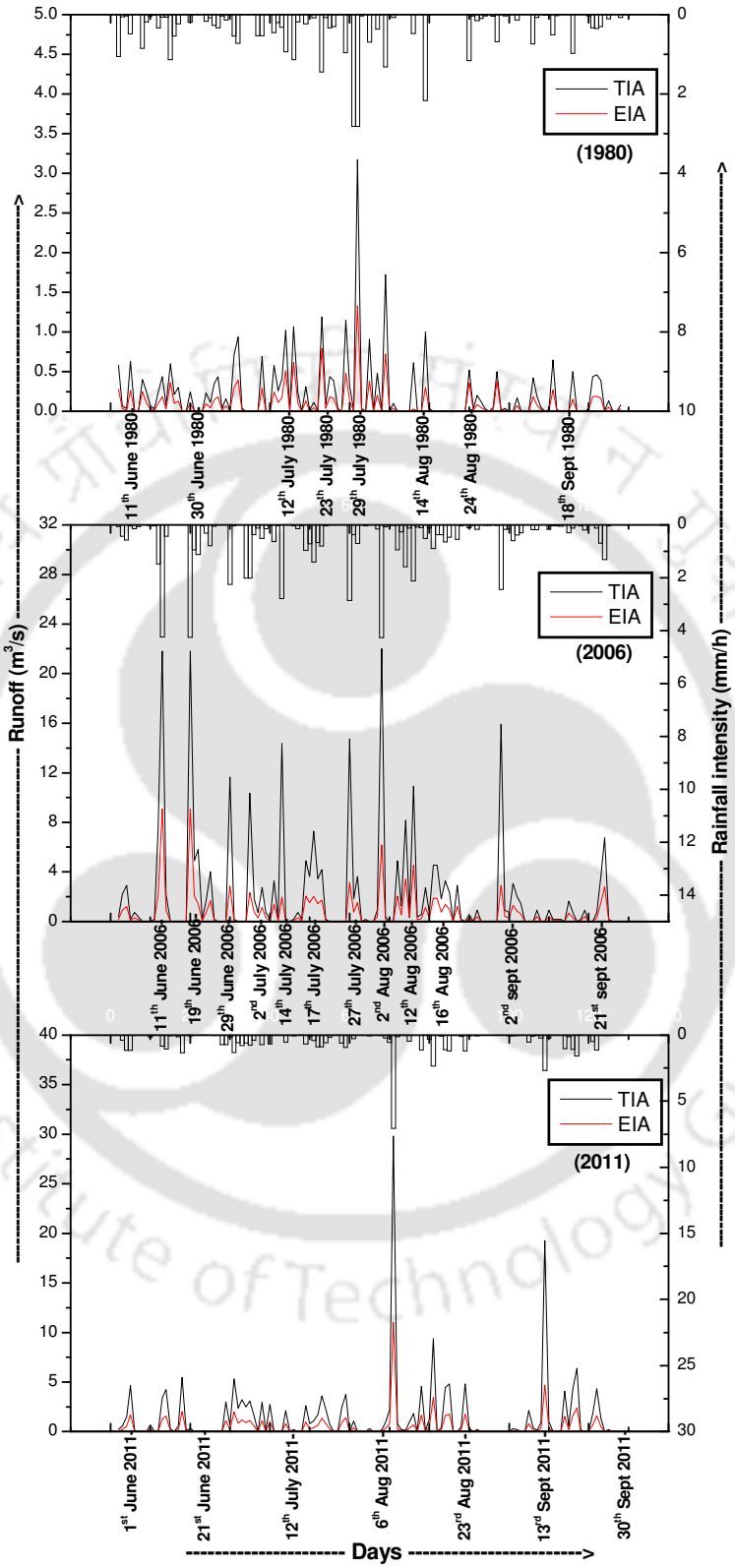

Fig. 6.7 Simulated runoff of watershed 5 using continuous rainfall data for TIA and EIA

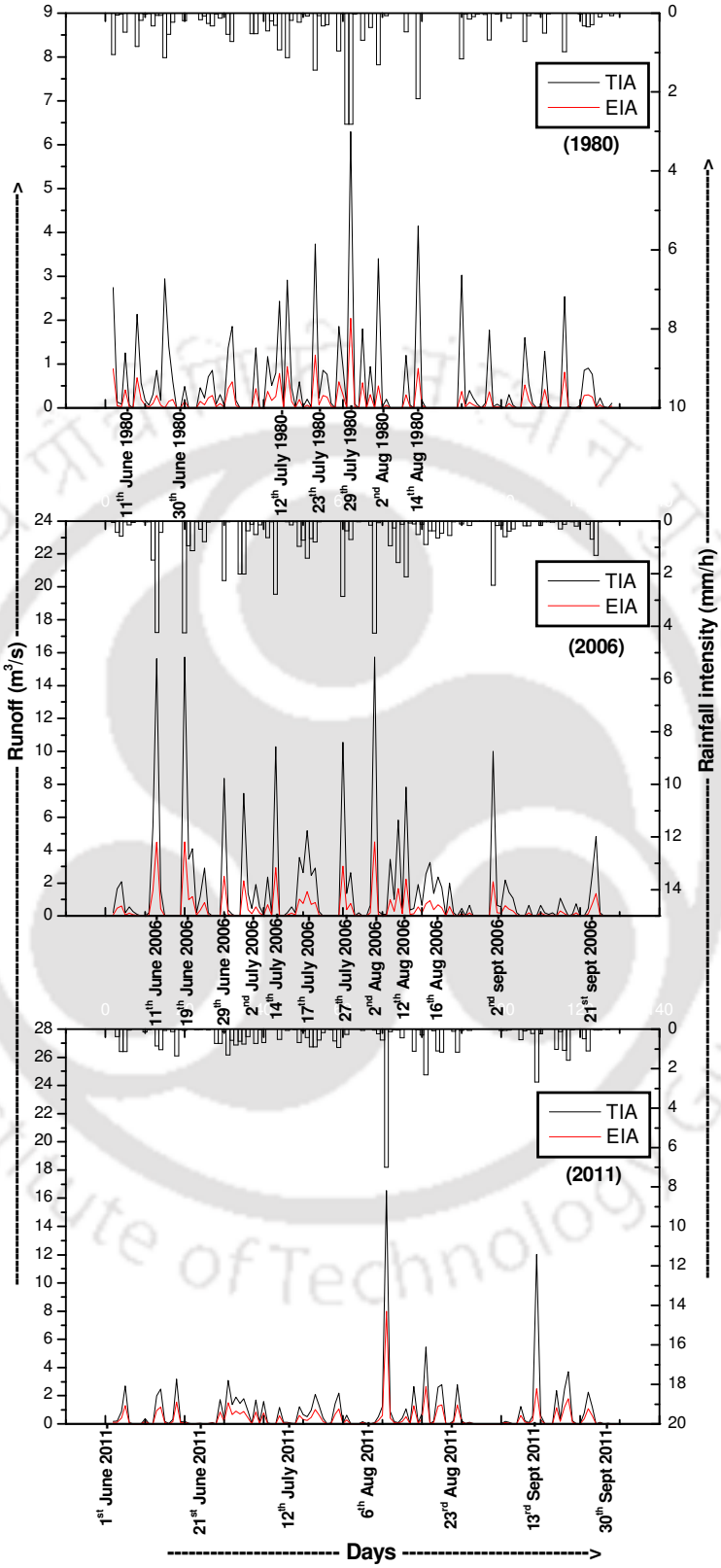

Fig. 6.8 Simulated runoff of watershed 6 using continuous rainfall data for TIA and EIA

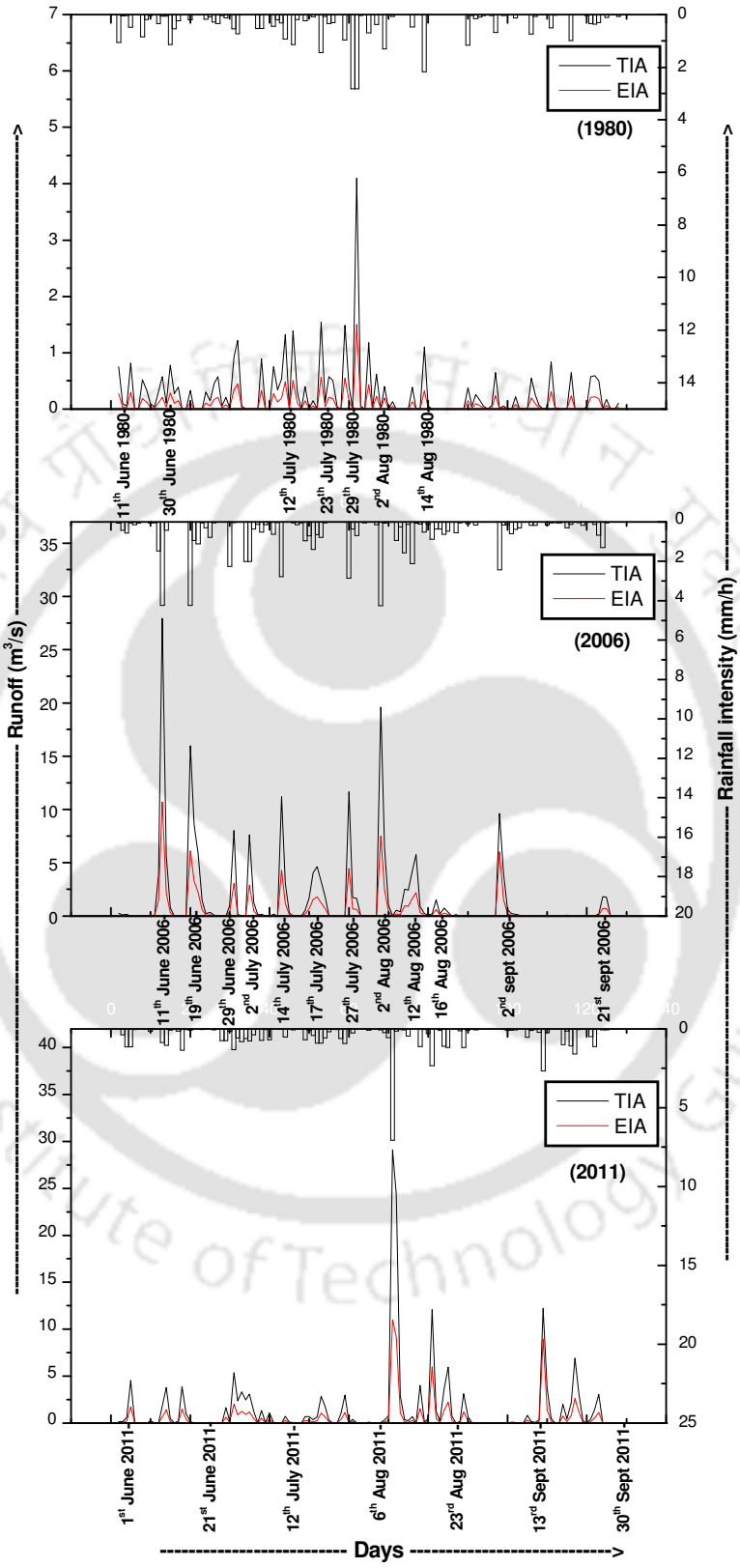

Fig.6.9 Simulated runoff of watershed 7 using continuous rainfall data for TIA and EIA

Table 6.1 Peak runoff simulated for different watersheds by considering TIA and EIA

Watershed	Year	Peak run off (m^3/s) by considering		(a)/(b)
		TIA (a)	EIA (b)	
1	1980	16.26	7.59	2.14
	2006	36.3	13.08	2.78
	2011	48.58	21.12	2.30
2	1980	9.06	4.11	2.20
	2006	36.79	13.14	2.80
	2011	57.64	41.67	1.38
3	1980	8.55	3.47	2.46
	2006	32.16	11.64	2.76
	2011	56.09	37.97	1.48
4	1980	2.81	1.2	2.34
	2006	16.66	8.01	2.08
	2011	28.58	10.7	2.67
5	1980	3.1	1.3	2.39
	2006	22.1	9.2	2.40
	2011	29.97	11.04	2.71
6	1980	6.15	2.0	3.08
	2006	15.65	4.5	3.48
	2011	16.56	8.0	2.07
7	1980	4.1	1.5	2.73
	2006	27.94	9.93	2.81
	2011	29.11	11.0	2.65

6.3.2 Runoff simulation using event wise rainfall data

This section shows the simulated runoff for different watersheds of the study area for different rainfall events described in section 3.3. From the last section, it is clear that TIA based prediction of runoff is overestimated. Hence for event wise rainfall data, runoff is determined by considering EIA only.

6.3.2.1 Runoff simulation for EIA determined using indirect method

In absence of fine resolution imageries the direct determination of EIA becomes difficult. To overcome this difficulty an attempt has been made to determine EIA indirectly from the corresponding TIA values by two empirical equations Eq. 4.6 and Eq. 4.8 (chapter 4). The runoff has been simulated in different watersheds for different rainfall events employing these EIA values. Figs. 6.10 to 6.12 show the simulated runoff for different watersheds of the study area for

rainfall events RE-1, RE-2 and RE-3, respectively, and by considering EIA estimated by Eq. 4.6 for the years 2006 and 2011. For RE-1, it is observed that watershed 3 produces maximum runoff and minimum for watershed 6 for both the years. The time to peak remains same for all the watersheds and maximum recession time is observed in watershed 7. Also it has been observed that runoff predicted in watershed 6 is increased by 25.3% from 2006 to 2011 for an increase in imperviousness of 46.25%, if EIA is estimated by Eq. 4.6. For RE-2, watershed 3 produces maximum runoff and minimum in watershed 7. The maximum recession time is observed in watershed 7. The difference in runoff is marginal for watershed 6 and 7. For RE-3, watershed 4 was found to show maximum increase in runoff of 44.36% and watershed 7 was found to show least increase in runoff of 3.16% from 2006 to 2011.

Similarly, Figs. 6.13 to 6.15 show the simulated flows for rainfall events RE-1, RE-2 and RE-3, respectively, and by considering EIA estimated by Eq. 4.8 for the years 2006 and 2011. For RE-1, the maximum increase in runoff (3.6%) occurred in watershed 4 from 2006 to 2011 subjected to maximum increase in EIA value estimated by Eq. 4.8. The increasing trend in runoff from 2006 to 2011 is true for all watersheds and all rainfall events. Such an increase in runoff is due to the increase in imperviousness.

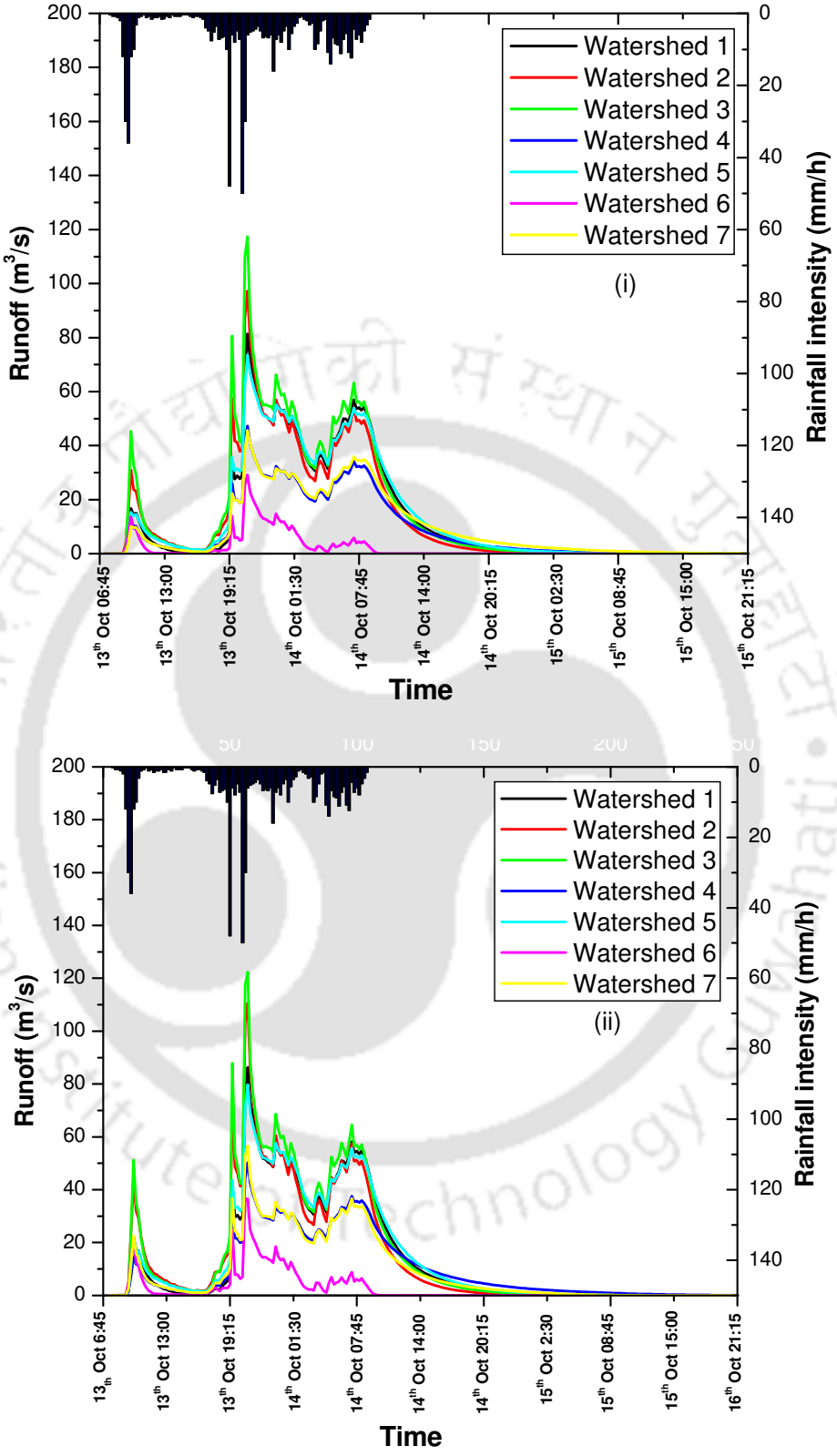

Fig 6.10 Flow simulation for RE-1 and EIA estimated by Eq. 4.6 for the year (i) 2006 and (ii) 2011

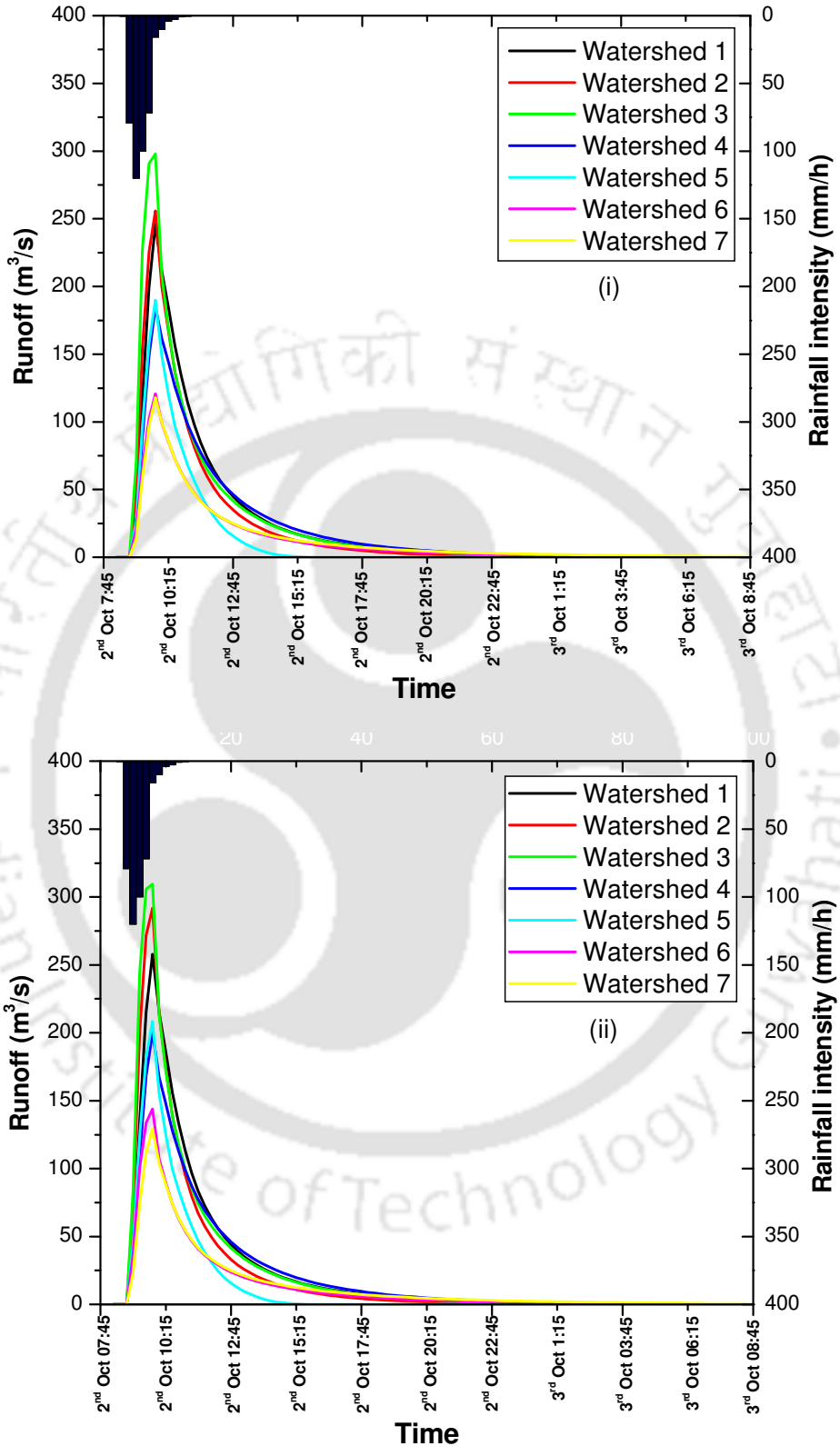

Fig 6.11 Flow simulation for RE-2 and EIA estimated by Eq. 4.6 for the year (i) 2006 and (ii) 2011

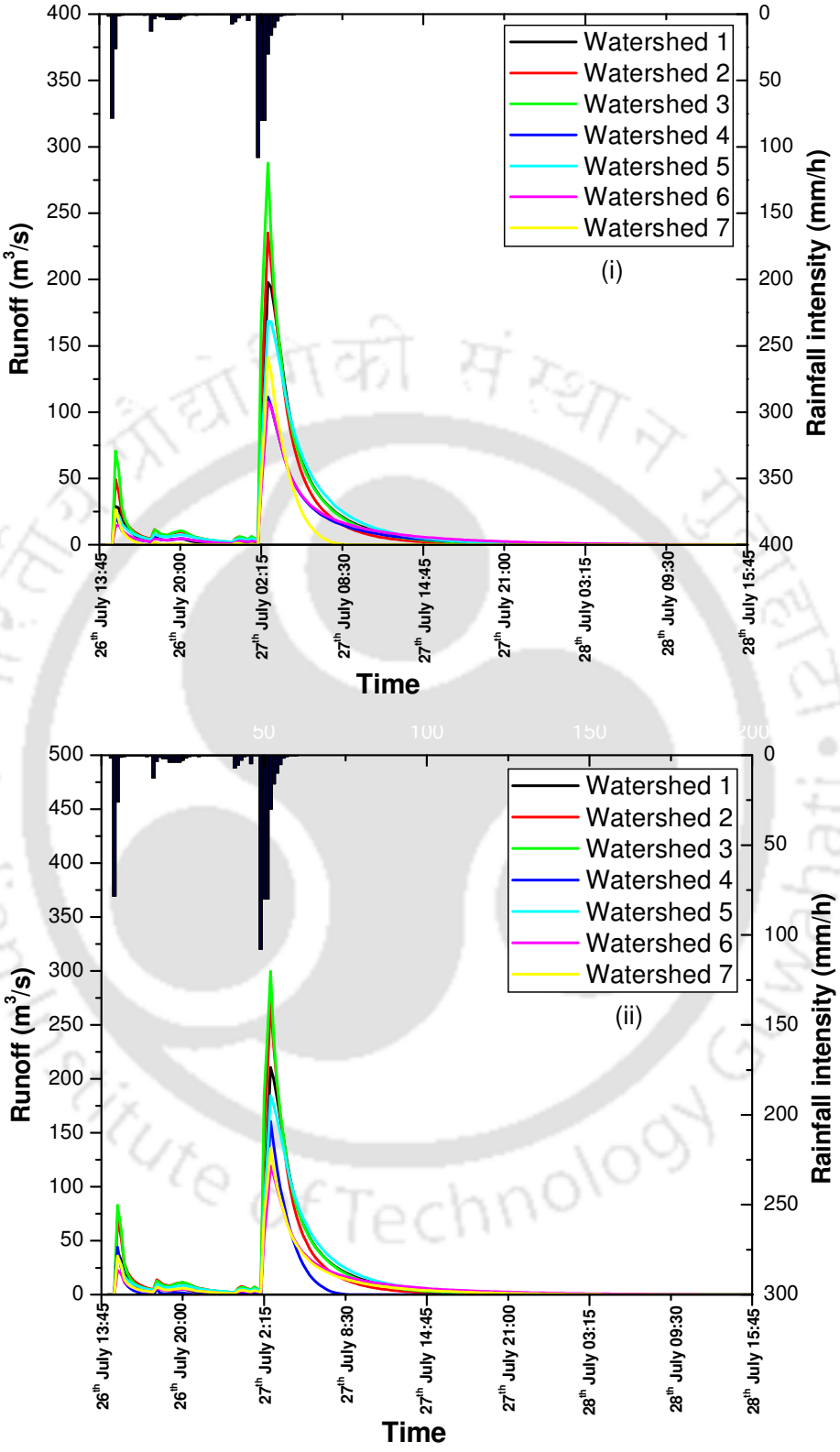

Fig 6.12 Flow simulation for RE-3 and EIA estimated by Eq. 4.6 for the year (i) 2006 and (ii) 2011

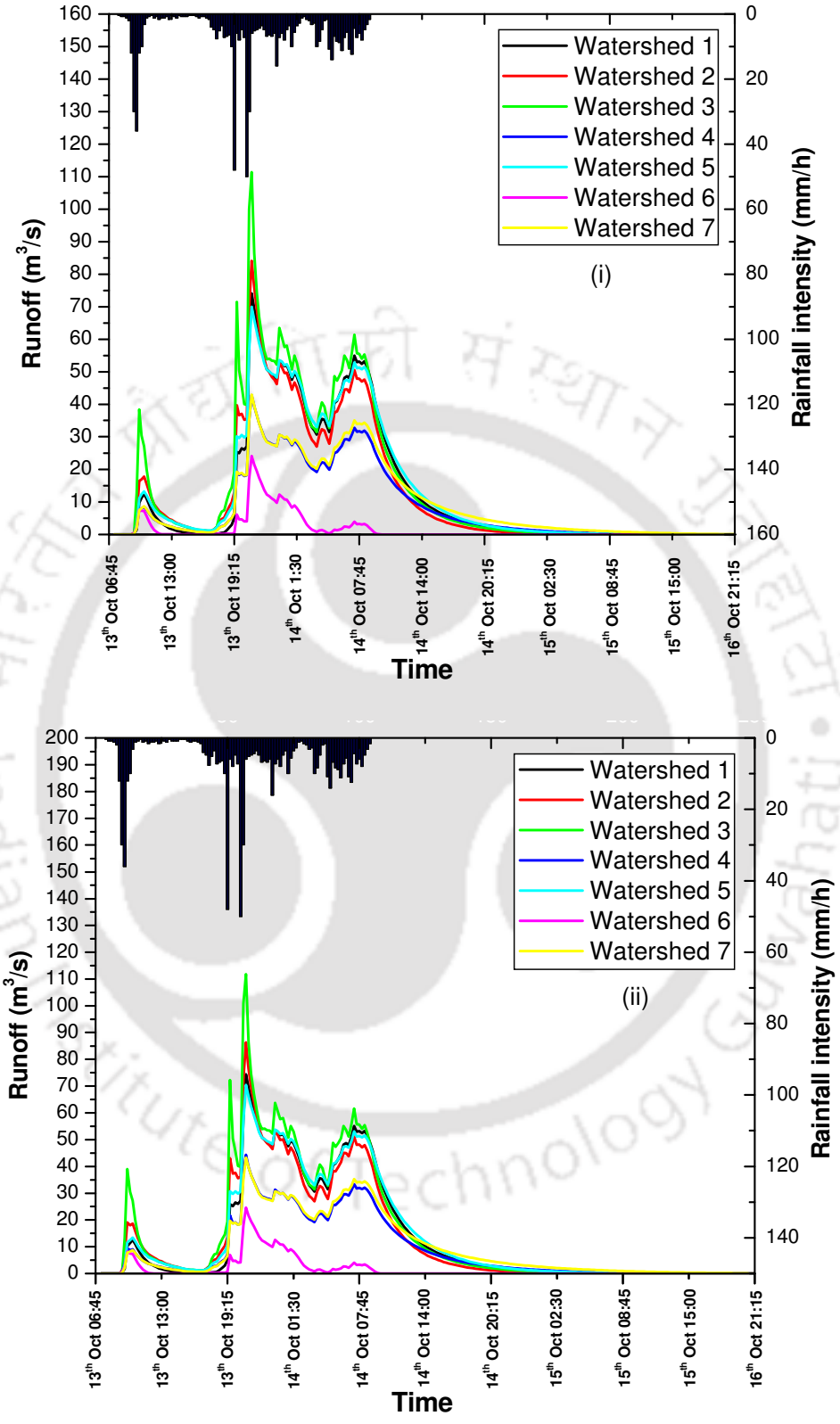

Fig. 6.13 Flow simulation for RE-1 and EIA estimated by Eq. 4.8 for the year (i) 2006 and (ii) 2011

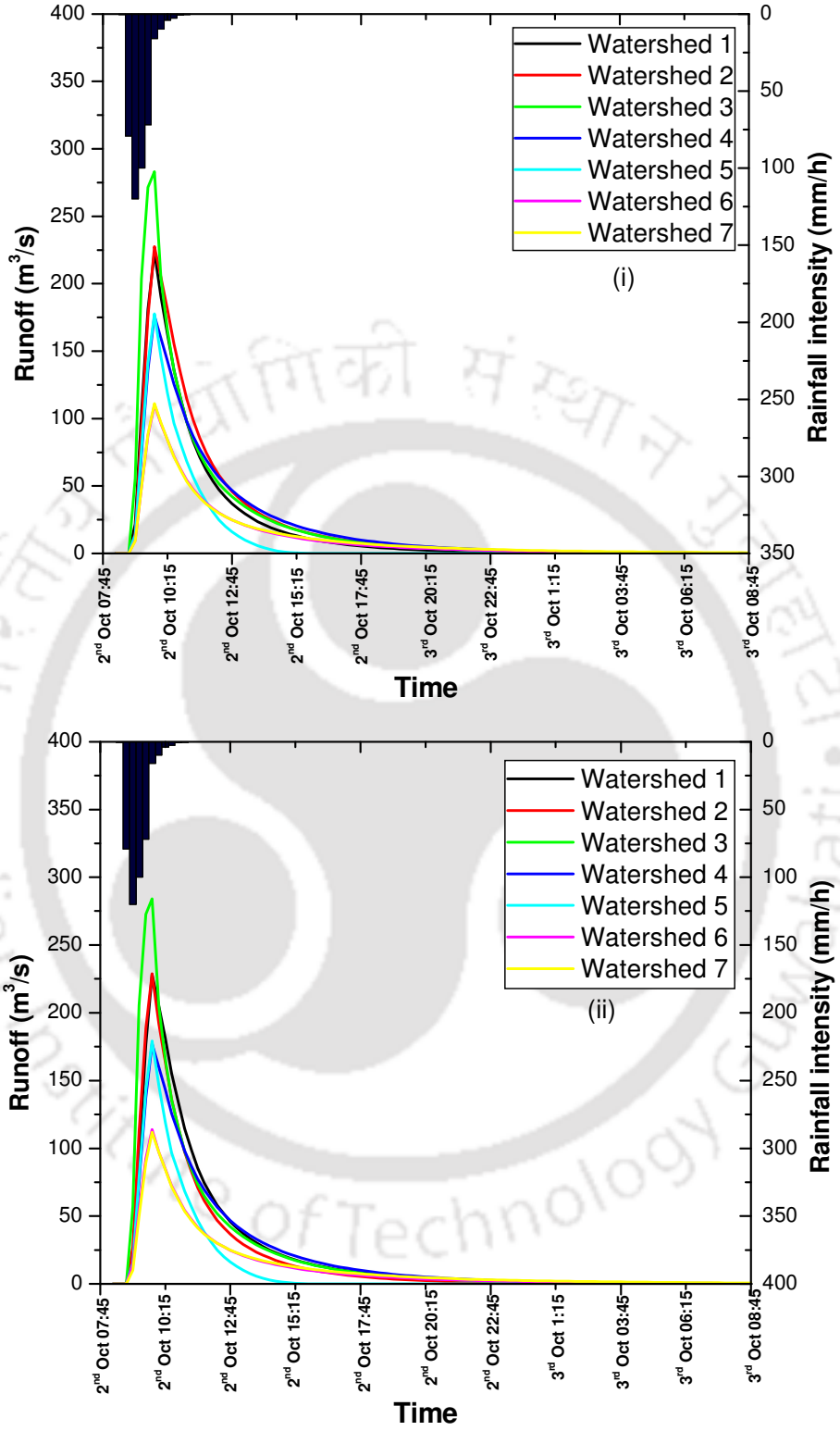

Fig. 6.14 Flow simulation for RE-2 and EIA estimated by Eq. 4.8 for the year (i) 2006 and (ii) 2011

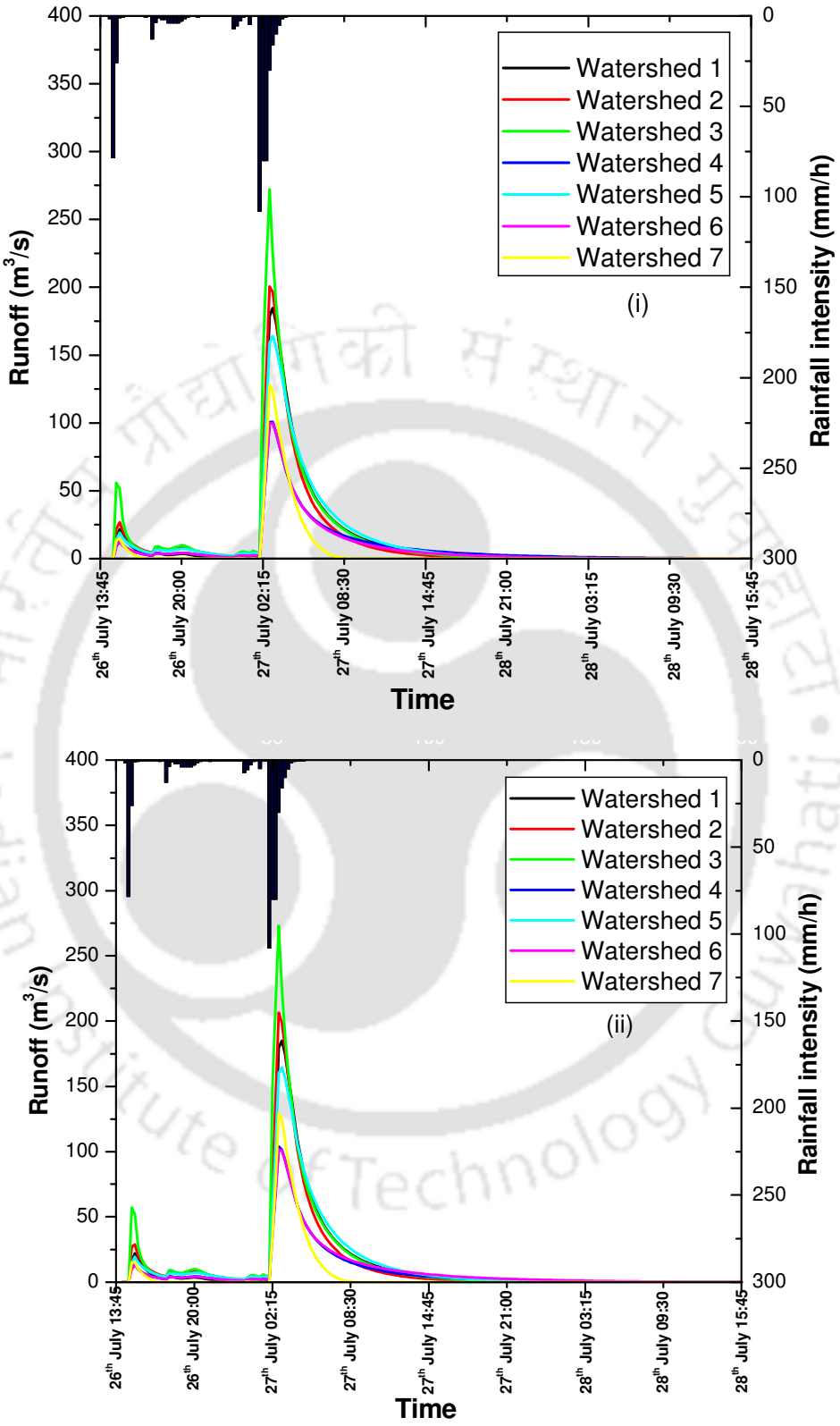

Fig. 6.15 Flow simulation for RE-3 and EIA estimated by Eq. 4.8 for the year (i) 2006 and (ii) 2011

It is also observed that for both the years all the watersheds predicted high peak runoff when EIA estimated by Eq. 4.6 is used as compared to Eq. 4.8. For eg: Watershed 6 shows 21.17% and 48.44% more peak runoff for the years 2006 and 2011, respectively if EIA estimated by Eq. 4.6 is used in the model instead of Eq. 4.8.

6.3.2.2 Runoff simulation based on EIA determined by direct method

Figs. 6.16 to 6.18 show simulated runoff for the study area for rainfall events RE-1, RE-2 and RE-3, respectively by considering EIA determined directly (section 4.6.5). For RE-1, the most urbanized watershed 3 shows 40.32% increase in runoff from 2006 to 2011. The time to peak is observed to remain same for all the watersheds and recession time is more for watershed 2. It is also observed that an increase in EIA by 32.73% increases the simulated runoff by 35% from 2006 to 2011 in watershed 2. For RE-2, the peak runoff has been found to increase by 30.84% from 2006 to 2011 for an increase in EIA by 54.68% in watershed 3. The recession time is observed to be more for watershed 2 and watershed 7 in 2006 and 2011, respectively. For RE-3, it is observed that watershed 3 shows 29.87% increase in runoff and the least urbanized watershed 6 shows 2.04% increase in runoff from 2006 to 2011. The time to peak remains same for all watersheds and recession time is found to be more for watershed 2. For RE-1, the maximum runoff is exhibited by watershed 3 and 5 (comparable) and for RE-2 and RE-3, watershed 5 shows the maximum runoff.

Table 6.2 shows the amount of over prediction in peak runoff in the year 2011 if EIA estimated by indirect method is employed in the model in place of EIA estimated by direct method. It is observed from Table 6.2 that peak runoff is largely overestimated in all the watersheds and for all rainfall events if EIA estimated by Eq. 4.6 is used for runoff prediction. However, the over prediction in runoff is comparatively less if EIA estimated by Eq. 4.8 is used in the model. The over prediction in runoff was 205% and 179% due to EIA estimated by Eqs. 4.6 and 4.8, respectively in the most urbanized watershed 3 due to RE-1. The same was 115% and 97.53% due to RE-2 and 157.5% and 134.6% due to RE-3. All these cases show that runoff is largely overestimated due to use of indirectly estimated EIA in the model. Hence effort should be made to estimate EIA by direct method ensuring the connectivity between the impervious area and the collection network.

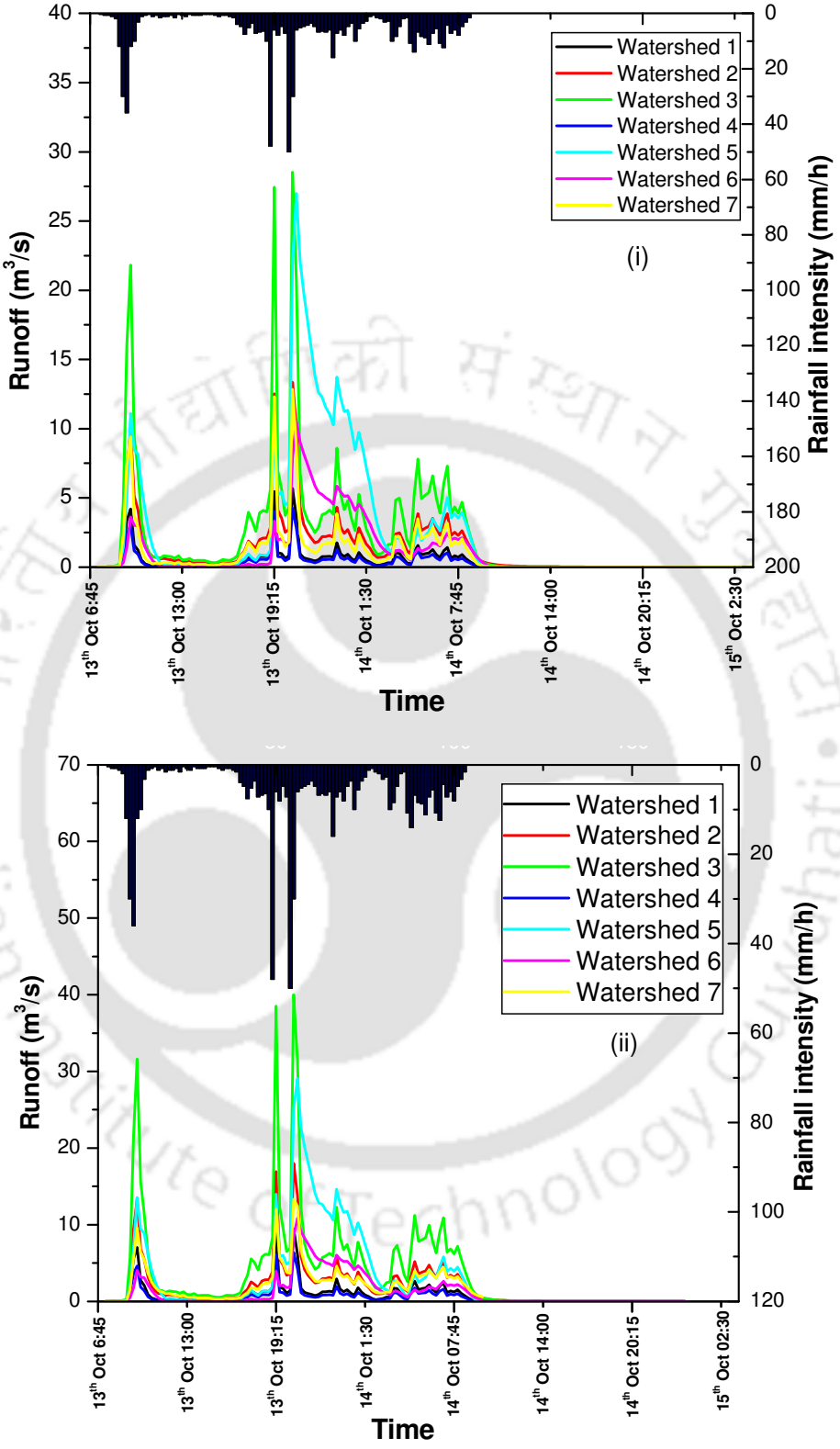

Fig. 6.16 Flow simulated in the study area for RE-1 and EIA estimated by direct method in the year (i) 2006 and (ii) 2011

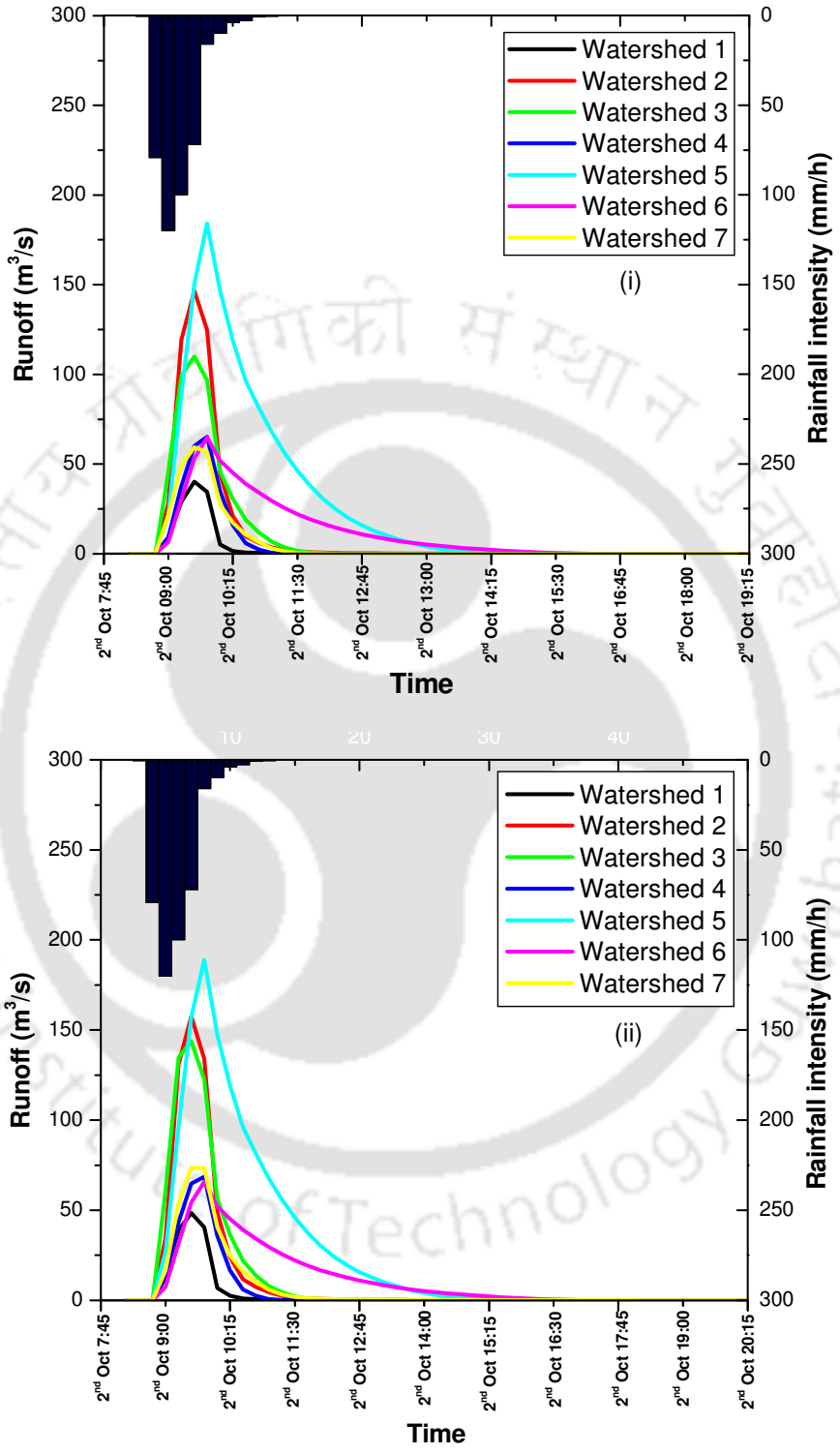

Fig. 6.17 Flow simulation in the study area for RE-2 and EIA estimated by direct method in the year (i) 2006 and (ii) 2011

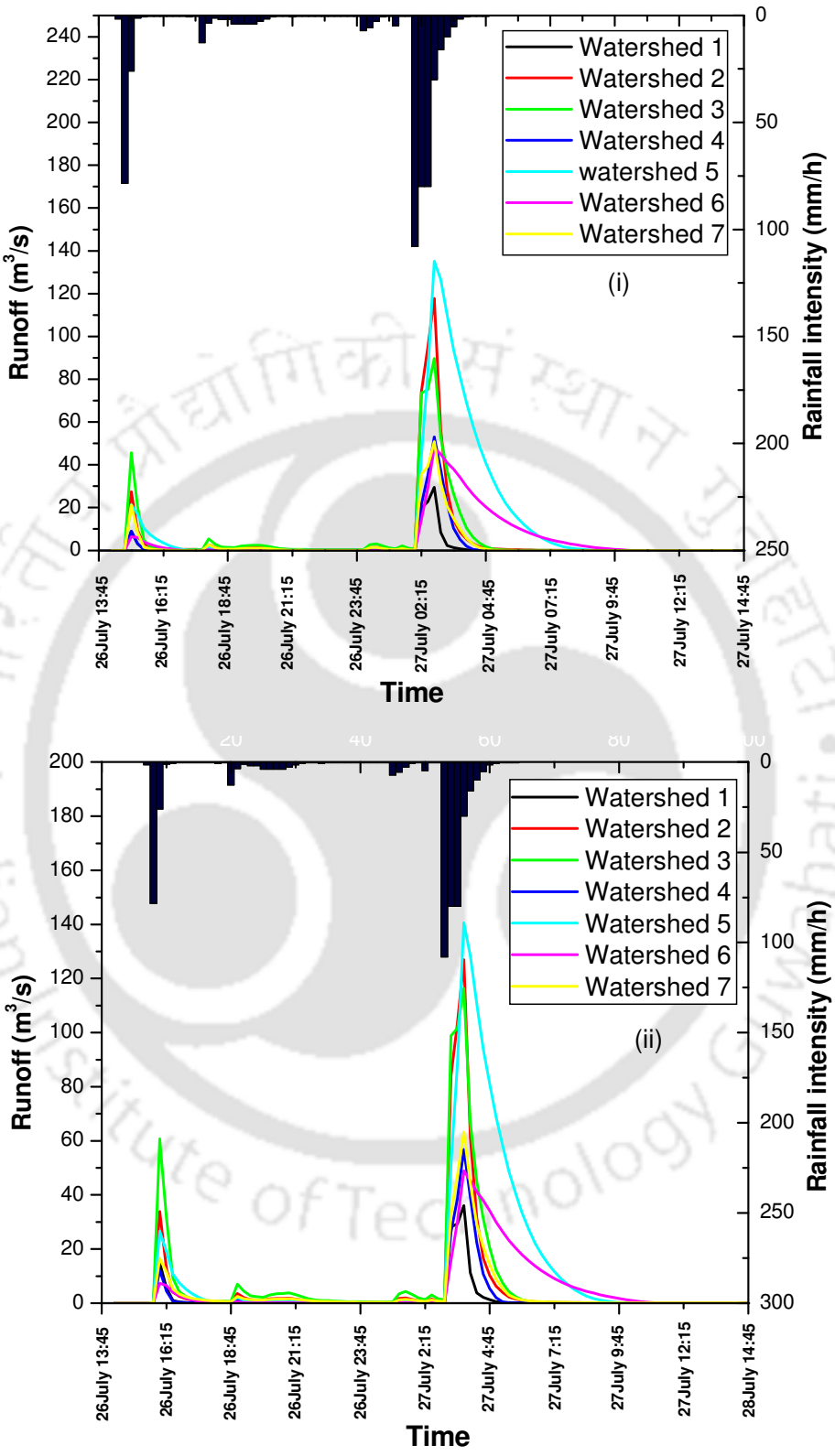

Fig. 6.18 Flow simulation in the study area for RE-3 and EIA estimated by direct method in the year (i) 2006 and (ii) 2011

Table 6.2 Comparison of peak runoff of 2011estimated based on EIA obtained by direct and indirect methods

Watershed No.	RE-1					RE-2					RE-3				
	Peak runoff (m^3/s)			Over prediction by indirect method (%)		Peak runoff (m^3/s)			Over prediction by indirect method (%)		Peak runoff (m^3/s)			Over prediction by indirect method (%)	
	Eq. 4.6	Eq. 4.8	Eq. 4.10	Eq. 4.6	Eq. 4.8	Eq. 4.6	Eq. 4.8	Eq. 4.10	Eq. 4.6	Eq. 4.8	Eq. 4.6	Eq. 4.8	Eq. 4.10	Eq. 4.6	Eq. 4.8
1	86.23	74.46	9.46	811	687	257.96	228.43	48.41	432	371	210.65	185.07	36.04	484	413
2	110.67	86.37	18.01	514	380	291.7	228.73	157.64	85	45.1	271.52	206.4	126.96	113	62
3	122.37	111.8	40.02	205	179	309.48	284.12	143.83	115	97.53	299.78	273.08	116.39	157.5	134.6
4	50.28	44.31	6.4	685	592	200.22	177.28	68.54	192	158.6	160.71	103.72	56.82	182	82.5
5	79.83	70.43	29.08	174	142	208.46	199.1	188.88	10.4	5.4	184.55	164.57	140.56	31.3	17.08
6	36.59	24.65	10.87	236	126	143.9	113.88	65.79	118	73.1	119.46	101.44	48.97	144	107
7	56.65	43.29	13.33	325	224	129.32	112.01	73.51	76	52.3	135.66	129.12	63.2	114.6	104

6.3.3 Comparison of simulated runoffs using continuous and event wise rainfall data

Many a time due to lack of short interval rainfall data, continuous simulation is performed. Therefore there is the need to evaluate the effect of continuous and event wise simulation on runoff prediction in an urban catchment. The runoff simulation has been carried out using continuous rainfall data from 1980 to 2012 and the rainfall event on 26th July 2011 (RE-3). The EIA estimated from 2011 image by direct method is used. Since land use is kept same, the difference in peak runoff is fully attributed to the change in rainfall characteristics (whether continuous or event).

Figs. 6.19 to 6.25 show the runoff simulation results based on continuous rainfall and RE-3 for all watersheds in the study area. From Fig. 6.19 (i and ii), it can be observed that the peak rainfall intensity is 0.93 mm/h on 26th July 2011 for continuous simulation as against 108 mm/h for RE-3 on the same date. This observation remains same for all the watersheds. Such a huge disparity in peak rainfall intensity will under predict runoff when continuous rainfall data is used instead of rainfall event RE-3. Table 6.3 summarizes under prediction in peak runoff corresponding to 26th July 2011 for all watersheds. It can be noted that peak runoff based on continuous rainfall is under predicted by an average of 0.012 times as compared to runoff obtained by considering RE-3. From flood management perspective, such an underprediction is unacceptable for urban catchment and hence it is mandatory to use event rainfall with realistic peak rainfall intensity for runoff determination. In the absence of event rainfall data, there is a need to apply a factor of safety to the runoff determined from continuous rainfall. However, further research is required to propose such factor of safety for runoff in urban catchment when continuous rainfall is used.

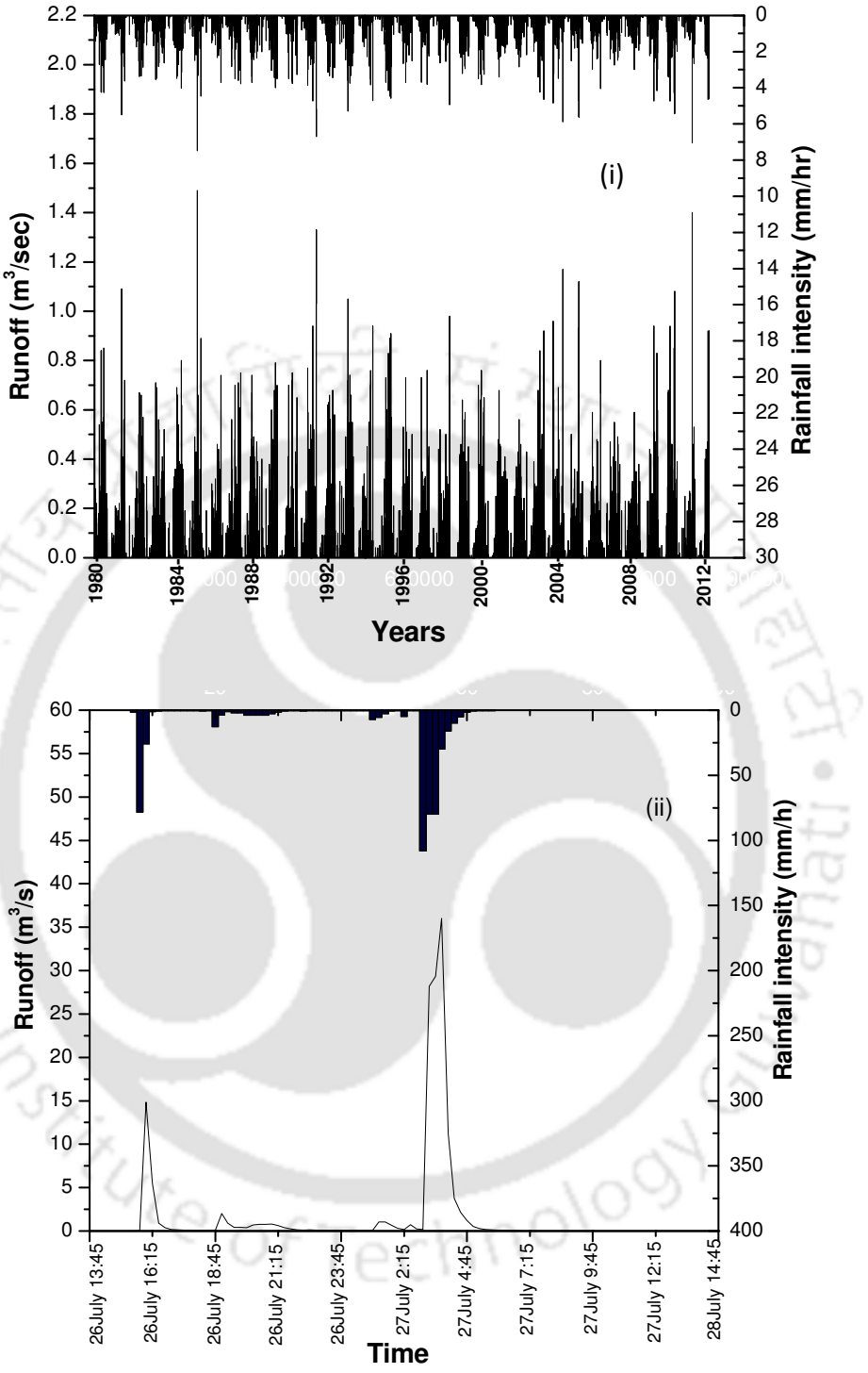

Fig. 6.19 Comparison of runoff simulated in watershed 1 using (i) continuous rainfall and (ii) RE-3

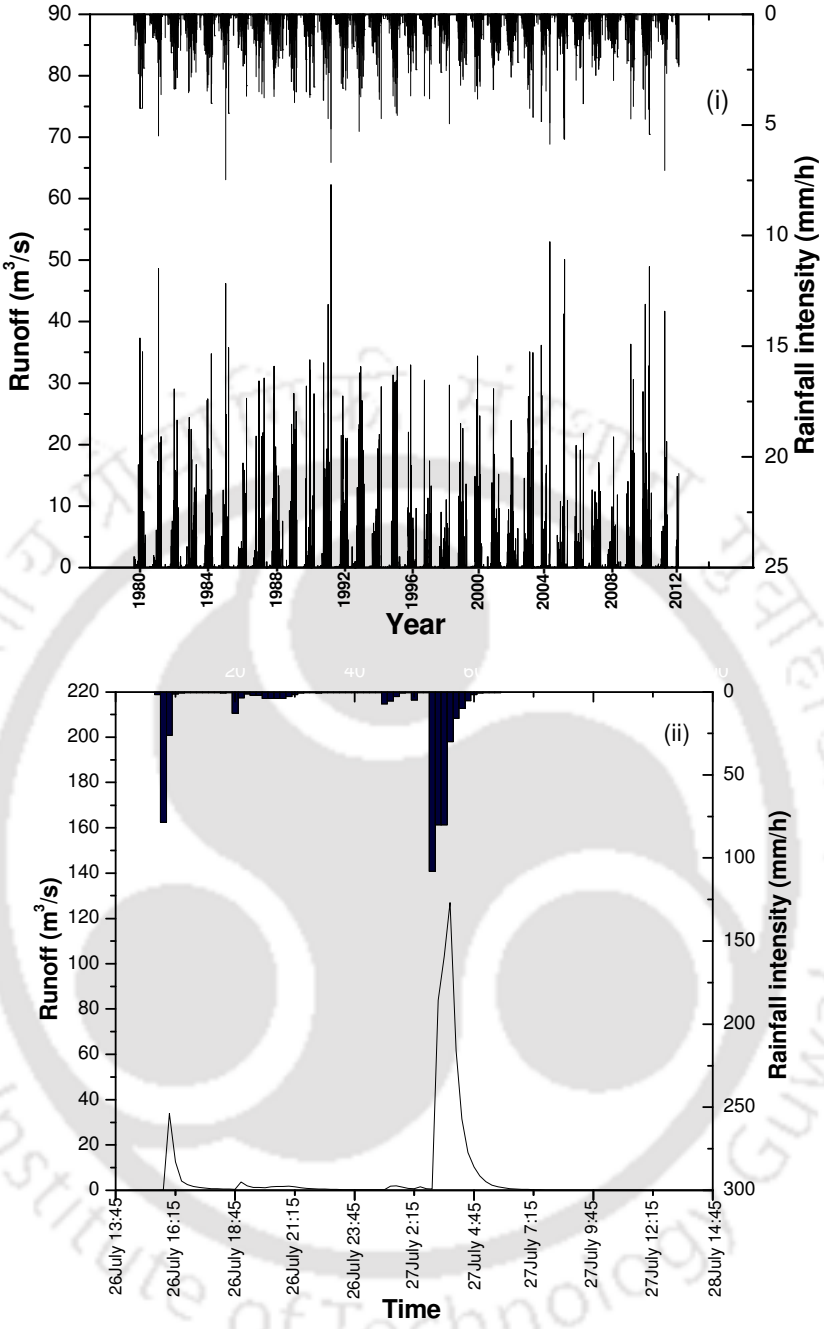

Fig. 6.20 Comparison of runoff simulated in watershed 2 using (i) continuous rainfall and (ii) RE-3

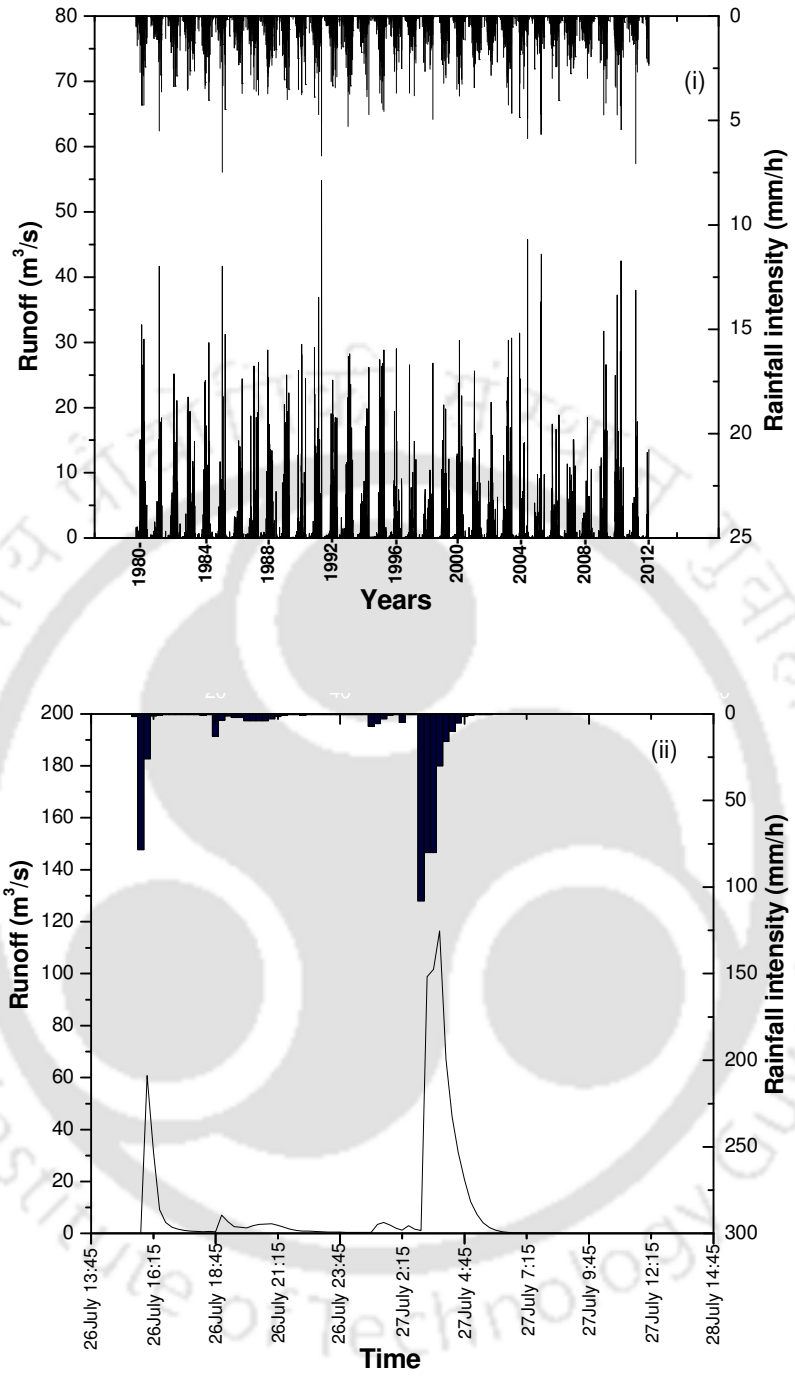

Fig. 6.21 Comparison of runoff simulated in watershed 3 using (i) continuous rainfall and (ii) RE-3

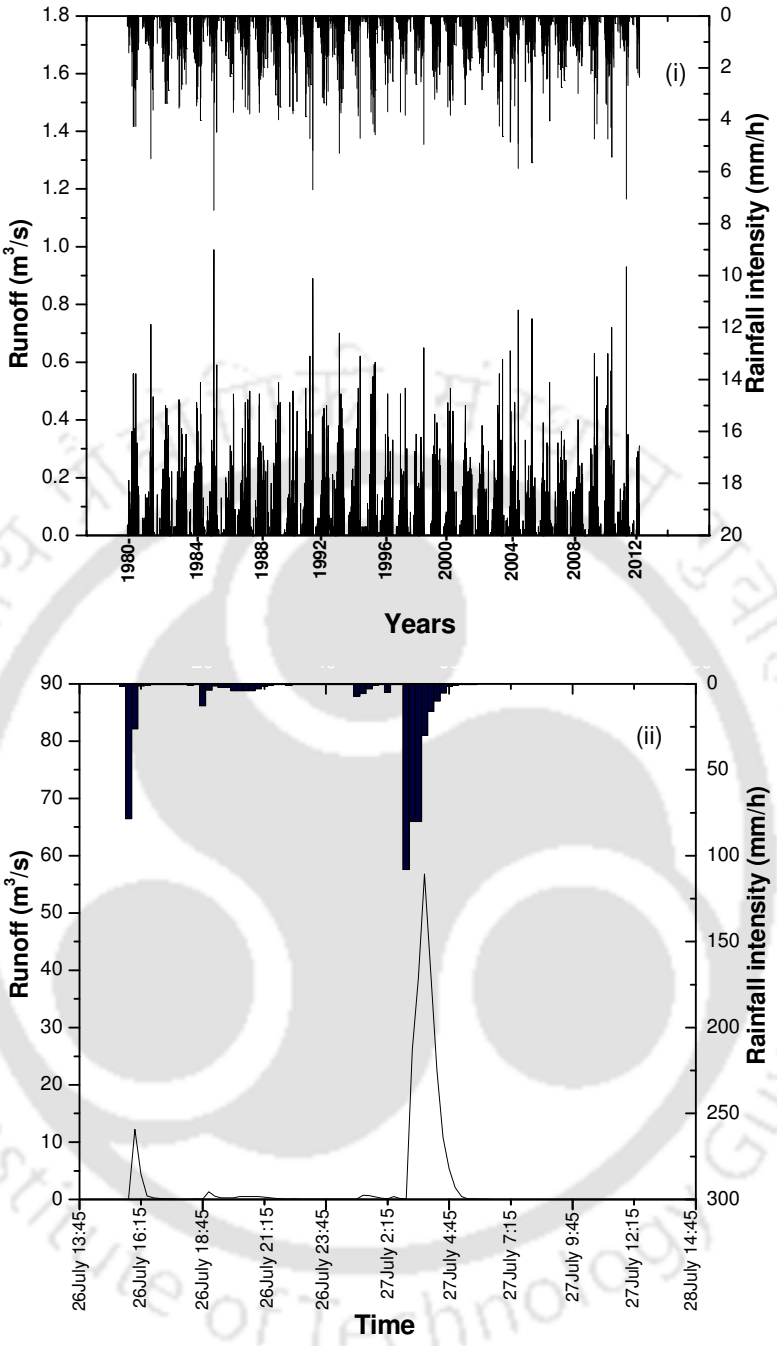

Fig. 6.22 Comparison of runoff simulated in watershed 4 using (i) continuous rainfall and (ii) RE-3

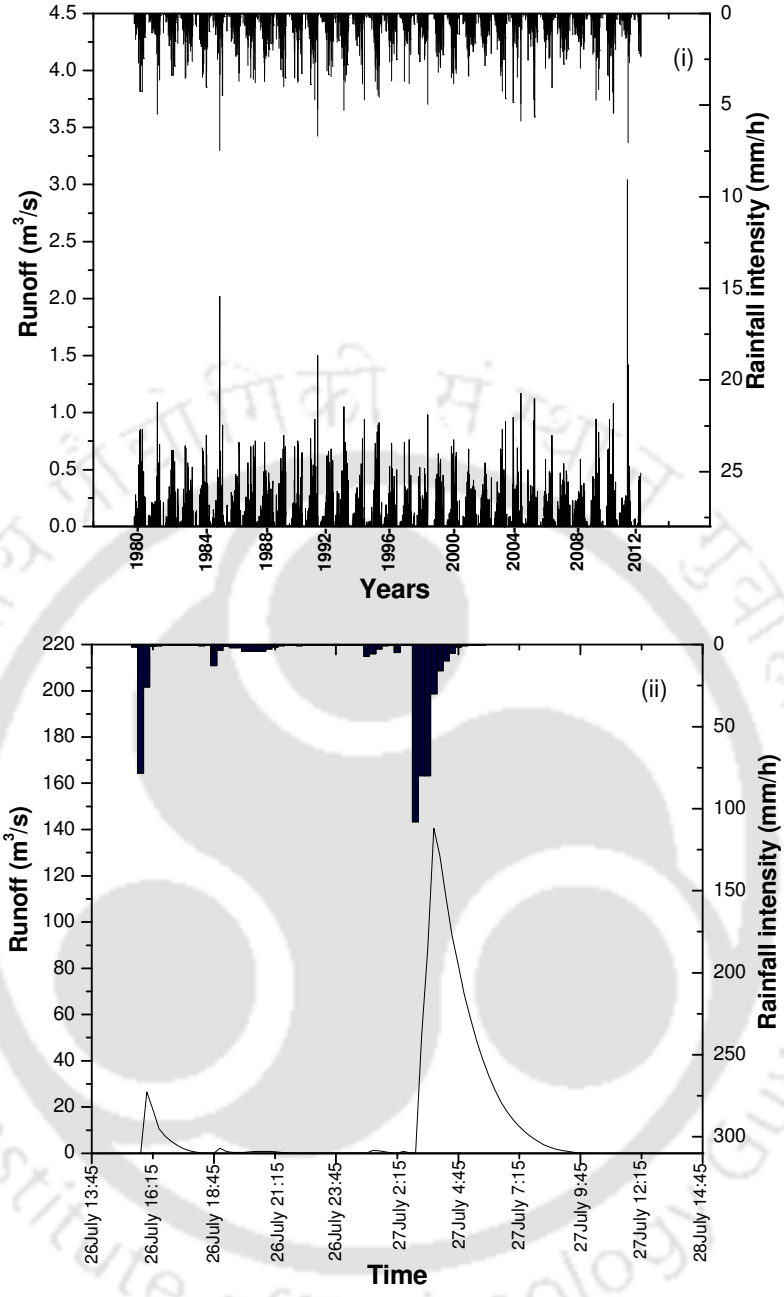

Fig. 6.23 Comparison of runoff simulated in watershed 5 using (i) continuous rainfall and (ii) RE-3

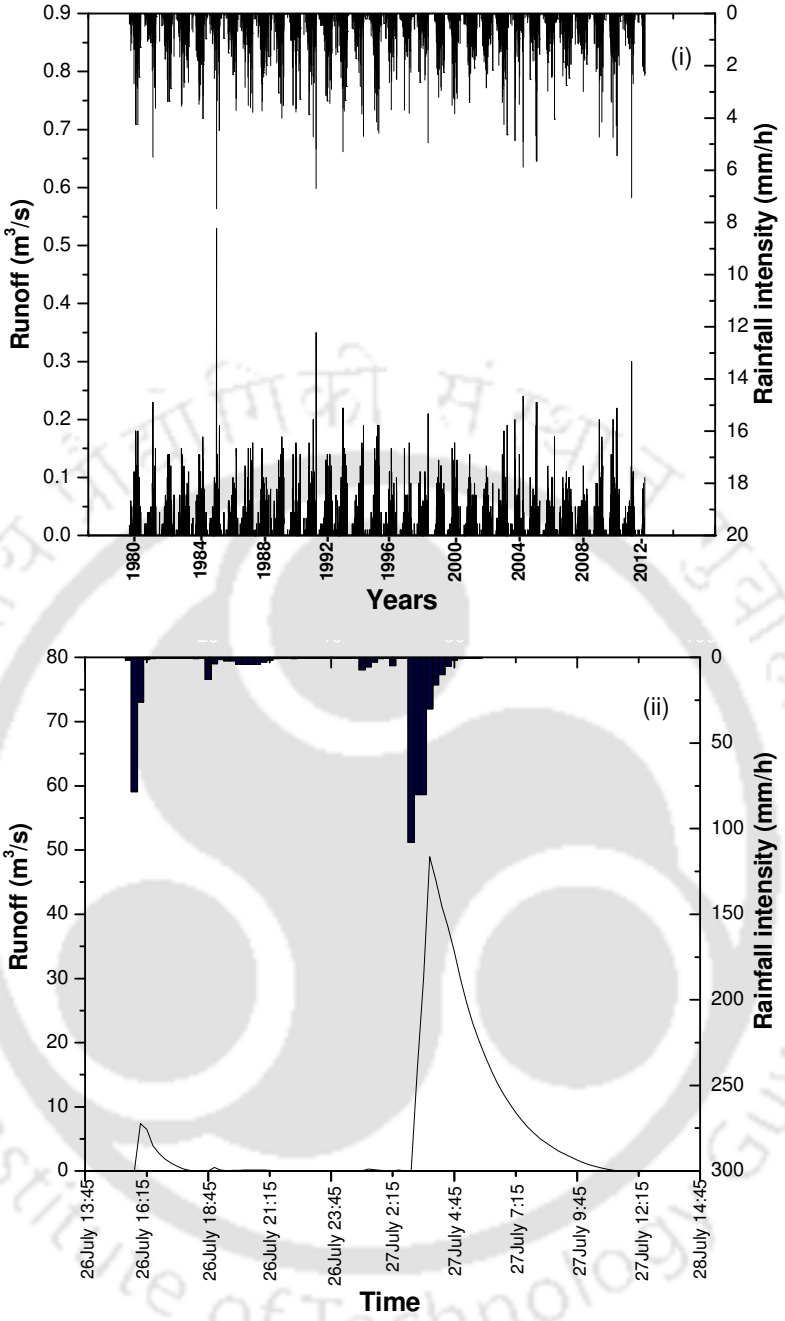

Fig. 6.24 Comparison of runoff simulated in watershed 6 using (i) continuous rainfall and (ii) RE-3

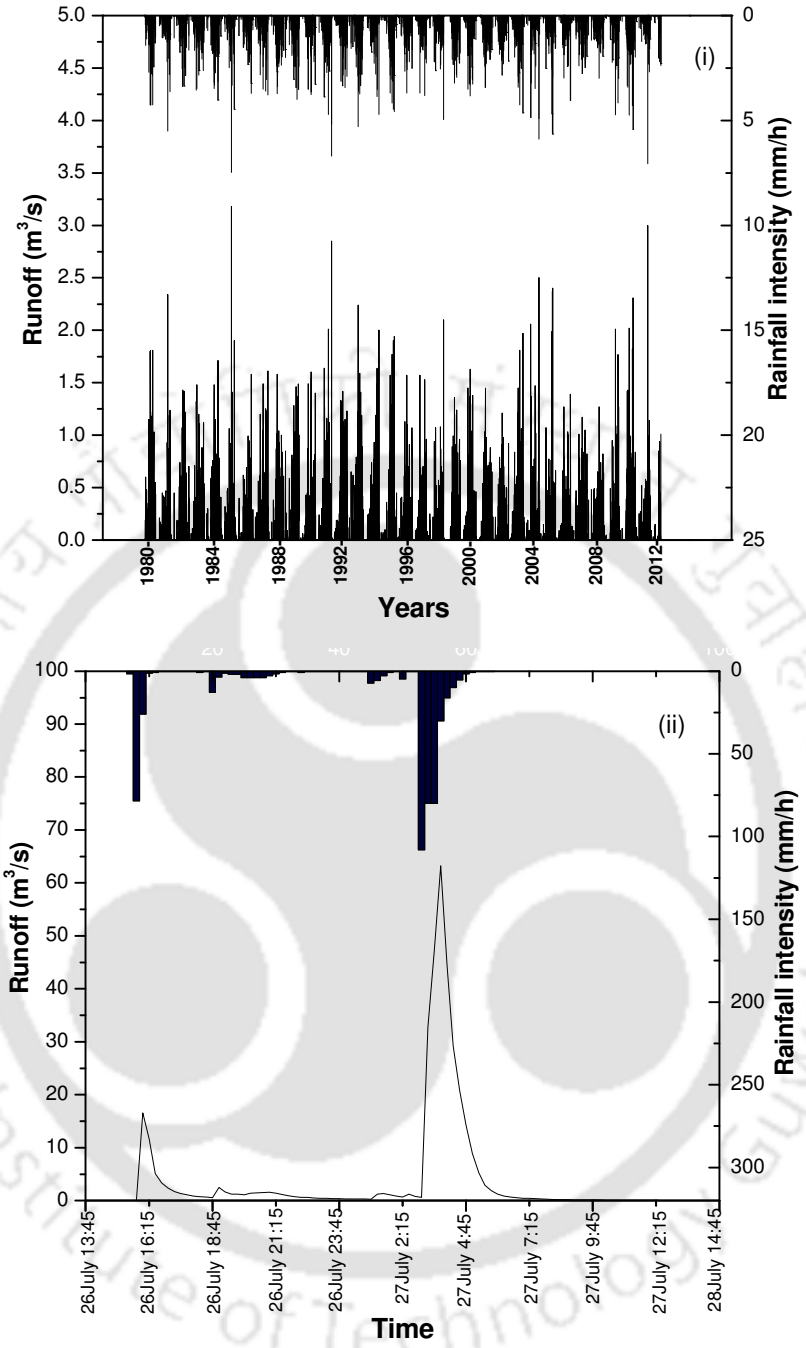

Fig. 6.25 Comparison of runoff simulated in watershed 7 using (i) continuous rainfall and (ii) RE-3

Table 6.3 Summary of under prediction of peak runoff when continuous rainfall is considered

Watershed No.	Peak runoff (m^3/s) based on		Under prediction (a/b)
	Continuous rainfall (a)	Rainfall event RE-3 (b)	
1	0.04	36.04	0.001
2	2.99	126.94	0.023
3	2.9	116.39	0.025
4	0.19	56.82	0.004
5	3.04	140.56	0.021
6	0.12	48.97	0.003
7	0.4	63.2	0.006

6.4 Effect of Using GIS Data with RS Images on Runoff Simulation

To improve the degree of accuracy of runoff prediction, imperviousness has been determined by integrating GIS data with satellite image as discussed in Section 4.6.4. Without GIS data, the satellite image has been classified based on the capability of the chosen training areas only. The classification process is not supported by the use of available data like building foot prints and road networks. This information is used while integrating GIS data with satellite image thereby minimizing misclassification and improving accuracy. The following section attempts to evaluate the difference in runoff due to misclassification by not considering GIS data. TIA estimated from the fine resolution imagery for the year 2006 by using GIS data and without using GIS data have been considered for determination of runoff.

6.4.1 Continuous rainfall data

Fig. 6.26 to 6.28 show the comparison of runoffs obtained in 2006 for all the seven watersheds with and without using GIS data. The summary of peak runoff obtained from these figures is listed in Table 6.4. In general, TIA estimated by considering GIS is always greater than the case where GIS is not integrated with remote sensing images (Section 4.6.4). Such an increase in TIA resulted in an average increase in peak runoff by 1.22 times when GIS is considered for imperviousness determination. The underprediction of runoff by not considering GIS data would influence flood management schemes. To minimize misclassification in land use and for ensuring better accuracy in runoff prediction in ungauged urban catchments, it is recommended to use GIS data along with satellite imageries for determining imperviousness.

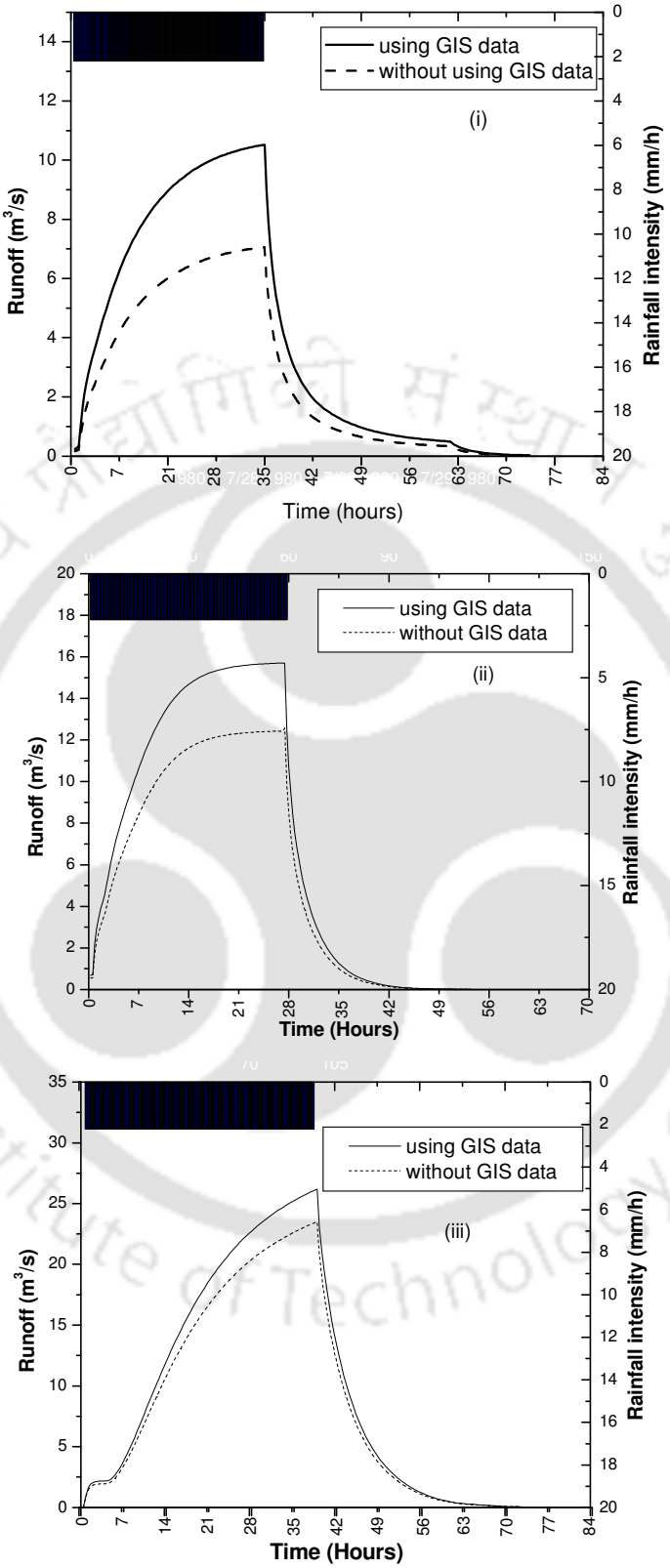

Fig. 6.26 Simulated runoff based on TIA estimated using GIS data and without using GIS data for (i) watershed 1, (ii) watershed 2 and (iii) watershed 3

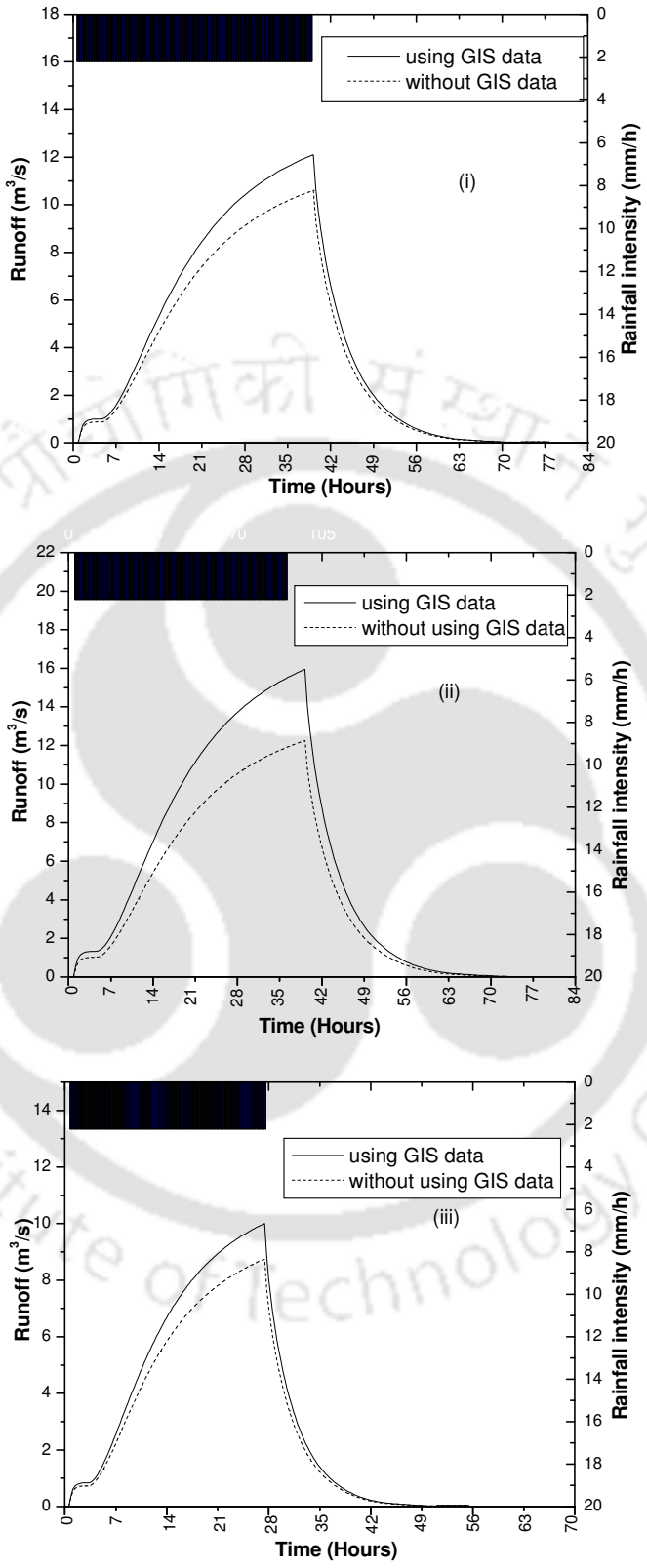

Fig. 6.27 Simulated runoff based on TIA estimated using GIS data and without using GIS data for (i) watershed 4, (ii) watershed 5 and (iii) watershed 6

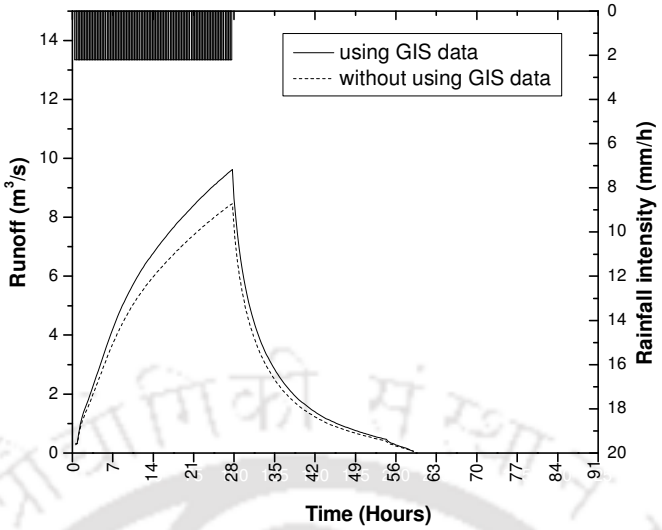

Fig. 6.28 Simulated runoff based on TIA estimated using GIS data and without using GIS data for watershed 7

Table 6.4 Summary of over prediction of peak runoff when GIS data is considered

Watershed No.	Peak runoff (m^3/s) by		(a)/(b)
	considering GIS data (a)	not considering GIS data (b)	
1	10.51	7.05	1.49
2	15.7	12.56	1.25
3	26.12	23.5	1.11
4	12.1	10.6	1.14
5	15.93	12.25	1.3
6	10.0	8.74	1.14
7	9.62	8.47	1.13

6.4.2 Event wise rainfall data

Fig. 6.29 to Fig. 6.31 show the simulated runoff for all the watersheds by employing TIA for the years 2006 and 2011 obtained by using GIS data. Fig. 6.32 to Fig. 6.34 show the simulated runoff for all the watersheds by employing TIA for the years 2006 and 2011 obtained without using GIS data. The land use classification Cl 1 (Section 4.6.4) has been considered for determining imperviousness without GIS data and Cl 4 (Section 4.6.4) has been considered as the imperviousness with GIS data for both the years of 2006 and 2011. Tables 6.5 and 6.6 summarize the peak runoff corresponding to RE-3 with and without considering GIS data for the years 2006 and 2011, respectively. When GIS data is considered, the average increase in peak

runoff is 1.23 and 1.14 times for the years 2006 and 2011, respectively when rainfall event RE-3 is considered. The average increase in peak runoff for rainfall event RE-3 is similar to those obtained for continuous rainfall data. This further reiterates the observation that integrating GIS with satellite image helps in better prediction of runoff in ungauged urban catchments.

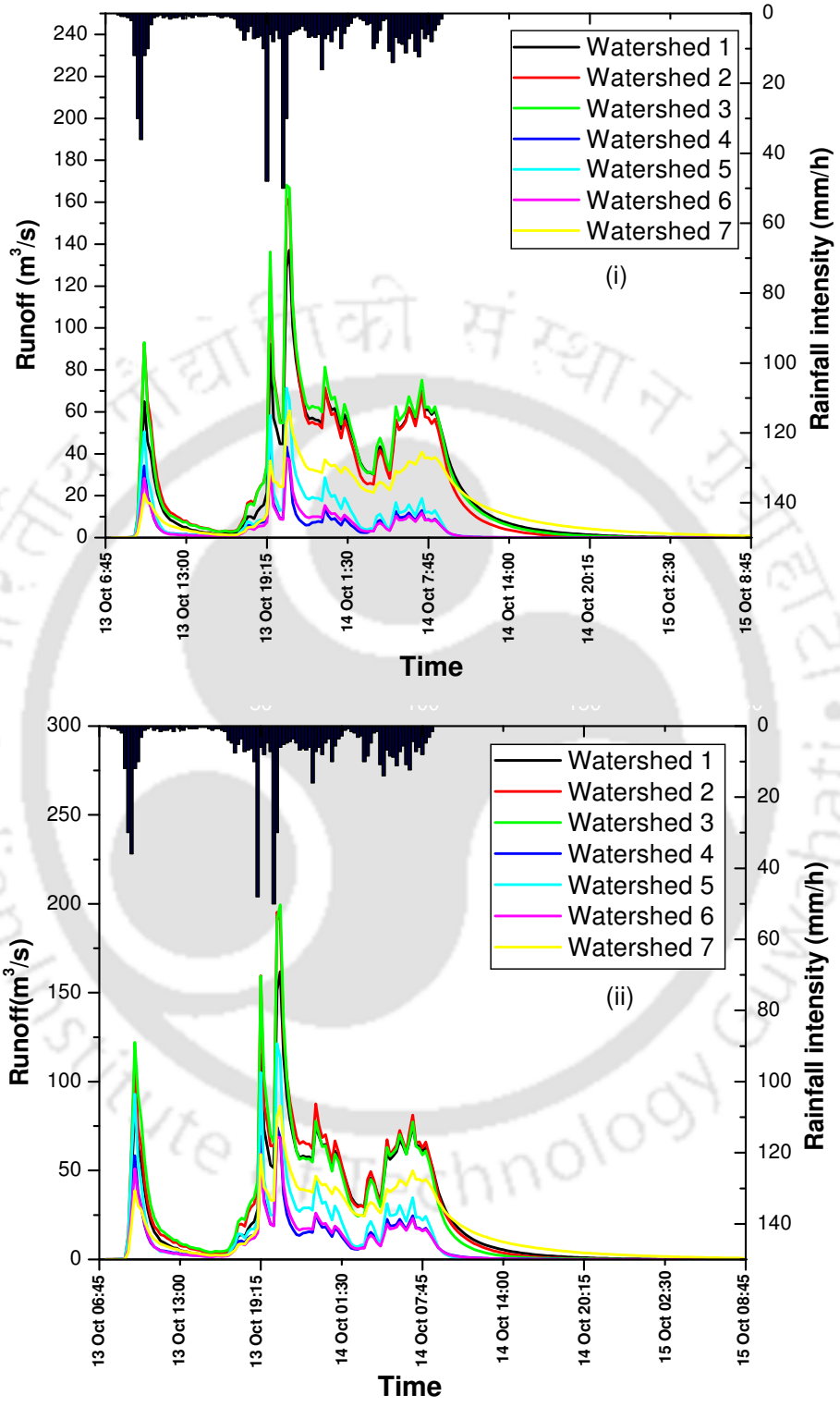

Fig. 6.29 Flow simulation for RE-1 and TIA estimated using GIS data for year (i) 2006 and (ii) 2011

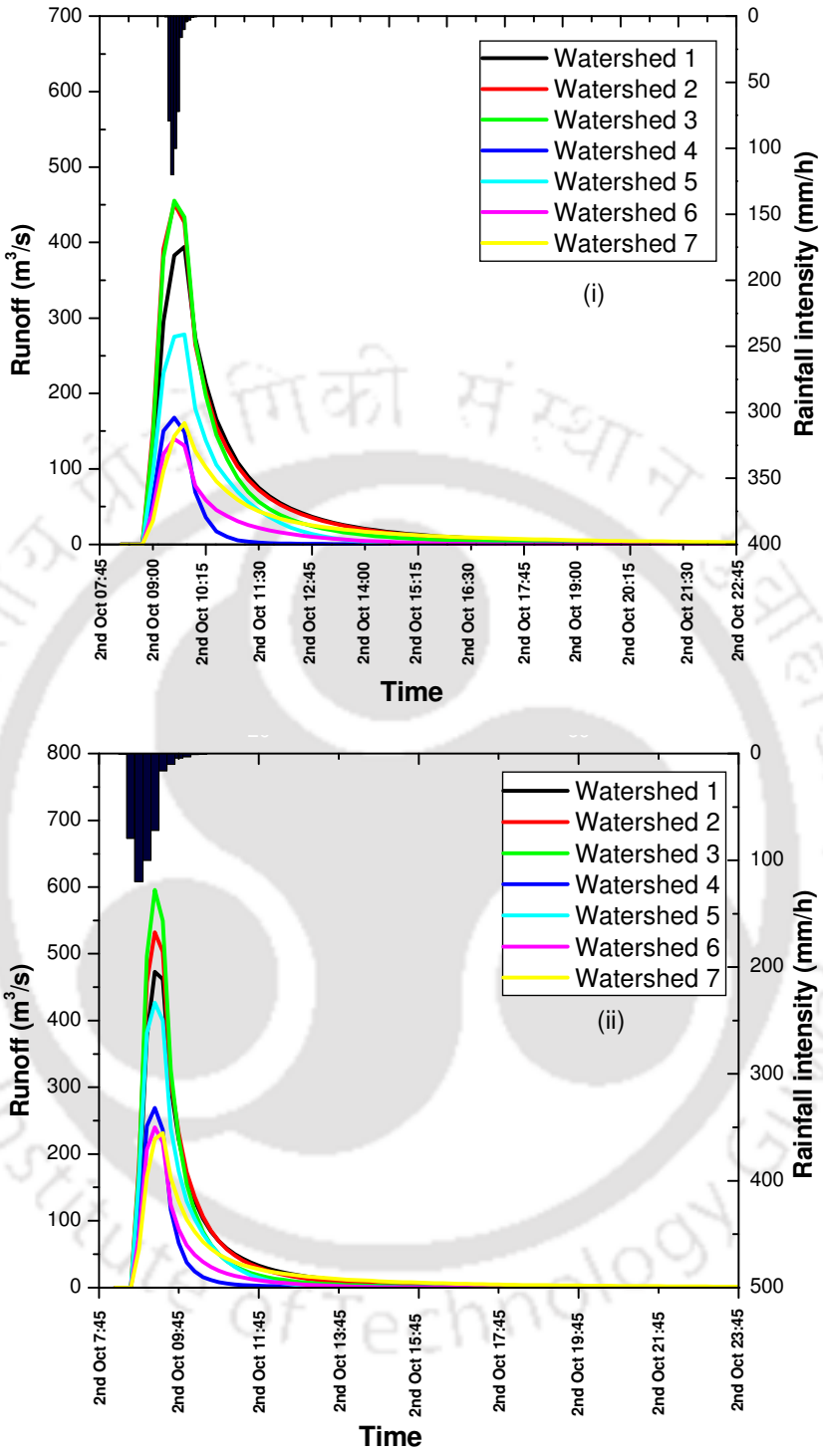

Fig. 6.30 Flow simulation for RE-2 and TIA estimated using GIS data for year (i) 2006 and (ii) 2011

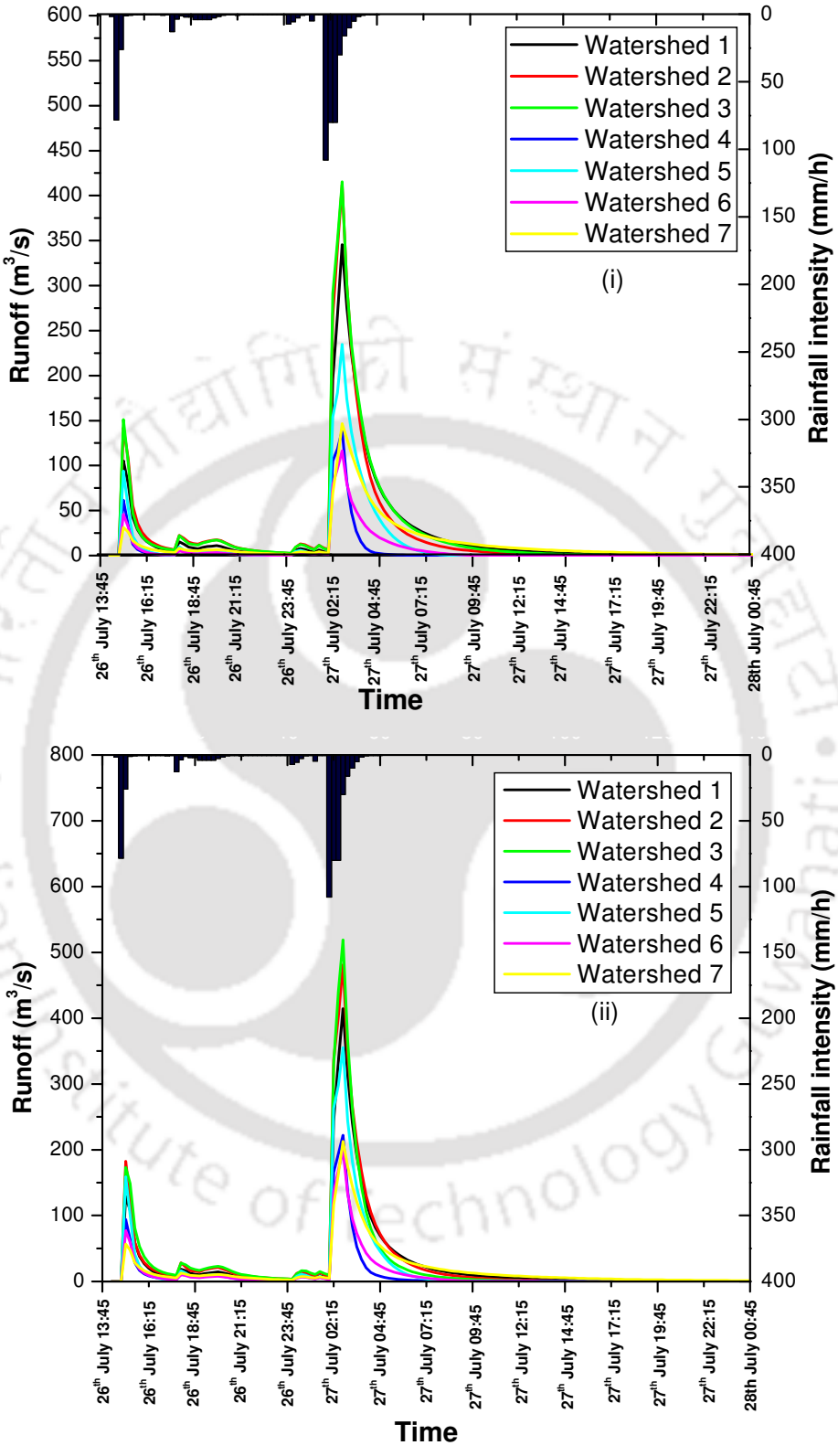

Fig. 6.31 Flow simulation for RE-3 and TIA estimated using GIS data for year (i) 2006 and (ii) 2011

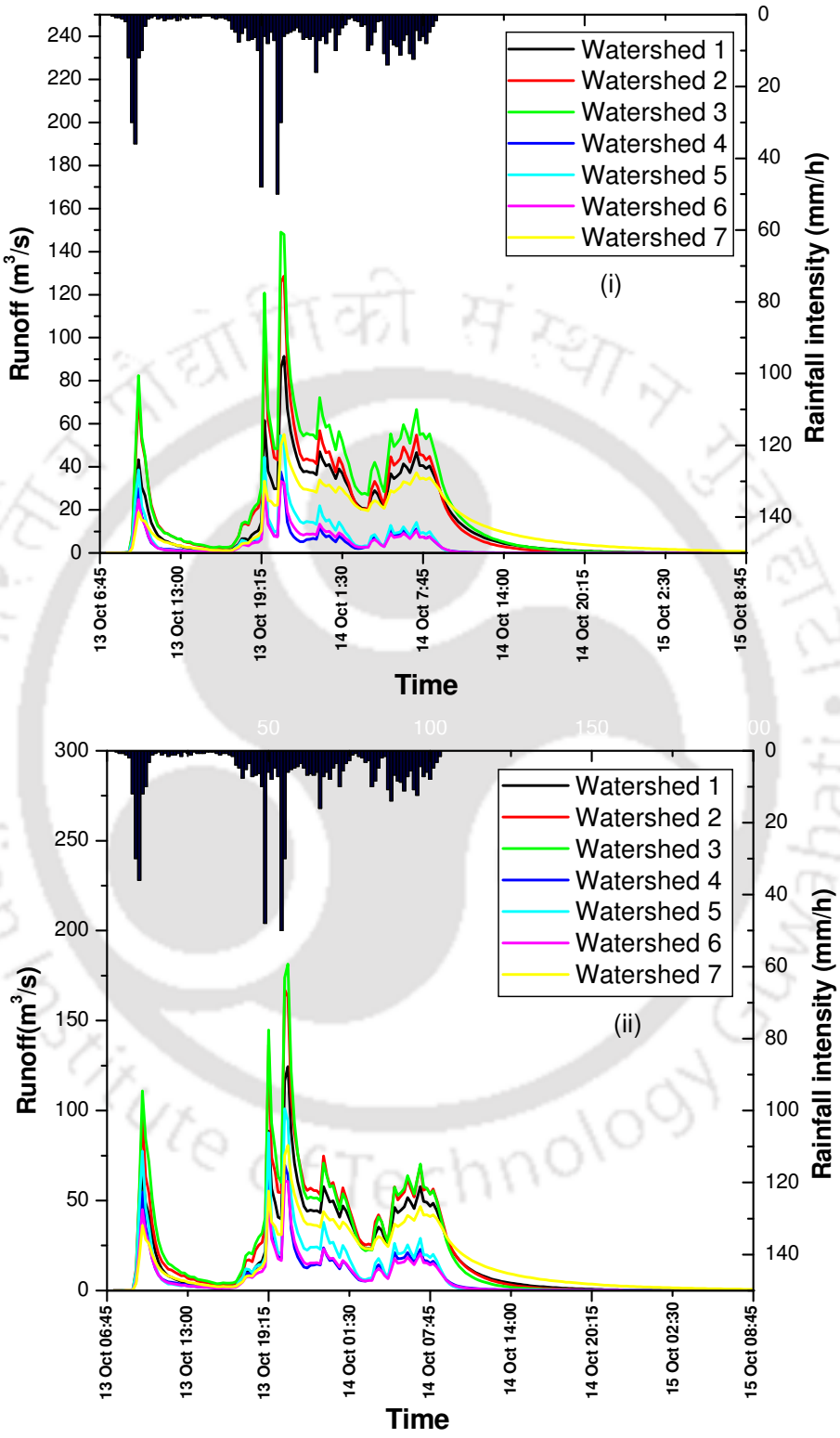

Fig. 6.32 Flow simulation for RE-1 and TIA estimated without using GIS data for year (i) 2006 and (ii) 2011

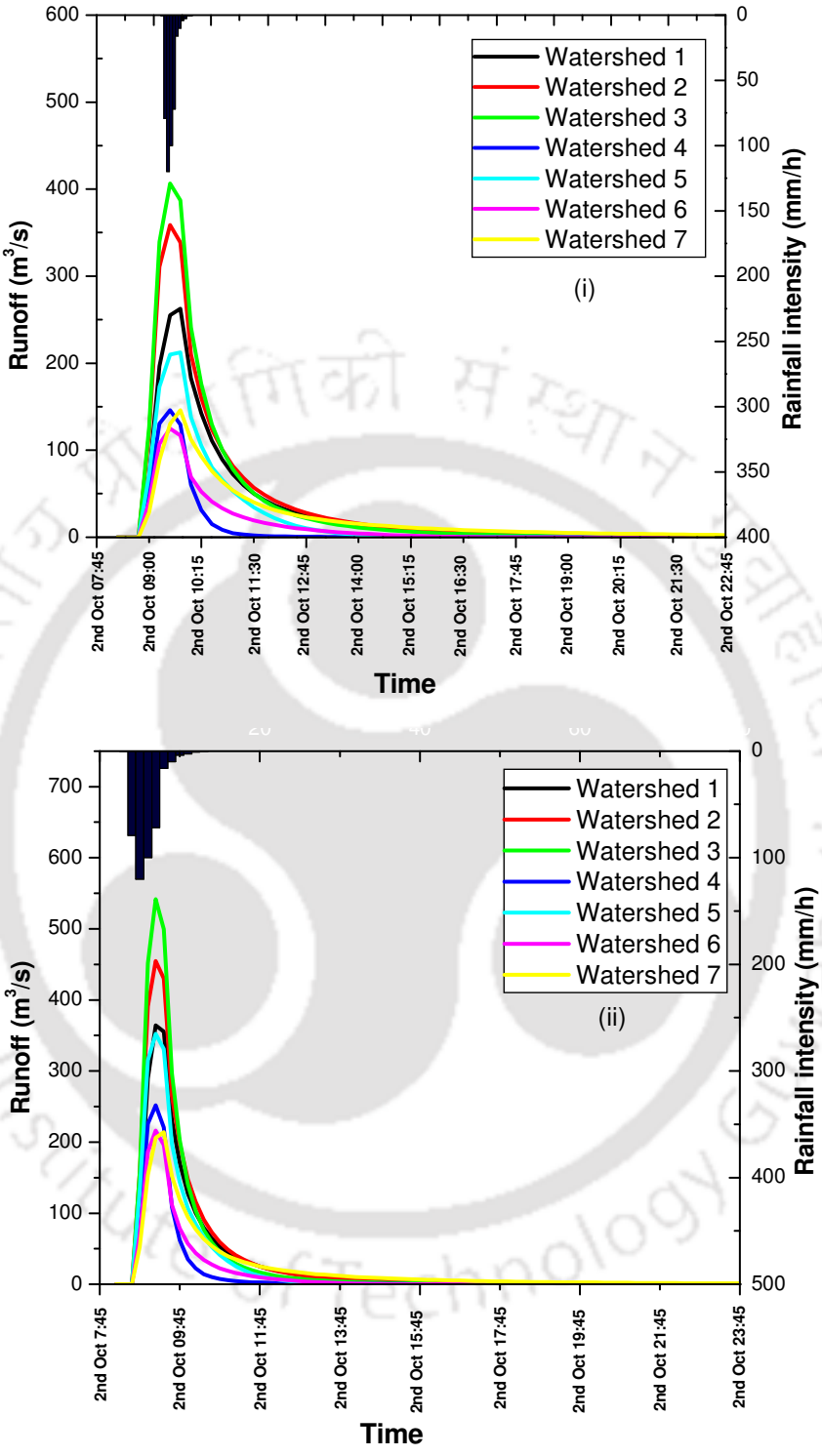

Fig. 6.33 Flow simulation for RE-2 and TIA estimated without using GIS data for year (i) 2006 and (ii) 2011

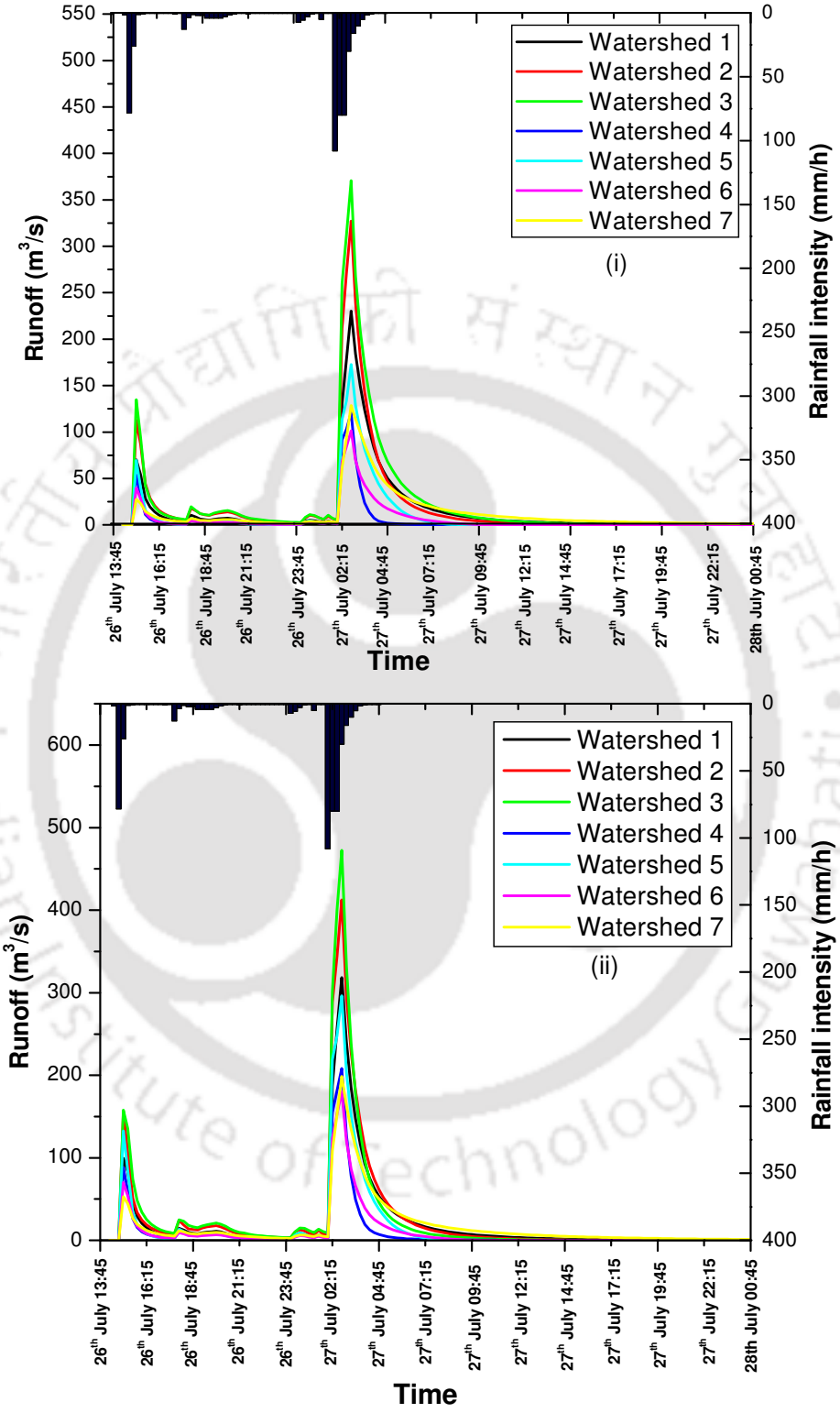

Fig. 6.34 Flow simulation for RE-3 and TIA estimated without using GIS data (i) 2006 and (ii) 2011

Table 6.5 Effect of using GIS data on peak runoff for year 2006 and rainfall event RE-3

Watershed No.	Peak runoff (m^3/s) by		(a)/(b)
	considering GIS data (a)	not considering GIS data (b)	
1	345.56	230.4	1.5
2	412.27	327.01	1.26
3	415.47	371.2	1.12
4	139.12	120.98	1.15
5	234.53	172.94	1.34
6	116.49	101.3	1.15
7	146.61	128.6	1.14

Table 6.6 Effect of using GIS data on peak runoff for year 2011 and rainfall event RE-3

Watershed No.	Peak runoff (m^3/s) by		(a)/(b)
	considering GIS data (a)	not considering GIS data (b)	
1	414.74	318.13	1.3
2	481.03	412.29	1.16
3	518.8	472.38	1.09
4	221.95	208.17	1.06
5	355.71	296.5	1.2
6	198.42	180.38	1.1
7	212.59	198.7	1.07

6.5 Role of Urbanization in Runoff Simulation

With all physical characteristics of the study area remaining constant, the increase in runoff from the year of 1980 to 2011 is a combined effect of the change in rainfall intensity and imperviousness (due to urbanization growth). To assess the actual effect of urbanization on runoff, the rainfall data is kept constant and land use of years varying from 1980 to 2011 has been used to determine runoff and the results are presented in the following sub sections.

6.5.1 Continuous rainfall data

Peak rainfall intensity of 2.2 mm/h is considered and the corresponding runoff for the land use of 1980, 2006 and 2011 has been estimated. EIA estimated from Eq. 4.10 (developed for the study area) has been used as the imperviousness for runoff prediction. Figs. 6.35 to 6.38 depict the impact of urbanization on runoff estimated based on continuous rainfall data for all watersheds. In the figures, (i) and (ii) are runoff estimated based on TIA and EIA (using Eq.

4.10), respectively. The summary of simulated runoff variation in response to the growth in imperviousness (effect of urbanization) is listed in Table 6.7. In general, runoff for the year 1980 is quite meager due to very low urbanization. Based on Fig. 6.35, the peak runoff in watershed 1 was found to increase by 160.8% from 1980 to 2006 for an increase in TIA from 4.2% to 23.85%. Similarly there is an increase in peak runoff of watershed 1 by 13.13% for TIA increase of 7.33% from 2006 to 2011. Fig. 6.35 a(ii) indicates an increase in peak runoff from 1.97 m^3/s in 1980 to 3.2 m^3/s in 2006 and 4.91 m^3/s in 2011 which contributes to 149% increase from 1980 to 2011. This can be attributed to the increased EIA of watershed as shown in Table 6.7. From Fig. 6.35b (i) it can be noted that an increase in TIA in watershed 2 from 32.92% in 2006 to 43.25% in 2011 causes 12.36% increase in peak runoff. Also 32.73% increase in EIA in watershed 2 increases the runoff by 26.3% from 2006 to 2011.

The highly urbanized watershed 3 exhibits 10% increase in runoff from 2006 to 2011 due to 21% increase in TIA and 75.32% increase in runoff from 2006 to 2011 due to 54.68% increase in EIA. Watershed 4 indicates an increased peak runoff of 116% from 2006 to 2011 due to TIA and 53.34% increase in runoff from 2006 to 2011 due to increase in EIA. For watershed 5 there is 21% and 62% increase in peak runoff from 2006 to 2011 due to increase in TIA and EIA, respectively. For watershed 6 there is 20.4% and 20% increase in peak runoff from 2006 to 2011 due to increase in TIA and EIA, respectively. It can be noted from Fig. 6.38 that for watershed 7, 59.06% increase in TIA from 2006 to 2011 causes the peak runoff to increase by 26.82%. An increase in EIA by 35.41% from 2006 to 2011 causes the peak runoff to increase by 49%.

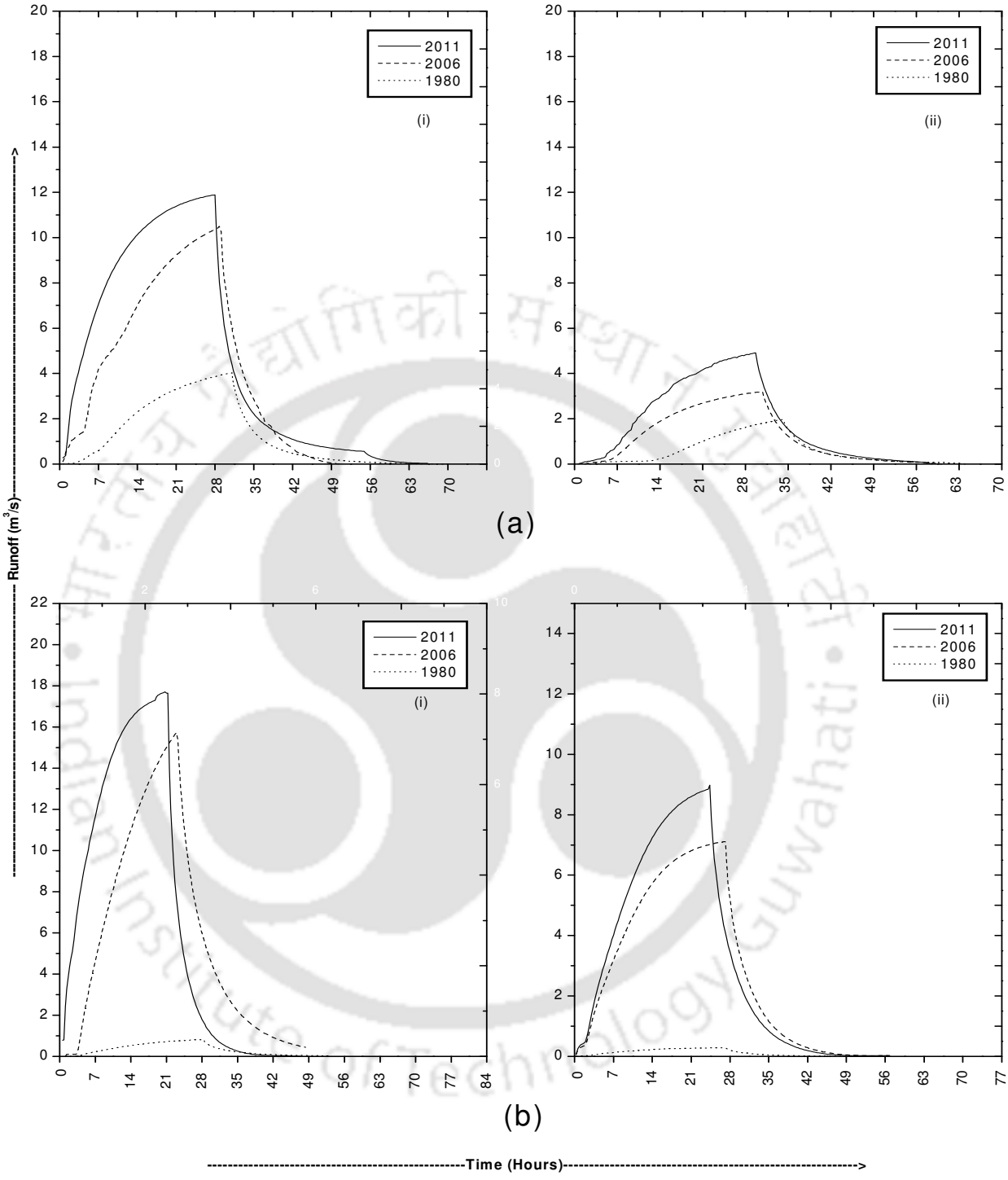

Fig. 6.35 Effect of urbanization growth on simulated runoff of (a) watershed 1 and (b) watershed 2 by considering (i) TIA and (ii) EIA

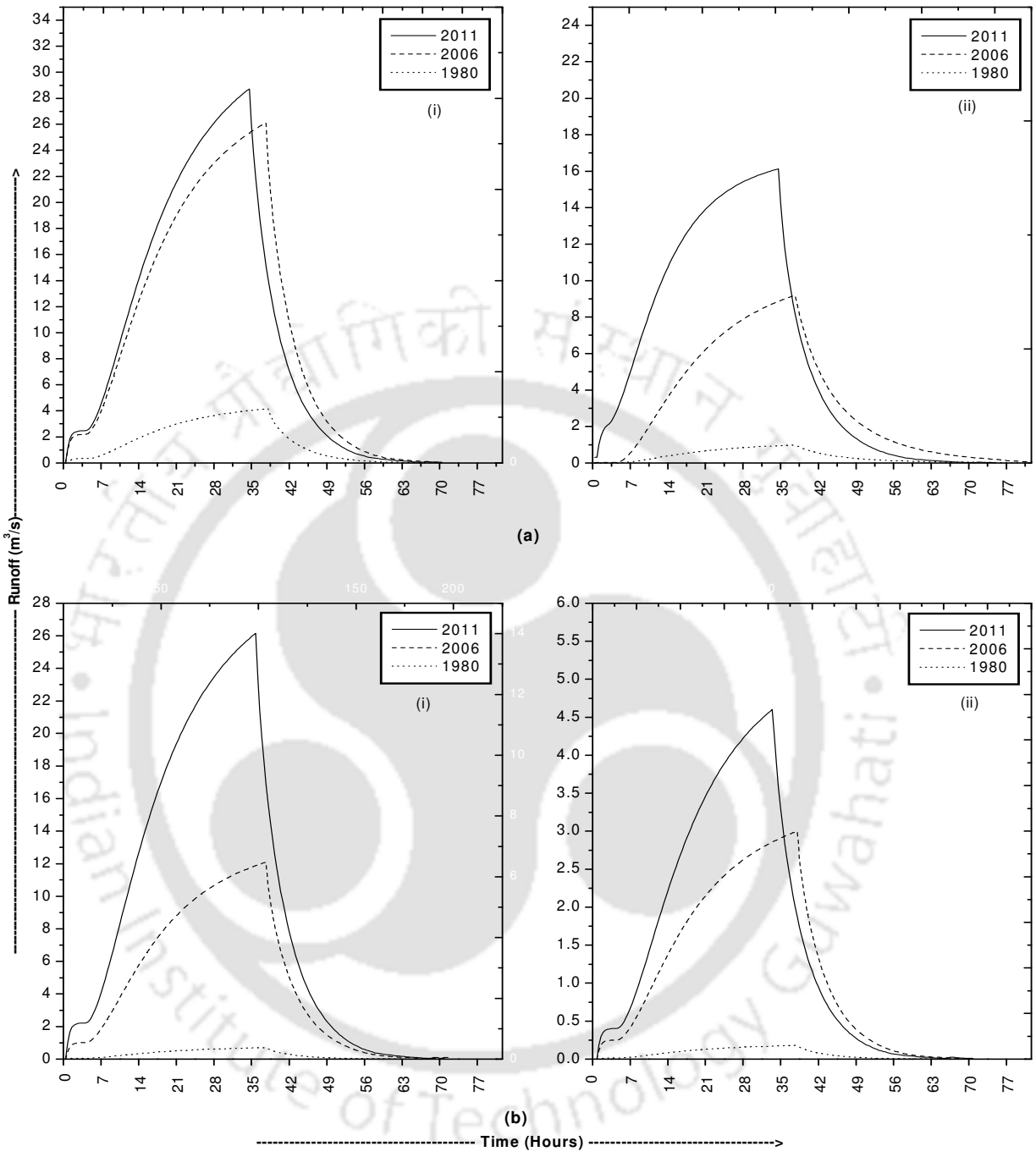

Fig. 6.36 Effect of urbanization growth on simulated runoff of (a) watershed 3 and (b) watershed 4 by considering (i) TIA and (ii) EIA

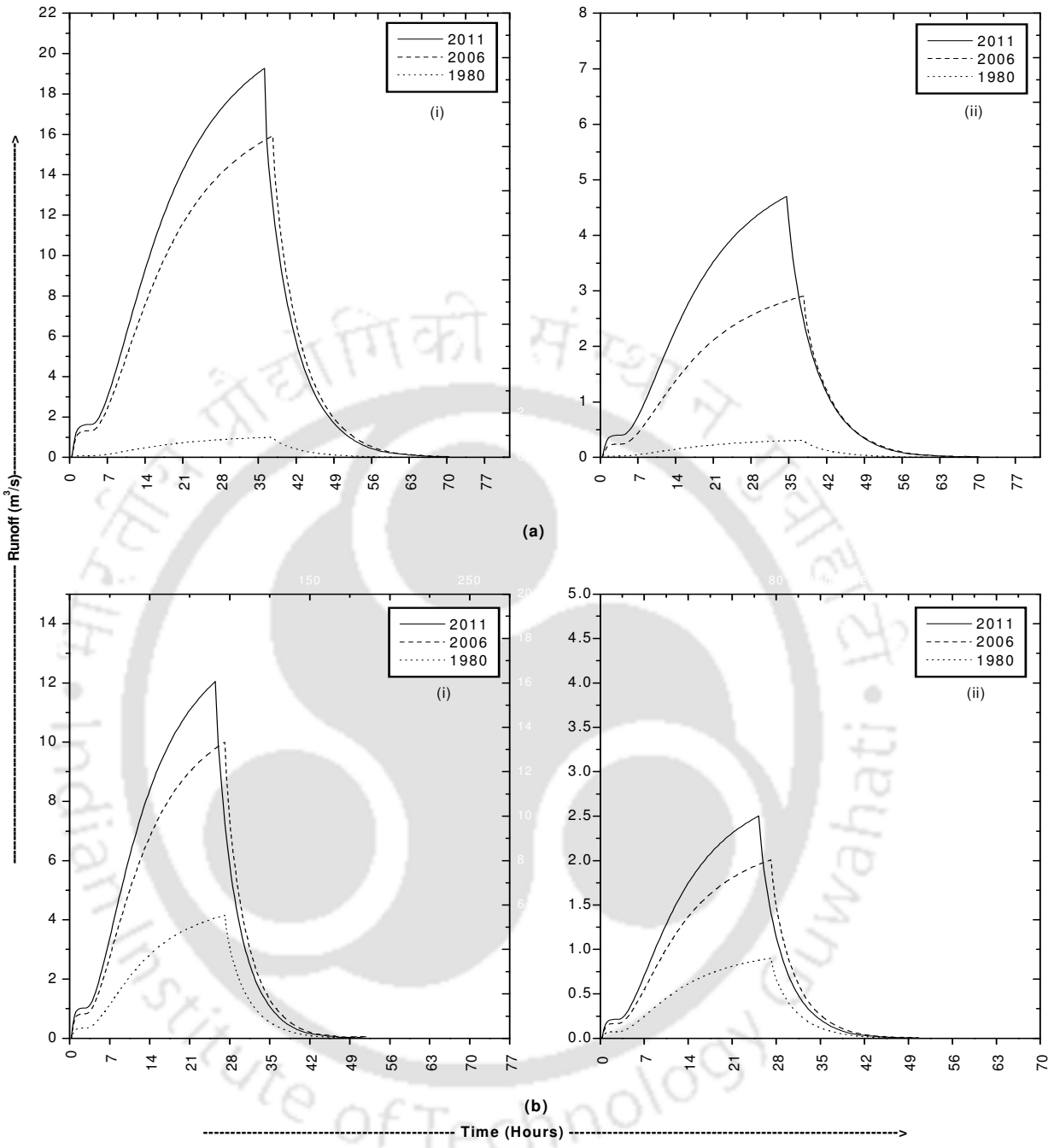

Fig. 6.37 Effect of urbanization growth on simulated runoff of (a) watershed 5 and (b) watershed 6 by considering (i) TIA and (ii) EIA

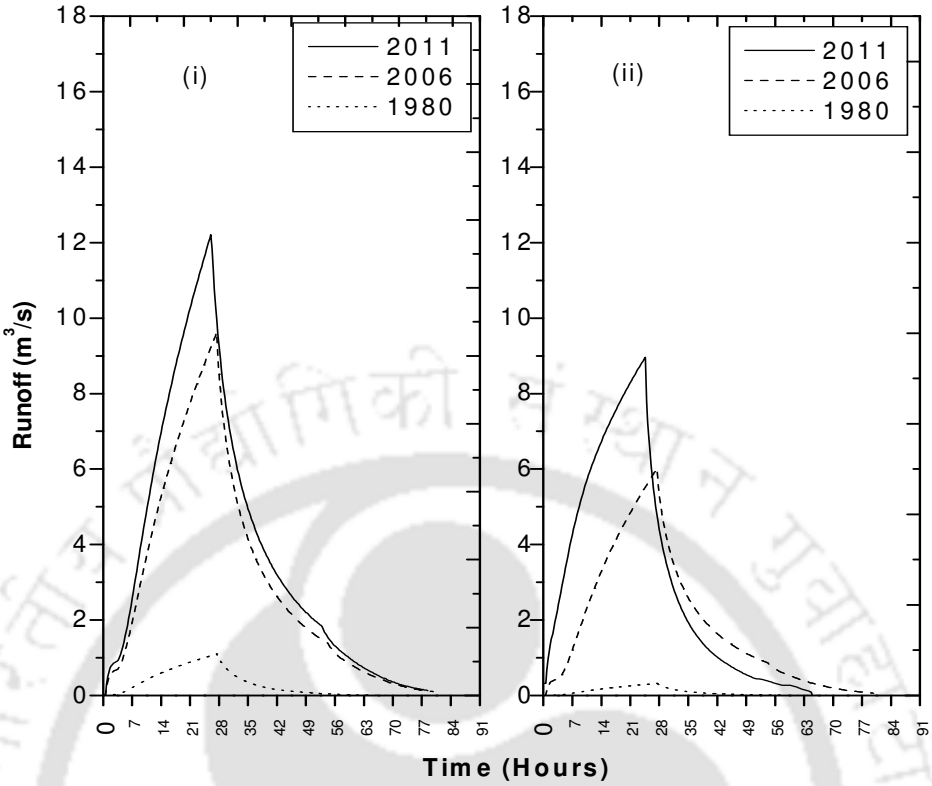

Fig. 6.38 Effect of urbanization growth on simulated runoff of watershed 7 by considering (i) TIA and (ii) EIA

Table 6.7 Effect of urbanization on simulated runoff in the study area based on continuous rainfall

Watershed	Year	Impervious area (%)		Peak runoff (m^3/s) due to	
		TIA	EIA	TIA	EIA
1	1980	4.2	0.34	4.03	1.97
	2006	23.85	1.28	10.51	3.2
	2011	25.6	2.51	11.89	4.91
2	1980	0.58	0.0009	0.81	0.28
	2006	32.92	4.98	15.7	7.11
	2011	43.25	6.61	17.64	8.98
3	1980	6.0	0.16	4.16	0.98
	2006	53.17	7.9	26.12	9.2
	2011	64.3	12.22	28.75	16.13
4	1980	0.04	0.0000025	0.4	0.18
	2006	31.38	1.1	12.1	3
	2011	53.4	1.71	26.15	4.6
5	1980	2.6	0.03	1.0	0.3
	2006	36.17	1.07	15.93	2.9
	2011	48.5	1.74	19.28	4.7
6	1980	5.47	0.13	4.15	0.9
	2006	23.53	0.38	10	2.08
	2011	30.83	0.54	12.04	2.5
7	1980	3.63	0.06	1.1	0.32
	2006	19.74	4.8	9.62	6.01
	2011	31.4	6.5	12.2	8.96

6.5.2 Event wise rainfall data

Different rainfall events (RE-1, RE-2 and RE-3) have been used to assess the effect of urbanization on runoff simulation for the most urbanized watershed 3 by considering different methods of imperviousness determination. Fig. 6.39 shows the runoff predicted due to RE-1 at the outlet of watershed 3 for imperviousness estimated by different methods in the years 1980 and 2011. Fig. 6.39(i) indicates that the runoff is largely overestimated if imperviousness other than directly estimated EIA is employed in the model.

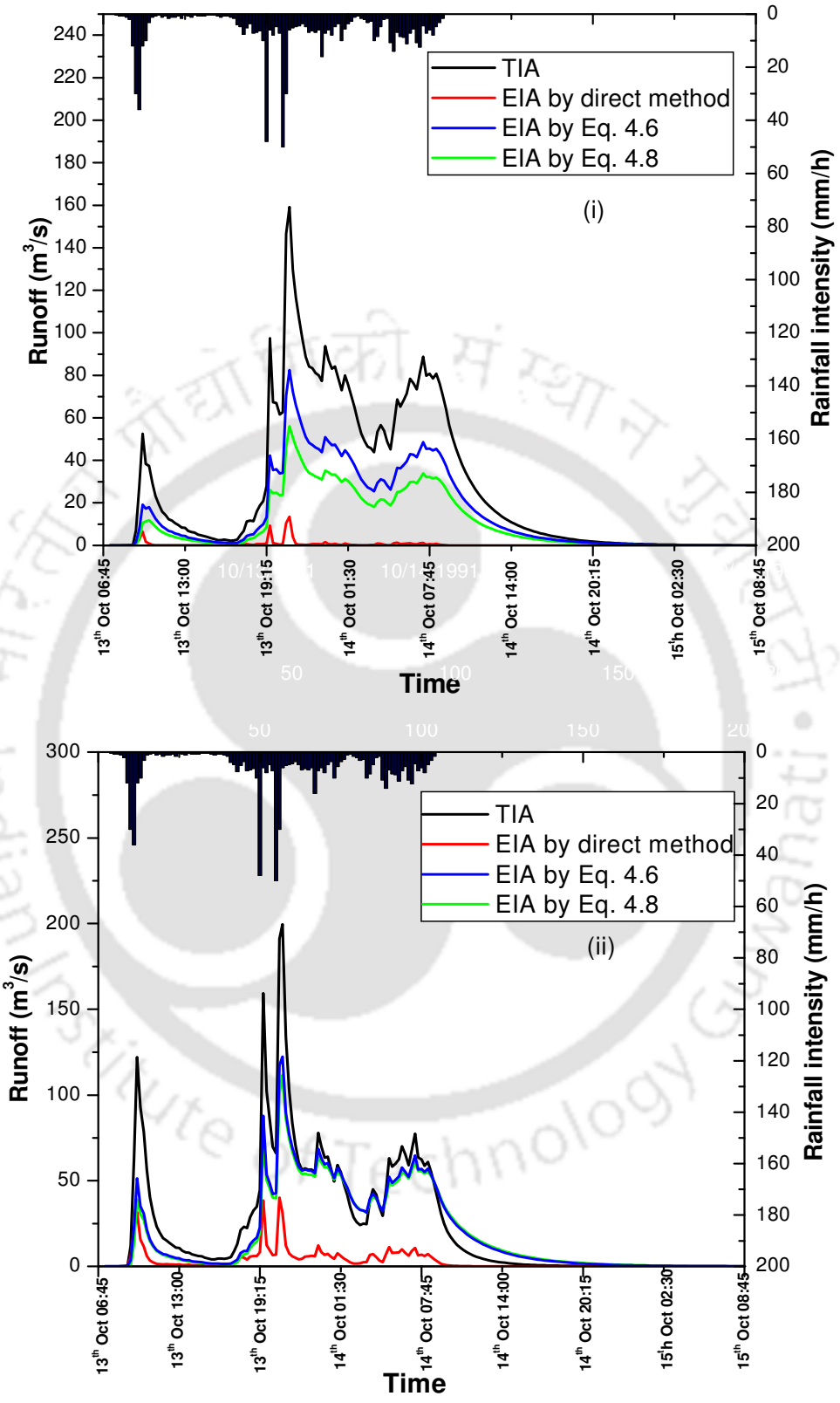

Fig. 6.39 Comparison of runoff simulated using RE-1 in watershed 3 corresponding to different imperviousness in the year (i) 1980 and (ii) 2011

From Fig. 6.39(ii) it is observed that the predicted runoff was 179.36% more if EIA estimated by Eq. 4.8 is used in the model in place of EIA estimated by direct method. Similarly predicted peak runoff was found to be 205% more if EIA estimated by Eq. 4.6 is used in the model in place of EIA estimated by direct method. The peak runoff is overestimated by 398% if TIA is used in the model instead of the EIA estimated by the direct method. Table 6.8 summarizes the increase in peak runoff values from 1980 for RE-1 and by considering different imperviousness. It can be noted that the increase in peak runoff was maximum (195.57%) from 1980 to 2011 when EIA estimated by direct method is used for runoff modeling.

Table 6.8 Effect of type of imperviousness on peak runoff of watershed 3 from 1980 to 2011 and RE-1

Type of imperviousness	Imperviousness (%) in 1980	Imperviousness (%) in 2011	Increase in peak runoff (%)
TIA	6.0	64.3	25.45
EIA by direct method	0.16	12.22	195.57
EIA by Eq. 4.6	1.87	33.31	48.38
EIA by Eq. 4.8	0.36	13.22	99.7

Fig. 6.40 shows the runoff predicted due to RE-2 at the outlet of watershed 3 for different imperviousness. From Fig. 6.40(ii), it is observed that the predicted runoff was 97.5% more if EIA estimated by Eq. 4.8 is used in the model in place of EIA estimated by direct method. Similarly the predicted runoff was 115.17% more if EIA estimated by Eq. 4.6 is used in the model in place of EIA estimated by direct method. Again it can be mentioned that increase in imperviousness increases the peak runoff by 314.3% at the outlet of watershed 3 if TIA is used in the model instead of the EIA estimated by the direct method. Table 6.9 shows the imperviousness of watershed 3 for the years 1980 and 2011 along with the increase in peak runoff values simulated for RE-2. It has been observed from the table that the increase in peak runoff was maximum (169.05%) from 1980 to 2011 when EIA values estimated by the direct method is considered.

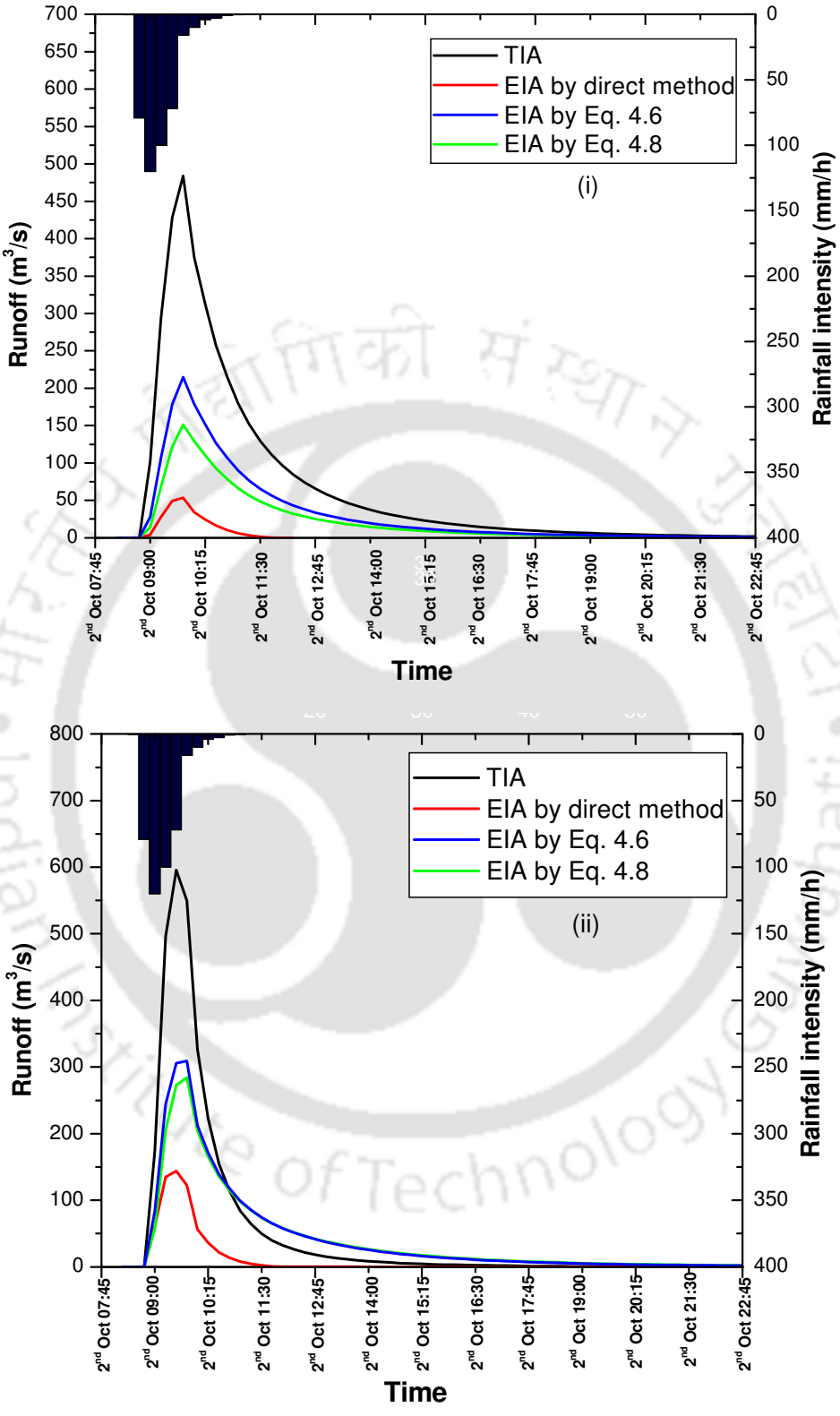

Fig. 6.40 Comparison of runoff simulated using RE-2 in watershed 3 corresponding to different imperviousness in the year (i) 1980 and (ii) 2011

Table 6.9 Effect of type of imperviousness on peak runoff of watershed 3 from 1980 to 2011 and RE-2

Type of imperviousness	Imperviousness (%) in 1980	Imperviousness (%) in 2011	Increase in peak runoff (%)
TIA	6.0	64.3	23.15
EIA by direct method	0.16	12.22	169.05
EIA by Eq. 4.6	1.87	33.31	44.0
EIA by Eq. 4.8	0.36	13.22	87.97

Fig. 6.41 shows the runoff predicted due to RE-3 at the outlet of watershed 3 for different imperviousness. From Fig. 6.41(ii) it is observed that the predicted runoff was 134.62% more if EIA estimated by Eq. 4.8 is used in the model in place of EIA estimated by direct method. When Eq. 4.6 is used in the model instead of direct method, predicted peak runoff was 157.5% more. Table 6.10 shows the imperviousness of watershed 3 for the years 1980 and 2011 along with the increase in peak runoff values simulated for RE-3. From table it can be noted that the increase in peak runoff was maximum (178.71%) from 1980 to 2011 when EIA is determined by direct method.

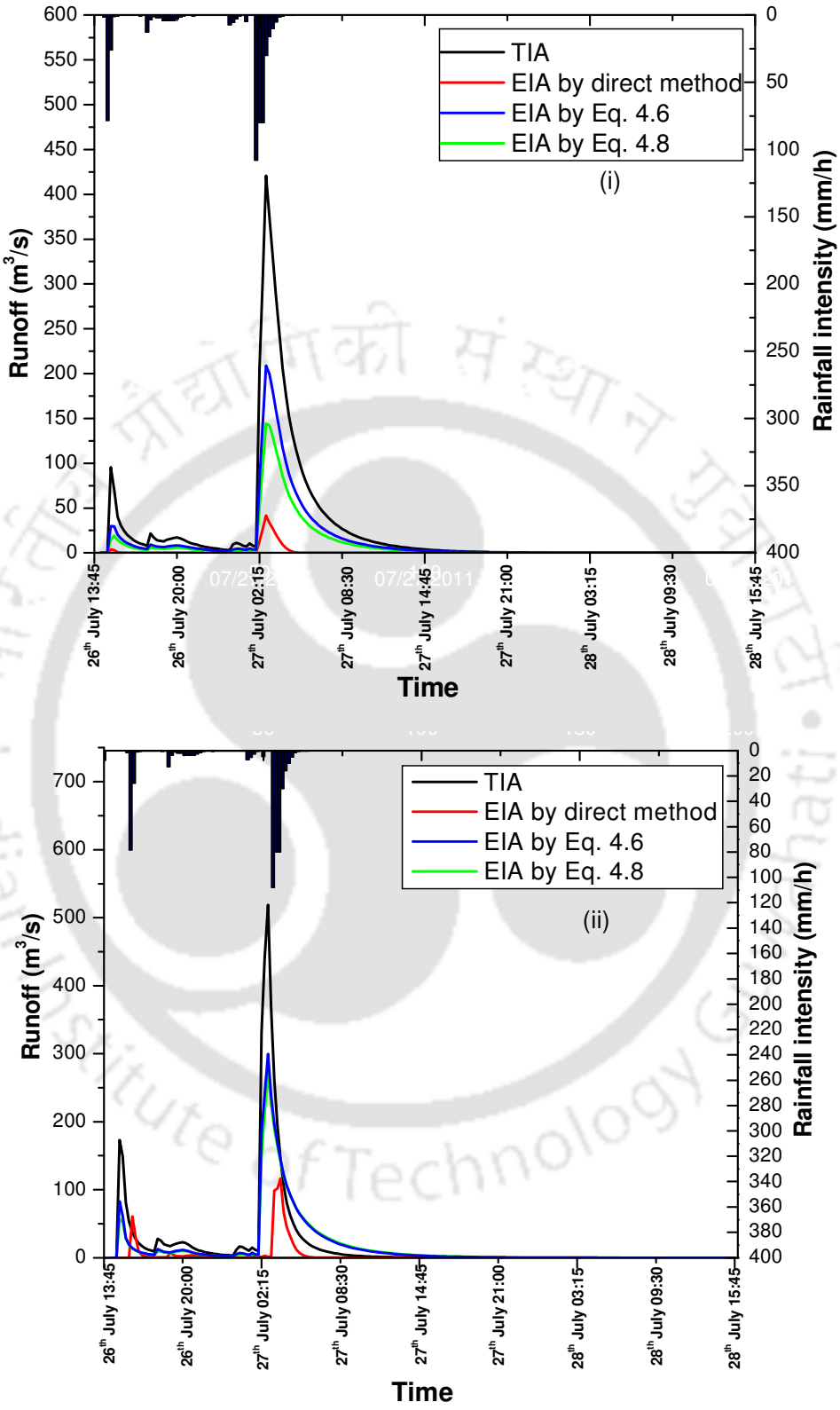

Fig. 6.41 Comparison of runoff simulated using RE-3 in watershed 3 corresponding to different imperviousness in the year (i) 1980 and (ii) 2011

Table 6.10 Effect of type of imperviousness on peak runoff of watershed 3 from 1980 to 2011 and RE-3

Type of imperviousness	Imperviousness (%) in 1980	Imperviousness (%) in 2011	Increase in peak runoff (%)
TIA	6.0	64.3	23.09
EIA by direct method	0.16	12.22	178.71
EIA by Eq. 4.6	1.87	33.31	45.5
EIA by Eq. 4.8	0.36	13.22	89.15

The impact of urbanization on runoff for all watersheds is shown in Figs. 6.42 to 6.44 and the same is listed in Table 6.11. EIA values for the year 1980 reported in the table is estimated from TIA by using Eq. 4.10 (developed for the study area). For the year 2011, EIA values are obtained from semi automated direct method (chapter 4). Table 6.11 shows that watershed 3 exhibits the maximum increase in peak runoff and watershed 6 exhibited least increase in runoff from 1980 to 2011 for all the rainfall events. It may be noted here that the urbanization is quite high in watershed 3 and hence the maximum increase in peak runoff is justified.

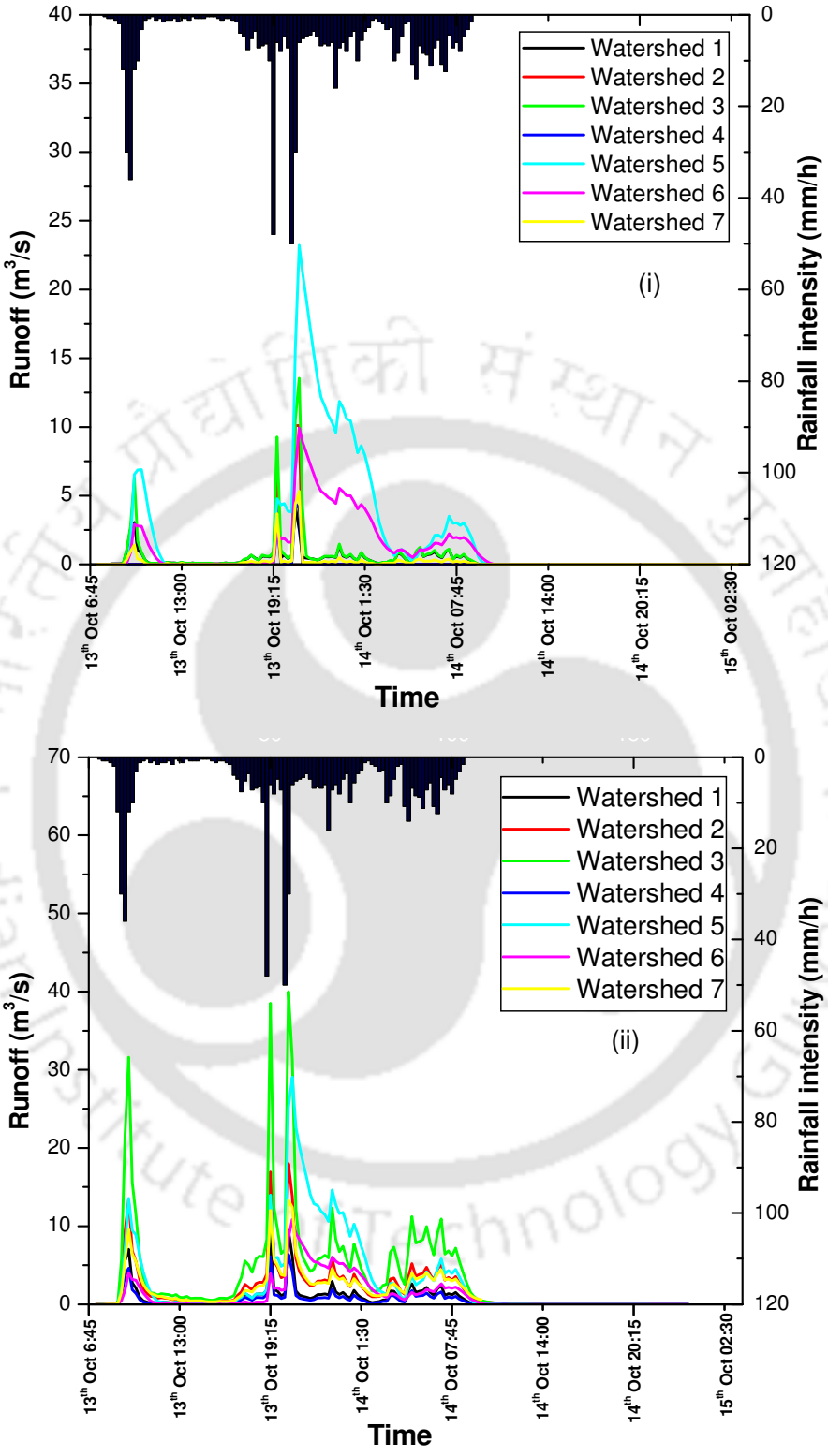

Fig. 6.42 Flow simulation in the study area for RE-1 by considering EIA of the year (i) 1980 (ii) 2011

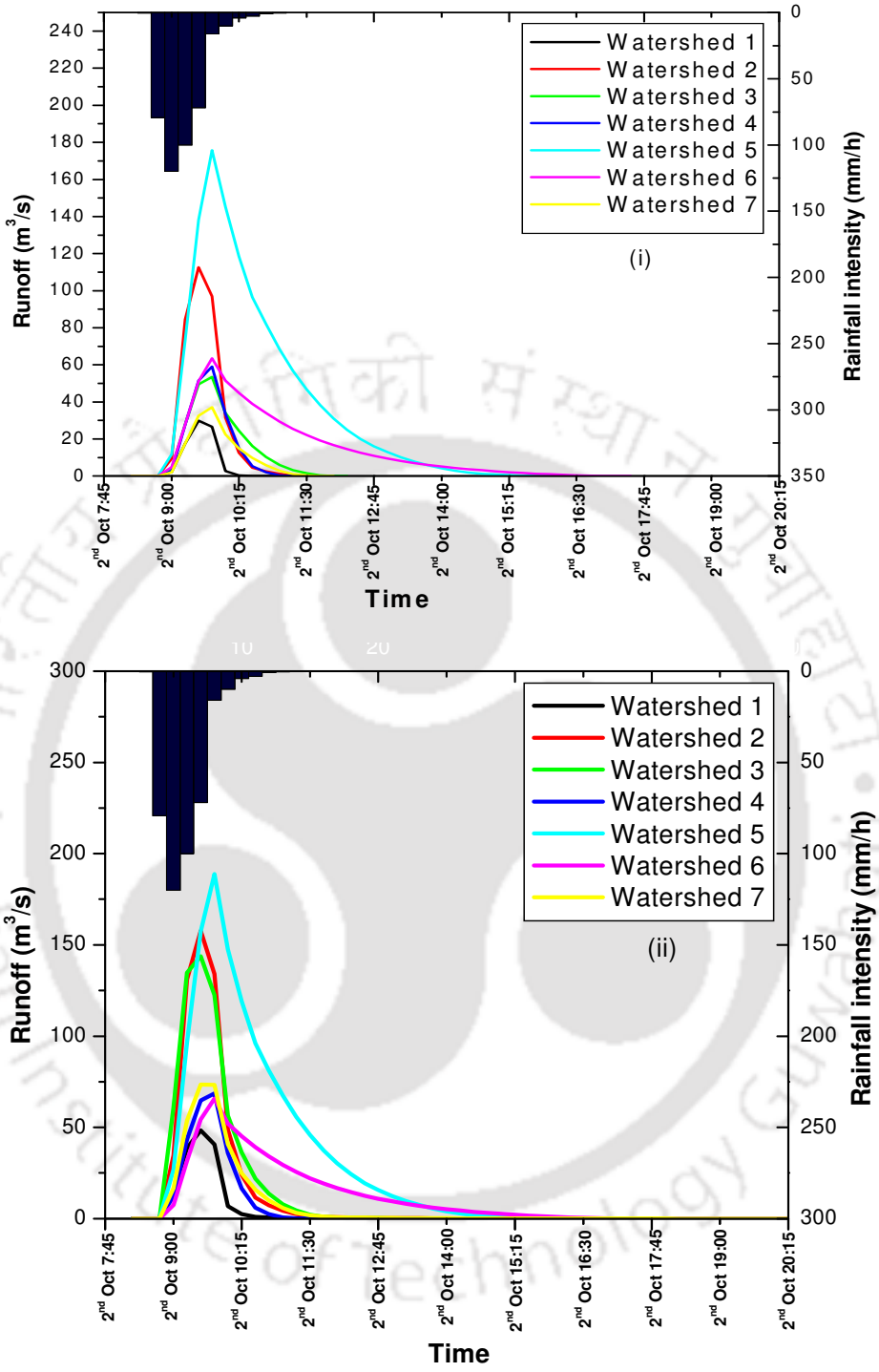

Fig. 6.43 Flow simulation in the study area for RE-2 by considering EIA of the year (i) 1980 (ii) 2011

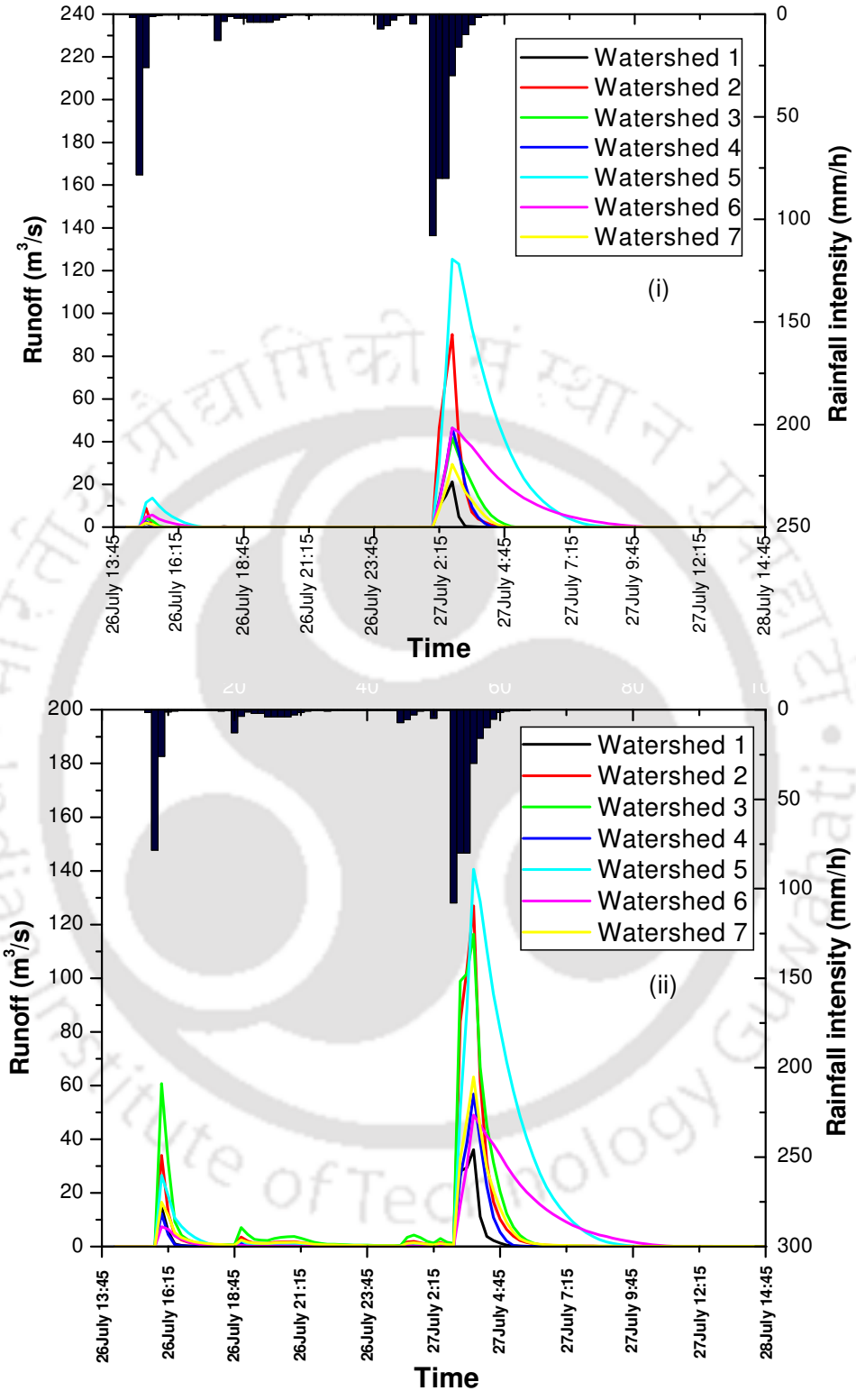

Fig.6.44 Flow simulation in the study area for RE-3 by considering EIA of the year (i) 1980 (ii) 2011

Table 6.11 Change in peak runoff due to EIA change from 1980 to 2011

Watershed	EIA (%) in 1980	EIA (%) in 2011	Increase in peak runoff (%) for		
			RE-1	RE-2	RE-3
1	0.34	2.51	124	62.23	70
2	0.0009	6.61	78.67	39.95	40.8
3	0.16	12.22	195.57	169.04	178.7
4	0.0000025	1.71	44.15	16.19	22.7
5	0.03	1.74	25.3	7.5	12.12
6	0.13	0.54	9.7	3.6	5.47
7	0.06	6.5	150.56	97.6	114.8

6.6 Simulated Runoff for Rainfall Intensities of Different Return Periods

The model was used to predict the runoff for a range of peak rainfall intensities corresponding to different return periods. The rainfall intensities were derived from the Intensity-Duration-Frequency (IDF) relationship of the region given by Eq. 6.5 (Rambabu et al. 1979; Subramanya 2011) for the duration of 15 minutes for different return periods (25 years, 50 years, 75 years and 100 years). Rambabu et al. (1979) analyzed rainfall characteristics for 42 rain gauge stations located in five different zones, namely, northern zone, western zone, central zone, eastern zone and southern zone, throughout India and developed the following relationship:

$$i = \frac{KT^a}{(t+b)^n} \qquad (6.5)$$

where i is the rainfall intensity in cm/h; T is the return period in years; t is the storm duration in hours; K, a, b and n are coefficients depending on location.

The value of the coefficients in Eq. 6.5 for a number of cities within India is also reported in the study. Hence, to get a close estimate of rainfall intensity for a particular return period for the study area Eq. 6.5 has been preferred over other IDF relationships available for Indian regions. The coefficients for the study area are K = 7.206; a = 0.156; b = 0.75; n = 0.94 (Rambabu et al. 1979). Based on these coefficients, the different rainfall intensities estimated for the study area are listed in Table 6.12.

Table 6.12 Rainfall intensities for different return periods

Return period (years)	Rainfall intensity (mm/h)
25	119.0
50	132.6
75	141.3
100	147.8

The simulated runoff for different watersheds of the study area are presented in Table 6.13 and plotted in Fig. 6.45. From Fig. 6.45, it is observed that watershed 5 produces maximum runoff and watershed 1 produces least runoff for all the design storms. Also it is noticed that there is a steep rise of simulated runoff for all watersheds from 25 year storm to 50 year storm and there is a steady marginal rise of the simulated runoff from 50 year storm to 100 year storm. Further it is observed that watershed 3 shows maximum rate of increase of simulated runoff (27.52%) from 2006 to 2011 for 100 year storm.

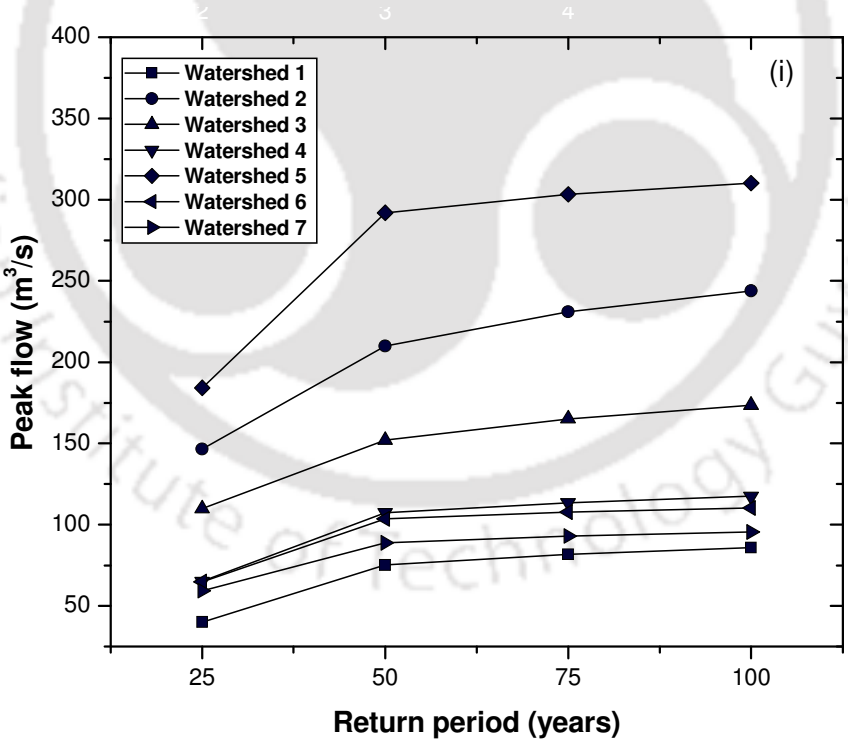

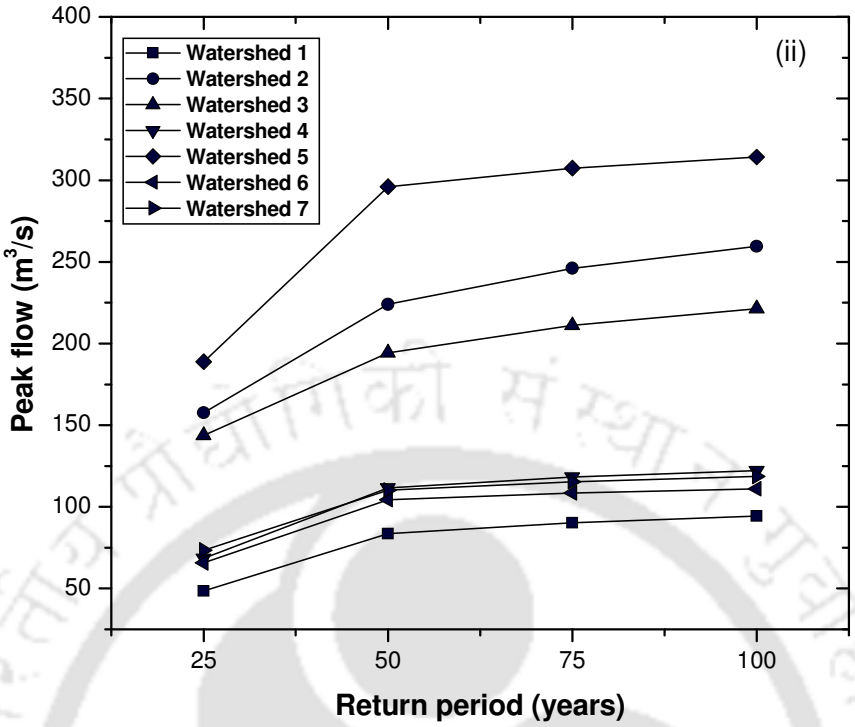

Fig. 6.45 Simulated runoff in the study area for different design storms for (i) 2006 LU and (ii) 2011 LU

Table 6.13 Peak flow for different design storms and for years 2006 and 2011

Watershed No.	Estimated Peak Flood (m^3/s)							
	25 yr flood		50 yr flood		75 yr flood		100 yr flood	
	2006 LU	2011 LU	2006 LU	2011 LU	2006 LU	2011 LU	2006 LU	2011 LU
1	40.11	48.41	75.13	83.59	81.78	90.27	85.87	94.38
2	146.5	157.64	209.96	224.11	231.01	246.1	243.88	259.54
3	109.92	143.83	152.05	194.4	165.13	211.15	173.61	221.4
4	65.13	68.54	107.42	111.62	113.51	118.24	117.55	122.29
5	184.26	188.88	291.96	296.13	303.32	307.45	310.2	314.3
6	64.91	65.79	103.55	104.4	107.67	108.52	110.19	111.04
7	59.33	73.51	88.81	110.24	92.99	115.42	95.54	118.56

Chapter 7

Development of Flood Inundation Maps and Flood Risk Assessment for the Study Area

7.1 General

Flood inundation map (FIM) is required to understand the impact of flooding in a particular area and on important structures such as roadways, railways, streets, buildings, airport, etc. FIM provides important information like depth and spatial extent of flooded zones, which is required by the municipal authorities to inform the citizens about the major flood prone areas and adopt appropriate flood management strategies. For proper flood management planning, it is very important to identify the flood risk from the interaction of hazard and vulnerability. Risk analysis quantifies the risk and risk quantification relies on flood hazard maps of the area (Apel et al. 2009). Hence flood hazard maps of the study area have been prepared corresponding to land use (LU) of different years by considering individual vulnerability parameters such as flood depth and inundated area, land use, affected population and road networks. In this chapter, FIM is determined by using Watershed Modeling System (WMS 8.4) and the risk assessment for the flood hazards also determined in the study area.

7.2 Flood Inundation Model

The runoff obtained at the outlet of each of the watersheds (using SWMM) and the drainage network details of the study area has been used to determine the inundated area. Runoff obtained from SWMM is used as the inflow hydrograph at the channel upstream. Further, unsteady flow modeling is carried out by using Hydrologic Engineering Centre-River Analysis System (HEC-RAS) in WMS platform to obtain water surface elevation in the channel and flow hydrograph at the downstream end of the channel. The details of the modeling procedure are discussed below.

7.2.1 Building the conceptual model

A schematic representation of the existing drainage system is prepared in WMS platform. The cross sections are positioned on the reaches and Manning's roughness is defined for different locations. The cross sectional details are derived from the TIN (triangulated irregular network) of the study area. Separate values of roughness are chosen for the impervious and

pervious fractions of sub-catchment. Manning's 'n' for impervious and pervious surfaces are taken as 0.01 and 0.1 (McCuen et al. 1996) corresponding to its value for concrete (for concrete drains) and vegetation (for natural drains) respectively. This conceptual model is then exported to HEC-RAS platform to simulate the water surface elevation in the channel.

7.2.2 Water surface profile determination using HEC-RAS

The cross section details of the concrete drains are modified with reference to the available cross section details of the collected drainage network. The water surface profiles for unsteady flow are computed by solving the continuity and momentum equations (Barkau 1982), which are expressed by Eqs. 7.1 to 7.6.

$$\frac{\partial A}{\partial t}+\frac{\partial \emptyset Q}{\partial x_c}+\frac{\partial (1-\emptyset)Q}{\partial x_f}=0 \tag{7.1}$$

$$\frac{\partial Q}{\partial t}+\frac{\partial}{\partial x_c}\left(\frac{\emptyset^2 Q^2}{A_c}\right)+\frac{\partial}{\partial x_f}\left(\frac{(1-\emptyset)^2 Q^2}{A_f}\right)+gA_c\left(\frac{\partial z}{\partial x_c}+S_c\right)+gA_f\left(\frac{\partial z}{\partial x_f}+S_f\right)=0 \tag{7.2}$$

$$\emptyset=\frac{K_c}{K_c+K_f} \tag{7.3}$$

$$K=\frac{A^{5/3}}{nP^{2/3}} \tag{7.4}$$

$$S_c=\frac{\emptyset^2 Q^2 {n_c}^2}{{R_c}^{4/3}{A_c}^2} \tag{7.5}$$

$$S_f=\frac{(1-\emptyset)^2 Q^2 {n_f}^2}{{R_f}^{4/3}{A_f}^2} \tag{7.6}$$

where Q is the total flow; A is the cross sectional area of flow which is equal to $A_c + A_f$; A_c is cross sectional area of flow in channel; A_f is cross sectional area of flow in floodplain; X_c is the distance along the channel between the cross sections; X_f is the distance along the floodplain between the cross sections; P is the wetted perimeter; R is the hydraulic radius (A/P); n is Manning's roughness coefficient; S is the friction slope; K_c is the conveyance of the channel; K_f is the conveyance of floodplain. Eqs 7.1 and 7.2 are solved by using four point implicit finite difference method in HEC-RAS. HEC-RAS computes water surface elevation at each cross section which is then imported to WMS platform.

7.2.3 Delineation of floodplain in WMS

WMS intersects the water surface elevation data with the TIN of the study area to delineate the floodplain. The study area is divided into flooded, non-flooded zones and the flood depth in the flooded zones is determined. The flood duration is derived from the flow hydrograph at the downstream of a particular reach. The flood spread is overlaid on the ward map of the study area which is depicted in Fig. 7.1 to know the flood inundated zones.

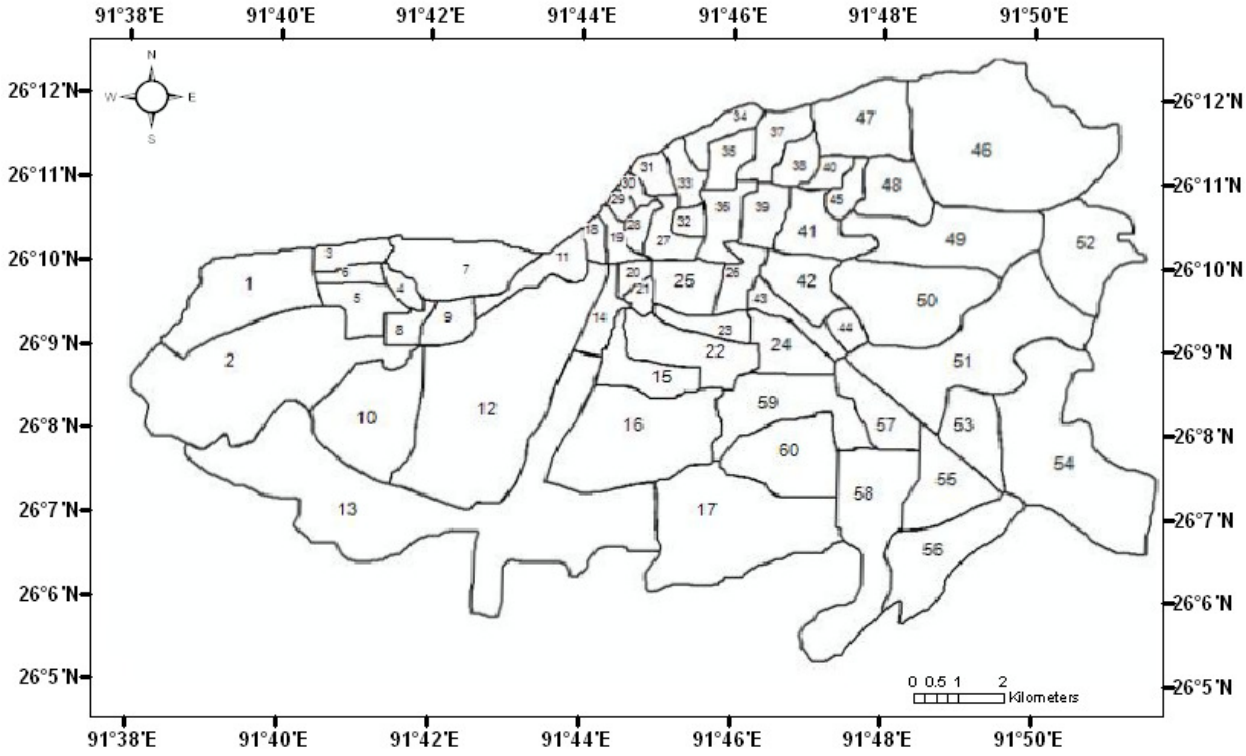

Fig. 7.1 Ward map of the study area showing 60 wards (Source: Guwahati Municipal Corporation)

7.2.4 Flood inundation map for the study area

To study the impact of land use change and the rainfall intensities on the flooding pattern of the urban study area, the inundation maps are prepared for the land use (LU) corresponding to the years 2006 and 2011. Series of historical rainfall events discussed in section 3.3 and rainfall intensities with different return periods discussed in section 6.6 have been considered for the preparation of flood inundation maps.

7.2.4.1 Flood inundation map for peak rainfall events

Fig. 7.2 shows the flood inundation map for the study area for 2006 LU and different rainfall events, RE-1 (13th October 1991), RE-2 (2nd October 2006) and RE-3 (26th July 2011). It is observed from Fig. 7.2 (i) that major portion of the city have been flooded with flood depth varying from 0.004 m to 0.47 m for a rainfall event of RE-1. The worst affected areas are ward number 25, 26, 44, 50 and 51 followed by ward numbers 14, 15, 16, 27, 32 and 59. From Fig. 7.2 (ii), it has been found that the flood depth varies between 0.006 m to 0.61 m throughout the study area for a rainfall of RE-2. The maximum flood depth is found to be in ward number 44, 50 and 51. Among busy residential areas, ward number 26 is the worst affected area where flood depth attains a maximum of 0.49 m and it remained for 59 hours. Though the flood depth in ward numbers 2 and 13 was found to be less, it remained for quite a long period of 83 hours. It can be observed from Fig. 7.2 (iii) that the maximum flood depth of 0.54 m has been found in ward number 50 for a rainfall of RE-3. Other worst affected areas are ward numbers 14, 15, 21, 25, 26, 27, 28, 32, 44, 51 and 59 with flood depth greater than 0.22 m. Land use remaining constant, the increase in flood depth is due to the increase in the rainfall intensity.

Fig. 7.3 shows flood inundation map of the study area for the rainfall events RE-1, RE-2 and RE-3 corresponding to 2011 LU. Flood depth varies from 0.005 m to 0.54 m in different places of the study area for RE-1. Maximum flood depth of 0.54 m is observed in ward number 44, 50 and 51. For the intense rainfall event of RE-2, the maximum flood depth was found to be 0.68 m in 2011. Comparing Fig. 7.2 (i) and Fig. 7.3 (i), it can be noted that the maximum flood depth in the study area increased by 16.7% from 2006 to 2011 for RE-1. Similarly, the increase in maximum flood depth corresponding to RE-2 and RE-3 is 10.2 % and 20.2 %, respectively. The average increase in maximum flood depth from 2006 to 2011 considering the three rainfall events is 15.7 %. This increase in flood depth in the study area is attributed to the increased imperviousness by 1.48 times from 2006 to 2011. The summary of results obtained from the flood inundation maps are listed in Table 7.1. It can be observed from Table 7.1 that the major portion of the city is affected by flood in both the years. It is also noticed that the duration of flood inundation increases in the affected wards from 2006 to 2011. This can be attributed to increased imperviousness in 2011.

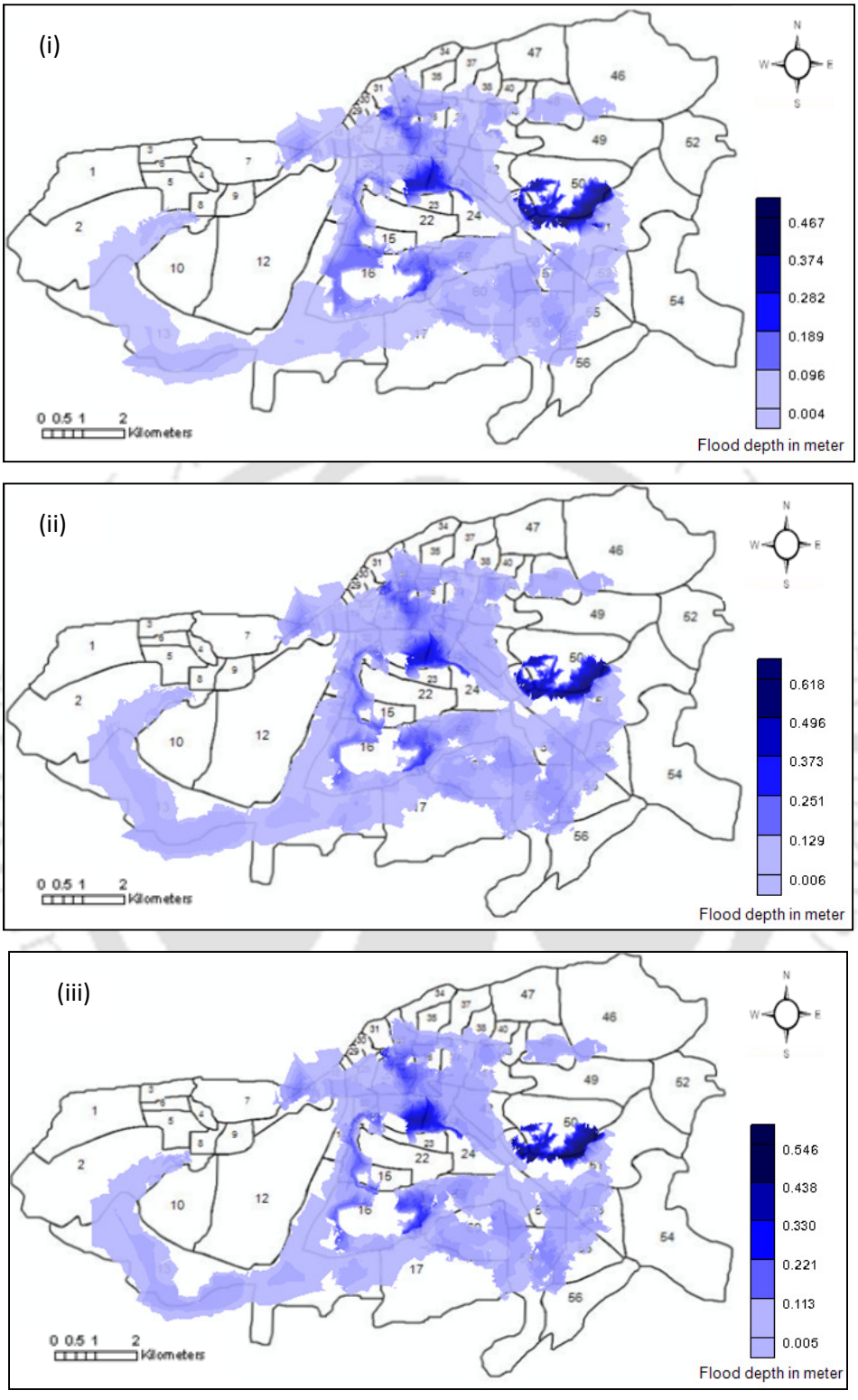

Fig. 7.2 Flood inundation map of the study area for LU of 2006 for (i) RE-1, (ii) RE-2 and (iii) RE-3

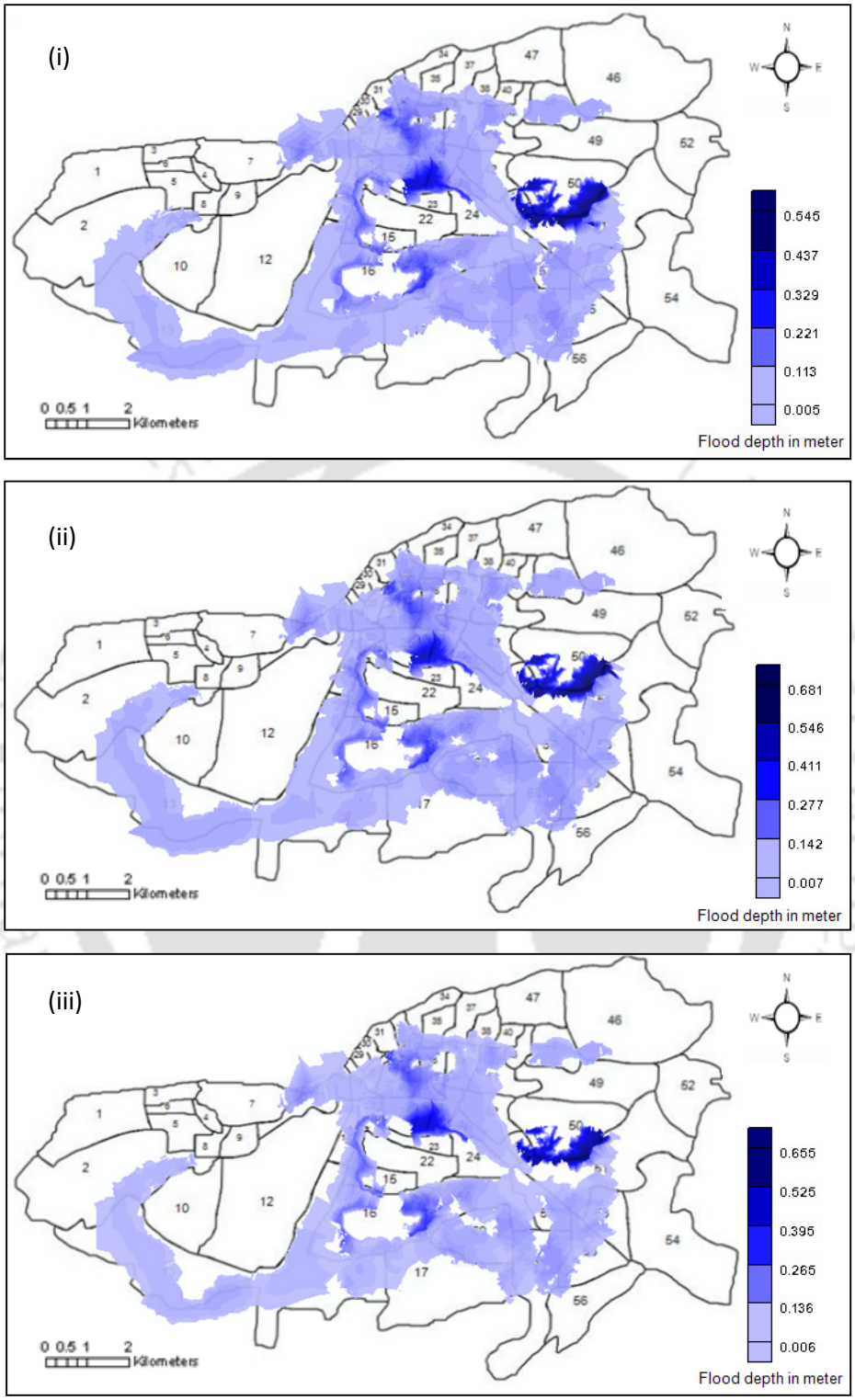

Fig. 7.3 Flood inundation map of the study area for LU of 2011 for (i) RE-1, (ii) RE-2 and (iii) RE-3

Table 7.1 Flood affected wards of the study area for different rainfall events and land uses

Year	Rainfall Events	Flood depth variation (m)	Flood affected Wards	Least affected Wards	Worst Affected Wards	Maximum Duration of Inundation
2006	RE-1	0.004 - 0.47	All wards except 1, 3, 4, 5, 6, 8, 9, 10, 12, 22, 24, 47, 49, 52, 54, 56	34, 35, 37, 45, 46, 56	14, 15, 16, 25, 26, 27, 32, 44, 50, 51, 59	50 hours
	RE-2	0.006- 0.62	All wards except 1, 3, 4, 5, 6, 8, 9, 10, 12, 22, 24, 47, 49, 52, 54, 56	34, 35, 37, 45, 46, 56	14, 15, 16, 25, 26, 27, 32, 44, 50, 51, 59	59 hours
	RE-3	0.005- 0.55	All wards except 1, 3, 4, 5, 6, 8, 9, 10, 12, 22, 24, 47, 49, 52, 54, 56	34, 35, 37, 45, 46, 56	14, 15, 16, 25, 26, 27, 32, 44, 50, 51, 59	55 hours
2011	RE-1	0.005 -0.55	All wards except 1, 3, 4, 5, 6, 8, 9, 10, 12, 22, 24, 47, 49, 52, 54, 56	34, 35, 37, 45, 46, 56	14, 15, 16, 25, 26, 27, 32, 44, 50, 51, 59	68 hours
	RE-2	0.007- 0.68	All wards except 1, 3, 4, 5, 6, 8, 9, 10, 12, 22, 24, 47, 49, 52, 54, 56	34, 35, 37, 45, 46, 56	14, 15, 16, 25, 26, 27, 32, 44, 50, 51, 59	73 hours
	RE-3	0.006 -0.66	All wards except 1, 3, 4, 5, 6, 8, 9, 10, 12, 22, 24, 47, 49, 52, 54, 56	34, 35, 37, 45, 46, 56	14, 15, 16, 25, 26, 27, 32, 44, 50, 51, 59	70 hours

7.2.4.2 Probabilistic flood inundation maps for the study area

Probabilistic flood inundation maps for the study area have been developed for a range of peak rainfall intensities corresponding to different return periods mentioned in section 6.6 of chapter 6. Fig. 7.4 shows the flood spread over the city for 25 year storm and for the land use of

the years of 2006 and 2011. The flood depth in the study area is 0.68 m in 2011 and a total area of 59.9 km^2 is found to be inundated. The maximum flood depth of 0.68 m remained for 60 hours in ward number 44 and a flood depth of 0.5 m was found to remain in ward number 26 for 73 hours. Also, it is observed that the maximum flood depth due to 25 year storm increased by 10.19% from 2006 to 2011.

Fig. 7.5 indicates the flood spread over the study area for 50 year storm and for the land use of 2006 and 2011. In 2011 the flood depth in the study area is found to vary between 0.01 m to 0.79 m and a total area of 61.5 km^2 is found to be inundated. Maximum flood depth of 0.79 m was found to remain for 63 hours in ward number 44 and a flood depth of 0.53 m was found to remain in ward number 26 for 76 hours. The maximum flood depth increased by 12.8% from 2006 to 2011 due to 50 year storm.

Fig. 7.6 shows the flood spread over the study area for 75 year storm and for the land use of 2006 and 2011. In 2011, the maximum flood depth is 0.88 m and a total area of 62.05 km^2 is found to be inundated. Maximum flood depth of 0.88 m was found to remain for 65 hours in ward number 44 and a flood depth of 0.63 m was found to remain in ward number 26 for 78 hours. There is an increase of maximum flood depth by 10.26% from 2006 to 2011 due to 75 year storm.

Fig. 7.7 depicts the flood spread over the study area for 100 year storm and for the land use of 2006 and 2011. In 2011, the maximum flood depth was found to be 0.94 m and a total area of 63.15 km^2 is found to be flooded. Maximum flood depth of 0.94 m was found to remain for 68 hours in ward number 44 and a flood depth of 0.7 m was found to remain in ward number 26 for 81 hours. The maximum flood depth increased by 6% from 2006 to 2011 for 100 year storm. The average increase in maximum flood depth from 2006 to 2011 is 9.81%.

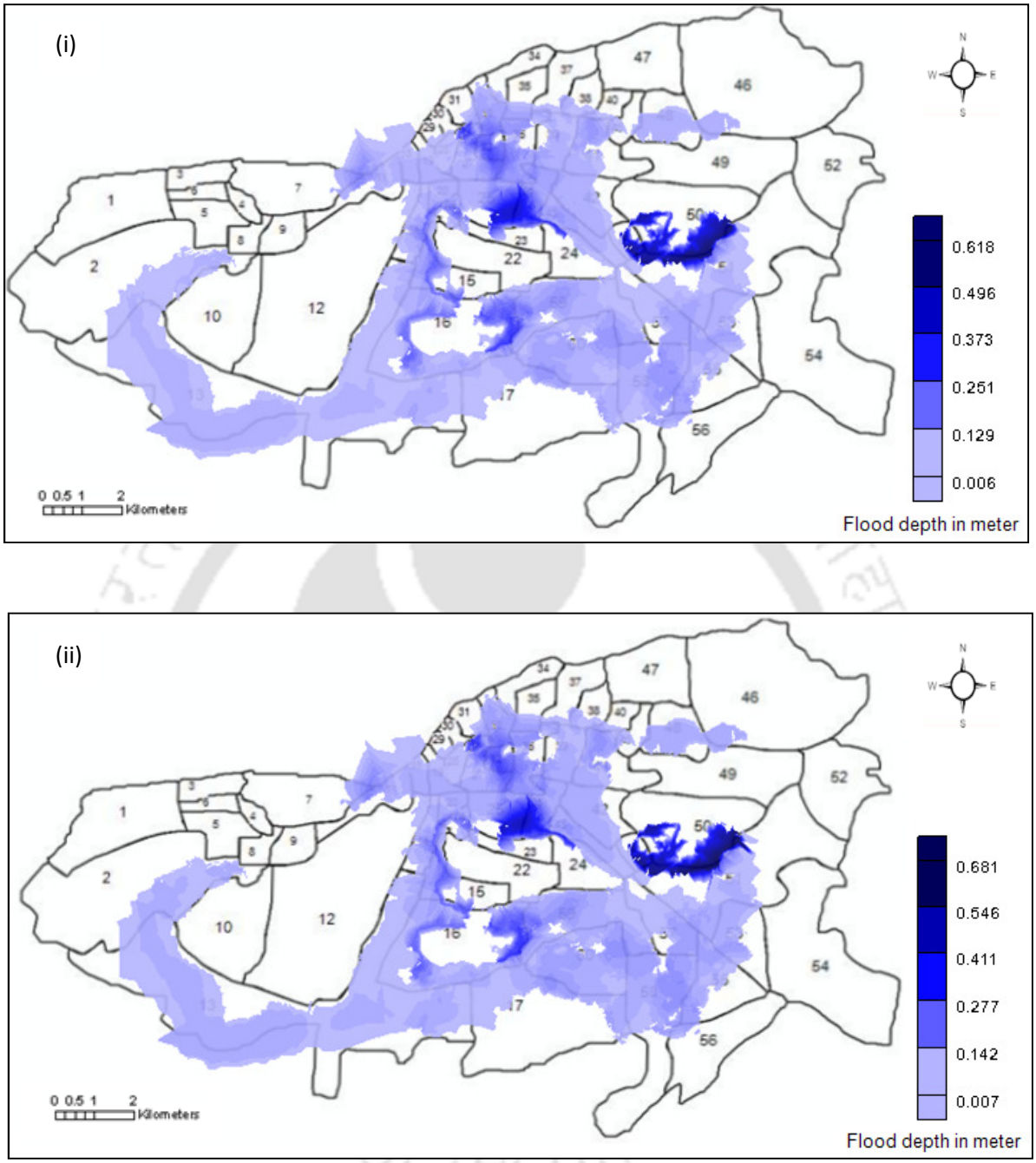

Fig. 7.4 Probabilistic flood inundation map of study area for a return period of 25 years with the LU of the year (i) 2006 and (ii) 2011

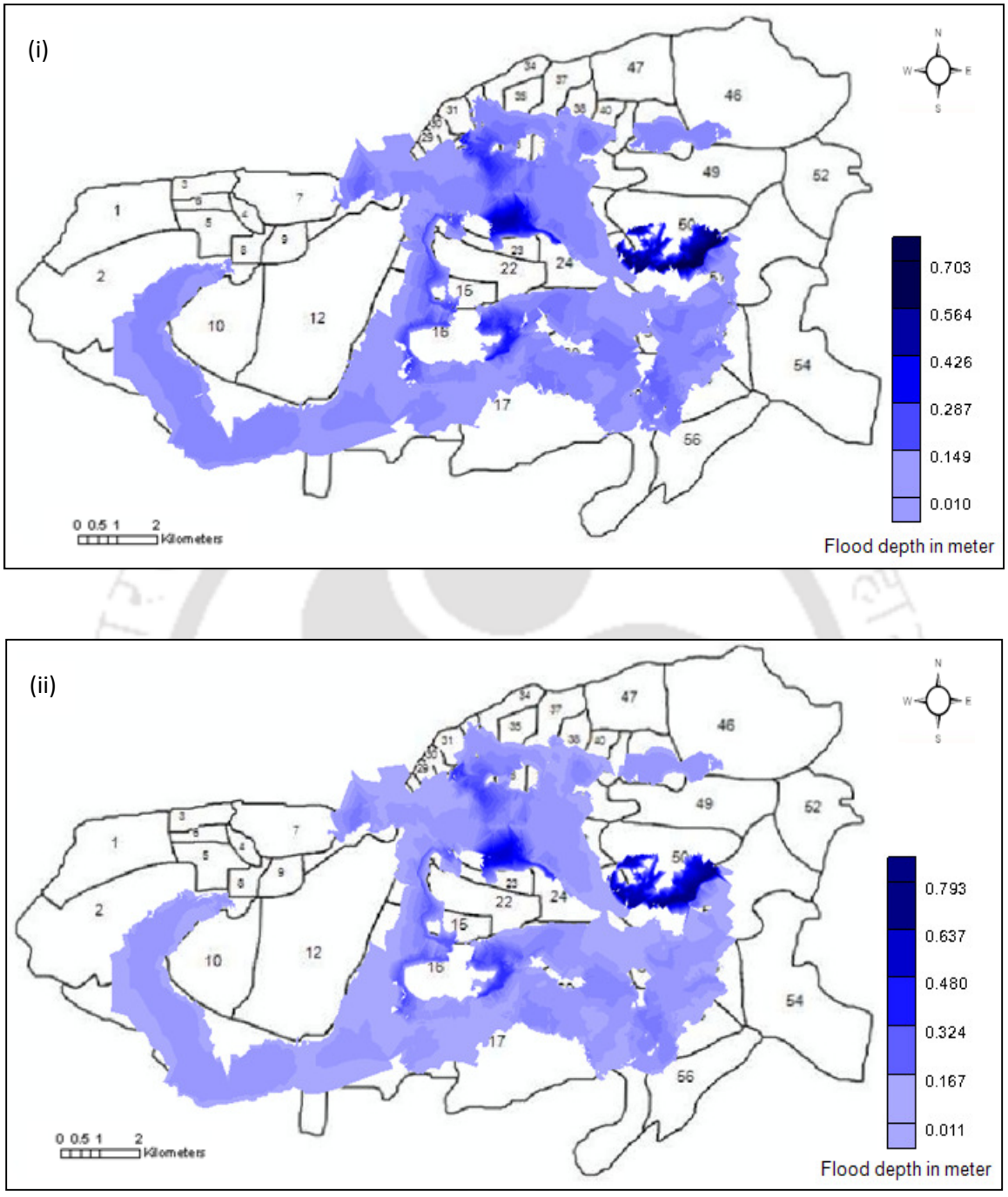

Fig. 7.5 Probabilistic flood inundation map of study area for a return period of 50 years with the LU of the year (i) 2006 and (ii) 2011

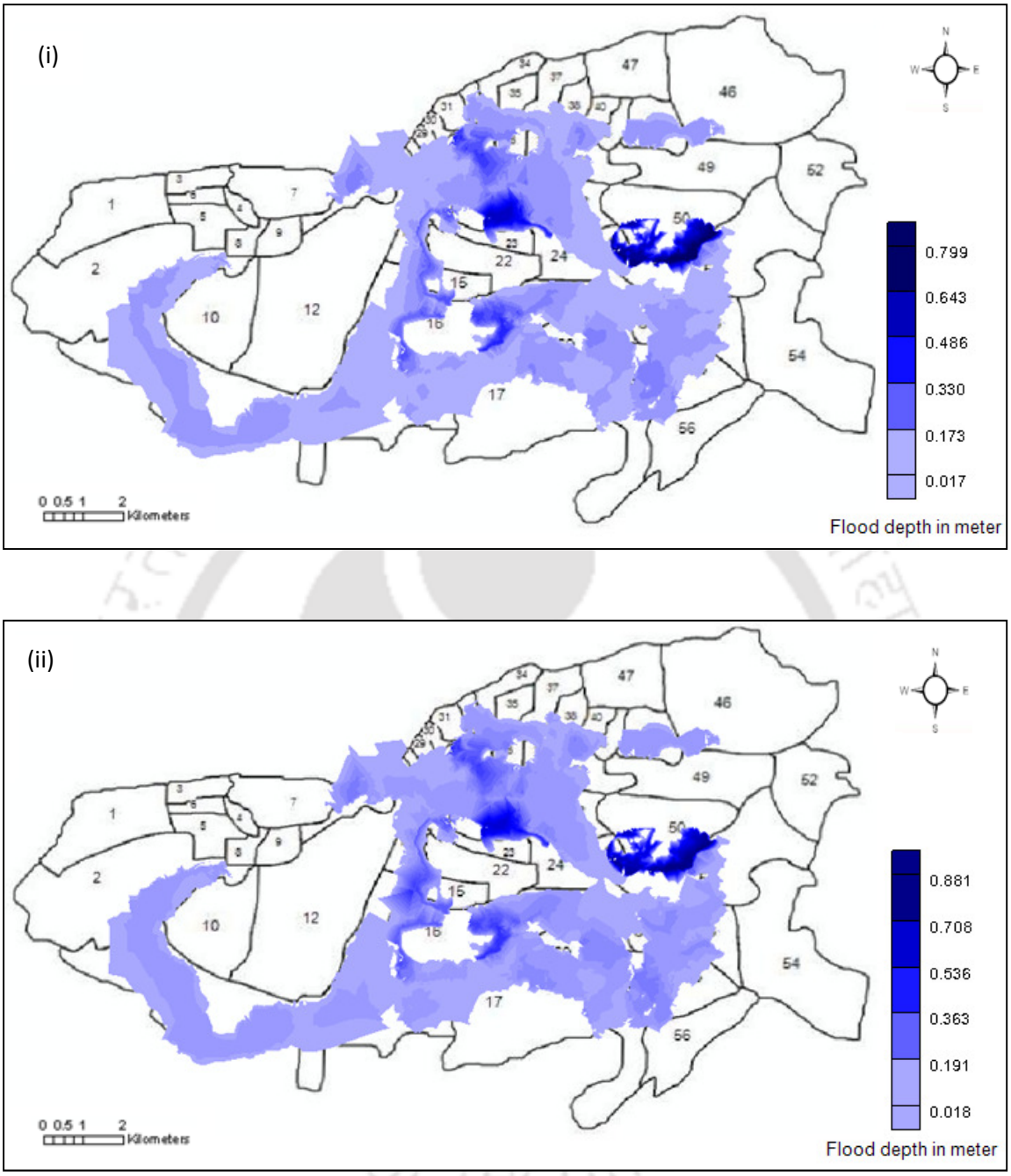

Fig. 7.6 Probabilistic flood inundation map of study area for a return period of 75 years with the LU of the year (i) 2006 and (ii) 2011

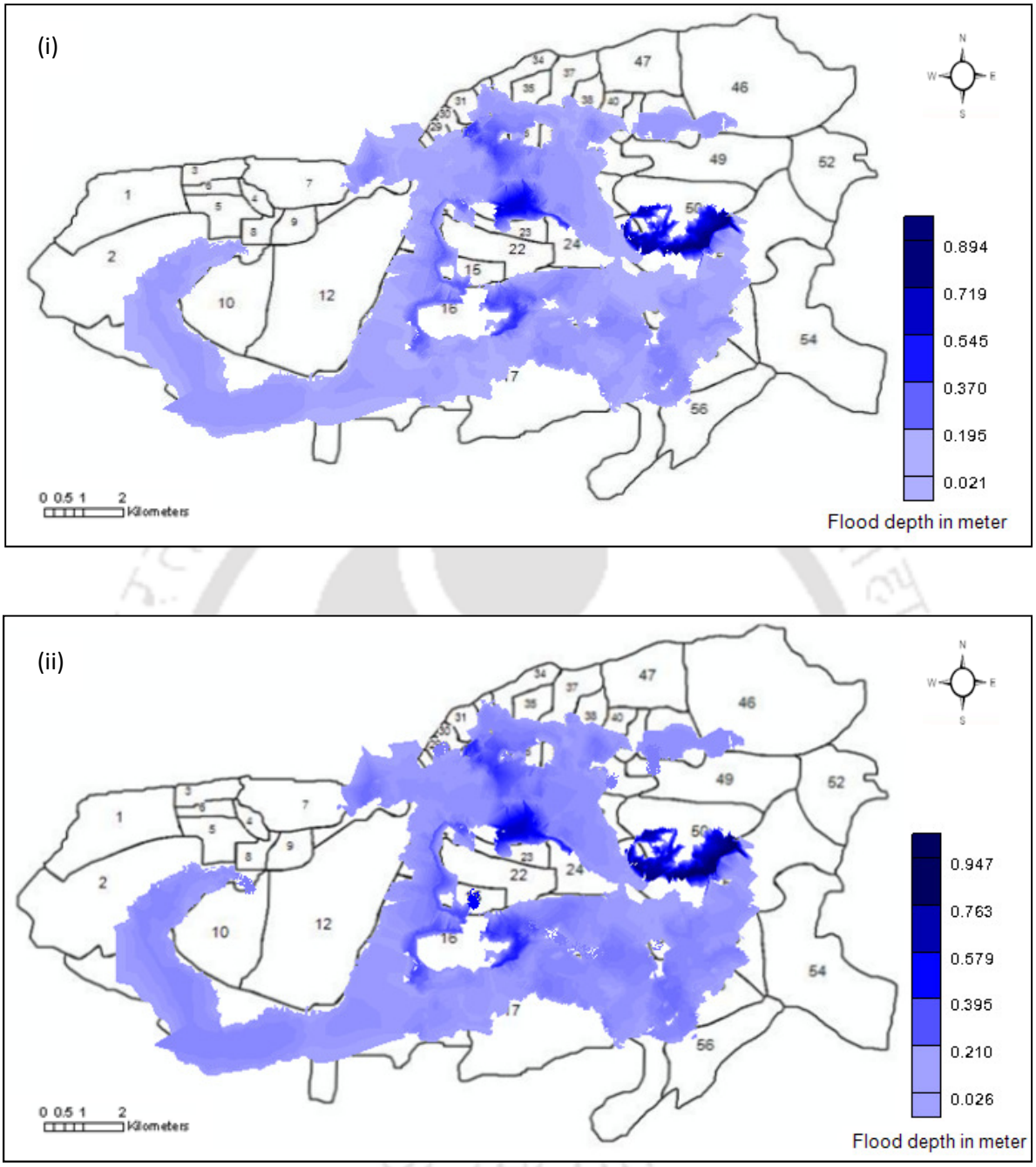

Fig. 7.7 Probabilistic flood inundation map of study area for a return period of 100 years with the LU of the year (i) 2006 and (ii) 2011

The details of flood affected areas by the storms of different return periods and land uses are presented in Tables 7.2 and 7.3. For better comparison, these data has been plotted as shown in Figs. 7.8 and 7.9. From Figs. 7.8 and 7.9, it is evident that watershed 3 is the worst affected zone of the study area having the flood affected area ranging from 64.5% in 2006 to 68.05% in 2011 for 100 year flood.

Table 7.2 Flood affected area (km^2) of the study area

Watershed No.	Flood affected area (km^2)							
	25 year flood		50 year flood		75 year flood		100 year flood	
	2006 LU	2011 LU	2006 LU	2011 LU	2006 LU	2011 LU	2006 LU	2011 LU
1	1.95	2.09	2.03	2.33	2.19	2.39	2.22	2.43
2	6.91	7.06	6.98	7.32	7.08	7.38	7.11	7.48
3	17.55	18.61	18.01	18.93	18.12	19.07	18.24	19.26
4	9.02	9.77	9.94	10.01	9.96	10.13	10.14	10.44
5	12.08	12.84	12.75	13.05	12.81	13.10	12.87	13.23
6	5.94	6.28	6.01	6.42	6.05	6.50	6.12	6.71
7	3.2	3.25	3.3	3.44	3.4	3.48	3.51	3.60

Table 7.3 Flood affected area (%) of the study area

Watershed No.	Flood affected area (%)							
	25 year flood		50 year flood		75 year flood		100 year flood	
	2006 LU	2011 LU	2006 LU	2011 LU	2006 LU	2011 LU	2006 LU	2011 LU
1	7.0	7.5	7.29	8.37	7.86	8.58	7.97	8.72
2	28.24	28.85	28.52	29.91	28.94	30.16	29.06	30.57
3	62.01	65.76	63.64	66.9	64.03	67.4	64.5	68.05
4	32.18	34.86	35.46	35.71	35.53	36.14	36.18	37.25
5	32.3	34.33	34.1	34.9	34.25	35.02	34.41	35.38
6	21.45	22.67	21.7	23.18	21.84	23.47	22.1	24.23
7	9.05	9.2	9.33	9.73	9.62	9.85	9.93	10.18

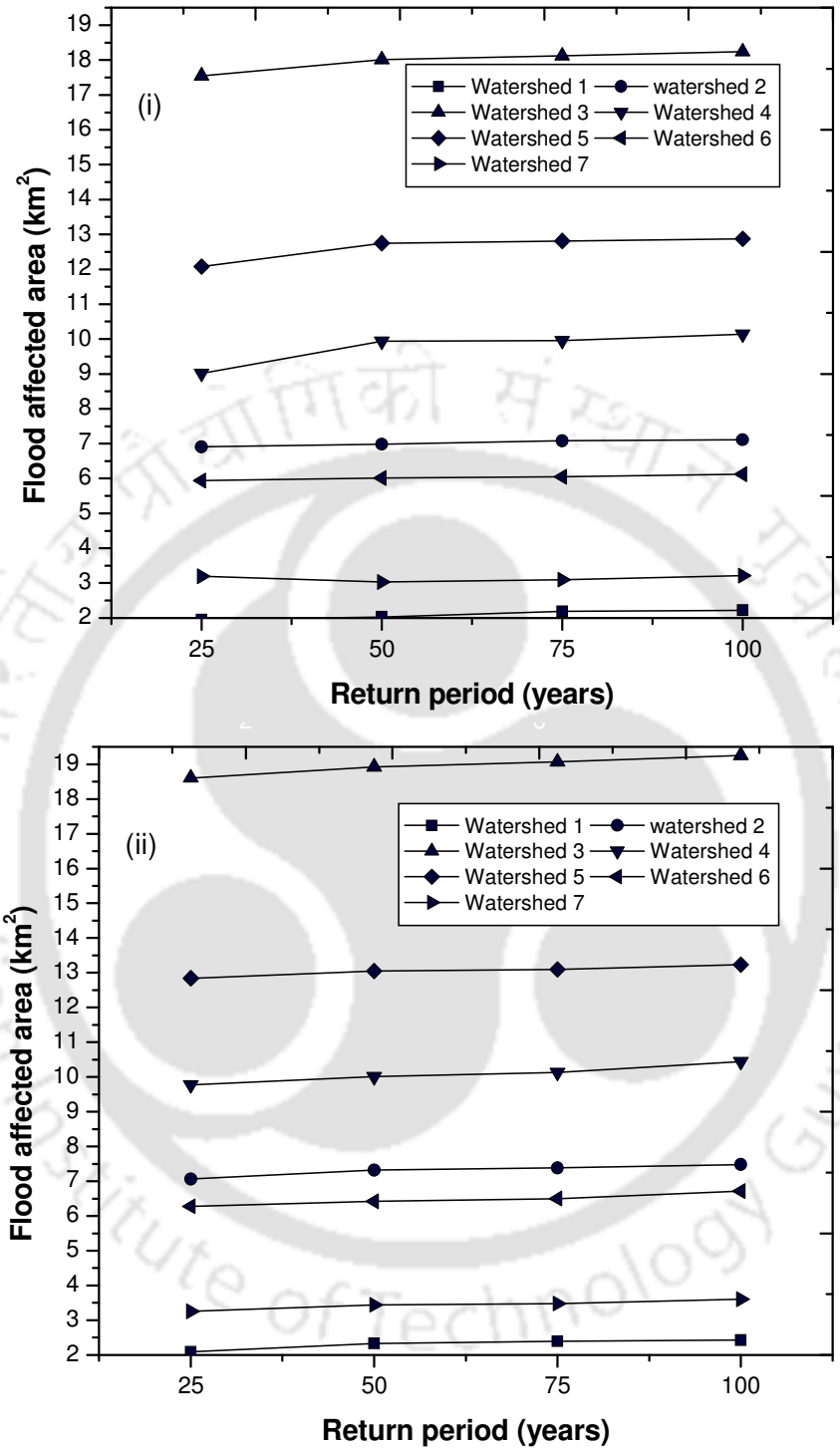

Fig. 7.8 Flood affected area (km^2) in the study area for different return periods and land use of (i) 2006 and (ii) 2011

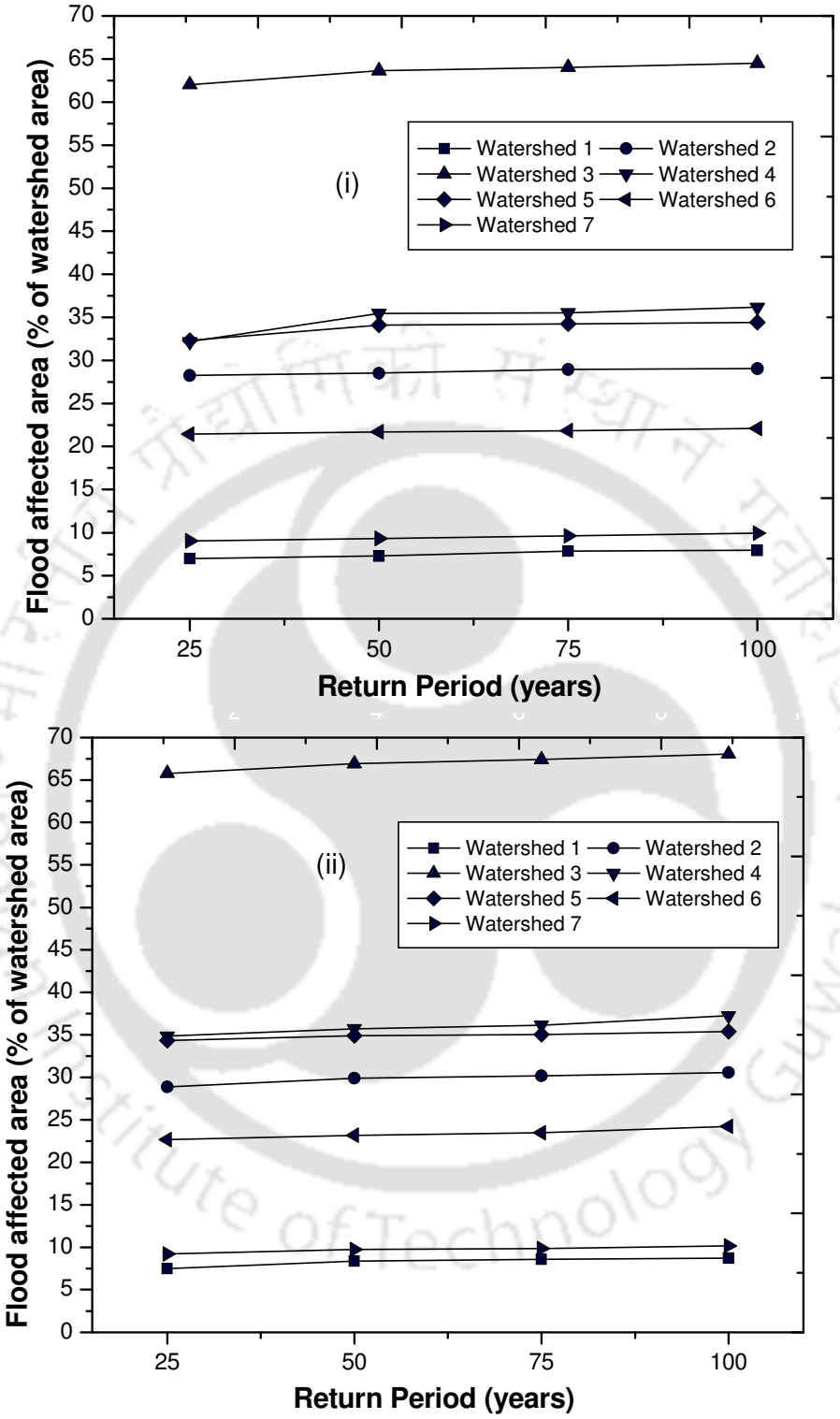

Fig. 7.9 Flood affected area (%) in the study area for different return periods and land use of (i) 2006 and (ii) 2011

Table 7.4 and Fig. 7.10 presents the maximum flood depth in different watersheds of the study area due to storms of different return periods and land uses of 2006 and 2011. It is observed from Fig. 7.10 that watershed 1 and 2 of the study area exhibits maximum flood depth for both 2006 LU and 2011 LU. It is observed from Tables 7.3 and 7.4 that watershed 1 and 2 are the critical zone of the study area if flood depth is considered and watershed 3 is the critical zone of the study area (which shows 68.05% of its area as affected by flood water) if spatial extent of flood is considered.

Table 7.4 Flood depth in different watersheds of the study area

Watershed No.	Maximum flood depth (m)							
	25 year flood		50 year flood		75 year flood		100 year flood	
	2006 LU	2011 LU	2006 LU	2011 LU	2006 LU	2011 LU	2006 LU	2011 LU
1	0.62	0.68	0.70	0.79	0.80	0.88	0.89	0.95
2	0.61	0.68	0.70	0.79	0.80	0.88	0.89	0.94
3	0.49	0.51	0.51	0.53	0.59	0.63	0.65	0.70
4	0.2	0.22	0.25	0.29	0.32	0.37	0.45	0.52
5	0.19	0.22	0.27	0.32	0.34	0.36	0.36	0.38
6	0.13	0.14	0.15	0.16	0.17	0.19	0.18	0.19
7	0.006	0.008	0.01	0.02	0.02	0.03	0.02	0.04

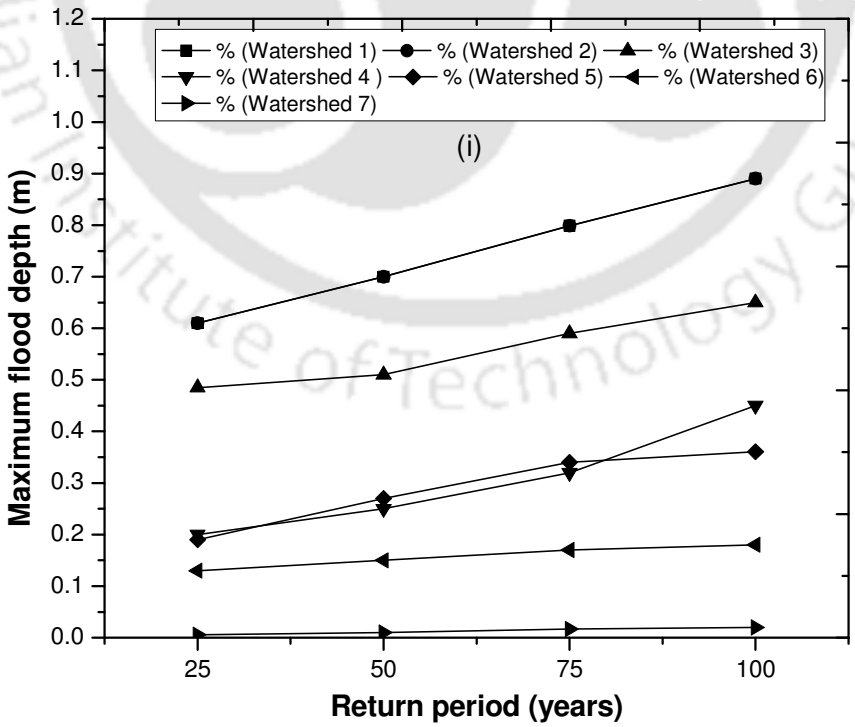

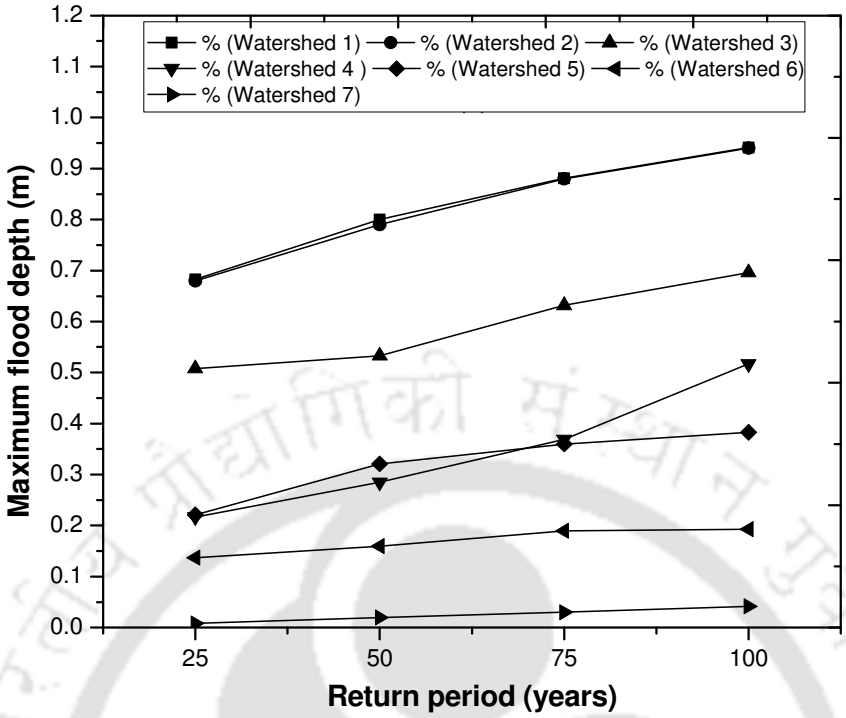

Fig. 7.10 Flood depth in the study area for different return periods for (i) 2006 LU (ii) 2011 LU

From the inundation maps for various past and probabilistic rainfall events, it can be noted that the entire urban city is getting flooded even for a minimum rainfall intensity of 50 mm/h (RE-1). Table 7.5 present details of flooding for different rainfall intensities and LU of 2011. It is observed that for an increase in rainfall intensity from 50 mm/h (as in RE-1) to 147.8 mm/h (as in case of 100 year storm), the maximum flood depth increases to 0.947 m. Some of the highly affected wards due to the above flood events are summarized in Table 7.6. Even though the flooding pattern remains same for 2006 and 2011 LU, the flood depth and inundated area is observed to increase with time. The rate of increase in flood depth with rainfall intensity is found to be more than the rate of spatial spreading of the flood. This is mostly attributed to the geography of the study area as shown in Fig. 7.11. The higher flood depths are noticed at various foothills in the study area. The worst affected areas of the city are ward numbers 25, 26, 44, 50 and 51 where the flood depth is maximum and remain for longer duration. During flooding, the discontinuous hills as shown in Fig. 7.11 does not allow further spreading of flood water causing the water depth to rise. Hence, additional flood management schemes need to be implemented in this area to adequately counter the problems due to flooding during high intensity rainfall.

Table 7.5 Details of flooding for different rainfall intensities and 2011 LU

Rainfall Events	Historical Rainfall Events			Probabilistic Storms			
	RE-1	RE-2	RE-3	25 year storm	50 year storm	75 year storm	100 year storm
Rainfall intensity (mm/h)	50.0	120.0	108.0	119.0	132.6	141.3	147.8
Max. Flood Depth (m)	0.545	0.681	0.655	0.681	0.793	0.881	0.947
Area Affected (km^2)	55.13	60.01	58.24	59.9	61.5	62.05	63.15

Fig. 7.11 Influence of geographical location of hills on flooding in the study area (image source- NRSC)

Table 7.6 Flood affected wards of study area

Ward Number	Area included
11	Part of Maligaon, Durgasarobar, Santipur
14	Bhaskarnagar, part of Fatasil
15	Fatasil, Udalbakra
16	Dakhingaon, Jyotikuchi
19	Kumarpara, Machkhowa
25	Ulubari, Rupnagar, Birubari
26	Lachitnagar, Bhangaghar, Srimantapur
27	Krishna nagar, Bahinnagar
29	Fancy Bazar, Pan Bazar
32	Paltan Bazar, Manupuribasti
39	Sarania, part of Chandmari,
41	Chandmari, part of Geetanagar
42	Anil nagar, Nabinnagar, zoo road
43	Tarunnagar, Ganeshguri, Dispur, RGB Road
44	Ganeshguri, Dispur
50	Hengerabari
51	Hengerabari, Satgaon
53	Sixmile, Punjabari
59	Dakhingaon, Kahilipara, Basisthapur

An effort has been made to correlate maximum flood depth (MFD) for the study area with peak rainfall intensity (PRI) (considered from sections 7.2.4.1 and 7.2.4.2) for particular land use as shown in Fig. 7.12. It can be noted that maximum flood depth versus rainfall intensity follows similar trend for 2006 and 2011 land use. An exponential curve represented by Eq. 7.7 has been fitted to these data with a regression coefficient close to unity.

$$MFD = A + B^* EXP (PRI/C) \quad (7.7)$$

where A, B and C are fitting parameters. The equations corresponding to years 2006 and 2011 are represented in Fig. 7.12. The difference in fitting parameters of equations corresponding to 2006 and 2011 is due to the variation in imperviousness. This is because MFD has been determined for the same PRI for both the years. The ratio of MFD in 2011 to 2006 varies between 1.06 and 1.21. Therefore, the average increase in MFD from 2006 to 2011 is 1.12, which is attributed to an increase in effective impervious area by 1.48 times from 2006 to 2011.

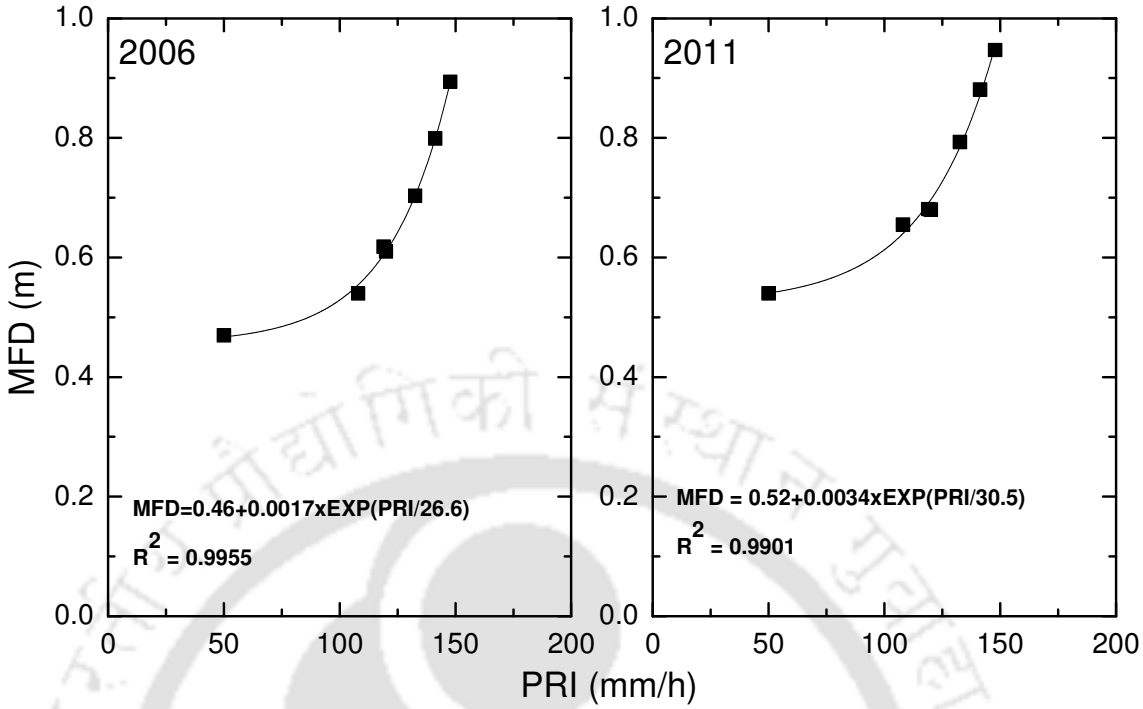

Fig. 7.12 Variation of maximum flood depth with peak rainfall intensity for years 2006 and 2011

The increasing trend of MFD attributed to an increase in imperviousness need to be analyzed further for future years. An effective flood management scheme should focus on minimizing MFD as imperviousness increases by providing suitable structural or non-structural flood control measures. The present study help to assess the magnitude of flood management schemes to be implemented for a study area with growing imperviousness due to urbanization.

7.3 Flood Hazard Assessment of the Study Area

Although the occurrence of flood cannot be prevented, the flood hazard can be minimized if flood risk areas are known in advance. A flood hazard map of the study area serves this purpose and is important for developing an effective and holistic flood management scheme. Hence an effort has been made to rank different wards of the study area based on the possible flood hazard caused by 100 year return period flood. Initially hazard ranks (HR) are developed by considering individual vulnerability parameters such as flood depth and inundated area, land use, affected population and roads (Kafle et al. 2006). Further, the overall HR for the study area has been determined by the interactive effect of all these vulnerability parameters. Such a study would

help to identify the predominant vulnerability parameter influencing the overall flood hazard ranking of the study area.

7.3.1 Flood hazard ranking on the basis of flood depth and inundated area

In this study, flood depth of 0.2 m has been fixed as the threshold value beyond which it can disrupt normal movement of population and transport. Depending on the total inundated area and the area inundated by flood depth of more than 0.2 m in a ward, two hazard indicators (HI) have been defined as follows (Kafle et al. 2006).

$$HI_1 = \frac{F_A}{T_A} \times 100 \quad (7.8)$$

$$HI_2 = \frac{F_D}{T_A} \times 100 \quad (7.9)$$

where F_A is the total flood affected area in the ward; F_D is the area with flood depth of more than 0.2 m in the ward; and T_A is the total area of the ward. Based on HI_1 and HI_2 values, hazard ranking of the wards were made using a rule, which is explained in the following section.

If both HI_1 and HI_2 for a ward are less than 50% it is ranked as 1 or low hazard region; If one of the two hazard indicators (HI_1 and HI_2) for a ward is less than 50% and other is more than 50% then it is ranked as 2 or medium hazard region; if both HI_1 and HI_2 for a ward are more than 50% it is ranked as 3 or high hazard region. Accordingly, each ward is assigned a hazard rank with respect to flood depth and inundated area. Fig. 7.13 shows the flood hazard ranking maps developed for the study area based on the flood depths and inundated area in 2006 and 2011. It can be noted that approximately 26.14% of the area falls under high flood hazard category in the year 2006.

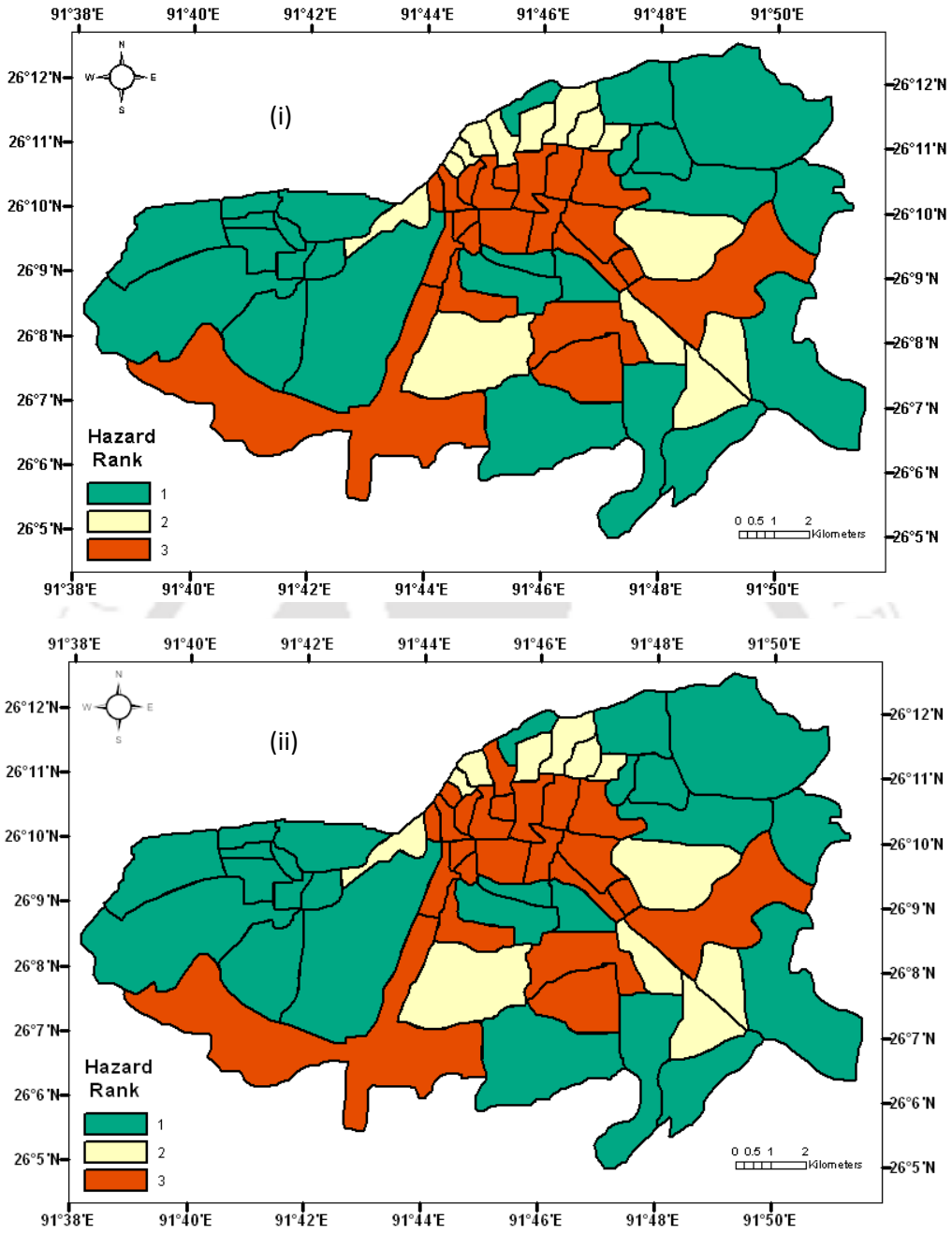

Fig. 7.13 Flood hazard ranking map of the study area based on flood depth and inundated area for the LU of the year (i) 2006 and (ii) 2011

It is noticed that central portion of the city is more vulnerable to flood hazard with respect to flood depth and inundated area for both the years. The geographical location of this area surrounded by hills as discussed in the previous section is the main cause of high hazard rank. Even though EIA in 2011 is 1.48 times more than the EIA in 2006, there is only a minimal increase in high flood hazard rank of the study area. Ward 29 and 33 changed from medium

hazard rank to high hazard rank in 2011 causing an increase in high hazard rank area as compared to 2006.

7.3.2 Flood hazard ranking on the basis of land use

From the classified satellite images of the study area corresponding to the years 2006 and 2011, flood hazard ranks are estimated based on a weighted score for different land uses. The weighted score has been estimated by Eq. 7.10 (Kafle et al. 2006).

$$\text{Weighted score} = 4.0 \times L_1 + 2.0 \times L_2 + 1.0 \times L_3 + 0.0001 \times L_4 \quad (7.10)$$

where L_1 is percentage of agricultural land; L_2 is percentage of forests and grass land; L_3 is percentage of swampy land and water bodies; L_4 is percentage of scrub land. It is felt that the degree of damage to the agricultural land will be the maximum due to flooding and hence assigned a highest coefficient of 4.0 for flood hazard calculation (Kafle et al. 2006). The forest and grass land categories will have comparatively less degree of damage and assigned a coefficient of 2.0. The swampy land and water body categories will have still less damage and a coefficient of 1.0 has been used for flood hazard calculation. The scrub land category is least effected due to flood with a coefficient of 0.0001.

The flood hazard ranks considering land use are estimated on the basis of linear interpolation between 0 and 100, where 0 corresponds to the minimum value of weighted score and 100 corresponds to the maximum value of weighted score. To quantify the flood hazard, three rankings for flood damage (HR from 1 to 3) are obtained for each ward from the allocated weighted score. HRs are fixed according to the corresponding value of interpolated weighted scores. If the interpolated weighted score for a ward is 0 to 33, it is assigned low HR 1, for 33 to 66 medium HR 2, and for 66 to 100 it is high HR 3. The flood HR maps for the study area are depicted in Fig. 7.14 for land use of 2006 and 2011. Unlike the flood HR map of the study area corresponding to flood inundation discussed in the previous section, it can be observed that the peripheral area of the city is highly vulnerable to flood hazard with respect to land use. The flood HR of ward 2 and 60 reduced from 2006 to 2011 due to decrease in agricultural land and corresponding increase in built up area.

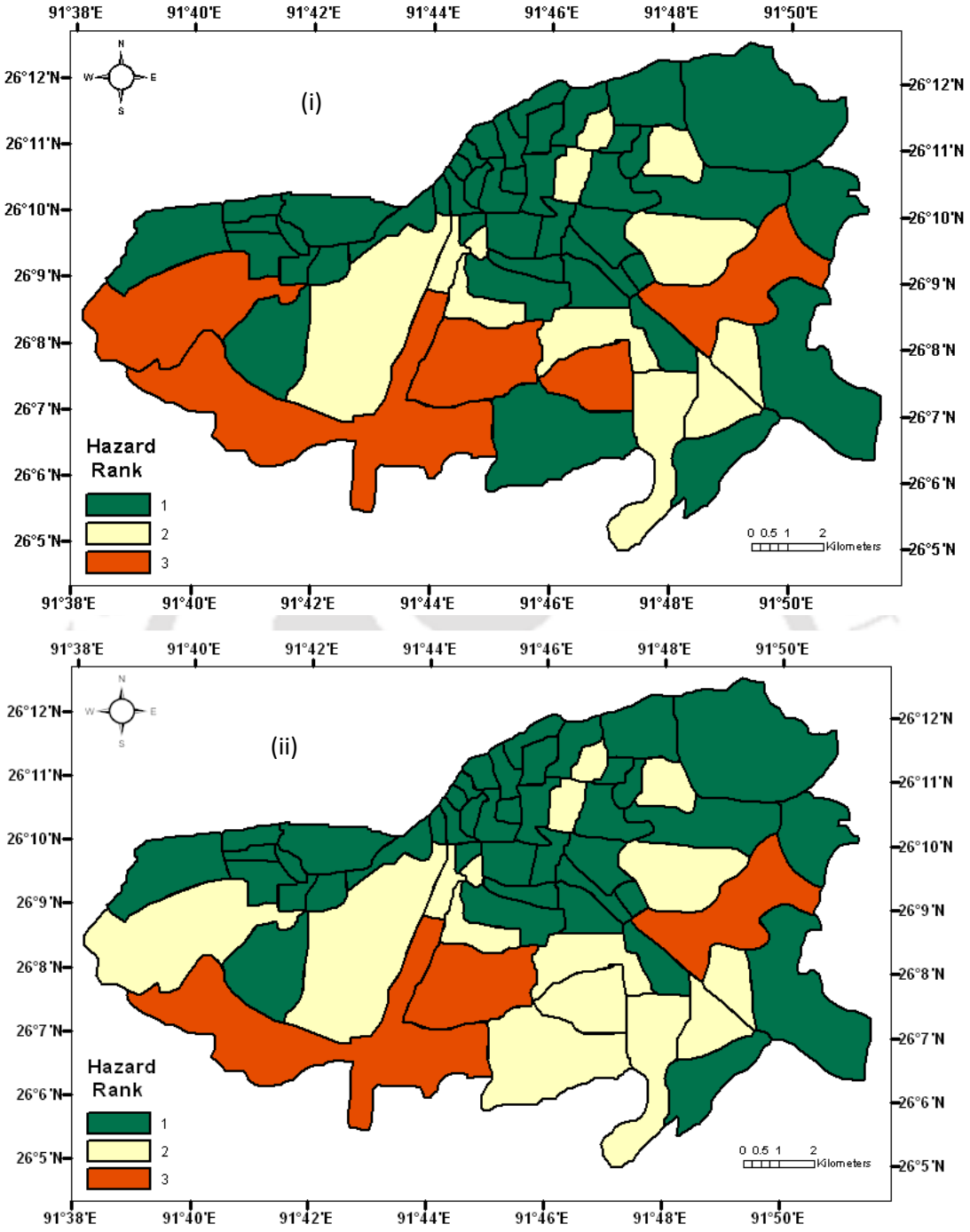

Fig. 7.14 Flood hazard ranking map of the study area based on land use in the year of (i) 2006 and (ii) 2011

7.3.3 Flood hazard ranking on the basis of population density and road network maps

The maximum population density in the study area is found to be 28760 persons per km^2 in ward number 29 for 2001 census. Based on the population density of the study area, the wards are distinguished into two categories. The wards having population density of less than 14380

persons per km^2 (half of the maximum population density) are kept under category 1 and the wards having population density of more than 14380 persons per km^2 are kept under category 2. The collected road network map of the study area gives details about the type of road depending on the location and width of the road. From the collected road network map of the study area, the type of the road (whether National Highway (NH) or major road or any other road) is assessed. The length of flood affected road is identified for each type of road in every ward. A weighted score is then estimated according to Eq. 7.11 (Kafle et al. 2006).

$$\text{Weighted score} = 4.0 \times R_1 + 2.0 \times R_2 + 1.0 \times R_3 \quad (7.11)$$

where R_1 is the percentage of NH affected by flood in the ward; R_2 is the percentage of major road affected by flood in the ward and R_3 is the percentage of any other road affected by flood in the ward. The coefficients 1.0, 2.0 and 4.0 in Eq. 7.11 were used to describe the weight to the flood damage (Kafle et al. 2006). The implication of flood on NH will be the maximum and hence given a highest coefficient of 4.0 for flood hazard calculation. Similarly, major road category will have comparatively less degree of damage as compared to NH and hence assigned a coefficient of 2.0. Any other road category will have least damage and hence given a coefficient of 1.0 for flood hazard calculation.

Two categories of affected roads are then estimated on the basis of linear interpolation between 0 and 100, where 0 corresponds to the minimum value of weighted score and 100 corresponds to the maximum value of weighted score. If weighted score is 0 to 50, it comes under category 1 and for 50 to 100 it falls under category 2. Based on these categories for population density and road network, the HR is assigned by the rule mentioned in Table 7.7. Further, the HR maps for the study area for the years 2006 and 2011 are developed as shown in Fig. 7.15. It is observed that major portion of the fully urbanized area falls under HR 3 imposing difficulties to people and transport facilities. It is also observed that the hazard ranking map does not change from 2006 to 2011. Comparing Figs. 7.14 (ii) and 7.15 (ii), it is observed that more number of wards of the study area is under HR 3 in 2011 if population density and flood affected roads are taken as vulnerability parameters as compared to land use.

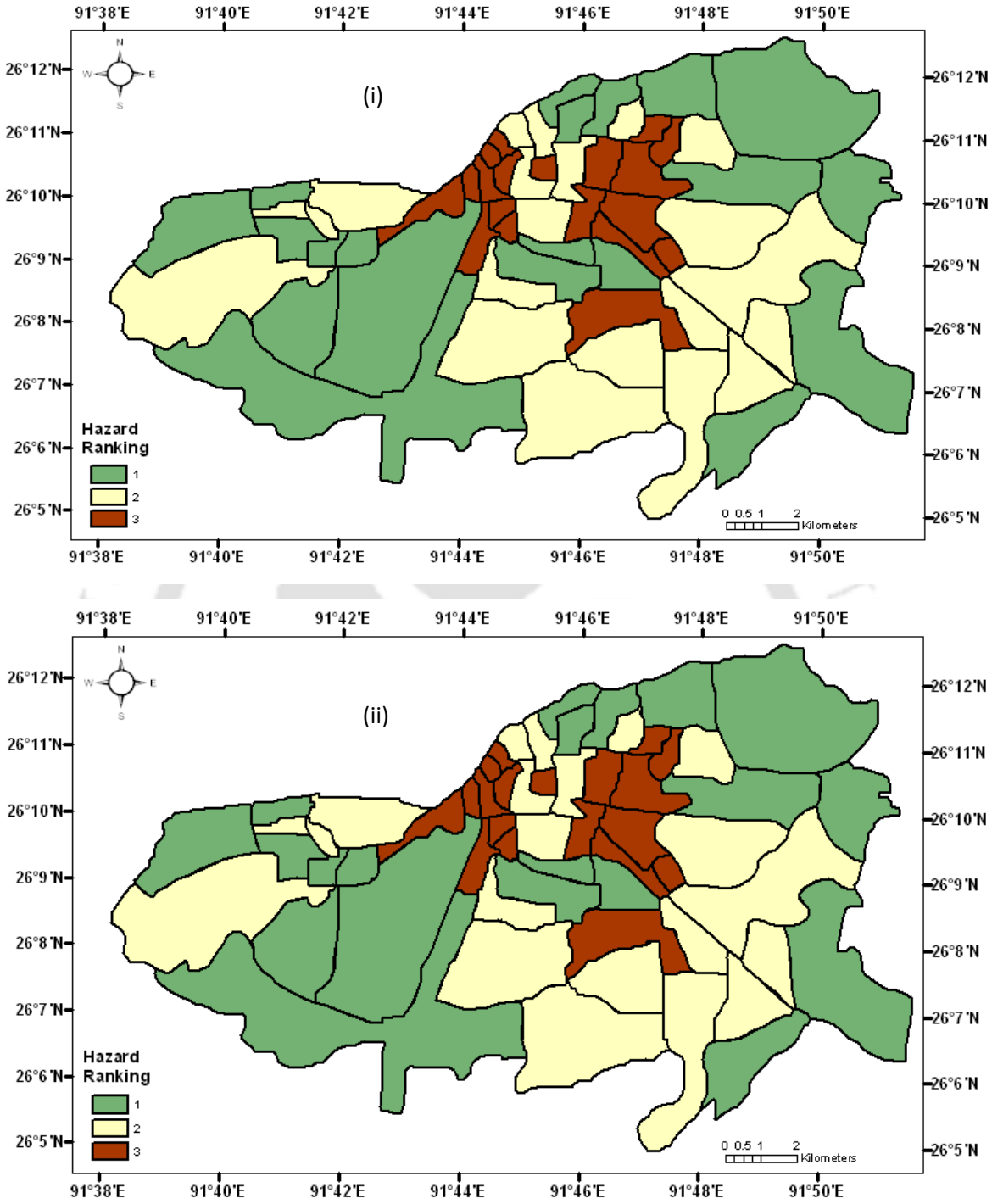

Fig. 7.15 Flood hazard ranking map for the study area based on population density and flood affected road in the year of (i) 2006 and (ii) 2011

Table 7.7 Hazard ranking based on population density and flood affected roads

Category		Hazard Rank
Based on population density	**Based on flood affected roads**	
Category 1	Category 1	1
Category 1	Category 2	2
Category 2	Category 1	2
Category 2	Category 2	3

7.3.4 Overall flood hazard ranking of the study area

The overall flood hazard rank of the study area has been determined by considering the interactive effect of all the vulnerability parameters, such as flood depth, land use, population density and flood affected roads. For this purpose, a three dimensional matrix multiplication mode was used to obtain the combined flood HR (Islam and Sado 2000; Islam and Sado 2002; Dewan et al. 2007) as explained by Fig. 7.16. Ranking was done from 1 to 9 for the interactive effect of two categories i.e., flood depth, inundated area and land use categories. The HRs obtained for different wards of the study area were 1, 2, 3, 4, 6, and 9. The numbers 7 and 8 will not appear because the combined HRs are the multiples of HRs obtained for land use (i.e.1, 2 and 3) and flood depth and affected road (i.e. 1, 2 and 3). These ranking is combined with the effect of population and flood affected road to get the overall hazard rankings from 1 to 27 as shown in Fig. 7.16. Again the combined HRs are calculated by multiplying the HRs obtained previously (i.e. HRs 1, 2, 3, 4, 6 and 9) with the HRs (i.e. 1, 2 and 3) that is obtained for population and flood affected road. Thus the overall HRs obtained for different wards of the study area were 1, 2, 3, 4, 6, 8, 9, 12, 18 and 27. The lower numerals represent low HR and the higher numerals represent high HR.

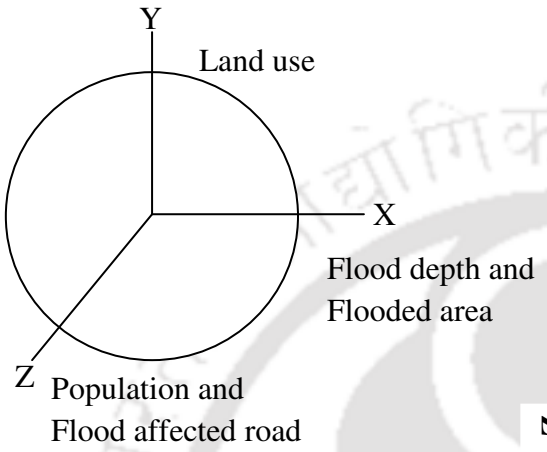

X

Flood depth and flooded area

Y Land use	**HR**	1	2	3
	1	1	2	3
	2	2	4	6
	3	3	6	9

XY

Flood depth and flooded area - land use

Z Population and flood affected road	**HR**	1	2	3	4	6	9
	1	1	2	3	4	6	9
	2	2	4	6	8	12	18
	3	3	6	9	12	18	27

Fig. 7.16 Ranking matrix for three dimensional multiplication mode (Islam and Sado 2002)

Figs. 7.17 shows the flood hazard ranking map for the study area based on the combined effect of two categories i.e. flood depth-area and land use in 2006 and 2011. It is observed that ward numbers 13 and 51 come under high hazard ranks (HR 9) in 2011 if interactive effect of both the categories (flood depth- inundated area and land use) is taken into account. Also it has been observed that the flood risk category of ward numbers 17, 29 and 33 have increased from 2006 to 2011. Fig. 7.18 shows the overall flood hazard ranking maps for the study area in the years 2006 and 2011, based on combined effect of flood depth, inundated area, land use, population density with flood affected road. In 2011, ward numbers 14, 21, 39, 51 and 59 come under maximum hazard rank of 18 followed by ward numbers 15, 16 and 60 that come under hazard rank of 12. It is also observed from Fig. 7.18 that more number of wards of the study area come under HR 12 in 2011 than in 2006. For the study area, there does not exist any ward that shows HR of 9 due to flood depth, flooded area and land use and HR of 3 due to population and flood affected road. Hence HR of 27 (9*3) does not appear in the ranking map.

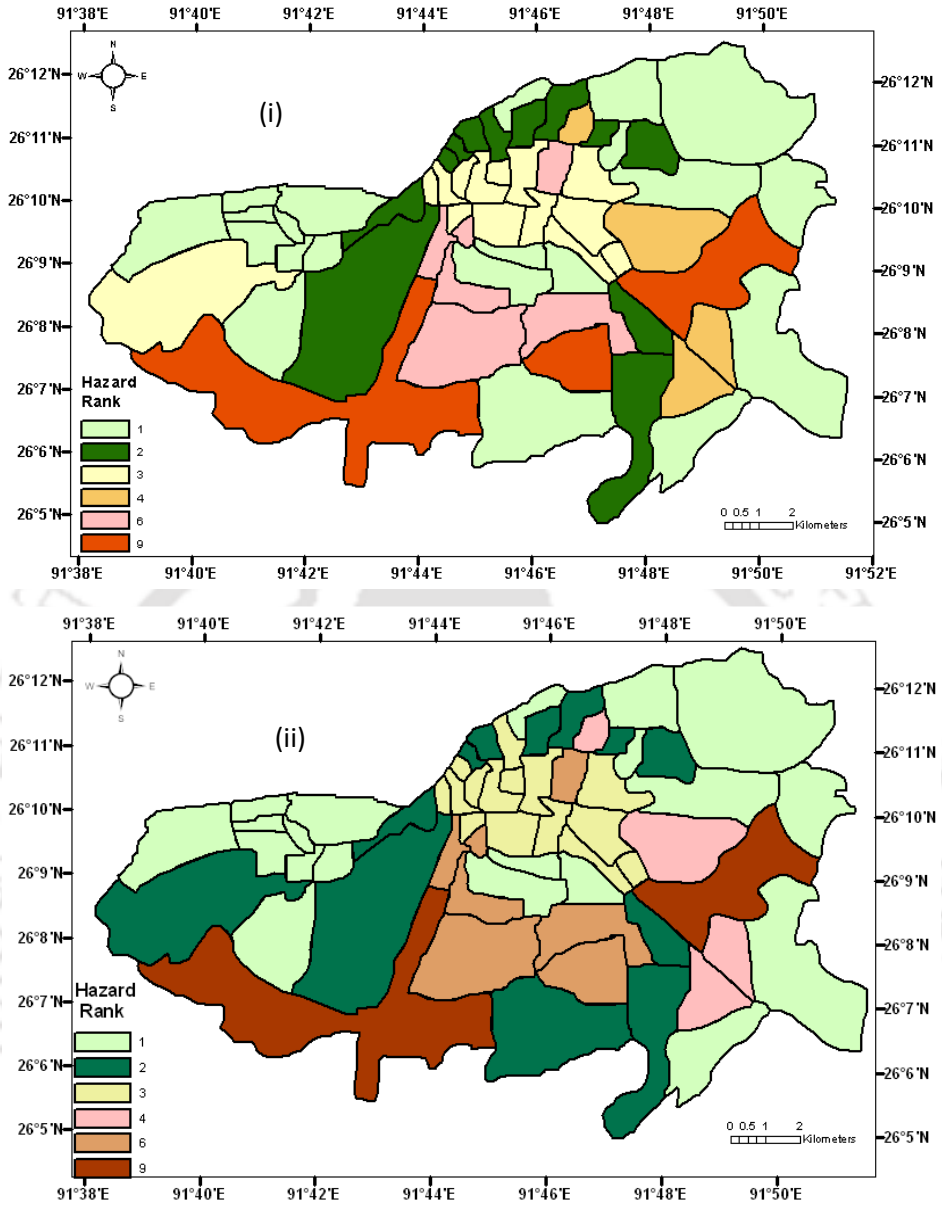

Fig. 7.17 Flood hazard ranking map for the study area based on flood depth, inundated area and land use in the year of (i) 2006 and (ii) 2011

The overall hazard ranks obtained in Fig. 7.18 were then regrouped into three groups designating HR 1, HR 2 and HR 3 as low flood risk zones; HR 4, HR 6 and HR 8 as medium flood risk zones; and HR 9, HR 12 and HR 18 as high flood risk zones. Based on these three groups, flood risk maps have been developed for the years 2006 and 2011 as depicted in Fig. 7.19 for the study area. It can be observed that except a few wards, the entire heart of the city is at high flood risk. Further comparing Figs. 7.13 (ii) and 7.19 (ii) it is observed that the flood

hazard ranking is comparable. Hence flood depth and flooded area are the most influential vulnerability factors in deciding the overall flood risk for the study area. Also more number of wards of the study area transforms to high flood risk in 2011 as compared to 2006. Owing to the importance of the central portion of the study area, which falls under high flood risk category, an effort has been made to reduce the impact of flooding by proposing a detention pond. The detail of the modeling procedure for the detention pond is explained in the following section.

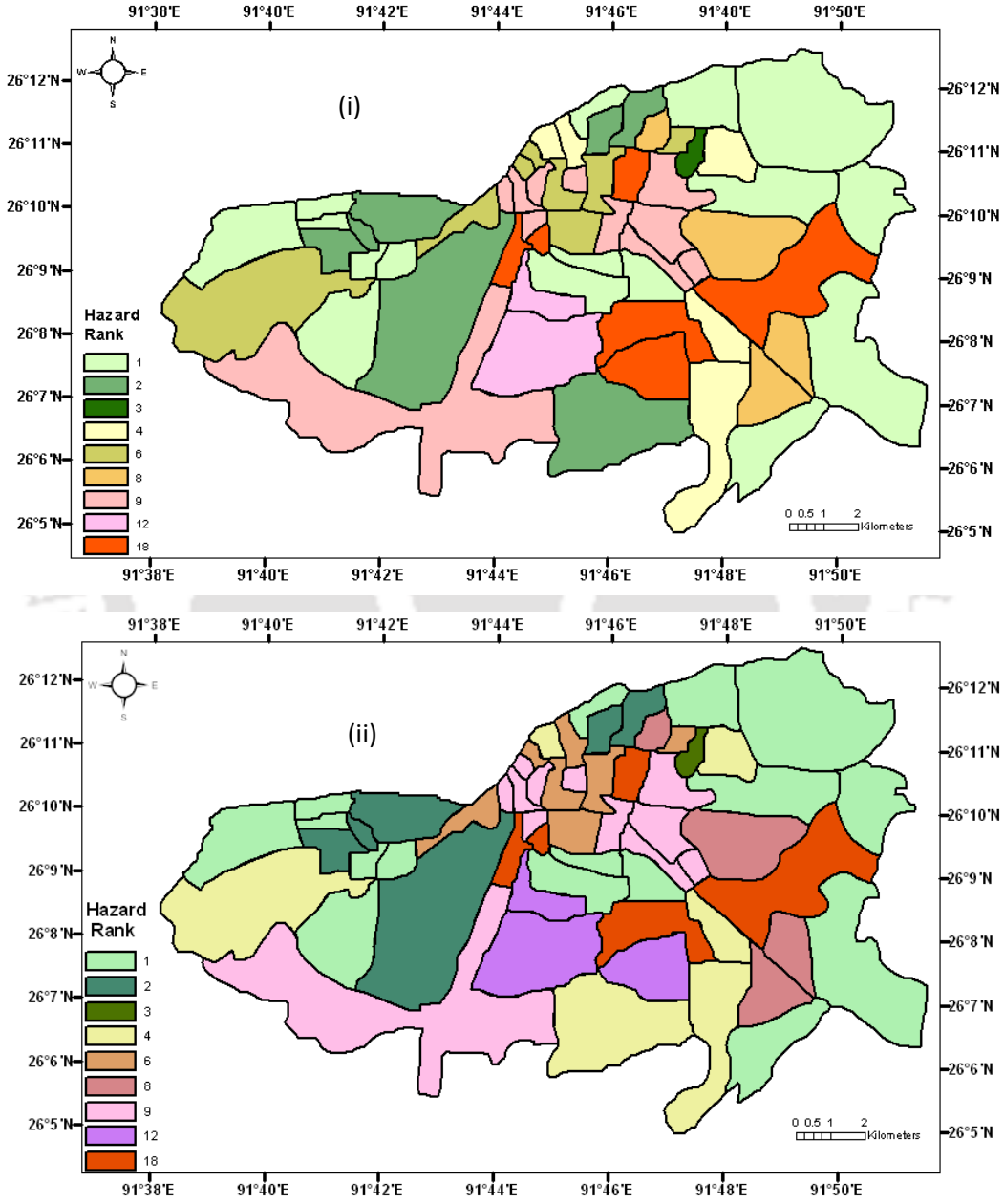

Fig. 7.18 Overall flood hazard ranking map for the study area based on flood depth, inundated area, land use, population density and flood affected road in the year of (i) 2006 and (ii) 2011

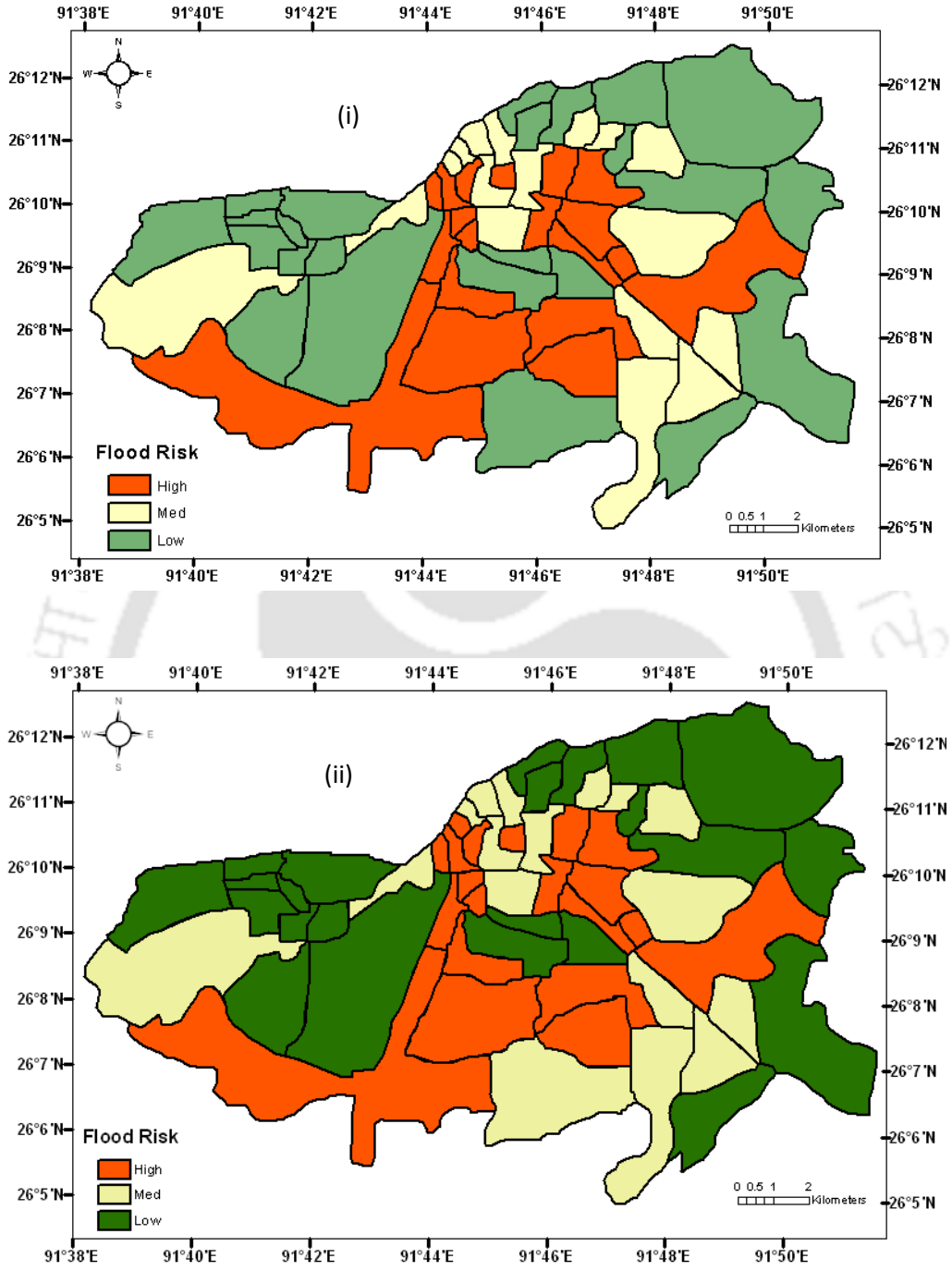

Fig. 7.19 Overall flood risk map of study area in the year of (i) 2006 and (ii) 2011

7.4 Provision of Detention Pond in the Study Area

The detention ponds are constructed as low lying basins with large water storage volume, which are used to reduce flooding by temporarily storing flood water and releasing later when the flood recedes. A volume based approach has been adopted in this study to fix the capacity of the detention pond (Guo 1999). In this approach, estimation of storage volume can be done without knowing the detailed outlet hydraulics. The basic concept used in the volume method is to find the maximum volume difference between the inflow and outflow volumes for the range of storm event in terms of rainfall duration. The capacity of the detention pond is estimated by using the continuity equation (Eq. 7.12) (Sahapure et al. 2011).

$$\Delta V = (Q_{in} - Q_{out})\Delta t \qquad (7.12)$$

where Q_{in} is inflow; Q_{out} is outflow; ΔV is change in storage in time Δt

According to Guo 2003, the design event for the detention basin should be the major event such as 100 year storm. Hence in the present study the capacity of the detention pond has been decided from the 100 years design rainfall duration, possible inflow and outflow at the proposed detention pond site. For predicting the inflow at the proposed site, a storage unit has been introduced in the model. The surface area of the wetland that can act as detention pond is measured in ArcGIS platform and certain initial depth is assumed to define the initial volume of the detention pond. Green Ampt infiltration parameters obtained from field experiment conducted at nearby site to the proposed detention pond have been used to model the infiltration characteristics. Due to lack of data, the evaporation component has not been considered in the analysis. The run off simulation has been performed using SWMM to determine inflow at the proposed site. The outflow hydrograph is chosen as the maximum capacity of the downstream drainage facility so that no flooding occurs at the downstream of the detention pond.

7.4.1 Impact of detention pond on flooding

As shown in Fig. 7.20, the wetland, Borosola Bil (natural lake), near the outlet of watershed 3 has been proposed to be used as detention pond to reduce the flooding in urban Guwahati city. Though there are many water bodies present in the study area (as shown in Fig. 3.8 in Chapter 3) Borosola Bil (Lake) has been chosen due to its large size and topographical location near the outlet of the watershed in the study site. The ideal location of this wetland would help to minimize flooding in major portion of the urban city and hence the storm water

load on river Bharalu will be reduced. Also being a natural wetland, it provides future scope for modification of the proposed detention pond unlike the artificial pond (R K Mission pond) present in the study area (Fig. 3.8).

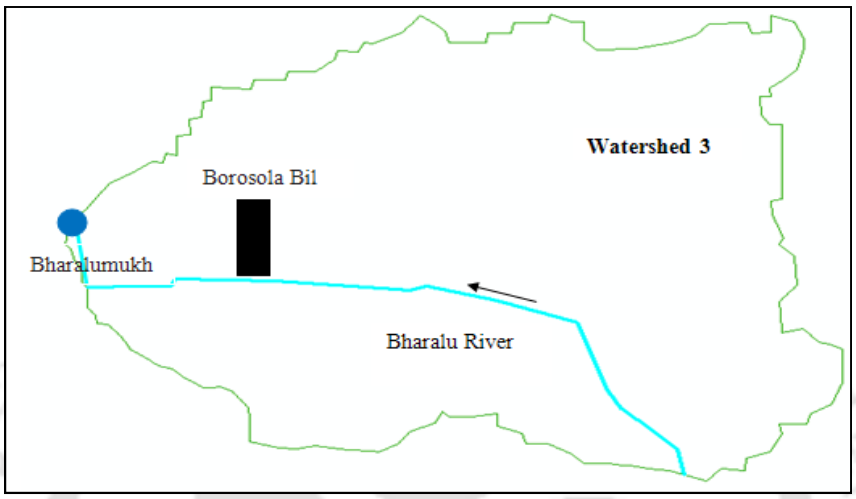

Fig. 7.20 Location of detention pond in the study area (Source: NRSC)

It has been found that by the introduction of the detention pond, the maximum flood depth reduced from 0.947 m as shown in Fig. 7.7 (ii) to 0.506 m as shown in Fig. 7.21. Hence the flood depth reduced by 46.5% due to the provision of detention pond. Also it can be mentioned that the inundated area in the city reduced from 63.15 km^2 to 35.98 km^2 (43%) for the land use of 2011 if detention pond is provided in the study area. However to achieve this much reduction in flooding, it has been found that the total area of the lake has to be maintained with a depth of 1.34 m assuming the lake to be rectangular. Even though there is a considerable decrease in flood extent in the city, it is not totally free from flooding by the use of Borosola Bil as detention pond. This is mainly due to the fact that this proposed detention pond receives the over loaded storm water discharge from one of the major natural drains, Bharalu River, of the study area. The flooding problem in other storm water drains need to be minimized by proposing further suitable flood management schemes for a holistic solution to urban flooding in the city. Such a flood management proposal requires further in depth investigation.

To assess the impact of introduction of detention pond on the flood risk of the study area, flood hazard of the city has been assessed by employing the methodology described in section 7.3. The overall flood risk map for the study area has been developed by including detention

pond and shown in Fig. 7.22. Comparing Fig. 7.19 (ii) and Fig. 7.22 it is observed that flood risk in many of the wards of the study area will be reduced from high risk to low risk if proposed detention pond is implemented. However the provision of one detention pond does not provide complete solution for the flooding problem of the study area. Further investigations are required to propose additional counter measures for flood management in the study area.

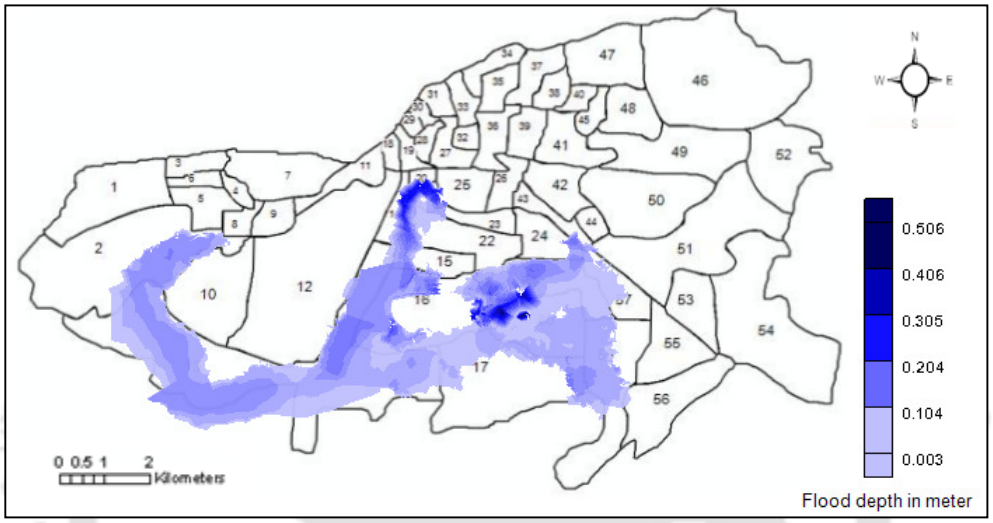

Fig. 7.21 Reduction in flooding in the study area by proposing detention pond

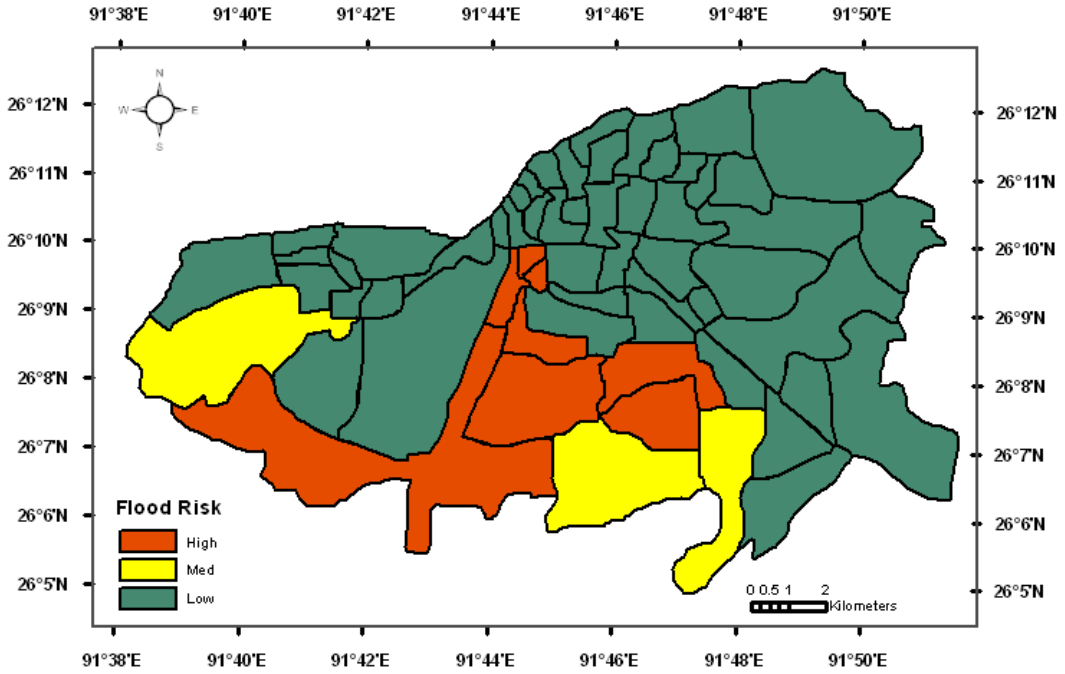

Fig. 7.22 Overall flood risk map of the study area for LU of 2011 by considering detention pond

Chapter 8

Summary and Conclusions

The research work deals with the quantification of imperviousness and its impact on urban flood modeling. The need of spatial technology for proposing effective flood management strategy for ungauged urban cities in developing countries like India is demonstrated. A fast growing urban Guwahati city is considered as the study area. This chapter summarizes the important observations from the present research work followed by the main conclusions. The future scope of research is presented as the last section of this chapter.

8.1 Summary of the Research Work

- The urbanization from 1980 to 2011 is quantified in terms of growth in imperviousness, which is defined as total impervious area (TIA) and effective impervious area (EIA). An exponential increase in imperviousness (built-up area) is noted for the study area.
- Determination of TIA is relatively easy compared to the more hydraulically relevant EIA. EIA is further estimated indirectly from TIA. However, there are no such relationships for Indian urban catchments. Therefore a semi-automated direct method is used for quantifying EIA using the fine resolution satellite imageries available for the year 2006 and 2011. A new relationship between TIA and EIA is proposed for the study area and it has been compared with those existing in the literature.
- EIA determined indirectly from coarse resolution imagery overestimate the imperviousness and hence fine resolution imageries are required for direct or indirect EIA estimation.
- The use of integrating GIS data with satellite imageries for preventing misclassification and better quantification of imperviousness has been demonstrated in this study. In the absence of GIS data, the rooftops were misclassified due to their colour and material. TIA estimated by coarse resolution imagery is 17.4% less than those estimated based on fine resolution imageries without using GIS data. However if GIS data are used, fine resolution imagery estimates TIA 30% more than that of the coarse resolution imagery. Such a difference by not considering the refined methods of space technology would impact the flood management scheme to be implemented for the study area.

- The difference in EIA value obtained by direct and indirect methods varies from 1.2% in watershed 1 to 427% in watershed 6.
- Tension infiltrometer was used to determine infiltration characteristics of 14 different locations of the study area. Saturated hydraulic conductivity (hydraulic conductivity at zero tension head) was found to vary from 6.48 mm/h to 75.6 mm/h. From the experimental result, Green Ampt infiltration parameters was determined and used as input for hydrologic runoff modeling.
- The percentage increase in runoff due to corresponding increase in TIA is less than that obtained due to EIA. This observation is similar to those reported by Alley and Veenhuis (1983).
- It is observed that the predicted runoff was 179.36% more if EIA estimated by Sutherland (1995) equation is used in the model instead of EIA estimated by direct method. Similarly predicted peak runoff was found to be 205% more if EIA estimated by Alley and Veenhuis (1983) equation is employed in the model in place of EIA estimated by direct method. The peak runoff is overestimated by 398% if TIA is used in the model instead of the EIA estimated by the direct method.
- The most urbanized watershed 3 shows the maximum increase (195.57%) in simulated runoff from 1980 to 2011. Watershed 6 exhibits least increase (9.7%) in simulated runoff from 1980 to 2011.
- TIA predicts peak runoff 2.14 times than EIA predicted runoff in 1980, 2.78 times of EIA predicted runoff in 2006 and 2.3 times of EIA predicted runoff in 2011. Hence the flood management strategies can be misleading if the modeling is based on TIA for an ungauged urban area. This indicates that more effort needs to be made to determine EIA precisely (either directly or indirectly).
- The peak flow predicted is found to be average 1.14 times more in 2011 when GIS data is used along with satellite imagery for imperviousness determination. Therefore, for better accuracy in runoff prediction in ungauged urban catchments, it is recommended to use GIS data along with remote sensing data (fine resolution satellite imagery) for improving the accuracy of runoff determination.

- Under estimation of rainfall intensity in continuous simulation than that of the event wise simulation, underestimates the simulated peak runoff. To avoid under estimation in runoff prediction, event wise simulation should be carried out in the watersheds where availability of short interval rainfall data is not a constraint.
- It is observed that the entire city is getting flooded even for a minimum rainfall intensity of 50 mm/hr.
- Higher flood depths are noticed at various foothills within the study area. The rate at which the flood depth is increasing with respect to different storm events is found to be more than the rate of spatial spreading of the flood. The spatial distribution of the flood water or the flooding pattern can be explained by the fact that during flooding, the topography of the area (with number of discontinuous hills) does not allow further spreading of flood water and thus the flood depth rises further at the flooded zones.
- The average increase in maximum flood depth from 2006 to 2011 was found to be 1.12, which is attributed to an increase in EIA by 1.48 times.
- Watershed 1 is found to be the critical zone of the study area if flood depth is considered and watershed 3 is the critical zone of the study area if spatial extent of flood is considered.
- Flood inundation maps for the study area have been developed for different peak rainfall intensities and for different land uses. Different wards of the study area have been ranked based on the possible flood hazard caused by 100 year return period flood and by considering individual vulnerability parameters such as flood depth and inundated area, land use, affected population and roads. Further, the overall HR for the study area has been determined by the interactive effect of all these vulnerability parameters. It has been observed that flood depth and flooded area are the most influential vulnerability factors in deciding the flood risk within the study area.
- Maximum flood depth exhibited an exponential relationship with peak rainfall intensity for a particular land use.
- It has been observed that by the introduction of a detention pond in the study area, the maximum flood depth reduced by 46.5% and the inundated area in the urban city reduced by 43% (from 63.15 km^2 to 35.98 km^2).

8.2 Conclusions

- Integrating GIS data with satellite imagery is mandatory to improve the accuracy of impervious quantification and runoff determination in ungauged urban catchment.
- Precise determination of hydraulically relevant effective impervious area is necessary for accurate assessment of runoff in urban catchment. The quantification of overestimation in runoff by considering total imperviousness or indirect estimation of effective imperviousness has been brought forth in this study.
- A semi-automated direct method has been used to determine effective imperviousness directly for the study area based on fine resolution satellite imageries. A new correlation has been developed to estimate effective impervious area based on total impervious area for the study area.
- It is recommended to use event rainfall for runoff analysis used in proposing flood management strategies. Use of continuous rainfall data considerably underestimates peak runoff. There is a need to apply a factor of safety to peak runoff estimated from continuous rainfall if the value is to be used for flood management.
- The average increase in maximum flood depth (MFD) from 2006 to 2011 was found to be 1.12, which is attributed to an increase in effective impervious area by 1.48 times from 2006 to 2011. From the exponential growth trend of urbanization in the city, the imperviousness for future years can be evaluated and hence the increasing trend of MFD attributed to an increase in imperviousness can be analyzed.
- It has been observed that flood depth and flooded area are the most influential vulnerability factors in deciding the flood risk within the study area.
- It is demonstrated in this study that geographical features such as hills play an important role in deciding the spatial extent and depth of flood.
- An exponential curve has been obtained for correlating maximum flood depth as a function of peak rainfall intensity for a particular land use.
- Provision of detention pond in the study area reduced maximum flood depth by 46.5% and inundated area by 43%. Therefore, improving existing depression or constructing additional detention ponds can be an effective tool for urban flood management.

8.3 Uncertainties involved in the current study

Uncertainty in model prediction arises from several sources. In the current study, sources of uncertainty can be categorized into two groups: uncertainty in image analysis and uncertainty in modeling. Uncertainty in image analysis may arise due to the use of satellite images from different sources, difference in resolution of the imageries and use of different classification algorithms to quantify land uses. Uncertainty in modeling can be due to the use of different hydrologic models, types of data input and different methodologies for modeling of hydrologic processes.

8.4 Future Scope of Research

Due to the uncertainties discussed above, the following section discuss about the limitations and possible scope of further research:

- Since details about the presence of gutters and inlets in the drainage network were not available, it is assumed that inflow occurs throughout the length of the drains. If the position of inlets and gutters are known precisely, then connectivity between the imperviousness and the drainage network can be ensured and thus effective imperviousness can be determined with more accuracy. Extensive field surveys need to be conducted to achieve this objective. The reliability of relationship between TIA and EIA can be ascertained.
- Exponential trend obtained for imperviousness and urbanization need to be evaluated for future years.
- The generality of correlation between effective imperviousness and total imperviousness needs to be evaluated for other urban catchments. A number of urban catchments having same range of TIA need to be considered to ensure the validity of Eq. 4.9 determined based on satellite imagery. Also the relationship can be generalized by considering some common parameter like drainage density for urban catchments. Thus the developed relationship will be applicable to other urban catchments showing similar TIA development and drainage density.
- A detailed study is required to determine the factor of safety to enhance the value of peak runoff estimated from continuous rainfall data.

- In the present research work, ward wise flood risk map has been developed for different vulnerability parameters. This can be extended to a more refined pixel wise flood risk map for the same vulnerability parameters.
- Proposing wetlands as detention ponds and its impact on reducing flooding pattern of the city need to be assessed.
- The usefulness of exponential relationship between maximum flood depth and peak rainfall intensity for proposing flood management schemes need to be further demonstrated.
- It was assumed in the present research work that the rainfall is uniform throughout the study area due to the availability of only one rain gauge station. By increasing the number of rain gauge station in the study area in future, the spatial variation of rainfall can be incorporated in the model to get a more realistic estimate of runoff and hence flooding.
- From the present study it is noticed that the variation in hydraulic conductivity is much at low tension heads and is less at high tension heads. This explains that the role of macro pores is dominant on infiltration property at low tension heads. Further studies need to be addressed to quantify the macro pore effect on the soil properties of the study area.
- Due to lack of time and resources, the experimental study to find out Green Ampt model parameters has been carried out in only 14 locations throughout the study area. However, to gain more confidence this study can be extended to subwatershed scale.
- In the present research work, flood risk map was derived for 2006 and 2011 LU. However fine resolution imageries of the study area for future years need to be collected for developing flood risk map and ascertaining the impact of EIA on flood risk presented in this study.
- Uncertainties while using different hydrologic models and different input parameters need to be studied in detail for urban catchments.

References

Abebe, A. J. and Price R. K. (2005). "Decision support system for urban flood management." *Journal of Hydroinformatics.* 7 (1), 3-15.

Alexander, D. P. and Rao, A. R. (1985). "Using remotely sensed data to estimate runoff." *Proceedings of the conference-Hydraulics and Hydrology in the small computer age, ASCE,* New York, 218-223.

Alley, W. M., and Veenhuis, Jack E., (1983). "Effective Impervious Area in Urban Runoff Modelling." *Journal of Hydraulic Engineering*, ASCE, 109 (2), 313-319.

Angullo-Jaramillo, R., Vandervaere, J. P., Roulier, S., Thony, J. L., Gaudet, J. P., and Vauclin, M. (2000). "Field measurement of soil surface hydraulic properties by disc and ring infiltrometers." A review and recent developments, *Soil and Tillage Research*, 55 (1-2), 1-29.

Ankeny, M.D, Ahmed, M., Kaspar, T.C., and Horton, R. (1991). "Simple field method for determining unsaturated hydraulic conductivity." *Soil Science Society of America, Journal,* 55 (2), 467-470.

Anselmo, V., Galeati, G., Palmieri, S., Rossi, U., and Todini, E. (1996). "Flood risk assessment using an integrated hydrological and hydraulic modeling approach: a case study." *Journal of Hydrology*, 175 (1-4), 533- 554.

Apel, H., Aronica, G. T., Kreibich, H. and Thieken, A. H. (2009). "Flood risk analyses- how detailed we need to be?" *Natural Hazards,* 49 (1), 79 – 98.

Arnell, N.W. (1986). "Average annual damage by flood frequency zone."*Journal of Water Resources Planning and Management,* ASCE, 112 (1), 104-113.

ASCE, (1982). Gravity Sanitary Sewer Design and Construction, ASCE Manual of Practice No. 60, New York.

ASCE, (1992). Design and construction of urban storm water management systems, ASCE-Manuals and reports on Engineering Practice No. 77, New York.

Bagarello, V., Iovino, M., and Tusa, G. (2000). "Factors affecting measurement of the near-saturated soil hydraulic conductivity." *Soil Science Society of America Journal,* 64 (4), 1203-1210.

Barkau, R. L. (1982). "Simulation of the July 1981 flood along the Salt river", Report for CE695BV, Special problems in Hydraulics, Department of Civil Engineering, Colorado State University, Fort Collins, Colorado.

Barco, J., Wong, K. M. and Stenstorm, M. K. (2008). "Automatic calibration of U.S. EPA SWMM model for a large urban catchment." *Journal of Hydraulic Engineering*, ASCE, 134 (4), 466-474.

Barron, O. V., Donn, M. J. and Barr, A. D. (2013). "Urbanization and shallow ground water: predicting changes in catchment hydrological responses." *Water Resources Management*, 27, 95-115.

Beighley, R. E., Kargar, M. and He, Y. (2009). "Effects of impervious area estimation methods on simulated peak discharges." *Journal of Hydrologic Engineering*, ASCE, 14 (2), 388-398.

Blade, E., Gomez, M., Dolz, J. and Sanchez, M. (2009). "Hydrodynamic modeling and risk analysis in RAMFLOOD project." *Flood Risk Management: Research and Practice,* Samuels et al. (eds), Taylor and Francis, UK, 25-30.

Bodhinayake, W., Si, B. C., and Noborio, K. (2004). "Determination of hydraulic properties in sloping landscapes from tension and double ring infiltrometers." *Vadose Zone Journal,* 3 (3), 964-970.

Boni, G., Ferraris, L., Giannoni, F., Roth, G., and Rudari, R (2007). "Flood probability analysis for un-gauged watersheds by means of a simple distributed hydrologic model." *Advances in Water Resources,* 30 (10), 2135-2144.

Bouwer, H. (1986). "Intake rate: Cylinder Infiltrometer." *Methods of Soil Analysis, Part-1, Physical and Minerological Methods, Agronomy Monograph No-9,* 2nd Ed., American Society of Agronomy, Soil Science Society of America, Madison, Wisconsin, 825-855.

Bouwer, H. (1994). "Estimating the ability of vadose zones to transmit liquids." *Handbook of vadose zone Characterization and monitoring,* L.G Wilson, L. G Everett and S. J. Cullen ed., Lewis, Boca Raton, Florida, 177-188.

Bouwer, H., Back, T., and Oliver, J. M. (1999). "Predicting infiltration and ground-water mounds for artificial recharge". *Journal of Hydrologic Engineering, ASCE,* 4 (4), 350-357.

Boyd, M. J., Bufil, M. C. and Knee, R. M. (1993). "Pervious and impervious runoff in urban catchments." *Hydrological Sciences Journal,* 38 (6), 463-478.

Boyd, M. J., Bufil, M. C. and Knee, R. M. (1994). "Predicting pervious and impervious storm runoff from urban drainage basins." *Hydrological Sciences Journal,* 39 (4), 321-332.

Bradley, A. A., Cooper, P. J., Potter, K. W., and Price, T. (1996). "Flood plain mapping using continuous hydrologic and hydraulic simulation models." *Journal of Hydrologic Engineering, ASCE,* 1 (2), 63-68.

Bruen, M. and Yang, J. (2006). "Combined hydraulic and black-Box models for flood forecasting in urban drainage systems." *Journal of Hydrologic Engineering*, ASCE, 11(6), 589–596.

Brun, A. C. and Band, L. E. (2000). "Simulating runoff behavior in an urbanized watershed." *Computers, Environment and Urban Systems,* 24, 5-22.

Buchele, B., Kreibich, H., Kron, A., Theiken, A., Ihringer, J., Oberle, P., Merz, B. and Nestmann, F. (2006). "Flood risk mapping: contribution towards an enhanced assessment of extreme events and associated risks." *Natural Hazards and Earth System Sciences,* 6, 485-503.

Burns, D., Vitvar, T., McDonnell, J., Hassett, J., Duncan, J. and Kendall, C. (2005). "Effects of sub urban development on runoff generation in the Croton river basin, New York, USA." *Journal of Hydrology,* 311, 266-281.

Cameira, M. R., Ahuja, L., Fernando, R. M. and Pereira, L. S. (2000). "Evaluating field measured soil hydraulic properties in water transport simulations using RZWQM." *Journal of Hydrology,* 236 (1-2), 78-90.

Canters, F., Chormansky, J., de Voorde, T. V., and Batelaan, O. (2006). "Effects of different methods for estimating impervious surface cover on runoff estimation at catchment level." Proceedings of 7th International Symposium on spatial accuracy assessment in natural resources and environmental sciences, M. Caetano and M. Painho edited, 557-566.

Chabaeva, A., Civco, D. L. and Hurd, J. D. (2009). "Assessment of imperviousness estimation techniques." *Journal of Hydrologic Engineering,* ASCE, 14 (4), 377-387.

Chu, X. and Steinman, A., (2009). "Event and continuous hydrologic modeling with HEC-HMS." *Journal of Irrigation and Drainage Engineering*, ASCE, 135 (1), 119-124.

Clothier, B. and Scotter, D. (2002). Unsaturated water transmission parameters obtained from infiltration, *Methods of soil analysis, Part 4-Physical methods, Soil Science Society of America, Madison, Wisconsin, USA.*

Crooks, S., and Davies, H. (2001). "Assessment of land use change in the Thames catchment and its effect on the flood regime of the river." *Physics and Chemistry of the Earth, part B: Hydrology, Oceans and Atmosphere,* 26 (7-8), 583-591.

Daniel, E. B., Camp, J. V., LeBoeuf, E. J., Penrod, J. R., Abkowitz, M. D., and Dobbins, J. P., (2010). "Watershed Modeling using GIS Technology: A Critical Review." *Journal of Spatial Hydrology,* 10 (2), 13-28.

Debo, T. N., and Reese, A. J. (1995). "Municipal Storm Water Management." Lewis Publishers, Boca Raton, Florida.

Delis, A. I., Skeels, C. P. and Ryrie, S. C. (2000)."Implicit high resolution methods for modelling dimensional open channel flow."*Journal of Hydraulic Research*, 38(5), 301–308.

Delleur, J. W. (2003): "The evolution of urban hydrology: Past, present, and future." *Journal of Hydraulic Engineering*, ASCE, 129 (8), 563–573.

Dewan, A. M., Islam, M. M., Kumamoto, T. and Nishigaki, M. (2007). "Evaluating flood hazard for land use planning in greater Dhaka of Bangladesh using remote sensing and GIS techniques." *Water Resources Management*, 21 (9), 1601 – 1612.

Dhar, O. N., and Nandargi, S. (2003). "Hydrometeorological aspects of floods in India." *Natural Hazards,* 28 (1), 1-33.

Dietrich, J., Schumann, A.H., Redetzky, M., Walther, J., Denhard, M., Wang, Y., Pfutzner, B. and Buttner, U. (2009). "Assessing uncertainties in flood forecasts for decision making:prototype of an operational flood management system integrating ensemble predictions." *Natural Hazards and Earth System Sciences,* 9, 1529-1540.

Donnay, P., Barnsely, M. J., Longley, P. A. (2001). *Remote Sensing and Urban Analysis*, Taylor and Francis, London.

Dutta, D., Hearath, S., and Musiake, K. (2003). "A mathematical model for flood loss estimation." *Journal of Hydrology,* 277 (1-2), 24-49.

Endreny, T. A. and Thomas, K. E. (2009): "Improving Estimates of Simulated Runoff Quality and Quantity using Road-Enhanced Land Cover Data." *Journal of Hydrologic Engineering,* ASCE, 14 (4), 346-351.

Faisal I. M., Kabir, M.R., and Nishat, A. (1999). "Non-structural flood mitigation measures for Dhaka city." *Urban Water*, 1 (2), 145-153.

Faisal I. M., Kabir, M.R., and Nishat, A. (2003). "The disastrous flood of 1998 and long term mitigation strategies for Dhaka city." *Natural Hazards*, 28 (2-3), 85-99.

Friedel, M. J., Smith, M. E., Chica, A. M. E., and Litke, D. (2008). "Probable flood predictions in ungauged coastal basins in EI Salvador." *Journal of Hydrologic Engineering,* ASCE, 13 (5), 321-332.

Gain, A. and Hoque, M. (2011). *Flood risk assessment in the eastern part of Dhaka city, Bangladesh: An application of hydrodynamic model and other geoinformatics tools.* LAP LAMBERT Academic Publisher.

Gain, A. and Hoque, M. (2012). "Flood risk assessment and its application in the eastern part of Dhaka city, Bangladesh." *Journal of Flood Risk Management*, Article first published online: 4th Nov 2012, DOI: 10.1111/jfr3.12003.

Gall, M., Boruff, B. J., and Cutter, S. L. (2007). "Assessing flood hazard zones in the absence of digital flood plain maps: comparison of alternative approaches." *Natural Hazards Review,* ASCE, 8 (1), 1-12.

Ghosh, I. and Hellweger, F. L., (2012). "Effects of spatial resolution in urban hydrologic simulations." *Journal of Hydrologic Engineering*, ASCE, 17 (1), 129-137.

Giacomoni, M. H., Zechman, E. M., and Brumbelow, K. (2012). "Hydrologic footprint residence: environmentally friendly criteria for best management practices." *Journal of Hydrologic Engineering*, ASCE, 17 (1), 99-108.

Giannoni, F., Roth, G., and Rudari, R. (2005). "A procedure for drainage network identification from geomorphology and its application to the prediction of hydrologic response." *Advances in Water Resources,* 28 (6), 567-581.

Gironas, J., Roesner, L. A., and Davis, J., 2009. Storm Water Management Model Applications Manual, Report No. EPA/600/R-09/000July 2009, 17, US Environmental Protection Agency.

Goetz, S., Wright, R., Smith, A., Zinecker, E., Schaub, E. (2003). "IKONOS imagery for resource management: Tree cover, impervious surfaces and riparian buffer analyses in the mid Atlantic region." *Remote Sensing of Environment,* 88, 195-208.

Green, W. and Ampt, G. (1911). "Studies on soil physics part I: the flow of air and water through soils". *Journal of Agricultural Science* 4 (1), 1–24.

Guo, J. C. Y. (1999). "Detention storage volume for small urban catchments." *Journal of Water Resources Planning and Management,* ASCE, 125 (6), 380-382.

Guo, J. C. Y.(2001a). "Design of circular infiltration basin under mounding effects."*Journal of Water Resources Planning and Management,* ASCE, 127 (1), 58–65.

Guo, Y. (2001 b). "Hydrologic design of urban flood control detention ponds."*Journal of Hydrologic Engineering*, ASCE, 6(6), 472–479.

Guo, J. C. Y. (2003). *Urban Storm Water Design*. Water Resources Publications, LLC, US.

Guo, J. (2006). "Storm-Water Predictions by Dimensionless Unit Hydrograph."*Journal of Irrigation and Drainage Engineering*, ASCE, 132(4), 410–417.

Gupta, R.P. (2003). *Remote Sensing Geology*, Springer-Verlag Berlin Heidelberg, NewYork.

Habili, J. M. and Heidarpour, M. (2011). "Estimating soil hydraulic parameters using Green Ampt Infiltration equation." *Journal of Hydrologic Engineering,* ASCE, 16 (10), 772-780.

Han, W., and Burian, S. J., (2005). "Classifying total and effective impervious surfaces for urban hydrologic modelling." In proceedings of the EWRI world water and environmental resources congress, ASCE, Anchorage, Alaska, 15-19 May.

Han, W., and Burian, S. J. (2009). "Determining Effective Impervious Area for Urban Hydrologic Modelling." *Journal of Hydrologic Engineering*, ASCE, 14 (2), 111- 120.

Heaney, J. P., Huber, W. C., and Nix, S. (1977). "Storm Water Management Model: Level I-Preliminary screening procedure." *U.S. Environmental Protection Agency Report, EPA-600/2-76-275, Washington, D. C.*

Horton, R. E. (1933). "The role of infiltration in the hydrologic cycle". *Transactions, American Geophysical Union,* 14, 446–460.

Huber, W. C. and Dickinson, R. E., 1988. Storm Water Management Model, User's Manual, Version 4.0, EPA-600/3-88-001a, U.S. Environmental Protection Agency, Athens, GA.

Islam, M. M. and Sado, K. (2000). "Development of flood hazard maps of Bangladesh using NOAA- AVHRR images with GIS." *Hydrological Sciences Journal,* 45 (3), 337-355.

Islam, M. M. and Sado, K. (2002). "Development priority map for flood countermeasures by remote sensing data with geographic information system." *Journal of Hydrologic Engineering,* ASCE, 7 (5), 346-355.

Jackson, T. J., Ragan, R. M., and Fitch, W. N. (1977). "Test of Landsat-based urban hydrologic modeling." *Journal of Water Resources Planning and Management Division,* ASCE, 103 (1), 141-158.

Jain, A. and Kumar, A. (2006). "An evaluation of artificial neural network technique for the determination of infiltration model parameters." *Applied Soft Computing,* 6 (3), 272-282.

Jain, M. K., Kothyari, U. C., and RangaRaju, K. G. (2004). "A GIS based distributed rainfall-runoff model." *Journal of Hydrology*, 299 (1-2), 107-135.

Jain, S. K., Singh, R. D., Jain, M. K. and Lohani, A. K. (2005). "Delineation of flood prone areas using remote sensing techniques." *Water Resources Management*, 19 (1-2), 333-347.

Jain, S. K., Saraf, A. K., Goswami, A. and Ahmad, T. (2006). "Flood inundation mapping using NOAA AVHRR data." *Water Resources Management,*, 20 (1-2), 949-959.

Jayaraman, V., Chandrasekhar, M. G., and Rao, U. R. (1997). "Managing the natural disasters from space technology inputs." *Acta Astronautica*, 40 (2-8), 291-325.

Joel, A., and I. Messing. (2000). "Application of two methods to determine hydraulic conductivity with disc permeameters on sloping land." *European Journal of Soil Science*, 51 (1), 93–98.

Joseph, G., (2003). *Fundamentals of Remote Sensing*. Universities Press Private Ltd, Hyderabad, India.

Jumadar, A. S., Pathirana, A., Gersonios, B., and Zevenbergen, C. (2008). "Incorporating infiltration modeling for urban flood management." *Hydrology and Earth System Sciences Discussions."* 5, 1533-1566.

Kafle, T. P., Hazarika, M. K., Shrestha, K. G., Prathumchai, K., and Samarakoon, L. (2006). "Integration of remote sensing and GIS with flood simulation model for flood hazard mapping in the Bagmati river, Nepal." In Proceedings, 5th International symposium on new technologies for urban safety of mega cities in Asia, November 16-17, 2006, Phuket Thailand, 257-268.

Karlsson, P., O., and Haimes, Y. Y. (1988). "Risk based analysis of extreme events." *Water Resources Research*, 24 (1), 9-20.

Kauffman, G. J., Belden, A. C., Vonck, K. J. and Homsey, A. R. (2009). "Link between impervious cover and base flow in the White Clay Creek wild and scenic watershed in Delaware." *Journal of Hydrologic Engineering, ASCE*, 14 (4), 324-334.

Koussis, A. D., Lagouvardos, K., Mazi, K., Kotroni, V., Sitzmann, D., Lang, J., Zaiss, H., Buzzi, A., and Malguzzi, P. (2003). "Flood forecasts for urban basin with integrated hydro-meteorological model." *Journal of Hydrologic Engineering, ASCE*, 8 (1), 1-11.

Kouwen, N. (1973). "Watershed modeling using a squire grid technique." *Proceedings of first Canadian Hydraulics conference,* CSCE, Edmonton, Alberta, 418-434.

Lee, J. G. and Heaney, J. P., 2003. Estimation of urban imperviousness and its impact on storm water systems. *Journal of Water Resources Planning and Management*, ASCE, 129 (5), 419-426.

Li, X. Y., Chau, K. W., Cheng, C. T., and Li, Y. S. (2006). "A web-based flood forecasting system for Shuangpai region." *Advances in Engineering software*, 37 (3), 146-158.

Luino, F., Cirio, C.G., Biddoccu, M., Agangi, A., Giulietto, W., Godone, F. and Nigrelli, G. (2009)."Application of a model to the evaluation of flood damage."*Geoinformatica*, (13) 339-353.

Lund, J. R. (2002). "Floodplain planning with risk based optimization." *Journal of Water Resources Planning and Management,* ASCE, 128 (3), 202- 207.

Lyon, J. G. (2010): *GIS for Water Resources and Watershed Management.* CRC Press, USA.

Maidment, D. R. (1983). Grid based computation of runoff: A preliminary assessment, Hydrologic Engineering Centre, US Army Corps of Engineers, Davis, CA, Contract DACW05-92-P-1983.

McCuen, R., Johnson P., and Ragan, R. (1996). Highway hydrology, hydraulic design series No.-2, Pub No.-FHWA-SA-96-067, Federal Highway Administration, Washington, DC, September, 326pp.

Mohapatra, P. K. and Singh, R. D. (2003). "Flood management in India." *Natural Hazards,* 28 (1), 131-143.

Molls, T. and Molls, F. (1998).“Space-time conservation method applied to Saint-Venant equations.”*Journal of Hydraulic Engineering*, ASCE, 124(5), 501–508.

Navarro, P. G. and Zorraquino, V. (1993).“Numerical modeling of flood propagation through system of reservoirs.”*Journal of Hydraulic Research*, 119(3), 380–389.

Nieto, J. D., Lerner, D. N., Saul, A. J., and Blanksby, J. (2012). “GIS water balance approach to support surface water flood risk management.” *Journal of Hydrologic Engineering*, ASCE, 17 (1), 55-67.

Noto, L. and Tucciarelli, T. (2001).“DORA- Algorithm for network flow models with improved stability and convergence properties.”*Journal of Hydraulic Engineering*, ASCE, 127(5), 380–391.

Novotny, V. and Olem, H. (1994). Water quality: Prevention, identification and management of diffuse pollution, Van Nostrand Reinhold Publisher, New York.

O’Brien, J. S., Julien, P. Y., and Fullerton, W. T.(1993). ‘‘Two-dimensional water flood and mudflow simulation.” *Journal of Hydraulic Engineering*, ASCE, 119(2), 244 –261.

Olsen, J. R., Beling, P. A., and Lambert, J. H. (2000). “Dynamic models for floodplain management.” *Journal of Water Resources Planning and Management,* ASCE, 126 (3), 167-175.

Pappas, E.A., Smith, D. R., Huang, C., Shuster, W. D. and Bonta, J. V. (2008). “Impervious surface impacts to runoff and sediment discharge under laboratory rainfall simulation.” *Catena,* 72, 146-152.

Perroux, K. M., and White, I. (1988). “Designs for Disc infiltrometers.” *Soil Science Society of America, Journal,* 52, 1205-1215.

Philip, J. (1957). “The theory of infiltration: 4. Sorptivity and albegraic infiltration equations”. *Soil Science,* 84 (3), 257–264.

Pingel, N. and Watkins Jr., D. (2010). “Multiple flood source expected annual damage computations.” *Journal of Water Resources Planning and Management,* ASCE, 136, (3), 319-326.

Plate, E. J. (2002). "Flood risk and flood management." *Journal of Hydrology*, 267 (1-2), 2-11.

Price, R. K. and Vojinovic, Z. (2008). "Urban flood disaster management." *Urban Water Journal,* 5 (3), 259-276.

Quader, A. and Guo, Y. (2006). "Peak discharge estimation using analytical probabilistic and design storm approaches." *Journal of Hydrologic Engineering*, ASCE, 11(1), 46–54.

Ragan, R. M. and Jackson, T. J. (1980). "Runoff synthesis using Landsat and SCS model." *Journal of Hydraulic Division, ASCE,* 106 (5), 667-678.

Rambabu, Tejwani, K. K., Agrawal, M. C., and Bhusan, L. S. (1979). "Rainfall intensity duration return period equations and nomographs of India, Bulletin No. 3, CSWCRTI, ICAR, Dehradun, India.

Ramlal, B., and Baban, S. M. J. (2008). "Developing a GIS based integrated approach to flood management in Trinidad, West Indies." *Journal of Environmental Management,* 88 (4) 1131-1140.

Ramos, T. B., Goncalves, M. C., Martins, J. C., van Genuchten, M. Th., and Pires, F. P. (2006). "Estimation of soil hydraulic properties from numerical inversion of tension disk infiltrometer data." *Vadose Zone Journal,* 5 (2), 684-696.

Ravagnani, F., Pellegrinelli, A., and Franchini, M. (2009). "Estimation of urban impervious fraction from sattelite images and its impact on peak discharge entering a storm sewer system." *Water Resources Management*, 23 (10), 1893-1915.

Rawls, W. J., Brakensiek, D. L. and Miller, N. (1983). "Green Ampt infiltration parameters from soils data. "*Journal of Hydraulic Engineering*, ASCE, 109 (1), 62-70.

Richards A. (1931). "Capillary conduction of liquids through porous mediums". *Physics,* 1 (5), 318–333.

Richards, J.A., 1999. *Remote Sensing Digital Image Analysis*, Springer-Verlag, Berlin.

Rossman, L.A. (2005). Storm Water Management Model- Users manual version 5.0, EPA-United States, (http//www.epa.gov/ednnrmrl/models/swmm5/manual.pdf)

Sahapure, S. S., Eldho, T. I. and Rao, E. P. (2011). "Flood simulation in an urban catchment of Navi Mumbai city with detention pond and tidal effects using FEM, GIS and Remote Sensing." *Journal of waterway, port, coastal and ocean engineering,* ASCE, 137 (6), 286-299.

Salimi, S., Ghanbarpour, M. R., Solaimani, K., and Ahamadi, M. Z.(2008). "Flood plain mapping using hydraulic simulation model in GIS." *Journal of Applied Sciences* 8 (4), 660-665.

Sanders, B. F. (2007). "Evaluation of online DEMs for flood inundation modeling." *Advances in Water Resources*, 30 (8), 1831-1843.

Schwartz, R. C, Evett, S. R. (2002). "Estimating hydraulic properties of a fine textured soil using a disc infiltrometer." *Soil Science Society of America Journal,* 66 (5), 1409-1423.

Scotter, D. R., Clothier, B. E., and Harper, E. R. (1982). "Measuring saturated hydraulic conductivity and sorptivity using twin rings." *Australian Journal of Soil Research,* 20 (4), 295-304.

Sharif, H. O., Sparks, L., Hassan, A. A., Zeitler, J., and Xie, H., 2010. Application of a distributed hydrologic model to the November 17, 2004 flood, of Bull Creek watershed, Austin, Texas. *Journal of Hydrologic Engineering*, ASCE, 15 (8), 651-657.

Shuster, W. D., Pappas, E., and Zhang, Y. (2008). "Laboratory scale simulation of runoff response from pervious-impervious systems." *Journal of Hydrologic Engineering, ASCE,* 13(9), 886–893.

Shuster, W. D. and Pappas, E. (2011). "Laboratory simulation of urban runoff and estimation of runoff hydrographs with experimental curve numbers implemented in USEPA SWMM." *Journal of Irrigation and Drainage Engineering, ASCE*, 137 (6), 343-351.

Sikorska, A.E., Scheidegger, A., Banasik, K. and Rieckermann, J. (2012)."Bayesian uncertainty assessment of flood predictions in ungauged urban basins for conceptual rainfall-runoff models." *Hydrology and Earth System Sciences,* 16, 1221-1236.

Simonovic, S. P., and Akter, T. (2006). "Participatory floodplain management in the Red river basin, Canada." *Annual Reviews in Control*, 30 (2), 183-192.

Singh, R. D., Mishra, S. K. and Chowdhary, H. (2001). "Regional flow-duration models for large number of ungauged Himalayan catchments for planning microhydro projects." *Journal of Hydrologic Engineering*, ASCE, 6(4), 310–0316.

Smith, K. A., and Mullins, C. E. (2001). *Soil and environmental analysis: physical methods.* 2nd Ed., revised and expanded, Marcel Dekker, Inc., New York.

Spry, R., and Zhang, S. (2006): "Modelling of drainage systems and overland flow paths at catchment's scales." *Proc., Urban Drainage Modelling and Water Sensitive Urban Design*, Monash Univ., Melbourne, Australia.

Sreeja, P., and Gupta, K. (2006). "An Alternate Approach for Transient Flow Modeling in Urban Drainage Systems." *Water Resources Management*, Springer *Publication*, 21 (7), 1225-1244.

Stephens, D.B. (1995). *Vadose Zone Hydrology.* CRC Press, USA.

Subramanya, K. (2011). *Engineering Hydrology,* Tata McGraw Hill, New Delhi.

Sutherland, R. C. (1995). "Methodology for estimating the effective impervious area of urban watersheds." *Watershed Protection Techniques,* 2 (1), 282-284.

Swain, P. H. and Davis, S. M. (1978). *Remote Sensing: The Quantitative Approach,* McGraw Hill.

Tao, T., and Kouwen, N. (1989). "Remote sensing and fully distributed modeling for flood forecasting." *Journal of water resources planning and management,* ASCE, 115 (6), 809-823.

Theobald, D. M., Goetz, S. J., Norman, J. B. and Jantz, P. (2009). "Watersheds at risk to increased impervious surface cover in conterminous United States." *Journal of Hydrologic Engineering,* ASCE, 14 (4), 362-368.

Todini, E. (1996). "The ARNO rainfall-runoff model." *Journal of Hydrology,* 175 (1-4), 339-382.

vanManen, S. E., and Brinkhuis, M. (2005). "Quantitative flood risk assessment for polders." *Reliability Engineering and system safety*, 90 (2-3), 229-237.

Wahl, N. A., Bens, O., Buczko, U., Hangen, E., and Huttl, R. F. (2004). "Effects of conventional and conservation tillage on soil hydraulic properties of a silty-loamy soil." *Physics and Chemistry of the Earth,* 29 (11-12), 821-829.

Wang, K and Altunkayank, A. (2012). "Comparative case study of rainfall runoff modeling between SWMM and fuzzy logic approach." *Journal of Hydrologic Engineering,* ASCE, 17 (2), 283-291.

Wardah, T. (2008). "Use of geostationary meteorological satellite images in convective rain estimation for flash flood forecasting." *Journal of Hydrology,* 356 (3-4), 283-298.

Warrick, A. W. (1992). "Models for disc permeameters." *Water Resources Research*, 28 (5), 1319-1327.

Warwick, J. J. and Tadepalli, P. (1991). "Efficacy of SWMM application." *Journal of water resources planning and management,* ASCE, 117 (3), 352-366.

Wright, N. G., Villanueva, I., Bates, P. D., Mason, D. C., Wilson, M. D., Pender, G. and Neelz, S.(2008). "Case study of the use of remotely sensed data for modelling flood inundation on the river Severn, U. K." *Journal of Hydraulic Engineering,* ASCE, 134 (5), 533- 540.

Xiong, Y. and Melching, C. S. (2005). "Comparison of kinematic wave and non linear reservoir routing of urban watershed runoff." *Journal of Hydrologic Engineering,* ASCE, 10 (1), 39-49.

Yoon, Y., Kim J. G. and Hyun, S. (2007). "Estimating soil water retention in a selected range of soil pores using tension disk infiltrometer data." *Soil and Tillage Research,* 97 (1), 107-116.

Zhang, R. (1997). "Determination of soil sorptivity and hydraulic conductivity from the disk infiltrometer." *Soil Science Society of America Journal,* 61 (4), 1024-1030.

List of Publications

Journals

- Sahoo, S. N. and Sreeja, P. "Determination of urbanization based on imperviousness." *Urban Design and Planning*, ICE Publishing, Thomas Telford, UK (Accepted).
- Sahoo, S. N. and Sreeja, P. (2014). "A methodology for determining runoff based on imperviousness in an un-gauged peri-urban catchment." *Urban Water Journal*, Taylor and Francis, UK, 11 (1), 42-54.
- Sahoo, S. N. and Sreeja, P. (2013). "Role of rainfall events and imperviousness parameters in urban runoff modeling." *ISH Journal of Hydraulic Engineering*, Taylor and Francis, UK, 19 (3), 329-334.
- Sahoo, S. N. and Sreeja, P. (2013). "A review of Decision Support System Application in Flood Management." *International Journal of Hydrology Science and Technology,* Inderscience Publication, 3 (3), 206 - 220.
- Sahoo, S. N. and Sreeja, P. (2012). "Application of geospatial technologies to determine imperviousness in peri-urban areas." *International Journal of Remote Sensing Applications,* 2 (4), 47-51.
- Sahoo, S. N. and Sreeja, P (2011). "Total and Effective Impervious Area from low resolution satellite imageries." *International Journal of Earth Sciences and Engineering,* 4 (6 SPL), 334-337.
- Sahoo, S. N. and Sreeja, P. (2011). "Determination of infiltration parameters for urban flood modeling." *Journal on Civil Engineering, imanager publications, India,* 1 (3), 7-12.

Conferences

- Sahoo, S. N. and Sreeja, P. "Evaluation of near saturation infiltration characteristics of a locally available soil." In proceedings of 6th International Congress in Environmental Geotechniques (6ICEG)-2010, New Delhi.
- Sahoo, S. N. and Sreeja, P. "Indirect Determination of Effective Impervious Area (EIA) of an urban city in North East India." In proceedings of World Environmental Water Resources Congress, EWRI, ASCE, May 22 to 26-2011, California.
- Sahoo, S. N. and Sreeja, P. "Determination of Effective Impervious Area in Guwahati city: A Case Study." In proceedings of AMTID, September 28 to 30, 2011, NIT Calicut, Kerala, India.
- Sahoo, S. N. and Sreeja, P. "Total and Effective Impervious Area from low resolution satellite imageries." In proceedings of ACE, October 21 – 23, KLU, Hyderabad, India.
- Sahoo, S. N. and Sreeja, P. "Impact of total and effective impervious area on runoff prediction." In Proceedings of ENSURE-2012, February 24- 26, IIT Guwahati, India.
- Sahoo, S. N. and Sreeja, P. "Role of rainfall events and imperviousness parameters in urban runoff modeling." In Proceedings of HYDRO-2012, December 7-8, IIT Mumbai, India.
- Sahoo, S. N. and Sreeja, P. "Flood inundation mapping (FIM): An effective tool for urban flood management." In Proceedings of HYDRO-2013, December 4-6 2013, IIT Madras, India.